

UNIVERSITY OF NAPLES “FEDERICO II”

Polytechnic and Basic Science School

Ph.D. School in Chemical Sciences



Bioactive metabolites produced by pathogenic fungi of forest plants

Roberta Di Lecce

Supervisor:

Prof. Antonio Evidente

Co-supervisor:

Dr. Marco Masi

Examiner:

Prof. Alessandra Napolitano

XXXIV Cycle 2018-2021

Coordinator: Prof. Angelina Lombardi

ABSTRACT

Pathogenic fungi are the main causes of forest plant disease. They induce alterations during developmental stages and the development of diseases, in particular canker, which determine huge economic and environmental losses, especially for plant nurseries and wood industries. Fungal-plant host interactions represent biochemically complex systems that are being studied also by metabolites involved. Pathogenic fungi are able to produce phytotoxins, i.e. secondary metabolites, which are involved at different stages of plant pathogenesis. Considering the strong economic and ecological impact of forest plant diseases, the study of the plant-pathogen interaction and the metabolites involved is of remarkable importance.

The aim of this PhD project has been on the investigation of phytotoxins produced by forest plants fungal pathogens. Culture filtrates have been obtained from *Hymenoscyphus fraxineus*, responsible of ash dieback, from *Fimetariella rabenhorstii* and *Stilbocrea macrostoma*, two fungi associated to *Quercus brantii* decline, from *Diplodia olivarum*, an aggressive pathogen of different plants in Italy, from *Alternaria argyroxiphii*, responsible of leaf spot of mahogany (*Khaya senegalensis*), and from *Diplodia sapinea*, associated to canker of Tunisian pine (*Pinus pinaster*). They have been exhaustively extracted and, the corresponding phytotoxic extracts have been purified to obtain metabolites by bio-guided chromatographic processes.

A new metabolite, named hyfraxinic acid, has been isolated and characterized from the culture filtrates of *H. fraxineus* together with four furano diterpenoids. Among them, the relative and the absolute configurations have been assigned to 1-deoxyviridiol by crystallographic analyses and by the application of the advanced Mosher's method. The new compound has been showed the most toxic effect in the phytotoxic assay.

A new chromenone and a new benzophenone, named rabenchromenone and rabenzophenone, have been isolated from the culture filtrate of *F. rabenhorstii* together with moniliphenone and coniochaetone A. The absolute configuration of rabenchromenone has been determined by application of electronic circular dichroism (ECD) spectroscopy supported by quantum mechanical calculations compared with the experimental spectrum. In the leaf puncture assay, rabenzophenone has proved to be the most toxic compound.

From the culture filtrate of *S. macrostoma*, three well-known compounds have been identified as 2,5-dihydroxymethylfuran, 5-hydroxymethyl-2-furaldehyde and tyrosol. All metabolites have been phytotoxic in the biological assay, but in particular the phytotoxicity of the two furan derivatives has been concentration-dependent.

A new cleistanthane *nor*-diterpenoid, named olicleistanone, has been isolated and characterized from the culture filtrate of *D. olivarum*, which has showed to be a racemate. Other four pimarane

diterpenoids and an isocoumarin has been identified. In the bioassays, olicleistanone has been showed a zootoxic activity against *Artemia salina* L.

From the culture filtrate of *A. argyroxiphii*, three new metabolites, named argyrottoxins A-C, have been isolated and characterized. The absolute configuration of argyrottoxin A has been determined by quantum chemical calculations and electronic circular dichroism experiments using a chiroptical probe. Other known compounds have been identified as porritoxinol, its phthalide, the phthalide carboxylic acid derivative, zinniol, alternariol and its 4-methyl ether. In the leaf puncture assay, argyrottoxin A and B have been phytotoxic on *Phaseolus vulgaris* L. leaves only.

Two new trisubstituted furanones, named pinofuranoxins A and B, have been isolated and characterized from the culture filtrate of *D. sapinea*. Their relative and absolute configurations have been assigned by NOESY experiment and by computational and ECD analyses, respectively. Both compounds have presented phytotoxic, antifungal and zootoxic activities and in details pinofuranoxin A has been more active than pinofuranoxin B.

INDEX

1 INTRODUCTION	1
1.1 Forest plants	1
1.1.1 Relevance of forest plants	1
1.1.2 Forest plant diseases	1
1.2 Fungal secondary metabolites	2
1.2.1 Classification of toxins	4
1.2.2 Biological activities	4
1.3 Previous studied pathogenic fungi involved in forest plant disease	8
1.3.1 <i>Diplodia africana</i>	8
1.3.2 <i>Diplodia cupressi</i>	12
1.4 Pathogenic fungi of forest plant diseases, studied in this thesis	16
1.4.1 Fungi involved in the decline of Iranian oak trees (<i>Quercus brantii</i>)	16
1.4.1.1 <i>Fimetariella rabenhorstii</i>	17
1.4.1.2 <i>Stilbocrea macrostoma</i>	18
1.4.2 Fungi involved in ash decline and lentisk canker in Europe	19
1.4.2.1 <i>Hymenoscyphus fraxineus</i>	23
1.4.2.2 <i>Diplodia olivarum</i>	24
1.4.3 Fungi involved in the diseases of maritime pine in Africa and mahogany in Brazil	25
1.4.3.1 <i>Diplodia sapinea</i>	26
1.4.3.2 <i>Alternaria argyroxiphii</i>	29
2 OBJECTIVES	31
3 MATERIAL AND METHODS	32
3.1 Fungal strains	32
3.1.1 <i>Hymenoscyphus fraxineus</i>	32
3.1.2 <i>Fimetariella rabenhorstii</i>	32
3.1.3 <i>Stilbocrea macrostoma</i>	32
3.1.4 <i>Diplodia olivarum</i>	33
3.1.5 <i>Alternaria argyroxiphii</i>	33
3.1.6 <i>Diplodia sapinea</i>	33
3.2 General procedures	33
4 EXPERIMENTAL	35
4.1 Production, extraction and purification of secondary metabolites from	35

<i>Hymenoscyphus fraxineus</i> culture filtrates	
4.1.1 Hyfraxinic acid	37
4.1.2 1-Deoxyviridiol	37
4.1.3 Viridiol	37
4.1.4 Nodulisporiviridin M	37
4.1.5 Demethoxyviridiol	37
4.1.6 2- <i>O</i> -Acetylhyfraxinic acid	37
4.1.7 2- <i>O-p</i> -Bromobenzoyl ester of hyfraxinic acid	38
4.1.8 3- <i>O-(S)-α</i> -Methoxy- α -trifluoromethyl- α -phenylacetate (MTPA) ester of 1-deoxyviridiol	38
4.1.9 3- <i>O-(R)-α</i> -Methoxy- α -trifluoromethyl- α -phenylacetate (MTPA) ester of 1-deoxyviridiol	38
4.2 Crystal structure determination of 1-deoxyviridiol	39
4.2.1 Crystallographic data of 1-deoxyviridiol	39
4.3 Leaf puncture assay of metabolites isolated from <i>H. fraxineus</i>	39
4.4 Production, extraction and purification of secondary metabolites from	40
<i>Fimetariella rabenhorstii</i> culture filtrates	
4.4.1 Rabenchromenone	42
4.4.2 Rabenzophenone	42
4.4.3 Moniliphenone	42
4.4.4 Coniochaetone A	42
4.5 Computational methods to afford absolute configuration (AC) of rabenchromenone	42
4.6 Biological assay on phytotoxins isolated from <i>F. rabenhorstii</i>	43
4.6.1 Leaf Puncture Assay	43
4.6.2 Tomato Cutting Assay	43
4.7 Production, extraction and purification of secondary metabolites from	44
<i>Stilbocrea macrostoma</i> culture filtrates	
4.7.1 2,5-Dihydroxymethylfuran	46
4.7.2 5-Hydroxymethyl-2-furaldehyde	46
4.7.3 Tyrosol	46
4.8 Crystal structure determination of 2,5-dihydroxymethylfuran	46
4.8.1 Crystallographic data of 2,5-dihydroxymethylfuran	47
4.9 Biological assay on phytotoxins isolated from <i>S. macrostoma</i>	47
4.9.1 Leaf Puncture Assay	47

4.9.2 Tomato Cutting Assay	47
4.10 Production, extraction and purification of secondary metabolites from <i>Diplodia olivarum</i> culture filtrates	48
4.10.1 Olicleistanone	51
4.10.2 Sphaeropsidin A	51
4.10.3 Sphaeropsidin C	51
4.10.4 Sphaeropsidin G	51
4.10.5 Diplopimarane	51
4.10.6 (-)-Mellein	52
4.11 Computational methods to determine the AC of olicleistanone	52
4.12 Biological assays on metabolites produced by <i>D. olivarum</i>	52
4.12.1 Leaf puncture assays	52
4.12.2 Antifungal assays	53
4.12.3 <i>Artemia salina</i> bioassays	53
4.13 Production, extraction and purification of secondary metabolites from <i>Alternaria argyroxiphii</i> culture filtrates	54
4.13.1 ArgYROtoxin A	56
4.13.2 ArgYROtoxin B	56
4.13.3 ArgYROtoxin C	56
4.13.4 Porritoxinol	56
4.13.5 6-(3',3'-Dimethallyloxy)-4-methoxy-5-methylphthalide	56
4.13.6 Phthalide derivative	56
4.13.7 Zinniol	57
4.13.8 Alternariol	57
4.13.9 Alternariol methyl ether	57
4.14 Determination of AC of argyrotoxin A by electronic circular dichroism	57
4.15 Leaf puncture assay of metabolites isolated from <i>A. argyroxiphii</i>	57
4.16 Production, extraction and purification of secondary metabolites from <i>Diplodia sapinea</i> culture filtrates	59
4.16.1 Pinofuranoxin A	61
4.16.2 Pinofuranoxin B	61
4.17 Biological assays on metabolites produced by <i>D. sapinea</i>	61
4.17.1 Leaf Puncture Assay	61
4.17.2 Antifungal Assays	61
4.17.3 <i>Artemia salina</i> bioassays	62

5 RESULTS AND DISCUSSION	63
5.1 Structural identification of secondary metabolites isolated from <i>H. fraxineus</i> culture filtrates	63
5.1.1 Structural determination of hyfraxinic acid	64
5.1.2 Determination of relative and absolute configurations of 1-deoxyviridiol	72
5.1.3 Novel data for nodulisporiviridin M and demethoxyviridiol	76
5.1.4 Leaf puncture assay	76
5.2 Structural identification of secondary metabolites isolated from <i>F. rabenhorstii</i> culture filtrates	78
5.2.1 Structural determination of rabenchromenone	79
5.2.2 Absolute configuration of rabenchromenone	86
5.2.3 Structural determination of rabenzophenone	87
5.2.4 Leaf puncture assay	94
5.3 Structural identification of secondary metabolites isolated from <i>S. macrostoma</i> culture filtrates	95
5.3.1 X-ray analyses of 2,5-dihydroxymethylfuran	96
5.3.2 Leaf puncture assay	98
5.4 Structural identification of secondary metabolites isolated from <i>D. olivarum</i> culture filtrates	100
5.4.1 Structural determination of olicleistanone	101
5.4.2 Relative and absolute configurations of olicleistanone	110
5.4.3 Biological assay	113
5.4.3.1 Leaf puncture assay	113
5.4.3.2 Antifungal assays	113
5.4.3.3 <i>Artemia salina</i> bioassay	113
5.5 Structural identification of secondary metabolites isolated from <i>A. argyroxiphii</i> culture filtrates	114
5.5.1 Structural determination of argyrotoxin A	116
5.5.2 Absolute configuration of argyrotoxin A	125
5.5.3 Structural determination of argyrotoxin B	127
5.5.4 Structural determination of argyrotoxin C	137
5.5.5 Leaf puncture assay	145
5.6 Structural identification of secondary metabolites isolated from <i>D. sapinea</i> culture filtrates	147
5.6.1 Structural determination of pinofuranoxins A and B	147

5.6.2 Relative configurations of pinofuranoxins A and B	160
5.6.3 Absolute configurations of pinofuranoxins A and B	163
5.6.4 Biological assay	168
5.6.4.1 Leaf puncture assay	168
5.6.4.2 Antifungal assays	169
5.6.4.3 <i>Artemia salina</i> bioassay	169
6 CONCLUSIONS	170
7 REFERENCES	173
8 APPENDIX A	200
9 PUBLICATIONS LIST	208
Acknowledgement	209

1 INTRODUCTION

1.1 Forest plants

Forest plants cover 31% of the Earth's land surface performing vital functions for human and wild life. Forests are the most biologically diverse ecosystems on Earth, in terms of genetic diversity, species and landscape, and they contain more than 80% of the terrestrial species of animals and plants. This biodiversity enables a wide range of services, named ecosystem services by experts, which include timber, nutrients, medicines, water, pest and pathogen regulation, maintenance of soil fertility, carbon, nitrogen and phosphorus cycle regulation.

1.1.1 Relevance of forest plants

Since 2013, March 21 of each year has been proclaimed "International Day of Forests" to sensitize on forest sustainable management and their use of resources. Forest plants are landscaped and ornamental heritage of each region and therefore connected to its tourist economy.

Nursery is a sector of the agricultural industry aimed at the propagation and production of plants for trade. In particular the forest plants are produced in the ornamental and forest nurseries. The ornamental nursery is a branch that produces plants for garden and parks. The forest nursery is a particular branch of the nursery that produces young seedlings, belonging exclusively to native woody species, intended mainly for the activities of afforestation.

Among the uses of wood obtained from forest plants, the largest is certainly in the wood industry, which includes many applications. One area is the production of products resulting from the decomposition of cellulose; as bioethanol from cellulose, cellophane (widely used for food preservation or for gifts), celluloid (used for the manufacture of common film), artificial textile fibres (like viscose, cupro, acetate and triacetate). An economically important application is the building industry, in particular the productions of houses, bridges, water mills, ships and boats. Another area is the manufacturing industry for the production of tools, toys but essentially furniture. The last application is its use as firewood.

1.1.2 Forest plant diseases

Forest plants diseases determine huge economic and environmental losses for nurseries, wood industries, landscape and forestry heritage.

The causes of plant diseases are divided in abiotic and biotic agents (Fig.1).

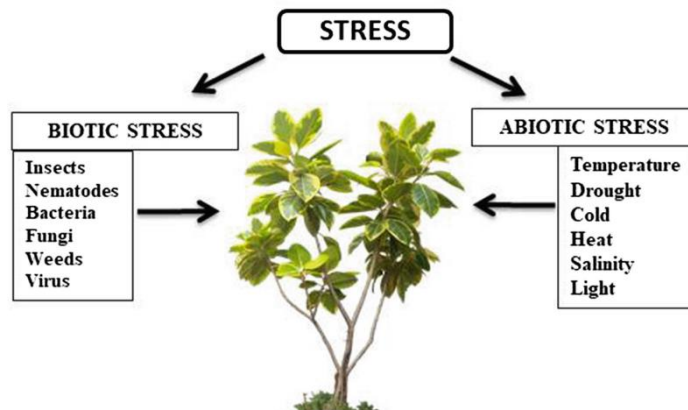


Figure 1: Biotic and abiotic agents of plant diseases.

The first group includes environmental, nutritional and chemical factors. Environmental factors are variation in temperature, moisture and light; nutritional factors are variation in nutrients; chemical factors result from improper soil pH, improper use of fertilizers and pesticides, chemical spills and air pollution. The resulting diseases are called non-infectious plant diseases and they cannot be transmitted from a plant to another.

The biotic causes are interactions with living organisms, known as pathogens, which cause infectious plant diseases. These organisms include nematodes, fungi, bacteria, viruses and insects (Luca *et al.*, 1992). Plants represent a nutrient-rich source for organisms and the resulting interactions could be of different types: symbiotic and pathogenic; this latter could be biotrophic, necrotrophic or hemibiotrophic. In the symbiotic interaction the organisms receive beneficients from each other. Biotrophs infect and colonise the plant without killing it, necrotrophs infect and colonise the dead plant, while hemibiotrophs adopt initially a biotrophic phase and then a necrotrophic one when the plant dies (Allwood *et al.*, 2008).

The organisms are able to produce primary and secondary metabolites. The first ones are essentially for development and for life, while the second are used for interactions with other organisms. Plant-pathogen interaction is one of the most biochemically complex system which is studied by the produced secondary metabolites too (Allwood *et al.*, 2008).

Fungi are the most dangerous microorganism among biotic stressors. They represent a wide reign composed by more than 3 million species (O'Brien *et al.*, 2005) and they are rich sources of secondary metabolites, originating from different biosynthetic pathways (Masi *et al.*, 2018). Their distribution and diversity cause severe damage to plants.

1.2 Fungal secondary metabolites

The diseases caused by fungal pathogens are one of the major problems for the wood industry and the natural and forestry heritage. The interest for these diseases and the associated fungi has been

increasing due their social and economic impact. For this reason, many fungi, isolated from infected plants, were grown *in vitro* in order to study their morphological characteristics and to establish a correct taxonomic classification. Fungi have the ability to produce phytotoxic secondary metabolites, called phytotoxins, that can be involved in the symptoms (Strobel, 1982). The production of phytotoxins is a fundamental step in the fungal-plant interaction, as the key role in infection and virulence processes (Allwood *et al.*, 2008; Möbius and Hertweck, 2009).

Since 1950 many studies allowed to demonstrate that phytotoxins, produced by phytopathogenic fungi, are involved in plant diseases. In plant pathology, these toxins are harmful at low concentrations reproducing some or all the symptoms of the disease caused by pathogen. Most of the plant pathogenic fungi are able to produce toxins *in vitro* culture and in their hosts (Graniti, 1991).

The toxins are able to move from the site of their production to the surrounding tissues or are translocated within the plant vessels *via* the apoplasts (Graniti, 1991). This migration allows different mode of actions: interacting with various cellular targets, altering gene expression, breaking membrane integrity, inhibiting the activity of plant enzymes or disrupting the biosynthesis of crucial metabolites (Evidente, 1997a; Evidente and Motta, 2001, 2002; Möbius and Hertweck, 2009).

In plant pathology, phytotoxins are identified as secondary metabolites produced by microbial pathogens, that interfere with the physiological mechanisms of infected plants. The virulence and the pathogenicity of fungi may depend on their ability to produce one or more toxins (Misaghi, 1982; Durbin, 1983; Graniti, 1991).

These toxins belong from different classes of natural compounds ranging from low molecular weight compounds, as terpenes, chromanones, butenolides, pyrones, macrolides, aromatic derivatives, aminoacids etc., to high molecular weight compounds such as proteins, glycoproteins and polysaccharides. From the biosynthetic point of view, they are synthesized through three most common ways of secondary metabolism. In particular, fatty acids and polyketides can be produced by acetate pathway, amino acids and aromatic phenylpropanoids are produced by shikimate pathway and terpenoids and steroids are produced by the mevalonate pathway (Dewick, 2009a and 2009b).

Initially, phytotoxins were isolated from infected plant tissues and germinating conidia of fungi, but this approach gave low amount of the target compounds. Actually, fungi are grown *in vitro* to obtain phytotoxins in an amount sufficient to study their chemical and biological properties. The production of phytotoxins strictly depends on several factors as the composition of culture medium and its pH, the duration and conditions of culturing (i.e. light, temperature, stirring); most of these factors are not identified in advance and need to be optimized (Berestetskiy, 2008). Furthermore, when fungi are stored and re-inoculated could change their ability to produce toxins (Kale and Bennett, 1992).

Thus, several studies are being conducted to understand the role of bioactive microbial metabolites in the pathogenesis processes and to find the best and rapid remedial tool to control plant diseases. These metabolites can be used to:

- develop specific and rapid diagnostic methods to identify the disease and to develop simple kits usable in the field (Del Sorbo *et al.*, 1994; Evidente *et al.*, 1997b; Andolfi *et al.*, 2009);
- perform genetical study aimed to select resistant plant species to the pathogen (Bani *et al.*, 2018);
- formulate new bio-pesticides (herbicides, fungicides, bactericides, insecticides, etc.) (Evidente and Motta, 2001; Schrader *et al.*, 2010; Evidente *et al.*, 2011a; Fernández-Aparicio *et al.*, 2013; Sarrocco *et al.*, 2015; Barilli *et al.*, 2017; Barilli *et al.*, 2019);
- develop new drugs with a new mechanism of action (antiviral, antimalarial, anticancer, etc.) to be applied in medicine (Bajsa *et al.*, 2007; Balde *et al.*, 2010; Evidente *et al.*, 2014; Singh and Datta, 2020).

1.2.1 Classification of toxins

The production of fungal phytotoxins has been investigated by different research groups and this has led to divide phytotoxins into two main groups according to their mode of action: host-specific and non-host specific toxins (Berestetskiy, 2008; Pusztahelyi *et al.*, 2015).

The host-specific phytotoxins are active against host plant only showing unique mode of action, moreover their production is essential for the virulence of the fungus (Otani *et al.*, 1995; Walton, 1996; Tsuge *et al.*, 2013; Pusztahelyi *et al.*, 2015).

The non-host-specific phytotoxins are not strictly related to the pathogenicity of the fungus, however they may contribute to its virulence. These metabolites possess a broad range of activity, causing symptoms on host and non-host plants (Walton, 1996; Pusztahelyi *et al.*, 2015).

Many studies have been performed to isolate and characterize the secondary metabolites produced by pathogenic fungi of forest plants. Most of the studied phytotoxins have shown a non-specific activity. The corresponding symptoms and disease on the plants are frequently due to a synergistic effect of the phytotoxins produced by the pathogen (Hohn, 1997; Evidente, 2011b).

1.2.2 Biological activities

The interest on studying of fungal secondary metabolites has been arising due to their other chemical and biological proprieties (Hohn, 1997), which could allow to apply them in agriculture and in medicine.

- *Screening of plant genotypes*: Phytotoxins could be used to obtain plants resistant to disease. This approach is successful in many cases, even though not perfect (Švábová and Lebeda, 2005). A way to select resistant cultivars seems to be the use of host-specific phytotoxins. This tool cannot be used for large-scale screening, because these toxins attack plants with a specific and relatively rare genotype, however, it is useful for screening plants that have the gene that determines the host-specific sensitivity. For example, the locus of sensitivity (*asc/asc*) to AAL-toxin produced by *Alternaria alternata* f. sp. *lycopersici*, specific for certain tomato cultivars, is detected in plants belonging to the genus *Nicotiana*, although they are not affected by this pathogen (Mesbah *et al.*, 2000; Brandwagt *et al.*, 2001).
- *Development of rapid diagnostic methods*: At the beginning the method used to identify fungal plant pathogens are related to the interpretation of visual symptoms and/or the isolation, the growth and the laboratory identification of the pathogen. This method requires a lot of time and the accuracy and reliability of the results depend on the abilities of the operators. Successively, immunological methods have been applied, DNA/RNA probe technology and polymerase chain reaction (PCR) amplification of nucleic acid sequences. The advantages of these techniques are speed, accuracy and ease of use also for operators with less experience in plant pathology. In the immunological techniques the antibodies are used to recognize specific antigens present on the surface or secreted by the pathogen. The most common immunological method is the enzyme-linked immunosorbent assay (ELISA) (Clark and Adams, 1977); this method consists in cheap and simple assays able to quantify the target pathogen and detect it. In the ELISA test, the low molecular weight phytotoxin, defined antigen, bounds to a specific carrier protein are used to produce antibodies when inoculate in the animal. The primary antibodies could be linked to an enzyme to generate a secondary antibody. Thus, in the presence of antigen, both antibodies recognize it as a sandwich. The specific substance is added and the enzyme linked to the secondary antibody catalyses the reaction which determine the colour change (Fig. 2) (Zheng *et al.*, 2006; Moises and Schäferling, 2009; Rahman *et al.*, 2019). Some phytotoxins with high molecular weight are natural antigens as exopolysaccharides (EPSs), which were isolated from the culture filtrates of a *Pseudomonas syringae* pv. *actinidiae* strain, the causal agent of bacterial canker of kiwifruit. They were partially identified and used to develop specific antibodies following the ELISA assay. The antibodies were used to develop a rapid and specific method to detect *P.s.* pv. *actinidiae* EPSs, and thus the presence of bacterium in infected plant samples (Cimmino *et al.*, 2017a).

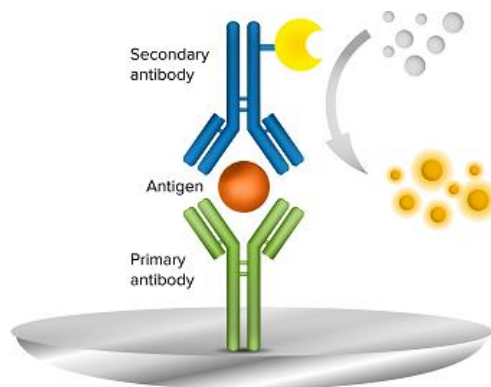


Figure 2: ELISA sandwich.

- *Formulation of bio-pesticides:* Usually in the agriculture the synthetic chemicals are used for pest control, crop protection and plant growth regulation due to their efficacy, reliability and quick knock down effect, although they have become a health hazard for humans and environment due to their toxicity and pollution. Biopesticides are potential alternatives to synthetic pesticides and they are obtained from plants, microorganisms and insects. These sources are readily available, easily biodegradable, presenting various modes of action, are less expensive and have low toxicity to humans and non-target organisms (Lengai and Muthomi, 2018; Marrone, 2019). Recently, the governments impose a deregistration of chemical pesticides and the public's concern of pesticide residues in food is increasing. This has motivated great interest in biological means of pest control (Whipps and Lumsden, 2001). Known sources of botanical pesticides are neem, pyrethrum, cotton and tobacco plants and they have already been commercialized (Dar *et al.*, 2014). Some biopesticides have been identified in the metabolites produced by fungi and bacteria belonging to species of *Trichoderma*, *Bacillus*, *Pseudomonas*, *Beauveria* and they have been commercialized as microbial pesticides (Kachhawa, 2017). These compounds are produced by microorganisms to defend themselves from the others. They present shorter environmental half-life than synthetic pesticides and are biodegradable, reducing potential environmental impact. In addition, biopesticides affect only the target pests or plant pathogens and do not show risk to non-target organisms. Most of the commonly used chemical pesticides have a single site of action, attacking one vulnerable metabolic pathway or process of the pest and these latter can develop resistance to that product. On the contrary, biopesticides typically have multiple modes of action, reducing the possibility to produce resistance by pests (Marrone, 2019).
- *Development of new drugs:* Natural products have always been played a key role in drug discovery in many fields (Keller, 2019; Newman and Cragg, 2020; Atanasov *et al.*, 2021), which include cancer and infectious diseases, cardiovascular diseases (for example, statins) and multiple sclerosis (for example, fingolimod). These metabolites own special features in

comparison with conventional synthetic molecules, which give advantages for the drug discovery process. They are characterized by scaffold diversity and structural complexity, that provide a variety of mode of action. These compounds usually have a high number of aliphatic carbons and oxygens but not many nitrogens and halogens, higher numbers of H-bond acceptors and donors and greater molecular rigidity. For example, this latter could be useful in drug discovery tackling protein–protein interactions (Atanasov *et al.*, 2021). Historically, the first drugs were obtained from natural products (Lahlou, 2007) and before the 20th century, the only medications were represented by crude and semi-pure extracts of plants, animals, microbes, and minerals. Successively, natural products have been displayed a key role in pharmacological research and about 40% of all medicines are based on natural products or their derivatives (John, 2009). A rich source of drugs is represented by fungi-derived natural products. The importance of investigating fungal secondary metabolites as sources of new medicines had been highlighted with the discovery of natural penicillins from the fungus *Penicillium* (Bérdy, 1980).

Ophiobolins, for example, are produced by phytopathogenic fungi belonging to the genus *Bipolaris* (Au *et al.*, 2000). The first member of the group that was isolated and characterized is ophiobolin A (Nozoe *et al.*, 1965), then other 25 biogenic analogues were isolated (Zhang *et al.*, 2012). These metabolites showed a cytotoxic activity against cancer cells (Ahn *et al.*, 1998). Ophiobolin A (Fig. 3) has proved to be an interesting candidate for the treatment of apoptosis-resistant cancer cells due to a unique mechanism of action (Masi *et al.*, 2019). In particular, it induces paraptosis in glioblastoma cells inhibiting BKCa ion channel activity (Bury *et al.*, 2013), giving an innovative strategy to treat this aggressive cancer. This cellular effect is also originated from pyrrolylation of primary amine groups abundant in human cells (Dasari *et al.*, 2015a), leading to lipid bilayer destabilization (Chidley *et al.*, 2016). Successively, α,β - and γ,δ -unsaturated ester analogues of polygodial and ophiobolin A were prepared; these compounds were capable of pyrrolylation of primary amines and demonstrated double-digit micromolar antiproliferative potencies in cancer cells (Dasari *et al.*, 2015b). Recently, some dimeric and trimeric species of this compound are prepared, obtaining that such dimeric compounds retain the ability to form pyrroles with primary amines. A polygodial dimer with the shortest linker length and both synthesized ophiobolin A dimers show a significant enhance of the antiproliferative activity compared with their monomeric analogues (Maslivet *et al.*, 2021).

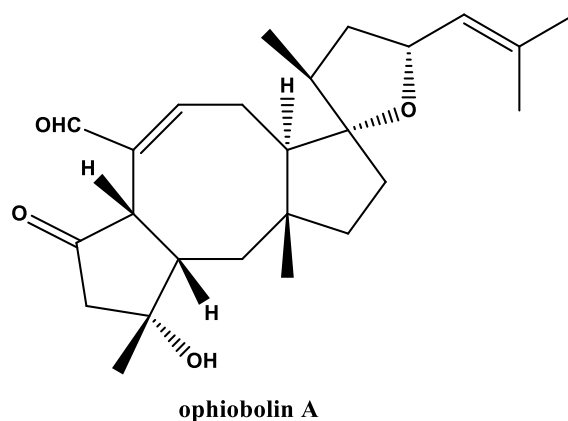


Figure 3: Structure of ophiobolin A.

1.3 Previous studied pathogenic fungi involved in forest plant disease

In the previous paragraphs, the economic and landscape implications of forest plants have been highlighted and the high potentials of secondary metabolites produced by pathogenic fungi has been discussed. In addition, forests are an immense reservoir of fungal diversity and thus of secondary metabolites with novel structures. In recent years, many studies have been performed to isolate metabolites produced by fungi pathogens for forest plants and to understand their role in the pathogenesis processes (Masi *et al.*, 2018). Prof. Evidente's group has been focusing on this field, studying the pathogenic fungi involved in various forest plant diseases, as *Diplodia africana*, pathogen of *Phoenicean juniper*, and *Diplodia cupressi*, pathogen of *Cupressus sempervirens* L..

1.3.1 *Diplodia africana*

Diplodia africana was originally identified as a pathogenic fungus associated with disease symptoms on prunus trees in South Africa (Damm *et al.*, 2007) and then it has also been reported as the causal agent of a branch dieback of *Phoenicean juniper* trees (Fig. 4) in a natural area on Caprera Island (Linaldeddu *et al.*, 2011).



Figure 4: Twig and branch dieback of *Phoenicean juniper* tree affected by *D. africana*.

From the organic extract of its liquid cultures, two new dihydrofuropyran-2-ones, named afritoxinones A and B, have been isolated and characterized, together with six known metabolites identified as oxysporone, sphaeropsidin A, episphaeropsidone, *R*-(-)-mellein, (3*R*,4*R*)-4-hydroxymellein and (3*R*,4*S*)-4-hydroxymellein (Fig. 5). The structures of new metabolites were determined, by spectroscopic and optical methods, as (3*aS**,6*R**,7*aS*)-6-methoxy-3*a*,7*a*-dihydro-3*H*,6*H*-furo[2,3-*b*]pyran-2-one and (3*aR**,6*R**, 7*aS*)-6-methoxy-3*a*,7*a*-dihydro-3*H*,6*H*-furo[2,3-*b*]pyran-2-one, respectively (Evidente *et al.*, 2012). The phytotoxicity of afritoxinones A and B and oxysporone were evaluated on host (*Phoenicean juniper*) and non-host plants (*Lycopersicon esculentum*, *Quercus ilex* L. and *Q. suber* L.) by cutting and leaf puncture assays and oxysporone showed the most toxic activity (Evidente *et al.*, 2012).

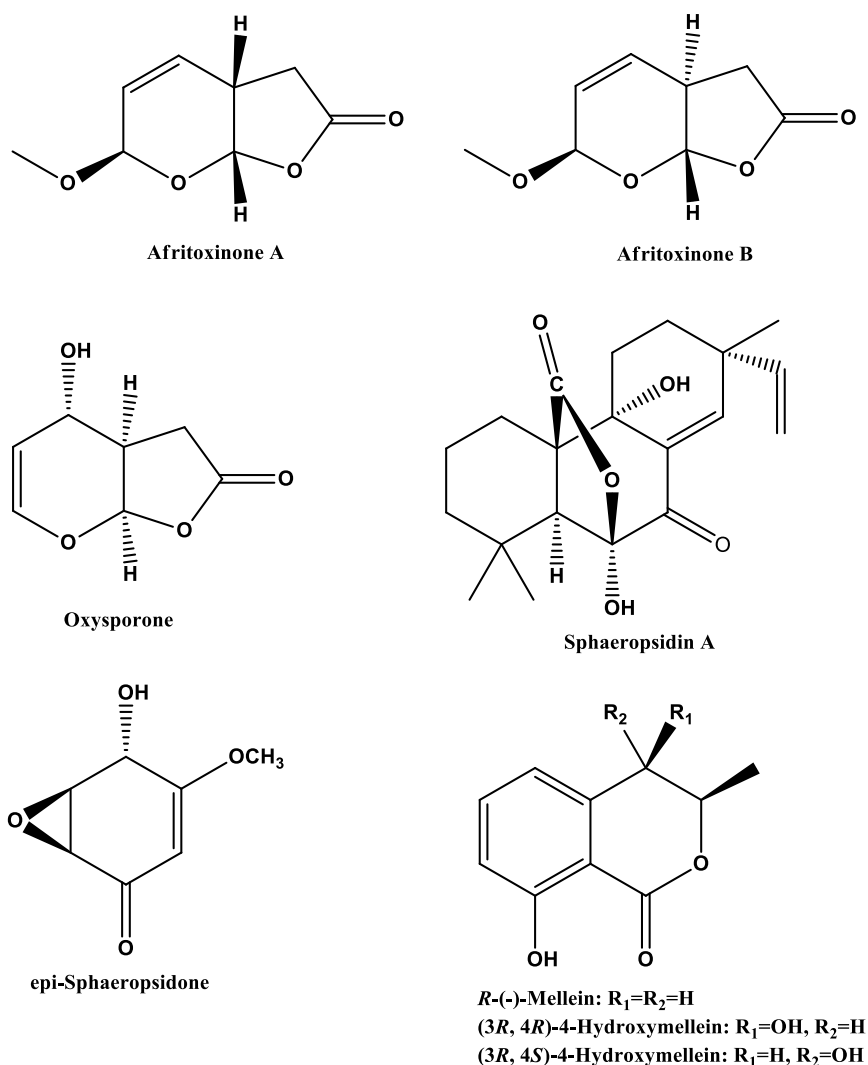


Figure 5: Phytotoxins isolated from *D. africana*.

The absolute configuration (AC) of oxysporone has been assigned by computational analysis of its optical rotatory dispersion (ORD), electronic circular dichroism (ECD), and vibrational circular dichroism (VCD) spectra. It has been found a good agreement between experimental and calculated ORD, ECD and VCD spectra of oxysporone also, taking into account the solvent effects. Thus, the combination of all three chiroptical methods allowed to assign the AC of (+)-oxysporone as (4*S*,5*R*,6*R*) (Mazzeo *et al.*, 2013).

Successively, structure-activity relationship (SAR) studies have been performed synthesizing eight oxysporone derivatives. All compounds have been tested in comparison to the parent compound on non-host plants (*Quercus suber* L., *Q. ilex* L. and *Vitis vinifera* L.) and against four plant pathogens (*Athelia rolfsii*, *Diplodia corticola*, *Phytophthora cinnamomi* and *P. plurivora*). These studies have been showed that the dihydrofuropyranone carbon skeleton and both the double bond and the hydroxy group of dihydropyran ring are essential features for the toxicity. Furthermore, the corresponding 4-*O*-bromobenzoyl ester of oxysporone has been showed a good antifungal activity towards three of the four fungi tested (Andolfi *et al.*, 2014a) (Fig. 6).

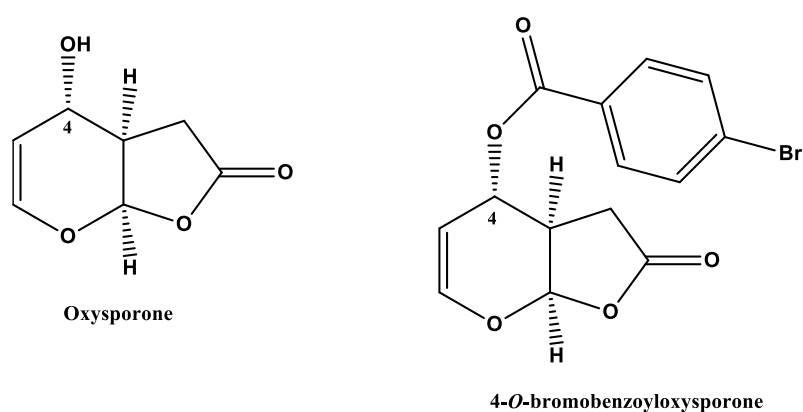


Figure 6: Structure of oxysporone and its 4-*O*-bromobenzoyl derivative.

1.3.2 *Diplodia cupressi*

Diplodia cupressi, previously recognized as *Sphaeropsis sapinea* f. sp. *cupressi*, was identified as the causal agent of canker diseases of Italian cypress (*Cupressus sempervirens* L.) (Alves *et al.*, 2006) (Fig. 7).



Figure 7: Canker symptoms induced on *Cupressus sempervirens* L. affected by *D. cupressi*.

The main metabolites, produced *in vitro* by this fungus, was a pimarane diterpenoid named sphaeropsidin A (Fig. 7). This metabolite showed phytotoxic activity on three species of cypress (*Cupressus sempervirens*, *C. macrocarpa* and *C. arizonica*) and antimicrobial activity when tested against *Seiridium cardinale* and *S. cupressi* (Evidente *et al.*, 1996). Then, from the same fungus other two pimarane diterpenes, the sphaeropsidin B and the sphaeropsidin C (Fig. 7), were isolated and they were assayed against *C. macrocarpa*, *C. sempervirens*, *C. arizonica*, *Quercus cerris*, *Q. ilex*, *Q. robur* and *Lycopersicon esculentum* showing phytotoxicity on host and non-host plants (Evidente *et al.*, 1997c). Successively, other three pimarane diterpenoids, named sphaeropsidins D, E and F, were isolated from the same fungus (Fig. 8). Sphaeropsidin D is the 11-hydroxylated sphaeropsidin A, sphaeropsidin E is the 7a,11b,14a-trihydroxypimara-8(9)15-diene and sphaeropsidin F is the 1,6,7,9-tetrahydroxypimara- 8(14),15-diene. When tested on cypress species, sphaeropsidin D caused leaf browning and necrosis on *C. macrocarpa* while sphaeropsidin F induced yellowing of the apical leaves of *C. sempervirens* (Evidente *et al.*, 2002; Evidente *et al.*, 2003).

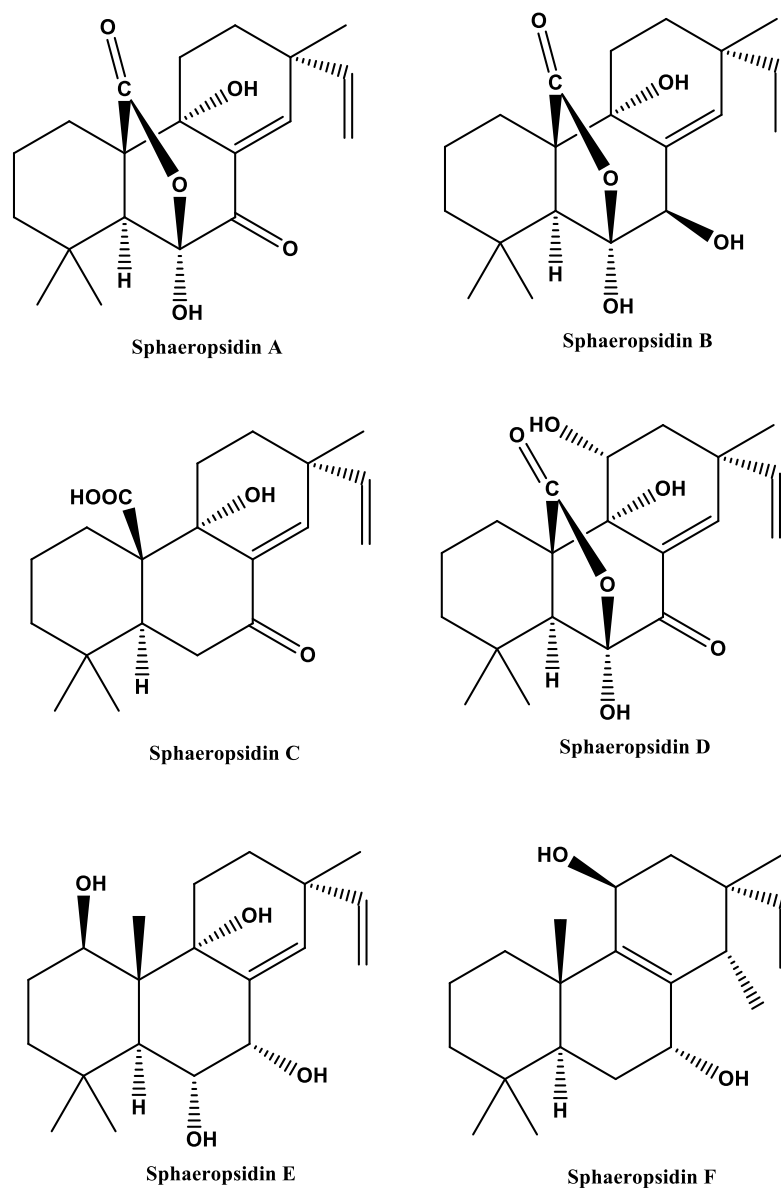


Figure 8: Sphaeropsidins isolated from *D. cupressi*.

A SAR study was carried out assaying the phytotoxic activity of sphaeropsidins A-F and eight derivatives. The metabolites showed to be non-selective toxins, causing symptoms on host and non-host plants. In addition, a modification of the ring A strongly reduced the biological activity (Sparapano *et al.*, 2004).

Sphaeropsidins A-C, together with 14 derivatives, were tested for antibacterial activity against *Xanthomonas oryzae oryzae*, *Pseudomonas fuscovaginae*, and *Burkholderia glumae*, the causal agents of severe bacterial rice diseases, obtaining a strong and specific activity of sphaeropsidin A against *Xanthomonas oryzae oryzae* (Evidente *et al.*, 2011c). Sphaeropsidin A showed a larvicidal activities against *Aedes aegypti* L., the major vector of the arboviruses responsible for dengue fever, yellow fever and Zika disease, while sphaeropsidin B was active as biting deterrent (Cimmino *et al.*, 2013). Recently, sphaeropsidin A has been tested, together with other fungal metabolites, for their reducing activity of development of several major rust fungi belonging from the genera *Puccinia* and *Uromyces*. It has been able to hamper strongly the germination of *U. pisi* at concentrations higher than 10^{-3} M and to inhibit moderately the germination of *U. viciae-fabae* at any concentration tested (Barilli *et al.*, 2016).

Sphaeropsidins A, B and C and 10 their semisynthetic derivatives were tested by *in vitro* anticancer assays, resulting that sphaeropsidin A, 6-*O*-acetylsphaeropsidin A and 15,16-dihydrosphaeropsidin A presented a 50% growth-inhibitory concentration in the low micromolar range for all cell lines analysed as A549 (NSCLC), OE21 (esophageal), Hs683 (glioma), U373 (glioma), SKMEL28 (melanoma) and B16F10 (melanoma) (Lallemand *et al.*, 2012). In particular, sphaeropsidin A proved to be an interesting compound because it was active as cisplatin and etoposide and more active than carboplatin and temozolomide, which are used to treat a large variety of human cancers. Then, the type of *in vitro* growth inhibition of sphaeropsidin A was investigated using quantitative videomicroscopy obtaining cytotoxic effects on mouse melanoma B16F10 cells and on human SKMEL-28 melanoma cells. This metabolite was active against drug-resistant cancer cell lines, including melanoma and renal cancer cells. Successively, mechanistic studies in melanoma and other multidrug-resistant *in vitro* cancer models demonstrated that sphaeropsidin A can overcome apoptosis via cell volume dysregulation and multidrug resistance by inducing a marked and rapid cellular shrinkage related to the loss of intracellular Cl^- and the decreased of HCO_3^- concentration in the culture supernatant (Mathieu *et al.*, 2015). Recently, a study has been performed regarding *in vitro* combination of sphaeropsidin A with cytotoxic chemotherapeutics. A surface response model has been built using four melanoma cell lines to determine the optimal *in vitro* combinations of this metabolite with two drugs, cisplatin and temozolomide. A combination of 4 μM of sphaeropsidin A with 75 μM cisplatin concomitantly for 72 h has improved its cytotoxic effect on melanoma cells in a synergistic manner and an optimal *in vitro* treatment schedule has been obtained for temozolomide (Ingles *et al.*, 2017). This study has highlighted that the combination of sphaeropsidin A with chemotherapeutic agents could improve the therapeutic benefits of conventional chemotherapies against advanced melanomas (Ingles *et al.*, 2017).

Considering the high potentially applications of this metabolites in many fields, its absolute configuration was recently confirmed by X-ray analysis of its 6-*O-p*-bromobenzoyl derivative (Masi *et al.*, 2016a).

The same fungus had produced two phytotoxic dimedone methyl ethers, named sphaeropsidone and *epi*-sphaeropsidone, and their chlorinated analogues, named chlorosphaeropsidone and *epi*-chlorosphaeropsidone (Fig. 9) (Evidente *et al.*, 1998; Evidente *et al.*, 2000). Sphaeropsidone and *epi*-sphaeropsidone are disubstituted 7-oxabicyclo[4.1.0]hept-3-en-2-ones epimers at C-5.

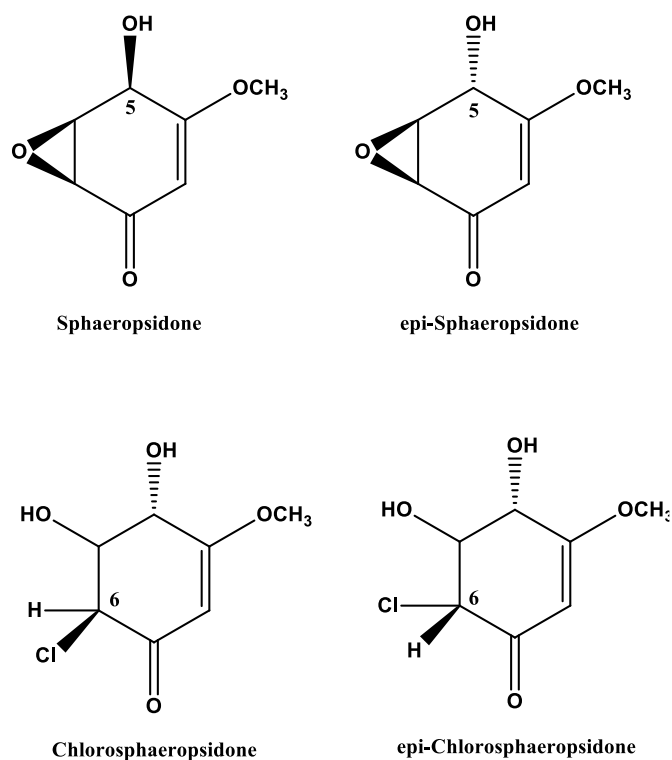


Figure 9: Phytotoxins isolated from *D. cupressi*.

Both compounds showed phytotoxic activity on host (*Cupressus sempervirens* L.) and non-host plants (*C. macrocarpa*, *C. arizonica* and *Lycopersicon esculentum*). These metabolites showed an antifungal activity against three species of *Seiridium*, *Botrytis cinerea* and *Phomopsis amygdali* and they enhanced the growth of *Verticillium dahliae* (Evidente *et al.*, 1998). The absolute stereochemistry at the three chiral centres of sphaeropsidone as 1*S*,5*R*,6*S* was determined through X-ray, ORD and ECD studies (Mennucci *et al.*, 2007; Tuzi *et al.*, 2012). Chlorosphaeropsidone and *epi*-chlorosphaeropsidone were two 6-chloro-4,5-dihydroxy-3-methoxycyclohex-2-en-1-one epimers at C-6 (Fig. 9). Their relative and AC were assigned by NMR, X-ray analysis and CD. When they were

assayed on host plant, both metabolites they did not show phytotoxic activity. This inactivity could be due to the opening of the epoxy ring compared with sphaeropsidones (Evidente *et al.*, 2000). A SAR study was carried out assaying the phytotoxic and antifungal activities of sphaeropsidone, *epi*-sphaeropsidone and their eight derivatives against non-host plants and five pathogenic oomycetes species. The structural features important for biological activity resulted to be the hydroxy group at C-5, the absolute C-5 configuration, the epoxy group, and the C-2 carbonyl group; while the conversion of sphaeropsidone into the corresponding 1,4-dione derivative led to a compound with a greater antifungal activity (Evidente *et al.*, 2011d).

Recently, sphaeropsidone and *epi*-sphaeropsidone were also tested for their stimulating and/or inhibitory activity of the seed germination and the radical growth of broomrapes species namely *Orobanche crenata*, *Orobanche cumana*, *Orobanche minor* and *Phelipanche ramosa*, root parasitic plants causing heavy yield losses on important crops. *Epi*-sphaeropsidone induced significant germination on *P. ramosa* and both compounds induced a strong and significant reduction on broomrape radicle length (Cimmino *et al.*, 2014). Thus, their ability to develop the haustorium, a parasitic plant organ that invades the host to absorb its water and nutrients, was investigated obtaining that sphaeropsidone and *epi*-sphaeropsidone induced haustorium development in radicles of the parasitic weeds *Striga hermonthica*, *O. crenata*, and *O. cumana* (Fernández-Aparicio *et al.*, 2016). In addition, a SAR study was carried out by testing the haustorium-inducing activity of these metabolites, using seven already known and four new hemisynthetic derivatives of sphaeropsidones. The haustorium-inducing activity might be correlated to the stereochemistry at C-5 and to the possibility to convert the natural sphaeropsidone and natural and hemisynthetic derivatives in the corresponding 3-methoxyquinone (Fernández-Aparicio *et al.*, 2016).

1.4 Pathogenic fungi of forest plant diseases, studied in this thesis

1.4.1 Fungi involved in the decline of Iranian oak trees (*Quercus brantii*)

Oak trees are affected by many pathogenic fungi which induce serious diseases such as canker, dieback and decline. In previous years, many fungi belonging to *Diplodia* species were identified as pathogens of oak trees and their phytotoxic metabolites were characterized to understand their role in the plant-pathogen interaction (Masi *et al.*, 2018).

Recent studies have been morphologically and molecularly identified many fungi associated to the decline of Persian oak trees (Alidadi *et al.*, 2019; Yousefshahi *et al.*, 2020) and in particular four species, *Biscogniauxia mediterranea*, *Didymella glomerata*, *Neoscytalidium dimidiatum* and *Obolarina persica*, were pathogens on the Persian oak seedlings in the greenhouse conditions (Alidadi *et al.*, 2019).

1.4.1.1 *Fimetariella rabenhorstii*

Fimetariella rabenhorstii (Niessl) N. Lundq. (Ascomycota, Sordariales, Lasiosphaeriaceae) was identified as endophytic fungus associated with *Aquilaria sinensis*, the main plant species used in China for the production of agarwood (Sanchez *et al.*, 2008; Wang *et al.*, 2009). This plant is the most precious resinous wood used as incenses, perfumes and traditional medicines in the world market. Sesquiterpenoids and phenylethyl chromone derivatives are the fragrant chemical constituents of agarwood (Jain and Bhattacharyya, 1959; Yang and Chen, 1986; Ishihara *et al.*, 1991; Konishi *et al.*, 1991; Konishi *et al.*, 2002). Agarwood may form in the cut, burned or withered and dying tissues, which are generally rich in endophytic fungi often associated with fungal diseases (Qi *et al.*, 2005; Phatik *et al.*, 2005). This led to believe that the fragrant chemical constituents of agarwood could be produced as phytoalexins by the host plant and by endophytic fungi during the agarwood-formation processes (Verma *et al.*, 2009).

A new sesquiterpenoid alcohol, named frabenol, was isolated from the organic extract of the liquid cultures of *Fimetariella rabenhorstii* (Tao *et al.*, 2011) (Fig. 10).

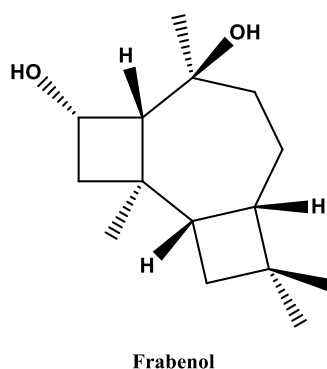


Figure 10: Structure of frabenol.

Its structure was obtained by spectroscopic methods (HRESIMS and 1D and 2D NMR) and its relative configuration was obtained from NOESY correlations. This metabolite had a carbon skeleton very close to koraiol, isolated from *Pinus koraiensis* (Khan *et al.*, 1979), and 5,8-cyclocaryophyllan-4-ol, a constituent of *Cangerana* oil (Weyerstahl *et al.*, 1996). The caryophyllene related compounds were known to be constituents of agarwood (Bhuiyan *et al.*, 2009; Okudera and Ito, 2009). Thus, the isolation of frabenol from *F. rabenhorstii* supported the theory that endophytic fungi of agarwood-producing plants could also contribute to the production of fragrant chemicals (Tao *et al.*, 2011).

Recently, *F. rabenhorstii* has been detected for the first time as the causal agent of decline and wood necrosis symptoms of oak trees (*Quercus brantii*) in Zagros Forest, in the west of Iran (Fig. 11).



Figure 11: a) *Quercus brantii* affected by *F. rabenhorstii*, b) necrosis in trunk section.

1.4.1.2 *Stilbocrea macrostoma*

Stilbocrea macrostoma was isolated from 12 different woody plants in New Zealand (<https://nt.ars-grin.gov/fungaldatabases>) (Gadgil, 2005) and from an unknown host plant in Sri Lanka (Voglmayr and Jaklitsch, 2019).

Recently, *S. macrostoma* has been isolated from branches of oak trees (*Quercus brantii*) in Zagros Forest (Paveh, Iran), showing wood necrosis (Fig. 12).



Figure 12: Wood necrosis of *Q. brantii* induced by *S. macrostoma*.

1.4.2 Fungi involved in ash decline and lentisk canker in Europe

Since 1995, serious dieback of European ash was observed in Poland, then diffused in all Europe, and the disease known as bark necrosis was detected at the shoot apices of 1–5-year-old plants. Eight species of fungi were identified and tested for their pathogenicity: *Cladosporium cladosporioides*, *Cytospora ambiens*, *Discula* sp., *Fusarium lateritium*, *Phoma* sp., *Phomopsis scobina*, *P. controversa* and *Diplodia mutila* (Przybył, 2002). Then, a specific pathogen, *Chalara fraxinea* (Kowalski, 2006), was associated to the ash tree mortality in Poland and in neighbouring countries, afterwards spread across all Europe (Pautasso *et al.*, 2013). This fungus caused various disease symptoms, from necrotic leaf spots to bark cankers associated with xylem necroses and wilting, and eventually the tree death (Pautasso *et al.*, 2013). Successively, another pathogen, named *Hymenoscyphus pseudoalbidus*, was identified as causal agent of ash dieback over entire countries, all Europe, Russia, Georgia, Armenia, Azerbaijan and Iran (Queloz *et al.*, 2011; Pautasso *et al.*, 2013). This fungus was able to penetrate directly into host cells and to cause brown to blackish necrotic lesions on ash leaflets and rachises (Cleary *et al.*, 2013), followed by wilting and leaf shedding (Bakys *et al.*, 2009; Cleary *et al.*, 2014; Gross *et al.*, 2014). These symptoms suggested that phytotoxic metabolites of the fungus are involved in the host-pathogen interaction and thus the metabolites produced by *H. pseudoalbidus* were studied. The first metabolites isolated from the liquid culture of this fungus were two viridin-related B-norsteroids, B-norviridiol lactone and B-norviridin enol, and a B-norsteroidal compound, 1 β -hydroxy-2 α -hydro-asterogynin A (Fig. 13).

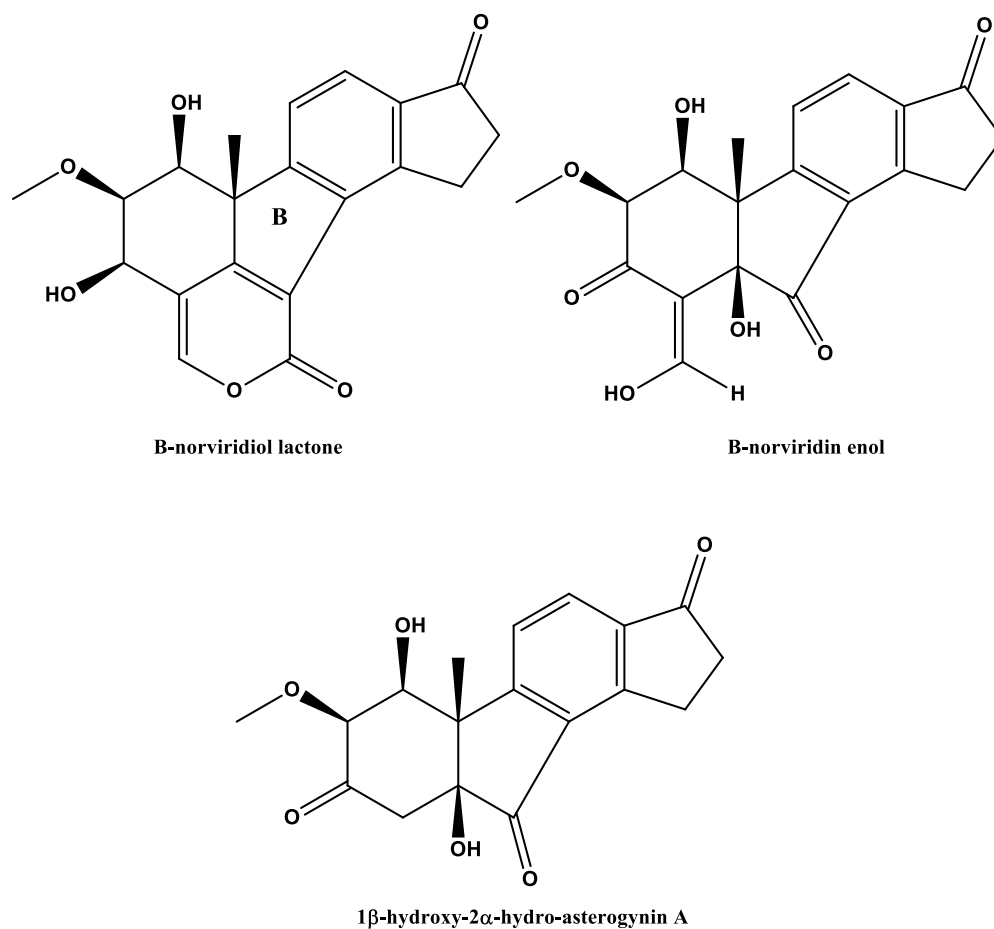


Figure 13: Structures of three B-norsteroids.

The 1β-hydroxy-2α-hydro-asterogynin A was a derivative of asterogynin A, from which could be formed through a β-elimination of water. The three viridin related B-norsteroids was proposed to be formed from either viridin or viridiol via a number of transformations. Among them, the ring contraction was proposed to be obtained by a benzylic acid rearrangement (Andersson *et al.*, 2012). Successively, three furanosteroids (1-deoxy-2-demethylviridiol, 1-deoxyviriol and 3-dihydrovirone) together with viridiol and demethoxyviridiol were isolated from the same fungus (Fig. 14), but they did not show phytotoxic effects on 2-week-old and 1-year-old ash seedlings (Andersson *et al.*, 2013a).

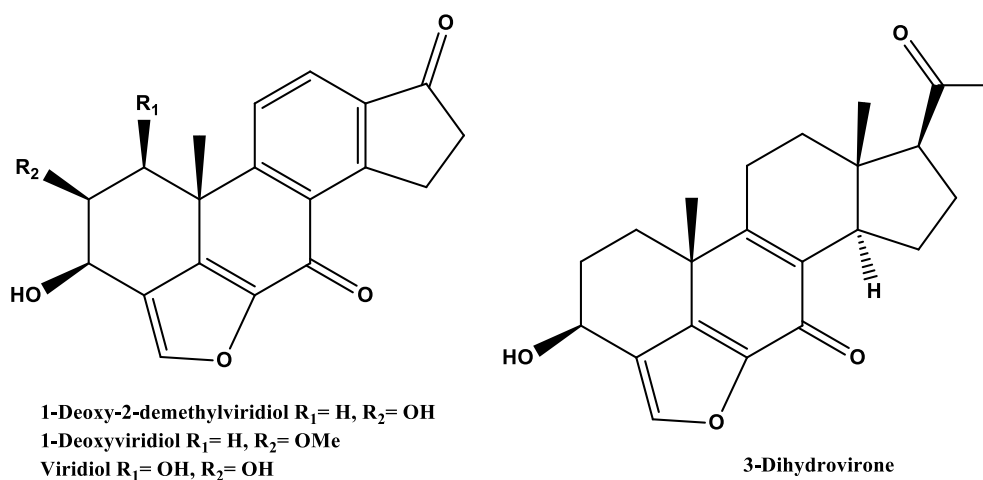


Figure 14: Structures of furanosteroids.

Even though viridiol was the most abundant metabolite produced by this fungus, it was demonstrated that there were no correlations between viridiol concentration and phytotoxicity of culture extracts in leaf segment tests or in the germination test (Junker *et al.*, 2014). The result suggested that further studies were needed to detect the phytotoxins. A 3-decalinoyltetramic acid, named hymenosetin (Fig. 15), was isolated from crude extracts of *H. pseudoalbidus* when it was grown in submerged cultures. This metabolite was inactive in the phytotoxic assays against *F. excelsior* and *A. stolonifera*, but exhibited a broad spectrum of antibacterial and antifungal activities, against various organisms tested, and cytotoxic effects against mouse fibroblast cell line L929 (Halecker *et al.*, 2014).

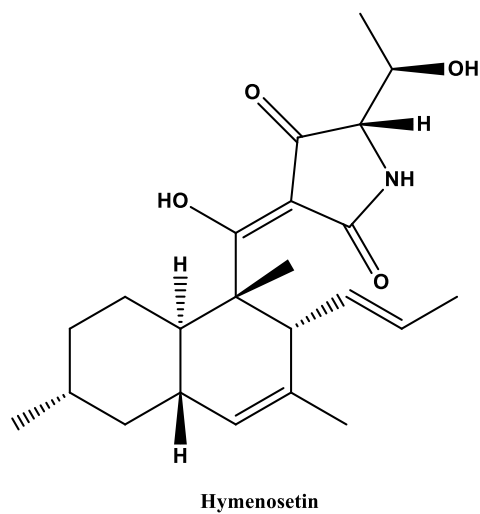


Figure 15: Structure of hymenosetin.

Then, four strains of *H. pseudoalbidus* (C494, C498, C505, and C506) were undergone to a GC-MS analyses to investigate their profile of volatile secondary metabolites. They proved to emit five compounds, identified as a methyl ester and four lactones as below reported in Fig. 16.

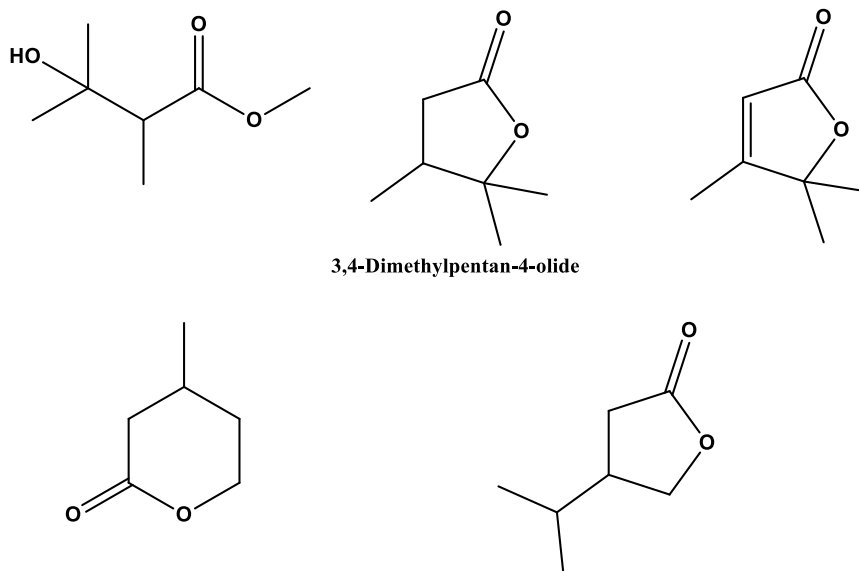


Figure 16: Structures of volatiles emitted by *H. pseudoalbidus*.

3,4-Dimethylpentan-4-olide caused necrotic lesions on the *F. excelsior* seeds and inhibition of the germination that were not observed in the solvent control and with the other volatiles (Citron *et al.*, 2014).

Lentisk dieback has been largely spread across Tunisian forests, but very few studies have been performed to identify the parasitic factors involved in this phenomenon. Recently, two *Botryosphaeriaceae* species, *Diplodia seriata* and *D. africana* have been isolated and identified from symptomatic branches of *Pistacia lentiscus* collected in the Rimel forest (Northern Tunisia). The results obtained from pathogenicity tests have been confirmed the virulence of the *Diplodia* species (Hlaïem *et al.*, 2020).

1.4.2.1 *Hymenoscyphus fraxineus*

The main cause of the common disease, known as “ash dieback”, is an alien and invasive pathogen *Hymenoscyphus fraxineus* (T. Kowalski) Baral, Queloz, and Hosoya (Fig. 17) (Baral *et al.*, 2014). *H. fraxineus* infects with a hemibiotroph interaction, based on an initial intracellular infection phase and then a necrotrophic stage (Mansfield *et al.*, 2019).



Figure 17: *F. excelsior* affected by *H. fraxineus*: a) shoot desiccation; b) wood lesion.

This fungus induces the same symptoms observed from *Diplodia* species infections, characterized by V-shaped necrotic sector visible in cross section (Fig. 18).



Figure 18: V-shaped necrosis in trunk section.

Recently, two new steroid-like glycosides, named hyfraxins A and B, have been isolated and chemical and biological characterized from the mycelial extract of *H. fraxineus* (Fig. 19) (Surup *et al.*, 2018).

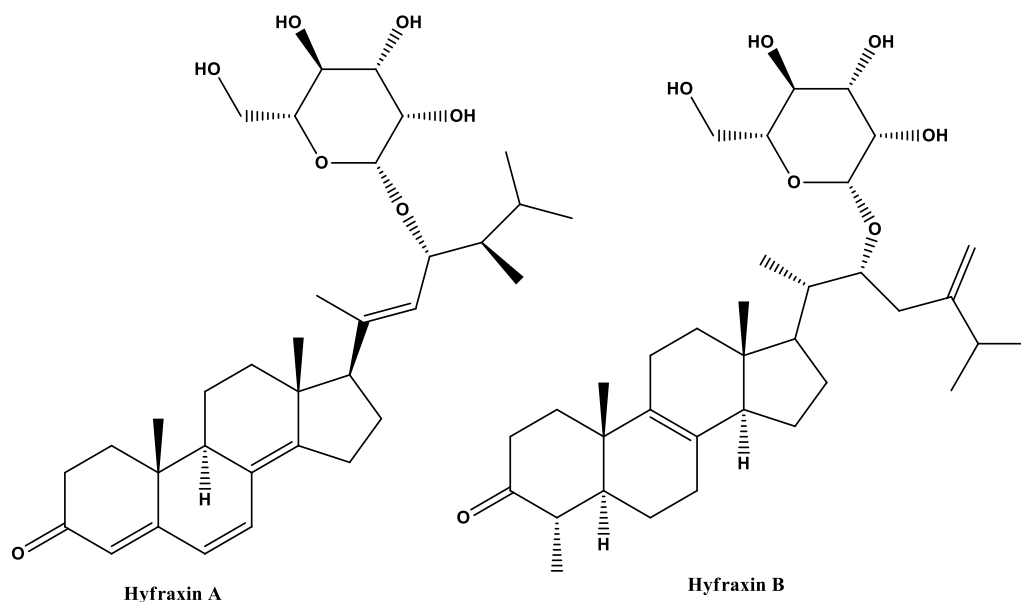


Figure 19: Structures of hyfraxins A and B.

Their structures have been elucidated by HR-ESIMS and NMR data. The relative stereochemistry has been assigned by ROESY correlations in conjunction with H,H and C,H coupling constants, while the absolute configuration have been determined based on ROESY correlations between the aglycons and the sugar moieties. The GC/MS analysis of the trimethylsilylated derivatives has been allowed to identify the sugars as D-mannose in both cases (Surup *et al.*, 2018).

The metabolites have been tested for their cytotoxic and antimicrobial activities. They have showed moderate to weak activity against the Gram-positive bacterium *Bacillus subtilis* and have been cytotoxic against the mouse fibroblast cell line L929 (Surup *et al.*, 2018).

1.4.2.2 *Diplodia olivarum*

Diplodia olivarum was detected as an aggressive pathogen on different host plants in Italy. Firstly, this fungus was isolated from different olive groves in southern Italy associated with their rotting drupes and it was described as a new species (Lazzizzera *et al.*, 2008). Then, *D. olivarum* was identified as a canker agent of carob tree inducing necrosis on trunk and branches, branch dieback and foliage reddening (Granata *et al.*, 2011). Recently, it has been associated to the canker of lentisk

(Linaldeddu *et al.*, 2016a) and wild olive (Manca *et al.*, 2020). The induced symptoms include sunken cankers with characteristic wedge-shaped wood necrosis on branches and stems, in addition foliar symptoms have also been observed on lentisk shoots (Fig. 20).



Figure 20: Foliar symptoms on *P. lentiscus* shoots infected by *D. olivarum*.

1.4.3 Fungi involved in the diseases of maritime pine in Africa and mahogany in Brazil

Maritime pine (*Pinus pinaster* Ait.) is a widespread tree species in the Western Mediterranean areas (Gea-Izquierdo *et al.*, 2019). Since 1800s, the maritime pine was largely diffused for afforestation, in part for its valuable resin production (Rodríguez-García *et al.*, 2016). It is found in sub-Mediterranean areas within the Mediterranean Region, forming dry-coniferous monospecific or mixed forests. In recent years symptoms of decline, including canopy defoliation and low regeneration, have been showed (Prieto-Recio *et al.*, 2015; Moreno-Fernández *et al.*, 2018).

In Tunisia, coniferous forests represent about 55% of the total afforested area, in which the most abundant species are Aleppo pine (*Pinus halepensis* Mill.), widespread in the central and southern regions, and Maritime pine (*Pinus pinaster* Ait.), diffused in the north. Over the past century, a progressive degradation of the Tunisian conifer forests was induced by human actions, as illegal clearing, logging, ploughing and handling of forest products (Mansoura *et al.*, 2001). Furthermore, phytopathogenic fungi associated with the bark beetles, *Tomicus piniperda* and *Orthotomicus erosus*, were reported in various pine forests of Tunisia (Ben Jamaa *et al.*, 2007).

Mahogany wood is very precious and largely used in wood industry due to its important technological characteristics. It is obtained from different species of the genus *Swietenia* and *Khaya*

(Falesi and Baena, 1999; Pinheiro *et al.*, 2001). *Khaya senegalensis* A. Juss. (Meliaceae), known as African mahogany, is a native species of tropical Africa and Madagascar. Since 1976 it was planted in Brazil (Falesi and Baena, 1999) because the native Brazilian mahogany, *Swietenia macrophylla* King in Hook, suffered a strong decrease induced by *Hypsipyla grandella* Zellar, a pest insect known as the mahogany shoot borer (Pinheiro *et al.*, 2001). Due to this problem, the exportation and marketing of native Brazilian mahogany wood was prohibited and since 2000 the commercial use of African mahogany has been increasing (Gasparotto *et al.*, 2001; Couto *et al.*, 2004).

Recently, a foliar disease of African mahogany has been detected and the study of the causal agents is still in progress. *Sclerotium coffeicola* has been the first pathogenic fungus associated to leaf spot of mahogany. It has been isolated in the commercial plantation of *Khaya senegalensis* with three years of age in Huimanguillo, Tabasco, Mexico (Perez-Vera *et al.*, 2017), but the involved phytotoxins are not reported yet.

1.4.3.1 *Diplodia sapinea*

In autumn 2006, symptoms of severe chlorosis, branch dieback, canker and shoot blight were observed in *Pinus pinaster* trees (Fig. 21), located in northwest Tunisia in the region of Djebel Khroufa near Tabarka. The associated pathogenic fungus was identified as morphotype A of *Diplodia pinea* (Desm.) J. Kickx f. (syn. *Sphaeropsis sapinea* [Fr.:Fr] Dyko & Sutton) described by Palmer *et al.* (1987) (Linaldeddu *et al.*, 2008).

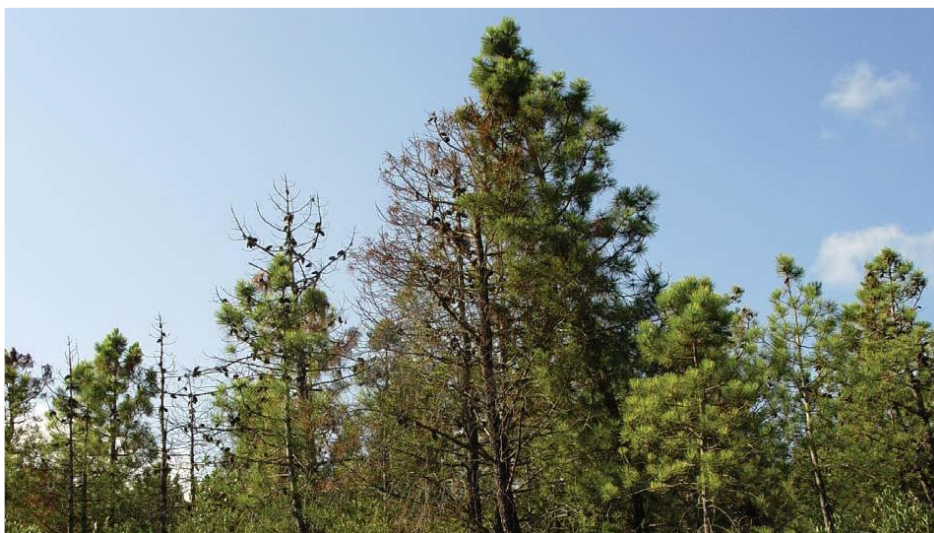


Figure 21: Disease symptoms of *P. pinaster* affected by *D. sapinea*.

Diplodia sapinea (Fr.) Fuckel is one of the most important and widespread pathogens of conifer and the typical observed symptoms are tip blight, resinous cankers on the main stem and branches, dieback and a blue stain in the sapwood. Historically, a hard attacks of *D. sapinea* in pine plantations happened as a consequence of environmental stresses such as hail and drought in the

southern hemisphere; this infection determined a large-scale dieback and tree mortality (Phillips *et al.*, 2013). This fungus was detected on exotic and native pine species in both Mediterranean and temperate climate regions (Fabre *et al.*, 2011). Recent studies have reported an ongoing expansion and affirmation of this pathogen in the low temperature habitats of northern Europe, as Estonia, Sweden and Finland, and in the southern coast of the Mediterranean Sea, as Tunisia and Algeria (Linaldeddu *et al.*, 2008; Müller *et al.*, 2019). However, many aspects of phytotoxicity still remain unknown, as its virulence mediated by phytotoxin production. Despite the high pathogenicity of *D. sapinea* and its ecological impact on different habits is well known, few studies were performed to understand the virulence factors involved in the pathogenesis. Until now, few phytotoxins were isolated and characterized from this pathogen (Masi *et al.*, 2018).

Four nonenolides, named diplodialides A-D, were initially isolated from *D. pinea* culture filtrates (Fig. 22) and their structures were determined by spectroscopic and chemical studies (Ishida and Wada, 1975; Wada and Ishida; 1979).

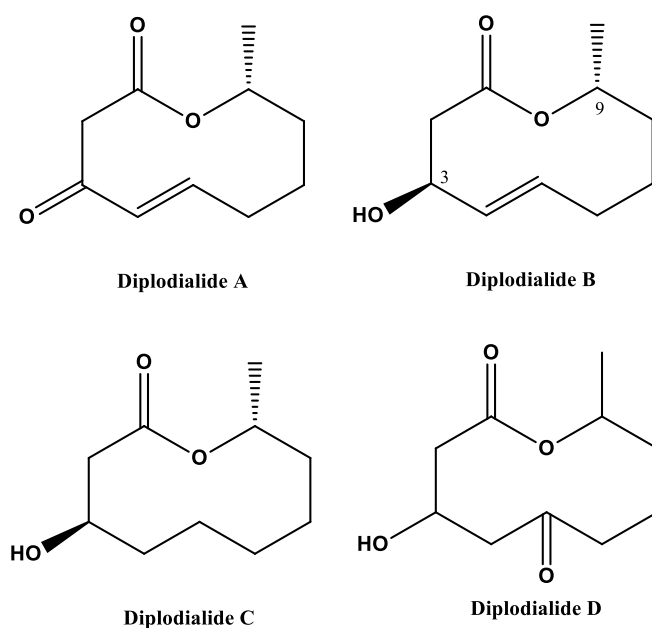


Figure 22: Structures of diplodialides A-D.

The absolute configuration (AC) *R* at C-9 of diplodialides A-C was determined by chemical degradations of the decanolid ring of diplodialide B to (-)-hexane-1,5-diol and comparing optical properties of the product with those reported in literature (Ishida and Wada, 1975). Then the ozonolysis of the acetate of diplodialide B, followed by oxidation and hydrolysis, let to determine the AC *3S* and *3R* at C-3 of diplodialides B and C, respectively (Wada and Ishida; 1979). Diplodialide A

imparting phytotoxic and antifungal activities were the pyridione, the oxiran ring and the carbonyl group of the side chain (Evidente *et al.*, 2006).

When *D. sapinea* was isolated in Sardinia (Italy) from symptomatic branches of declining Monterey pine (*Pinus radiata*), three metabolites, identified as *R*-(-)-mellein, (3*R*,4*R*)-4-hydroxymellein and (3*R*,4*S*)-4-hydroxymellein, were isolated for the first time from this fungus (Fig. 25). They were assayed for phytotoxic activity on host and non-host plants and antifungal activity and a significant activity was showed for *R*-(-)-mellein, while only a synergic activity was observed for the other two 3,4-dihydroisocoumarins in both tests (Cabras *et al.*, 2006).

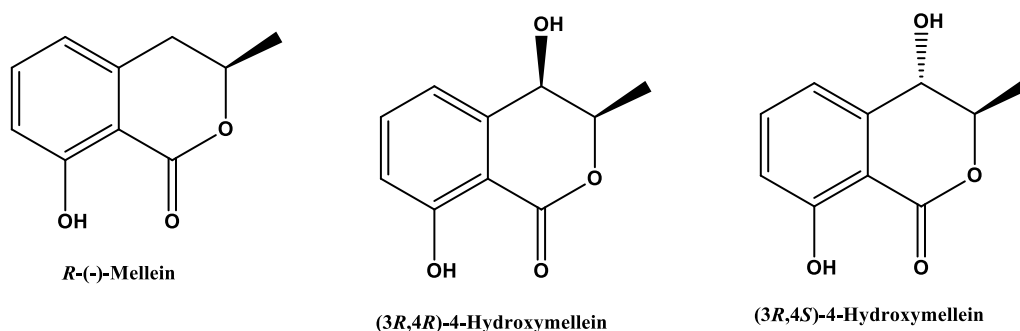


Figure 25: Structures of three dihydroisocoumarins

1.4.3.2 *Alternaria argyroxiphii*

In Brazil, the African mahogany was found to be affected by many pathogens. The leaf spot of African mahogany was a disease observed for the first time in Minas Gerais State, Brazil on October 2012 and few years ago, the pathogen *Alternaria argyroxiphii* E.G. Simmons & Aragaki (Simmons, 2007; Woudenberg *et al.*, 2013) has been associated to this disease. Recent phylogenic analyses and phytotoxic assays, carried out to fulfil Koch's postulates, have been identified *A. argyroxiphii* as a causal agent of leaf spot of *Khaya senegalensis* (Fig. 26) (Teixeira *et al.*, 2017).



Figure 26: Leaf spot symptoms caused by *A. argyroxiphii* on *K. senegalensis*.

Alternaria fungi are cosmopolitan fungi extensively distributed in nature and they are present as plant pathogens, weak facultative parasites, saprophytes and endophytes (Thomma, 2003). These fungi are well-known producers of metabolites toxic to plants and animals, which are defined as phytotoxins and mycotoxins, respectively (Lou *et al.*, 2013; Pontes *et al.*, 2020). Phytotoxins produced by *Alternaria* species belong to different classes of natural compounds and exhibit a variety of biological activities, such as phytotoxic, cytotoxic, and antimicrobial activities (Brase *et al.*, 2009; Tsuge *et al.*, 2013; Cimmino *et al.*, 2015).

2 OBJECTIVES

The aim of the present thesis has been the isolation and the chemical and biological characterization of phytotoxins produced by fungal pathogens of forest plants, in order to understand their role in the pathogenesis process. In particular, this thesis has been focused on the chemical and biological elucidation of metabolites produced by two fungi involved in the dieback of Iranian oak tree, *Fimetariella rabenhorstii* and *Stilbocrea macrostoma*, by a fungus causing the ash decline in Italy, *Hymenoscyphus fraxineus*, by a fungus associated to the Italian lentisk canker, *Diplodia olivarum*, by a fungus that induces canker to the Tunisian maritime pine, *Diplodia sapinea*, and by a fungus associated to leaf spot of African mahogany, *Alternaria argyroxiphii*.

Firstly, fungal culture filtrates of each fungus were obtained growing in the right medium and, successively, their production of phytotoxic secondary metabolites was investigated, as below reported:

- Production, extraction and purification of secondary metabolites from culture filtrates of *F. rabenhorstii*, *S. macrostoma*, *H. fraxineus*, *D. olivarum*, *D. sapinea* and *A. argyroxiphii*.
- Identification of the already known metabolites.
- Chemical characterization of new secondary metabolites by spectroscopic techniques.
- Assignment of their relative and absolute configurations by spectroscopic and chemical methods.
- Biological characterization.

These studies were carried out in collaboration with other groups which grown the fungi and performed the biological assay.

3 MATERIAL AND METHODS

3.1 Fungal strains

3.1.1 *Hymenoscyphus fraxineus*

The strain of *H. fraxineus* was isolated from a cankered branch of a *Fraxinus excelsior* L. (European ash) tree located in a declining ash forest in Veneto, Italy. The strain was identified by morphological study and the analysis of internal transcribed spacer (ITS) of rDNA using the same procedures previously reported (Linaldeddu *et al.*, 2016b). The ITS sequence is available in GenBank with the accession number MN428071. The fungal cultures were held on potato dextrose agar (PDA) and stored at 4 °C as CHA1 in the culture collection of the Dipartimento Territorio e Sistemi Agro-Forestali, (TeSAF), University of Padua.

3.1.2 *Fimetiariella rabenhorstii*

The strain SR84-1C of *F. rabenhorstii* was isolated from stems of infected *Quercus brantii* (Iranian oak) trees collected in Kurdistan, Iran. The fungus was identified on the basis of the analysis of internal transcribed spacer (ITS) sequence. Its pathogenicity was verified on 2-year-old oak trees in greenhouse conditions following Koch's postulates (Byrd and Segre, 2016). The pure cultures were maintained on PDA and stored at 4 °C in the fungal collection of the Department of Plant Protection, University of Kurdistan, Sanandaj, Iran.

3.1.3 *Stilbocrea macrostoma*

The strain 4B-212 of *S. macrostoma* was isolated from necrotic branches of *Quercus brantii* tree for the first time collected in Zagros Forest, in Paveh, Kermanshah Province, Iran. Its pathogenicity was confirmed by in greenhouse experiments on 2-year-old oak trees following Koch's postulates (Byrd and Segre, 2016). The molecular identification of the isolate 4B-212 was obtained extracting the total genomic DNA from fresh mycelia grown on PDA and using the method previously described by Abdollahzadeh *et al.* (2009). The D1/D2 variable domains of the 28S nrDNA (LSU) region of ribosomal DNA was amplified and sequenced using the primer pairs LR0R/LR5 (Vilgalys and Hester 1990). Phylogenetic analyses based on LSU sequence data using Bayesian method highlighted the isolate of *S. macrostoma* (*Bionectriaceae*) was close to the isolate G.J.S. 02-125 from Sri Lanka. The fungal strain was held on PDA at 4 °C in the fungal collection of the Department of Plant Protection, Agriculture Faculty, University of Kurdistan, Sanandaj, Iran.

3.1.4 *Diplodia olivarum*

The strain of *D. olivarum* was isolated from a cankered branch of *Pistacia lentiscus* (lentisk) collected in Caprera Island, Italy. The genetic sequences of this strain are available in GenBank with the accession numbers: ITS; KX833078), *tef1- α* ; KX833079) and MAT1-2-1; MG015783 (Lopes et al., 2018). Its cultures were maintained on PDA (Fluka, Sigma-Aldrich Chemic GmbH) and stored at 4°C in the collection of the Dipartimento di Agraria, University of Sassari, Italy, as BL96.

3.1.5 *Alternaria argyroxiphii*

The strain of *A. argyroxiphii* E.G. Simmons & Aragaki (CBS 117222) was purchased from Westerdijk Fungal biodiversity Institute, Utrecht, Netherlands. The fungal cultures were maintained on carrot-agar and stored at 4°C in the collection of the Dipartimento di Agraria, University of Sassari, Italy.

3.1.6 *Diplodia sapinea*

The strain of *D. sapinea* was isolated from a cankered branch of *Pinus pinaster* (maritime pine) tree collected in northwest Tunisia. The strain was identified through morphological study and analysis of internal transcribed spacer (ITS) rDNA. Fungal DNA extraction, PCR amplification reactions, and DNA sequencing were performed as reported by Linaldeddu *et al.* (2016b). The sequence of the ITS region is available in GenBank with accession number: MW436711. Pure cultures were held on PDA and stored at 4 °C as C3 in the collection of the Dipartimento di Agraria, University of Sassari, Italy.

3.2 General procedures

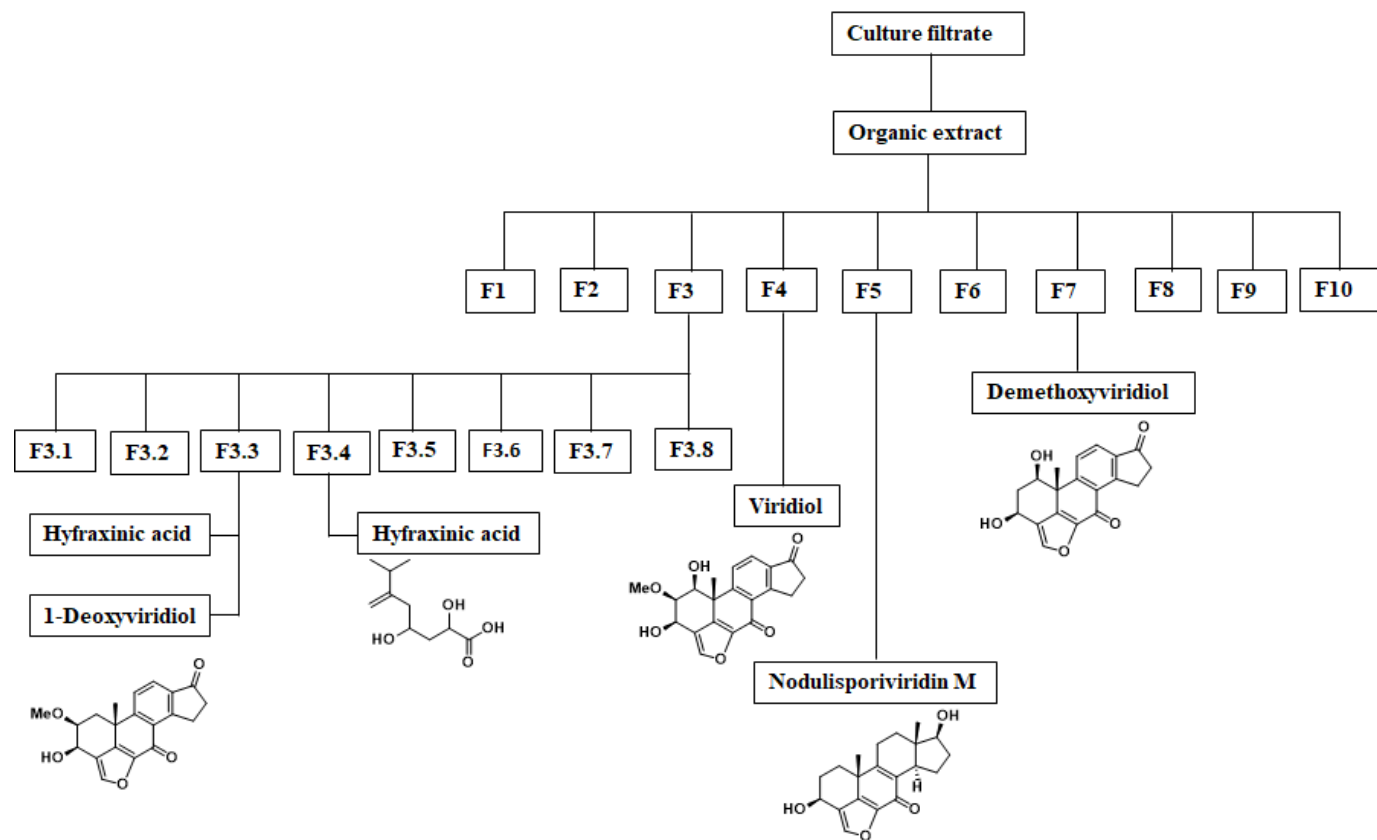
Optical rotation was measured on a Jasco P-1010 digital polarimeter (Jasco, Tokyo, Japan); IR spectra were recorded as a glass film deposits using a Perkin Elmer Spectrum 100 FT-IR spectrometer (Waltham, MA, USA). A Jasco V-530 spectrophotometer (Easton, MD, U.S.A.) was used to record UV spectra. A Jasco J-815 or J-715 spectropolarimeter was used to record ECD spectra. Bruker (Karlsruhe, Germany) and Varian (Palo Alto, CA, USA) instruments (400/100 MHz and 500/125 MHz respectively) were used to recorded ^1H , ^{13}C and 2D NMR spectra using suitable deuterated solvents. The same solvents were used also as internal standards. The carbon multiplicities were determined by DEPT spectra (Berger and Braun, 2004). DEPT, Correlated Spectroscopy (COSY-45), Heteronuclear Single Quantum Coherence (HSQC) and Heteronuclear Multiple Bond Correlation (HMBC) experiments (Berger and Braun, 2004) were performed using Bruker and Varian microprograms.

High resolution electrospray ionization mass spectrometry (HRESIMS), electrospray ionization mass spectrometry (ESIMS) and liquid chromatography mass spectrometry (LC/MS) analyses were performed using the LC/MS Time-of-flight (TOF) system AGILENT (Agilent Technologies, Milan, Italy) 6230B, HPLC 1260 Infinity. The HPLC separations were carried out with a Phenomenex (Bologna, Italy) LUNA column (C18 (2) 5 μ 150x4.6 mm). HRESIMS spectra were recorded on a 6120 Quadrupole LC/MS instrument (Agilent Technologies). Analytical, preparative, and reverse-phase thin-layer chromatography (TLCs) were carried out on silica gel (Kieselgel 60, F254, 0.25 and 0.5 mm and RP-18 F254s, respectively) plates (Merck, Darmstadt, Germany), while column chromatography was performed using silica gel (Kieselgel 60, 0.063-0.200 mm, Merck). The spots were visualized by exposure to UV light and/or iodine vapours and/or by spraying first with 10% H₂SO₄ in MeOH, and then with 5% phosphomolybdic acid in EtOH, followed by heating at 110°C for 10 min. Sigma-Aldrich Co. (St. Louis, MO, U.S.A.) supplied all of the reagents and the solvents.

4 EXPERIMENTAL

4.1 Production, extraction and purification of secondary metabolites from *Hymenoscyphus fraxineus* culture filtrates

Hymenoscyphus fraxineus was grown on 150 Petri dishes (90 mm diameter) containing 20 mL of malt extract agar (MEA) medium (Oxoid, Italy). The plates were separately inoculated with 6 mm agar plugs of 10-day-old cultures and incubated for 45 days at 20 °C in the dark. The corresponding culture filtrates were extracted by maceration with EtOAc for 24 h. The solvent, dehydrated on Na₂SO₄, was evaporated under reduced pressure to obtain a brown-red oil residue (2.9 g). The organic extract was fractionated by column chromatography (CC) on silica gel eluted with CHCl₃/*iso*-PrOH (9:1), yielding 10 homogeneous fractions (F1-F10, Scheme 1). The residue (526.6 mg) of F3 was further purified by CC eluted with CHCl₃/*iso*-PrOH (93:7) obtaining eight fractions (F3.1-F3.8). The residue (198.9 mg) of F3.3 was purified by CC on silica gel eluted with EtOAc/*n*-hexane (6:4), yielding a new metabolite named hyfraxinic acid (**1**, 25.4 mg, R_f 0.69) as an amorphous solid and a metabolite identified as 1-deoxyviridiol (**2**, 11.5 mg, R_f 0.19) as a white solid. Successively, compound **2** was crystallized using EtOAc/MeOH (5:1). The residue (111.8 mg) of F3.4 was purified by CC on silica gel eluted with *n*-hexane/EtOAc (6:4), obtaining a further amount of hyfraxinic acid (**1**, 8.0 mg, for a total of 33.4 mg). The residue (449.1 mg) of F4 was purified by CC on silica gel using CHCl₃/*iso*-PrOH (95:5, v/v) as the eluent, yielding a metabolite identified as viridiol (**3**, 160.1 mg, R_f 0.49), the main metabolite, as a yellow solid. The residue (167.4 mg) of F5 was further purified by a first step of CC on silica gel eluted with CHCl₃/*iso*-PrOH/MeOH (9:0.5:0.5) and a second step of preparative TLCs eluted with CHCl₃/*iso*-PrOH (9:1), obtaining a metabolite identified as nodulisporiviridin M (**4**, 17.4 mg, R_f 0.28) as a white solid. The residue (218.5 mg) of F7 was further purified by CC on silica gel, using CHCl₃/Me₂CO (93:7) as eluent, and then by preparative TLC eluted with CH₂Cl₂/MeOH (9:1), yielding a metabolite identified as demethoxyviridiol (**5**, 8.0 mg, R_f 0.48) as a yellow oil.



Scheme 1: Extraction and purification of *Hymenoscyphus fraxineus* culture filtrate.

4.1.1 Hyfraxinic acid (1)

Hyfraxinic acid (Fig. 27, Page 63) was obtained as an amorphous solid and had: $[\alpha]_{\text{D}}^{25} +192.3$ (c 0.6, EtOH); UV λ_{max} (log ϵ) <220 nm; IR ν_{max} 3460, 1771, 1645 cm^{-1} ; ^1H and ^{13}C NMR data are reported in Table 1; ESIMS (+) spectrum m/z : 427 $[2\text{M} + \text{Na}]^+$ and 225 $[\text{M} + \text{Na}]^+$; HRESIMS (+) spectrum m/z : 203.1287 $[\text{M} + \text{H}]^+$ (calcd for $\text{C}_{10}\text{H}_{19}\text{O}_4$ 203.1283).

4.1.2 1-Deoxyviridiol (2)

1-Deoxyviridiol (Fig. 27, Page 63) was a white solid and had: $[\alpha]_{\text{D}}^{25} -151$ (c 0.3, EtOH) [lit. (Andersson *et al.*, 2012): $[\alpha]_{\text{D}}^{25} -13$ (c 0.02, EtOH)]; ^1H and ^{13}C NMR data are in agreement with those previously reported (Andersson *et al.*, 2012); HRESIMS (+) spectrum m/z : 339.1237 $[\text{M} + \text{H}]^+$ (calcd for $\text{C}_{20}\text{H}_{19}\text{O}_5$, 339.1232).

4.1.3 Viridiol (3)

Viridiol (Fig. 27, Page 63), the main metabolite obtained as a yellow solid, had: $[\alpha]_{\text{D}}^{25} -47.1$ (c 0.2, CH_2Cl_2) [lit. (Del Bel *et al.*, 2017): $[\alpha]_{\text{D}}^{25} -53.3$ (c 0.22, CH_2Cl_2)]; ^1H and ^{13}C NMR data are in agreement with those previously reported (Lumsden *et al.*, 1992); ESIMS (+) spectrum m/z : 709 $[2\text{M} + \text{H}]^+$; HRESIMS (+) spectrum m/z : 355.1185 $[\text{M} + \text{H}]^+$ (calcd for $\text{C}_{20}\text{H}_{19}\text{O}_6$ 355.1182).

4.1.4 Nodulisporiviridin M (4)

Nodulisporiviridin M (Fig. 27, Page 63) was obtained as a white solid and had: $[\alpha]_{\text{D}}^{25} -51.4$ (c 0.2, EtOH); ECD spectrum and ^1H and ^{13}C NMR data agree with those reported in Wang *et al.*, 2018; ESIMS (+) spectrum m/z : 657 $[2\text{M} + \text{H}]^+$; HRESIMS (+) spectrum m/z : 329.1750 $[\text{M} + \text{H}]^+$ (calcd for $\text{C}_{20}\text{H}_{25}\text{O}_4$ 329.1753).

4.1.5 Demethoxyviridiol (5)

Demethoxyviridiol (Fig. 27, Page 63), yielded as a yellow oil, had: $[\alpha]_{\text{D}}^{25} -25.0$ (c 0.8, EtOH); ^1H and ^{13}C NMR data agree with those formerly reported (Cole *et al.*, 1975); HRESIMS (+) spectrum m/z : 363.0637 $[\text{M} + \text{K}]^+$ (calcd for $\text{C}_{19}\text{H}_{16}\text{KO}_5$ 363.0635).

4.1.6 2-O-Acetylhyfraxinic acid (6)

1.0 mg of hyfraxinic acid (1) was dissolved in 40 μL of pyridine and acetylated with 40 μL of acetic anhydride under stirring for 2 h at room temperature. Then the reaction was stopped adding MeOH and C_6H_6 , and the resultant azeotrope was evaporated under a nitrogen stream. The residue (1.2

mg) was purified by TLC eluted with $\text{CHCl}_3/\text{iso-PrOH}$ (98:2), yielding 2-*O*-acetylhyfraxinic acid (**6**, 1.1 mg), as an amorphous solid (Fig. 28, Page 66). Compound **6** had: UV λ_{max} ($\log \epsilon$) <220 nm; IR ν_{max} 3467, 1786, 1736, 1645, 1250 cm^{-1} ; ^1H NMR data are reported in Table 1; ESIMS (+) spectrum m/z : 245 $[\text{M} + \text{H}]^+$.

4.1.7 2-*O-p*-Bromobenzoyl ester of hyfraxinic acid (**7**)

1.0 mg of hyfraxinic acid (**1**) was dissolved in 100 μL of anhydrous MeCN and then 2.0 mg of DMAP and 2.0 mg of *p*-bromobenzoyl chloride were added. The reaction mixture was left under stirring for 4 h and then the solvent was evaporated under a nitrogen stream. Subsequently, the residue (1.5 mg) was purified by preparative TLC eluted with CHCl_3 , obtaining 2-*O-p*-bromobenzoyl ester of hyfraxinic acid (**7**, 1.4 mg) (Fig. 28, Page 66). This latter (**7**) had: UV λ_{max} ($\log \epsilon$), 245 nm (4.20); IR ν_{max} 3433, 1791, 1729, 1639, 1590 cm^{-1} ; ^1H NMR data are reported in Table 1; ESIMS (+) spectrum m/z : 387 $[\text{M} + 2 + \text{H}]^+$ and 385 $[\text{M} + \text{H}]^+$.

4.1.8 3-*O-(S)- α* -Methoxy- α -trifluoromethyl- α -phenylacetate (MTPA) ester of 1-deoxyviridiol (**8**)

1.0 mg of 1-deoxyviridiol (**2**) was dissolved in 20 μL of dry pyridine and 10 μL of (*R*)-(-)-MTPA-Cl was added. The reaction was left for 24 h at room temperature, then it was stopped with MeOH and the solvents were removed under a nitrogen stream. The residue (1.4 mg) was purified by TLC eluted with EtOAc/*n*-hexane (6:4), affording 3-*O-(S)*- MTPA ester of 1-deoxyviridiol (**8**, 1.2 mg) as a homogeneous oil (Fig. 39, Page 75). It (**8**) had: UV λ_{max} ($\log \epsilon$), 306 (3.90), 244 nm (4.25); IR ν_{max} 1743, 1705, 1669, 1628, 1579, 1165 cm^{-1} ; ^1H NMR data are in Table 2; ESIMS (+) spectrum m/z : 1109 $[2\text{M} + \text{H}]^+$ and 555 $[\text{M} + \text{H}]^+$.

4.1.9 3-*O-(R)- α* -Methoxy- α -trifluoromethyl- α -phenylacetate (MTPA) ester of 1-deoxyviridiol (**9**)

10 μL of (*S*)-(+)-MTPA-Cl was added to 1.0 mg of 1-deoxyviridiol (**2**) dissolved in 20 μL of dry pyridine, and the reaction was conducted in the same conditions used for obtaining compound **8**. The residue (1.7 mg) obtained was purified by TLC eluted with EtOAc/*n*-hexane (6:4), affording 3-*O-(R)*- MTPA ester of 1-deoxyviridiol (**9**, 1.4 mg) as a homogeneous oil (Fig. 39, Page 75). It (**9**) had: UV λ_{max} ($\log \epsilon$), 306 (3.90), 244 nm (4.25); IR ν_{max} 1743, 1705, 1669, 1628, 1579, 1165 cm^{-1} ; ^1H NMR data are in Table 2; ESIMS (+) spectrum m/z : 1109 $[2\text{M} + \text{H}]^+$ and 555 $[\text{M} + \text{H}]^+$.

4.2 Crystal structure determination of 1-deoxyviridiol

Single crystals of 1-deoxyviridiol (**2**), suitable for X-ray structure analysis, was obtained by slow evaporation of its solution in EtOAc/MeOH (1:5). One selected crystal was fitted at ambient temperature on a Bruker-Nonius Kappa charge-coupled device (CCD) diffractometer (graphite monochromated Mo K α radiation, $\lambda = 0.71073 \text{ \AA}$, CCD rotation images, thick slices, and φ and ω scans to fill the asymmetric unit), and a semi-empirical absorption correction (multiscan, SADABS) was applied. The structure was determined by direct methods using the SIR97 program (Altomare *et al.*, 1999) and anisotropically refined by the full matrix least squares method on F2 against all independent measured reflections using the SHELXL-2016/6 program (Sheldrick, 2015). The hydroxy H atom was located in difference Fourier maps and freely refined with $U_{\text{iso}}(\text{H})$ equal to $1.2U_{\text{eq}}$ of the carrier atom, while the other hydrogen atoms were placed in calculated positions and refined according to the riding model with C–H distances in the range of 0.93–0.96 \AA and with $U_{\text{iso}}(\text{H})$ equal to $1.2U_{\text{eq}}$ or $1.5U_{\text{eq}}$ (C_{methyl}) of the carrier atom. Crystals presented a thin needle shape and weakly diffracting at high θ values, this did not allow to assign the absolute configuration due to the absence of strong anomalous scatterer atoms in the compound. The relative configuration is $2S^*,3R^*,9R^*$. The Figure 34 (Page 72) was generated using ORTEP-3 (Ferrugia, 2012) and Mercury CSD 3.9 (Macrae *et al.*, 2008).

4.2.1 Crystallographic data of 1-deoxyviridiol

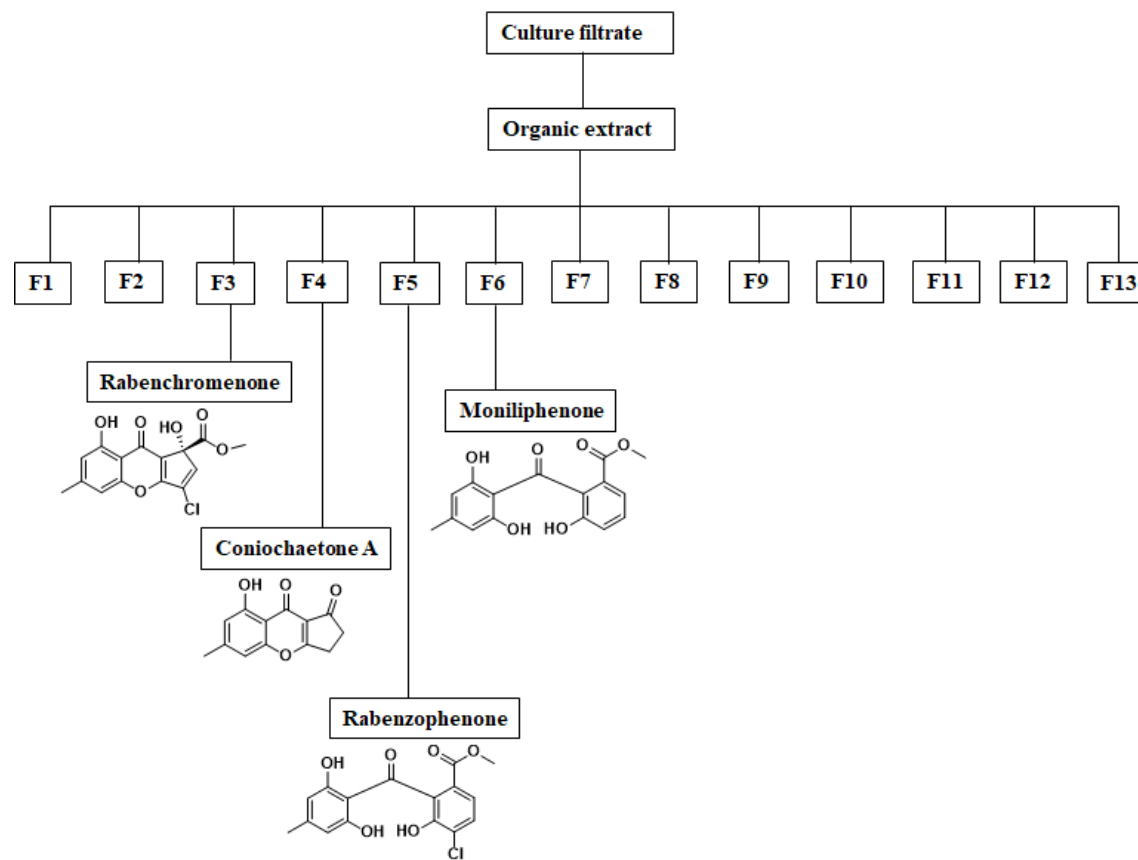
Empirical formula: $\text{C}_{20}\text{H}_{18}\text{O}_5$; formula weight: $338.34 \text{ g mol}^{-1}$; monoclinic: $P2_1$; unit cell parameters: $a = 8.423(5) \text{ \AA}$; $b = 8.266(5) \text{ \AA}$; $c = 11.452(7) \text{ \AA}$; $V: 796.2(8) \text{ \AA}^3$; $Z: 2$; $D_x: 1.411 \text{ Mg/m}^3$. All crystallographic data for compound **2** were deposited in the Cambridge Crystallographic Data Centre with deposition number CCDC 1955835.

4.3 Leaf puncture assay of metabolites isolated from *H. fraxineus*

Each compound was assayed at 1.0 and 0.5 mg/mL on mature leaves of *Celtis australis* L., *Quercus suber* L., *Hedera elix* L., *Juglans regia* L., and *Fraxinus angustifolia* L., using the procedure previously described (Andolfi *et al.*, 2014b). Leaves were observed every day and scored for symptoms after 7 days, but the effect of the toxins on the leaves persisted for up to 10 days. Lesions were estimated using APS Assess 2.0 software (Lamari, 2002) and their size was expressed in millimeters squared.

4.4 Production, extraction and purification of secondary metabolites from *Fimetariella rabenhorstii* culture filtrates

Fimetariella rabenhorstii was grown under stationary conditions in 10 flasks containing 500 mL of modified Czapek–Dox medium at pH 6.8. They were incubated at 25 °C in the dark for 30 days and then the mycelium was removed by filtration through filter paper (Whatman No. 4). The filtrates were lyophilized and stored at –20 °C. Successively it was dissolved in 500 mL of H₂O and exhaustively extracted with EtOAc. The solvent, dehydrated by Na₂SO₄, was evaporated under reduced pressure, obtaining an orange–red oil residue (196 mg). The corresponding organic extract was fractionated by CC on silica gel eluted with CHCl₃/MeOH (9:1), yielding 13 homogeneous fractions (F1-F13, Scheme 2). The residue (11.9 mg) of F3 was further purified by reversed-phase TLC eluted with MeOH/H₂O (8:2), yielding a new metabolite named rabenchromenone (**10**, 1.7 mg, R_f 0.36) as an amorphous solid. The residue (10.0 mg) of the F5 was furthermore purified by TLC using CH₂Cl₂/*iso*-PrOH (95:5), obtaining another new metabolite named rabenzophenone (**11**, 1.1 mg, R_f 0.45) as an amorphous solid. The residue (17.3 mg) of the F6 was purified by TLC eluted with CHCl₃/MeOH (9:1), yielding a metabolite identified as moniliphenone (**12**, 1.8 mg, R_f 0.31) as an amorphous solid. Finally, the residue (10.8 mg) of the F4 was purified by TLC, eluted with CHCl₃/*iso*-PrOH (95:5), affording a metabolite identified as coniochaetone A (**13**, 5.3 mg, R_f 0.56) as an amorphous solid.



Scheme 2: Extraction and purification of *Fimetariella rabenhorstii* culture filtrate.

4.4.1 Rabenchromenone (10)

Rabenchromenone (Fig. 40, Page 78), obtained as an amorphous solid, had: $[\alpha]_D^{25} +47$ (c 0.06, MeOH); IR ν_{\max} 3423, 1742, 1654, 1618, 1596, 1462 cm^{-1} ; UV λ_{\max} (log ϵ), 341 (3.80), 272 (4.46) nm; ^1H and ^{13}C NMR data are present in Table 5; HRESIMS (+) spectrum m/z : 685.0119 and 683.0139 $[2\text{M} + \text{K}]^+$, 669.0384 and 667.0417 $[2\text{M} + \text{Na}]^+$, 347.0126 and 345.0155 $[\text{M} + \text{Na}]^+$, 325.0113 and 323.0334 $[\text{M} + \text{H}]^+$ (calcd for $\text{C}_{15}\text{H}_{12}\text{ClO}_6$ 325.0293 and 323.0322).

4.4.2 Rabenzophenone (11)

Rabenzophenone (Fig. 40, Page 78) was obtained as an amorphous solid and had: IR ν_{\max} 3346, 1733, 1635, 1588, 1465 cm^{-1} ; UV λ_{\max} (log ϵ), 284 (2.50) nm; ^1H and ^{13}C NMR data are reported in Table 6; HRESIMS (+) spectrum m/z : 339.0458 and 337.0469 $[\text{M} + \text{H}]^+$ (calcd for $\text{C}_{16}\text{H}_{14}\text{ClO}_6$ 339.0449 and 337.0479), 216.0013 and 214.0039 $[\text{C}_9\text{H}_7\text{ClO}_4 + \text{H}]^+$.

4.4.3 Moniliphenone (12)

Moniliphenone (Fig. 40, Page 78) was an amorphous solid and had: ^1H and ^{13}C NMR are in agreement with those previously (Kachi and Sassa, 1986). HRESIMS (+) spectrum m/z : 627.1488 $[2\text{M} + \text{Na}]^+$, 325.0749 $[\text{M} + \text{Na}]^+$, 303.0882 $[\text{M} + \text{H}]^+$ (calcd for $\text{C}_{16}\text{H}_{15}\text{O}_6$ 303.2867).

4.4.4 Coniochaetone A (13)

Coniochaetone A (Fig. 40, Page 78), yielding as an amorphous solid, had: ^1H and ^{13}C NMR data agree with those previously reported (Wang *et al.*, 1995). HRESIMS (+) spectrum m/z : 483.0391 $[2\text{M} + \text{Na}]^+$, 253.4308 $[\text{M} + \text{Na}]^+$, 231.5853 $[\text{M} + \text{H}]^+$ (calcd for $\text{C}_{13}\text{H}_{11}\text{O}_4$ 231.2240).

4.5 Computational methods to afford absolute configuration (AC) of rabenchromenone

The AC of rabenchromenone (**10**) was determined using molecular mechanics and preliminary DFT calculations were performed with Spartan'18 (Wave function, Inc., Irvine, CA, U.S.A.), with standard parameters and convergence criteria. DFT and time-dependent density functional theory (TDDFT) calculations were carried out with Gaussian 16, with default grids and convergence criteria (Frisch *et al.*, 2016). Conformational searches and the optimizations of the conformers obtained were performed as previously described (Cimmino *et al.*, 2016). Final optimizations were carried out at the $\omega\text{B97X-D/6-311+G(d,p)}$ level, including the Solvation Model based on Density (SMD) for CH_3CN . TD-DFT calculations were run with several functionals (CAMB3LYP, B3LYP, BH&HLYP, M06-2X,

and ω B97X-D) and def2-TZVP basis set, including a polarizable continuum solvent model (PCM) for CH₃CN. Average ECD spectra were calculated as previously described (Cimmino *et al.*, 2016). Two conformers for compound **10**, with a population >1% at 300 K, were considered; they differed in the orientation of the ester moiety. ECD spectra were generated using the program SpecDis (Bruhn *et al.*, 2017), as previously described (Cimmino *et al.*, 2017b).

4.6 Biological assay on phytotoxins isolated from *F. rabenhorstii*

4.6.1 Leaf Puncture Assay

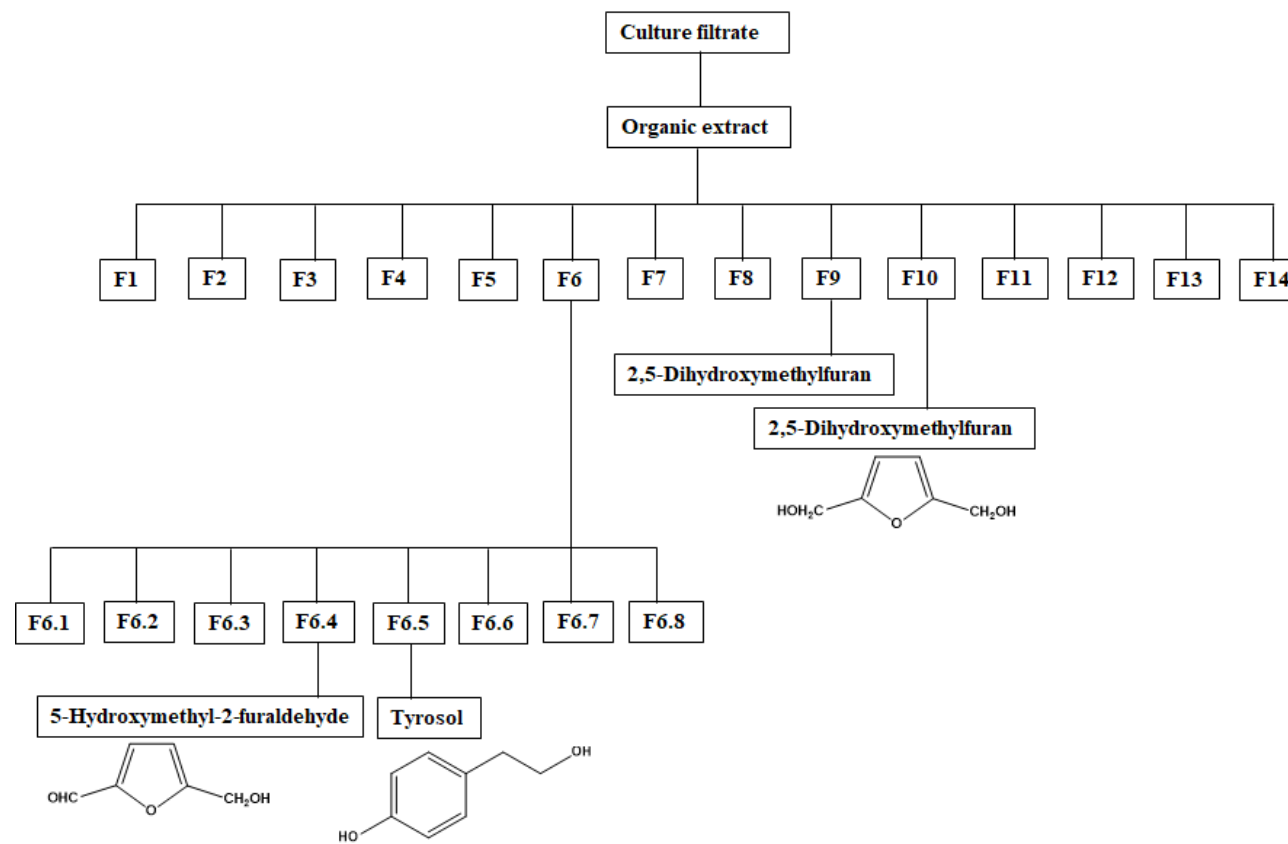
All compounds (**10-13**) were assayed on *Quercus ilex* L. and *Lycopersicon esculentum* L. young leaves. Fungal culture filtrates, organic extracts and each compound (**10-13**) were tested at 1.0 mg/mL using the same procedure previously described (Cimmino *et al.*, 2018). Leaves were observed every day and scored for symptoms after 7 days, but the effect of the toxins on the leaves persisted for up to 10 days. The phytotoxicity was expressed using a visual scale from 0 (no symptoms) to 4 (wide necrosis up to 1 cm in diameter).

4.6.2 Tomato Cutting Assay

The fungal culture filtrates, its organic extracts and the chromatographic fractions were assayed at 1 mg/mL on 21-day-old seedlings of *Lycopersicon esculentum* L. following the procedure previously described (Cimmino *et al.*, 2018). Symptoms were evaluated visually after 7 days and the phytotoxicity was expressed with the same scale reported above.

4.7 Production, extraction and purification of secondary metabolites from *Stilbocrea macrostoma* culture filtrates

Stilbocrea macrostoma was grown under stationary conditions in 10 flasks containing 500 mL of PDB medium at pH 4.5. The cultures were incubated at 25 °C in the dark for 30 days and then the mycelium was removed by filtration through filter paper (Whatman No. 4). The filtrates were lyophilized and stored at -20 °C. Subsequently, the lyophilized was dissolved in 600 mL of H₂O and extracted with EtOAc. The organic extract, dehydrated by Na₂SO₄, and evaporated under reduced pressure, yielding a brown-red oil residue (947 mg). It was fractioned by CC on silica gel eluted with CHCl₃/*iso*-PrOH (9:1), yielding 14 homogeneous fractions (F1-F14, Scheme 3). The residue (37.8 mg) of the F9 was purified by preparative TLC using CH₂Cl₂/MeOH (8:2) as eluent, obtaining a metabolite identified as 2,5-dihydroxymethylfuran (**14**, 8.1 mg, R_f 0.65) as crystals. The residue (42.1 mg) of the F10 was purified by preparative TLC eluted with CHCl₃/*iso*-PrOH (7:3) affording further amount of 2,5-dihydroxymethylfuran (**14**, 20.1 mg, for a total of 28.2 mg). The residue (102.4 mg) of the F6 was purified by CC on silica gel eluted with CHCl₃/*iso*-PrOH (95:5) obtaining eight fractions (F6.1-F6.8). The residue (27.0 mg) of the F6.4 was further purified by preparative TLC eluted with CHCl₃/*iso*-PrOH (95:5), yielding a metabolite identified as 5-hydroxymethyl-2-furaldehyde (**15**, 5.5 mg, R_f 0.25) as yellow oil. The residue (10.9 mg) of the F6.5 was successively purified by TLC using CHCl₃/*iso*-PrOH (9:1) as eluent, obtaining a metabolite identified as tyrosol (**16**, 1.3 mg, R_f 0.43) as an amorphous solid.



Scheme 3: Extraction and purification of *Stilbocrea macrostoma* culture filtrate.

4.7.1 2,5-Dihydroxymethylfuran (14)

2,5-Dihydroxymethylfuran (Fig. 52, Page 95) was obtained as crystals and had: ^1H and ^{13}C NMR data agree with those previously reported (Schneider *et al.*, 1996; Mancilla *et al.*, 2009); ESIMS (+) spectrum m/z : 151 $[\text{M} + \text{Na}]^+$.

4.7.2 5-Hydroxymethyl-2-furaldehyde (15)

5-Hydroxymethyl-2-furaldehyde (Fig. 52, Page 95), yielded as yellow oil, had: ^1H and ^{13}C NMR data were in agreement with those previously reported (Dohnal and Kisiel, 1993; Li *et al.*, 2007; Guo *et al.*, 2016); ESIMS (+) spectrum m/z : 127 $[\text{M} + \text{H}]^+$.

4.7.3 Tyrosol (16)

Tyrosol (Fig. 52, Page 95), obtained as an amorphous solid, had: ^1H NMR data agree with those previously reported (Kimura and Tamura, 1973; Capasso *et al.*, 1992; Cimmino *et al.*, 2017c; Masi *et al.*, 2020); ESIMS (+) spectrum m/z : 295 $[2\text{M} + \text{Na}]^+$, 159 $[\text{M} + \text{Na}]^+$.

4.8 Crystal structure determination of 2,5-dihydroxymethylfuran

A solution of 2,5-dihydroxymethylfuran (14) gave crystals, suitable for X-ray structure analyses, by slow evaporation of CDCl_3 in a NMR glass tube at ambient temperature. Single crystals with two different crystal habitus were found (Fig. 53, Page 96). The majority of crystals was formed at the bottom of NMR tube in a rare snow-like habitus, while rhombe-plate crystals were formed on the wall of NMR tube aligning as little flags hanging on a strand. Single crystals of both habitus were analysed by X-ray diffraction, proving that they belong to the same crystalline phase.

Data were collected in flowing N_2 at 173 K on a Bruker-Nonius KappaCCD diffractometer equipped with Oxford Cryostream apparatus (graphite monochromated $\text{MoK}\alpha$ radiation $\lambda = 0.71073 \text{ \AA}$, CCD rotation images, thick slices, φ and ω scans to fill asymmetric unit). A semiempirical absorption correction (multi-scan, SADABS) was applied. The structure was determined by direct methods using SIR97 program (Altomare *et al.*, 1999) and anisotropically refined by the full matrix least-squares techniques using SHELXL-2016/6 program (Sheldrick, 2015). The hydroxy H atoms were placed in difference Fourier maps and freely refined ($U_{\text{iso}}(\text{H})$ equal to $1.2U_{\text{eq}}$ of the carrier atom). The hydrogen atoms were introduced in calculated positions and refined as a riding model with C-H distances in the range 0.95-0.99 \AA and $U_{\text{iso}}(\text{H}) = 1.2U_{\text{eq}}(\text{C})$. Figure 54 (Page 96) was generated using ORTEP-3 (Farrugia, 2012) and Mercury CSD 3.9 (Macrae *et al.*, 2008).

4.8.1 Crystallographic data of 2,5-dihydroxymethylfuran

Empirical formula: C₆H₈O₃, formula weight: 128.12 g mol⁻¹; T: 173 K; orthorhombic: space group *P* n a 21; unit cell parameters: a = 16.2960(10), b = 7.7050(11), c = 4.879(3) Å; V: 612.6(4) Å³; Z: 4; D_{calc}: 1.389 g/cm³; F(000): 272; μ: 0.112 mm⁻¹. 3164 total reflections collected, 1059 independent reflections. The final refinement gave *R*1 = 0.0376; *wR*2 = 0.0622 [*I* > 2σ(*I*)].

All crystallographic data for compound **14** were deposited in the Cambridge Crystallographic Data Centre with deposition number CCDC 2005394.

4.9 Biological assay on phytotoxins isolated from *S. macrostoma*

4.9.1 Leaf Puncture Assay

All compounds (**14-16**) were assayed on *Quercus ilex* L. and *Lycopersicon esculentum* L. young leaves. Each compound was tested at a concentration of 5.0, 1.0 and 0.1 mM, preparing test solutions obtained dissolving compounds in a H₂O solution with 4% of MeOH, which was also used as the negative control. A droplet (20 μL) of test solution was applied on leaves, that had previously been needle punctured. The treatment was repeated three times and the leaves were kept in a moistened chamber to preserve the droplets from drying. Leaves were observed every day and scored for symptoms after 48 hours, but the toxic effect of phytotoxins on the leaves remained up to 7 days. The phytotoxicity was expressed using a visual scale from 0 (no symptoms) to 4 (wide necrosis up to 1 cm in diameter).

4.9.2 Tomato Cutting Assay

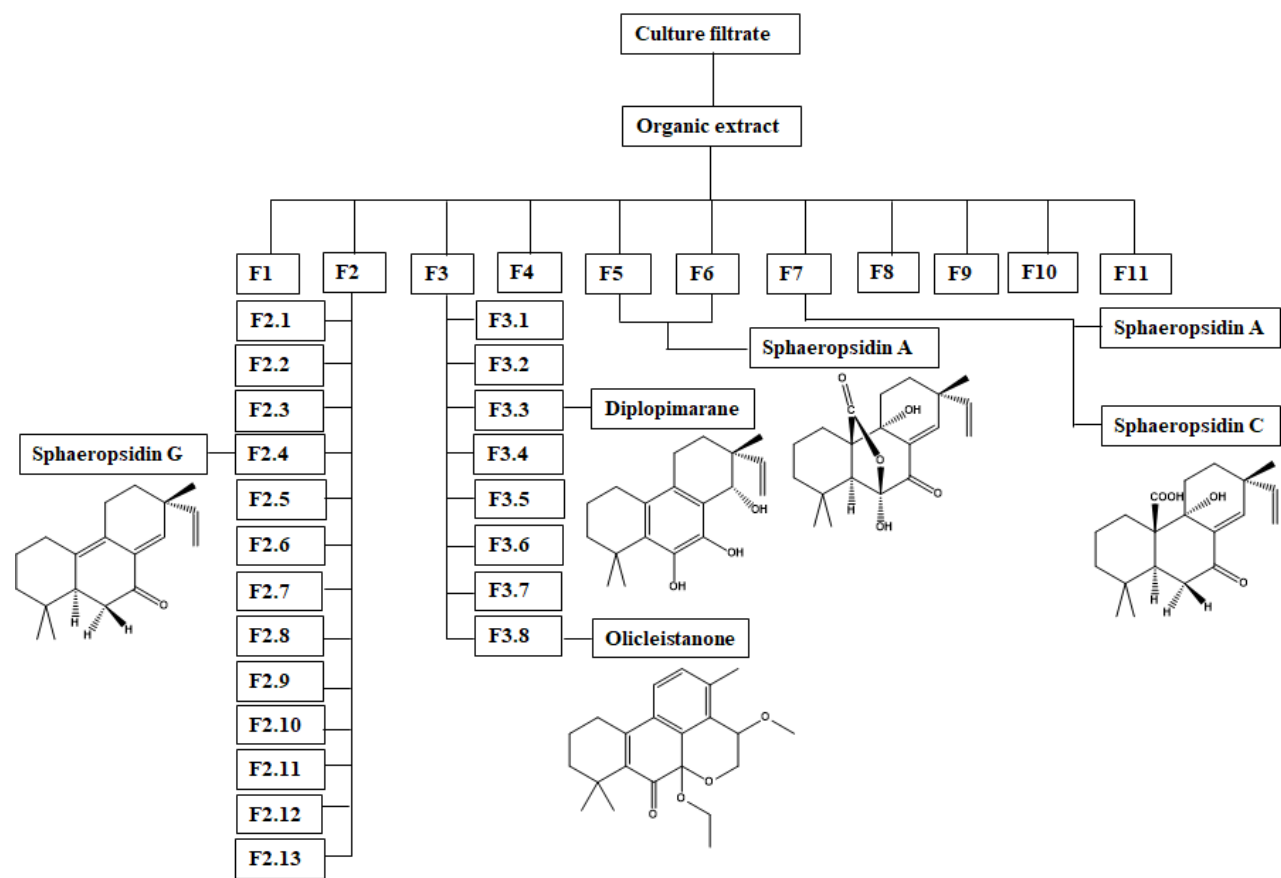
The phytotoxicity of the fungal culture filtrates, its organic extracts and the chromatographic fractions were tried at 1 mg/mL using tomato cutting assay using the procedure previously described (Cimmino *et al.*, 2018). Symptoms were evaluated visually up to 7 days.

4.10 Production, extraction and purification of secondary metabolites from *Diplodia olivarum* culture filtrates

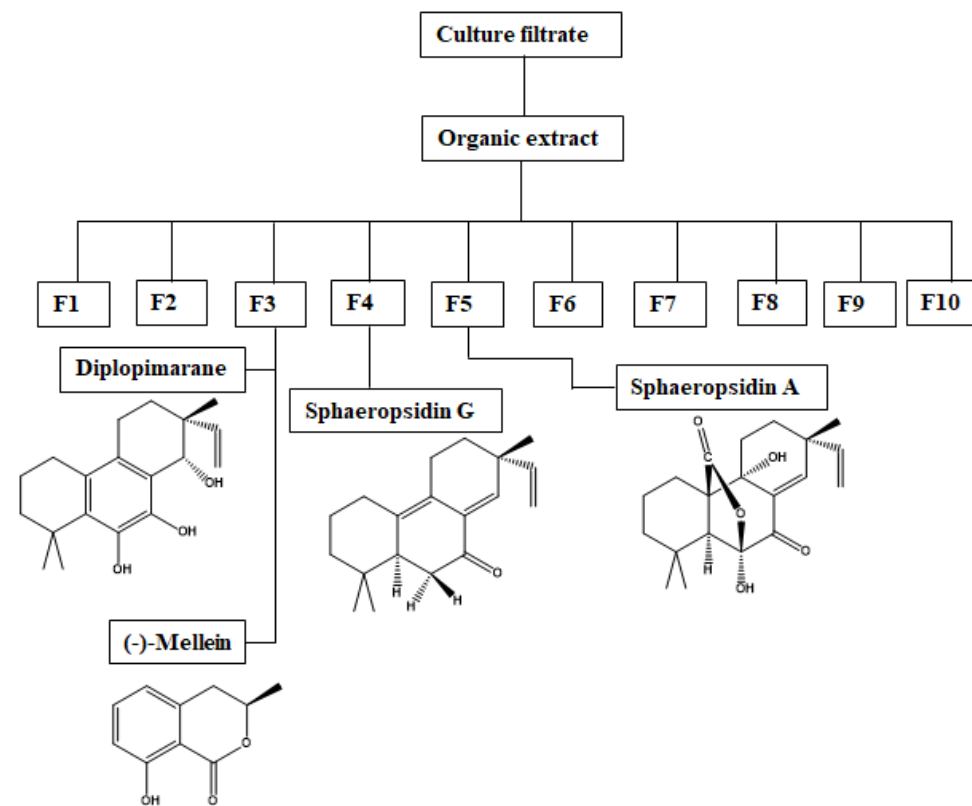
Diplodia olivarum was grown on Czapek broth amended with 2% yeast extract or on mineral salt medium (Pinkerton and Strobel, 1976), both in Erlenmeyer flasks each containing 250 mL of medium at pH 5.7. They were incubated at 25°C for 30 days and the corresponding culture filtrates were obtained removing the mycelium by filtration through filter paper in a vacuum system.

The culture filtrates, obtained growing the fungus on Czapek medium, were acidified to pH 4 with 2 N HCl and extracted exhaustively with EtOAc. The solvent was dried with Na₂SO₄ and evaporated under reduced pressure, yielding a brown-red oil residue recovered (4.5 g). This latter was fractionated by CC on silica gel eluted with *n*-hexane/EtOAc (7:3) obtaining 11 homogeneous fractions (F1-F11, Scheme 4). The residue (195.2 mg) of F2 was further fractionated by CC on silica gel eluted with petroleum ether/EtOAc (9.5:0.5), yielding 13 homogeneous fractions (F2.1-F2.13). The residue (11.0 mg) of F2.4 was purified by TLC using *n*-hexane/Me₂CO (8.5:1.5), affording a metabolite identified as sphaeropsidin G (**20**, 6.7 mg, R_f 0.82), as an amorphous solid. The residue (103.2 mg) of F3 was fractionated by CC on silica gel eluted with CHCl₃/*iso*-PrOH (93:7), obtaining 8 homogeneous fractions (F3.1-F3.8). The residue (23.0 mg) of F3.3 was crystallized with EtOAc/*n*-hexane (1:5) to afford a metabolite identified as diplopimarane (**21**, 14.2 mg, R_f 0.7), as white crystals. The residue (56.4 mg) of F3.8 was purified by preparative TLC using *n*-hexane/CHCl₃/*iso*-PrOH (8:1.5:0.5), yielding a new metabolite named olicleistanone (**17**, 5.8 mg, R_f 0.45) as an amorphous solid. The residues (290.3 mg) and (278.9 mg) of F5 and F6 respectively were combined and crystallized with EtOAc/*n*-hexane (1:5) obtaining a metabolite identified as sphaeropsidin A (**18**, 312.6 mg, R_f 0.5) as white crystals. The residue (135.1 mg) of F7 was purified by CC on silica gel eluted with *n*-hexane/EtOAc/Me₂CO (6:2.5:1.5), giving a metabolite identified as sphaeropsidin C (**19**, 53.3 mg, R_f 0.52) as a white solid, and a further amount of sphaeropsidin A (**18**, 33.2 mg, for a total amount of 345.8 mg).

The culture filtrates, obtained growing the fungus on modified mineral medium, were extracted using the same procedure to give 3.2 g of organic extract. This latter was fractionated by CC on silica gel eluted with *n*-hexane/EtOAc (7:3), yielding 10 homogeneous fractions (F1-F10, Scheme 5). The residue (302.3 mg) of F3 was purified by CC on silica gel eluted with *n*-hexane/CHCl₃/*iso*-PrOH (7.5:2:0.5), obtaining a metabolite identified as diplopimarane (**21**, 1.4 mg) and a metabolite identified as (-)-mellein [**22**, 105.8 mg, R_f 0.65), as amorphous solids. The residue (8.2 mg) of F4 was purified by TLC using *n*-hexane/Me₂CO (8.5:1.5) as eluent, affording a metabolite identified as sphaeropsidin G (**20**, 1.5 mg). The residue (815.9 mg) of F5 was crystallized with EtOAc/*n*-hexane (1:5) to give sphaeropsidin A (**18**, 677 mg).



Scheme 4: Extraction and purification of *Diplodia olivarium*, grown on Czapek medium, culture filtrate.



Scheme 5: Extraction and purification of *Diplodia olivarum*, grown on mineral salt medium, culture filtrate.

4.10.1 Olicleistanone (17)

Olicleistanone (Fig. 57, Page 100) was obtained as an amorphous solid and had: UV λ_{\max} (log ϵ) 333 (2.98), 241 (3.55) nm; IR ν_{\max} 1725, 1610, 1592, 1560, 1458 cm^{-1} ; ^1H and ^{13}C NMR data are reported in Table 12; ESIMS (+) spectrum m/z : 735 $[\text{2M} + \text{Na}]^+$, 395 $[\text{M} + \text{K}]^+$ and 311 $[\text{M} + \text{H} - \text{CH}_3\text{CH}_2\text{OH}]^+$; HRESIMS (+) spectrum m/z : 379.1876 $[\text{M} + \text{Na}]^+$ (calcd. for $\text{C}_{22}\text{H}_{28}\text{NaO}_4$ 379.1885).

4.10.2 Sphaeropsidin A (18)

Sphaeropsidin A (Fig. 57, Page 100), yielded as white crystals, had: $[\alpha]_{\text{D}}^{25} +104$ (c 0.4, MeOH) [lit. (Evidente *et al.*, 1996): $[\alpha]_{\text{D}}^{25} +109.6$ (c 0.2, MeOH)]; ^1H NMR data are in agreement with those previously reported (Evidente *et al.*, 1996); ESIMS (+) spectrum m/z : 715 $[\text{2M} + \text{Na}]^+$ and 369 $[\text{M} + \text{Na}]^+$; HRESIMS (+) spectrum m/z : 347.1820 $[\text{M} + \text{H}]^+$ (calcd. for $\text{C}_{20}\text{H}_{27}\text{O}_5$, 347.1780).

4.10.3 Sphaeropsidin C (19)

Sphaeropsidin C (Fig. 57, Page 100), obtained as a white solid, had: $[\alpha]_{\text{D}}^{25} +18.3$ (c 0.7, MeOH) [lit. (Evidente *et al.*, 1997c): $[\alpha]_{\text{D}}^{25} + 16.8$ (c 1.0, MeOH)]; ^1H NMR data agree with those previously reported (Evidente *et al.*, 1997c); ESIMS (+) spectrum m/z : 703 $[\text{2M} + \text{K}]^+$, 687 $[\text{2M} + \text{Na}]^+$ and 665 $[\text{2M} + \text{H}]^+$; HRESIMS (+) spectrum m/z : 333.2037 $[\text{M} + \text{H}]^+$ (calcd. for $\text{C}_{20}\text{H}_{29}\text{O}_4$ 333.2066).

4.10.4 Sphaeropsidin G (20)

Sphaeropsidin G (Fig. 57, Page 100) was yielded as an amorphous solid and had: $[\alpha]_{\text{D}}^{25} +48.6$ (c 0.8, CHCl_3) [lit. (Cimmino *et al.*, 2016): $[\alpha]_{\text{D}}^{25} +51.4$ (c 0.56, CHCl_3)]; ^1H NMR data agree with those previously reported (Cimmino *et al.*, 2016); ESIMS (+) spectrum m/z : 309 $[\text{M} + \text{K}]^+$, 293 $[\text{M} + \text{Na}]^+$, 271 $[\text{M} + \text{H}]^+$.

4.10.5 Diplopimarane (21)

Diplopimarane (Fig. 57, Page 100), yielded as white crystals, had: $[\alpha]_{\text{D}}^{25} +23.0$ (c 0.1, CHCl_3) [lit. (Andolfi *et al.*, 2014b): $[\alpha]_{\text{D}}^{25} +25.8$ (c 0.6, CHCl_3)]; ^1H NMR data are in agreement with those previously reported (Andolfi *et al.*, 2014); ESIMS (+) spectrum m/z : 623 $[\text{2M} - 4\text{H} + \text{Na}]^+$, 339 $[\text{M} - 2\text{H} + \text{K}]^+$, 325 $[\text{M} + \text{Na}]^+$, 323 $[\text{M} - 2\text{H} + \text{Na}]^+$.

4.10.6 (-)-Mellein (22)

(-)-Mellein (Fig. 57, Page 100), yielded as an amorphous solid, had: $[\alpha]_{\text{D}}^{25}$ -93.0 (c 0.3 MeOH) [lit. (Masi *et al.*, 2020): $[\alpha]_{\text{D}}^{25}$ -90 (c 0.2, MeOH)]; ^1H NMR data are agree with those previously reported (Masi *et al.*, 2020); ESIMS (+) spectrum m/z : 179 $[\text{M} + \text{H}]^+$.

4.11 Computational methods to determine the AC of olicleistanone

The absolute configuration (AC) of olicleistanone (**17**) was determined by molecular mechanics, Hartree-Fock (HF) and density functional theory (DFT) calculations performed with Spartan'18 (Wavefunction, Inc. 2018), with standard parameters and convergence criteria. The conformers of (7*S*,15*S*)-**17** and (7*S*,15*R*)-**17** were explored with the Monte Carlo algorithm using Merck molecular force field (MMFF), then they were screened by geometry optimizations at HF/3-21G level, single-point calculations at B3LYP/6-31G(d) level, and final geometry optimizations at the same level. Energies and populations were estimated at the B97M-V/6-311+G(2df,2p) level. This procedure provided six energy minima for (7*S*,15*S*)-**17** and ten minima for (7*S*,15*R*)-**17** within the final energy threshold (10 kJ mol⁻¹ at the B97M-V/6-31G(d) level). The GIAO method at the B3LYP/6-31G(d) level was used to calculate the ^{13}C NMR chemical shifts. An empirical correction was applied to each molecule depending on the number of bonds to the carbon and their bond lengths (Hehre *et al.*, 2019). 3J coupling constants were determined as Boltzmann averages of all the DFT structures described above, either with Karplus equations or at B3LYP/pcJ-0 levels (Fermi contact term only).

4.12 Biological assays on metabolites produced by *D. olivarum*

4.12.1 Leaf puncture assays

All compounds (**17-22**) were tested at 1.0 mg/mL on leaves of *Phaseolus vulgaris* L., *Juglans regia* L. and *Quercus suber* L. using the same procedure previously described (Andolfi *et al.*, 2014b). Each compound was dissolved in MeOH and then a stock solution with sterile distilled water was prepared. A droplet (20 μL) of test solution was applied on the adaxial sides of leaves that had previously been needle punctured. MeOH in distilled water (4%) was used as control. Each treatment was repeated three times. The leaves were kept in a moistened chamber to prevent the droplets from drying. Leaves were observed daily and scored for symptoms after 5 days, even if the effects of the toxins were observed up to 10 days. Lesions were estimated using APS Assess 2.0 software following the tutorials in the user's manual (Lamari 2002) and were expressed in mm².

4.12.2 Antifungal assays

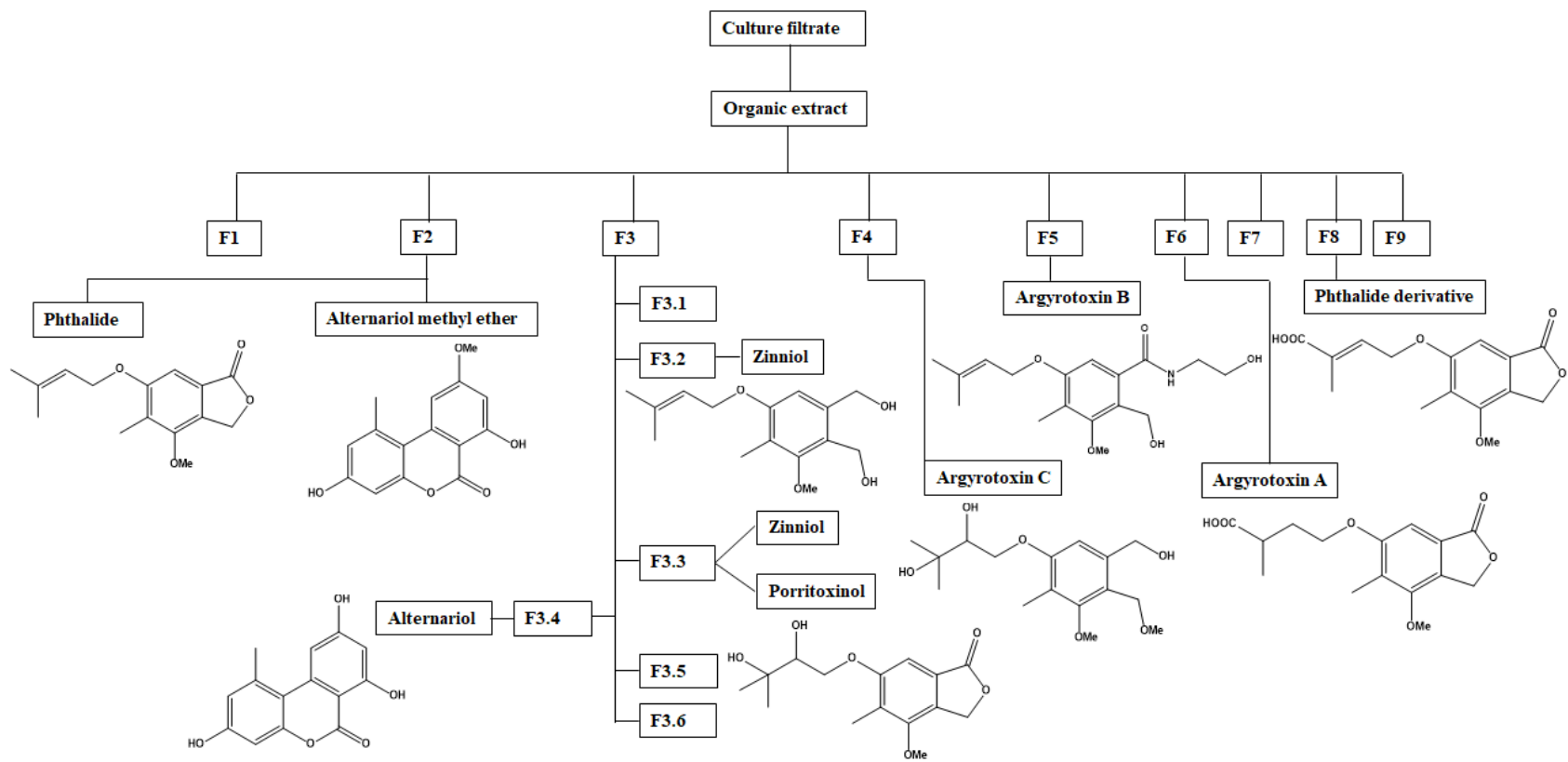
The metabolites (17-22) were preliminarily assayed on four different plant pathogens including the two fungi (*Athelia rolfsii* and *D. corticola*) and the two oomycetes (*Phytophthora cambivora* and *P. lacustris*). The sensitivity of four species to these compounds was estimated, depending on the species, on carrot agar (CA) or PDA, as inhibition of the mycelium radial growth. The assays were carried out as previously reported (Masi *et al.*, 2016b), testing each metabolite at 200 µg per plug. In brief, a flamed cork borer was used to cut mycelial plugs (6 mm diameter) from the margin of actively growing 4-day-old colonies. One plug was placed in the center of a 9 cm diameter Petri dish with the mycelia in contact with the medium and then 20 µL of the test solution, at different concentrations (50, 100, and 200 µg/plug), was applied on the top of each plug. MeOH was used as negative controls. The solvent was evaporated in a laminar flow cabinet and the plates were incubated at 20°C for 4–7 days, depending on the fungal species, until in the negative control the target fungi covered the plate's surface. Metalaxyl-M (mefenoxam; p.a. 43.88%; Syngenta), a synthetic fungicide to oomycetes, and PCNB (pentachloronitrobenzene), for ascomycetes and basidiomycetes, were used as positive controls. Each treatment consisted of three replicates and the experiment was repeated two times.

4.12.3 *Artemia salina* bioassays

The metabolites (17-22) were tested at 100 mg/mL on brine shrimp larvae (*Artemia salina* L.) in cell culture plates with 24 cells (Corning) as previously described (Favilla *et al.*, 2006). Brine shrimp eggs were hatched in Petri dishes containing artificial sea water (3.3% (wt/vol) marine salts in distilled water) and incubated in the dark at 27 °C for 36–48 h. The newly hatched brine shrimps (nauplii) were separated the others, transferred to fresh sea water and immediately used for bioassays. Each well contained 30–40 larvae in 500 µL of marine water. 5 µL of test solution of the toxins was transferred to the wells. Untreated control and 1% solvent control were assayed along with compound tests. Tests were performed in quadruplicate. The percentage (%) of larval mortality was determined after 36 h incubation at 27°C in the dark.

4.13 Production, extraction and purification of secondary metabolites from *Alternaria argyroxiphii* culture filtrates

Alternaria argyroxiphii was grown on liquid medium (Czapek amended with 2 % yeast extract and malt extract) at pH 5.7. The corresponding culture filtrates were extracted exhaustively with EtOAc at pH 4.0, yielding an oily brown residue (1.4 g). The organic extract was fractionated by CC on silica gel eluted with CHCl₃/*iso*-PrOH (9:1) obtaining 9 homogeneous fractions (F1-F9, Scheme 6). The residue (63.2 mg) of F2 was purified by preparative TLC eluted with *n*-hexane/EtOAc (7:3), yielding a metabolite identified as 6-(3',3'-dimethyallyloxy)-4-methoxy-5-methylphthalide (**27**, 7.3 mg, R_f 0.76) as an amorphous solid and another metabolite identified as alternariol methyl ether (**31**, 4.5 mg, R_f 0.50) as white solid. The residue (108.5 mg) of F3 was further fractionated by CC using CHCl₃/Me₂CO (8:2), obtaining six homogeneous fractions F3.1-F3.6. The residue (10.0 mg) of F3.2 was purified by TLC eluted with CHCl₃/MeOH (95:5), obtaining a metabolite identified as zinniol (**29**, 4.1 mg, R_f 0.43) as an amorphous solid. The residue (35.3 mg) of F3.3 was purified by preparative TLC using petroleum ether/Me₂CO (7:3) as eluent, affording further amount of zinniol (**29**, 4.6 mg, for a total of 8.7 mg) and another metabolite identified as porritoxinol (**26**, 17.4 mg, R_f 0.41) as an amorphous solid. The residue (43.7 mg) of F3.4 was purified by preparative TLC using CHCl₃/MeOH (9:1) as eluent, yielding a metabolite identified as alternariol (**30**, 15.0 mg, R_f 0.54) as an amorphous solid. The residue (32.4 mg) of F4 was purified by reverse phase TLC eluted with MeCN/H₂O (7:3), affording a new metabolite named argyrotxin C (**25**, 2.7 mg, R_f 0.58) as a yellow oil. The residue (32.6 mg) of F5 was purified by preparative TLC eluted with CHCl₃/MeOH (9:1), yielding a new metabolite named argyrotxin B (**24**, 1.9 mg, R_f 0.62) as an amorphous solid. The residue (64.7 mg) of F6 was purified by preparative TLC using CHCl₃/*iso*-PrOH (95:5) as eluent, obtaining a new metabolite named argyrotxin A (**23**, 3.5 mg, R_f 0.73) as an amorphous solid. The residue (36.6 mg) of F8 was purified by preparative TLC using CHCl₃/MeOH (9:1), obtaining a metabolite identified as phthalide carboxylic acid derivative (**28**, 10.0 mg, R_f 0.93) as an amorphous solid.



Scheme 6: Extraction and purification of *Alternaria argyroxiphii* culture filtrate.

4.13.1 Argyrotoxin A (23)

Argyrotoxin A (Fig. 64, Page 115) was afforded as an amorphous solid and had: UV λ_{\max} nm (log ϵ) 298 (3.2), 254 (3.6); IR ν_{\max} 3400, 1754, 1700, 1618, 1466, 1423, 1125 cm^{-1} ; ^1H and ^{13}C NMR data are reported in Table 15; ESIMS (+) spectrum m/z : 333 $[\text{M} + \text{K}]^+$, 295 $[\text{M} + \text{H}]^+$ and 277 $[\text{M} + \text{H} - \text{H}_2\text{O}]^+$; HRESIMS (+) spectrum m/z : 317.1010 $[\text{M} + \text{Na}]^+$ (calcd for $\text{C}_{15}\text{H}_{18}\text{NaO}_6$, 317.1001).

4.13.2 Argyrotoxin B (24)

Argyrotoxin B (Fig. 64, Page 115) was obtained as an amorphous solid and had: UV λ_{\max} nm (log ϵ) 291 (3.3), 254 (3.7); IR ν_{\max} 3409, 1660, 1620, 1561, 1453, 1424, 1124 cm^{-1} ; ^1H and ^{13}C NMR are in Table 16; ESIMS (+) spectrum m/z : 344 $[\text{M} + \text{K} - \text{H}_2\text{O}]^+$ and 306 $[\text{M} - \text{H}_2\text{O} + \text{H}]^+$; HRESIMS (+) spectrum m/z : 328.1534 $[\text{M} + \text{Na} - \text{H}_2\text{O}]^+$ (calcd for $\text{C}_{17}\text{H}_{23}\text{NNaO}_4$ 328.1525).

4.13.3 Argyrotoxin C (25)

Argyrotoxin C (Fig. 64, Page 115) was yielded as an amorphous solid and had: UV λ_{\max} nm (log ϵ) 273 (3.2); IR ν_{\max} 3369, 1605, 1582, 1456, cm^{-1} ; ^1H and ^{13}C NMR are present in Table 17; ESIMS (+) spectrum m/z : 353 $[2\text{M} + \text{K}]^+$ and 283 $[\text{M} + \text{H} - \text{MeOH}]^+$; HRESIMS (+) spectrum m/z : 337.1635 $[\text{M} + \text{Na}]^+$ (calcd for $\text{C}_{16}\text{H}_{26}\text{NaO}_6$ 337.1627).

4.13.4 Porritoxinol (26)

Porritoxinol (Fig. 64, Page 115), obtained as an amorphous solid, had: ^1H NMR data agree with those previously reported (Suemitsu *et al.*, 1994). ESIMS (+) spectrum m/z : 297 $[\text{M} + \text{H}]^+$.

4.13.5 6-(3',3'-Dimethallyloxy)-4-methoxy-5-methylphthalide (27)

6-(3',3'-Dimethallyloxy)-4-methoxy-5-methylphthalide (Fig. 64, Page 115), obtained as an amorphous solid, had: ^1H NMR data are in agreement with those previously reported (Suemitsu *et al.*, 1992). ESIMS (+) spectrum m/z : 263 $[\text{M} + \text{H}]^+$.

4.13.6 Phthalide derivative (28)

Phthalide derivative (Fig. 64, Page 115), yielded as an amorphous solid, had: ^1H NMR data are in agreement with those previously reported (Yang *et al.*, 2011). ESIMS (+) spectrum m/z : 315 $[\text{M} + \text{Na}]^+$.

4.13.7 Zinniol (29)

Zinniol (Fig. 64, Page 115), obtained as an amorphous solid, had: ^1H NMR data agree with those previously reported (White and Starrat, 1967). ESIMS (+) spectrum m/z : 289 $[\text{M} + \text{Na}]^+$.

4.13.8 Alternariol (30)

Alternariol (Fig. 64, Page 115) was yielded as an amorphous solid and had: ^1H NMR data are in agreement with those previously reported (Tan *et al.*, 2008). ESIMS (+) spectrum m/z : 259 $[\text{M} + \text{H}]^+$.

4.13.9 Alternariol methyl ether (31)

Alternariol methyl ether (Fig. 64, Page 115) was obtained as a white solid and had: ^1H NMR data agree with those previously reported (Tan *et al.*, 2008). ESIMS (+) spectrum m/z : 273 $[\text{M} + \text{H}]^+$.

4.14 Determination of AC of argyroxin A by electronic circular dichroism

The AC of argyroxin A (**23**) was determined through ECD by applying the biphenyl chiroptical probe approach to overcome its high molecular flexibility and the very weak chiroptical response. Compound **23** (1 equiv., 0.05 M), 1-[3-(dimethylamino)propyl]-3-ethylcarbodiimide hydrochloride (EDC.HCl) (1.7 equiv.) and *N,N'*-dimethylamino pyridine (DMAP) (1 equiv.) were added in sequence to a solution of the biphenylazepine **32** (1.25 equiv.) in anhydrous CH_2Cl_2 . The mixture of reaction was stirred overnight, then diluted with CH_2Cl_2 , washed with 10 % aqueous NaHCO_3 , brine and finally dried over anhydrous Na_2SO_4 . The solvent was evaporated under reduced pressure and the resulting residue was used without further purification. The UV and ECD spectra of **23** in CH_3CN solution were recorded in the range 180–350 nm.

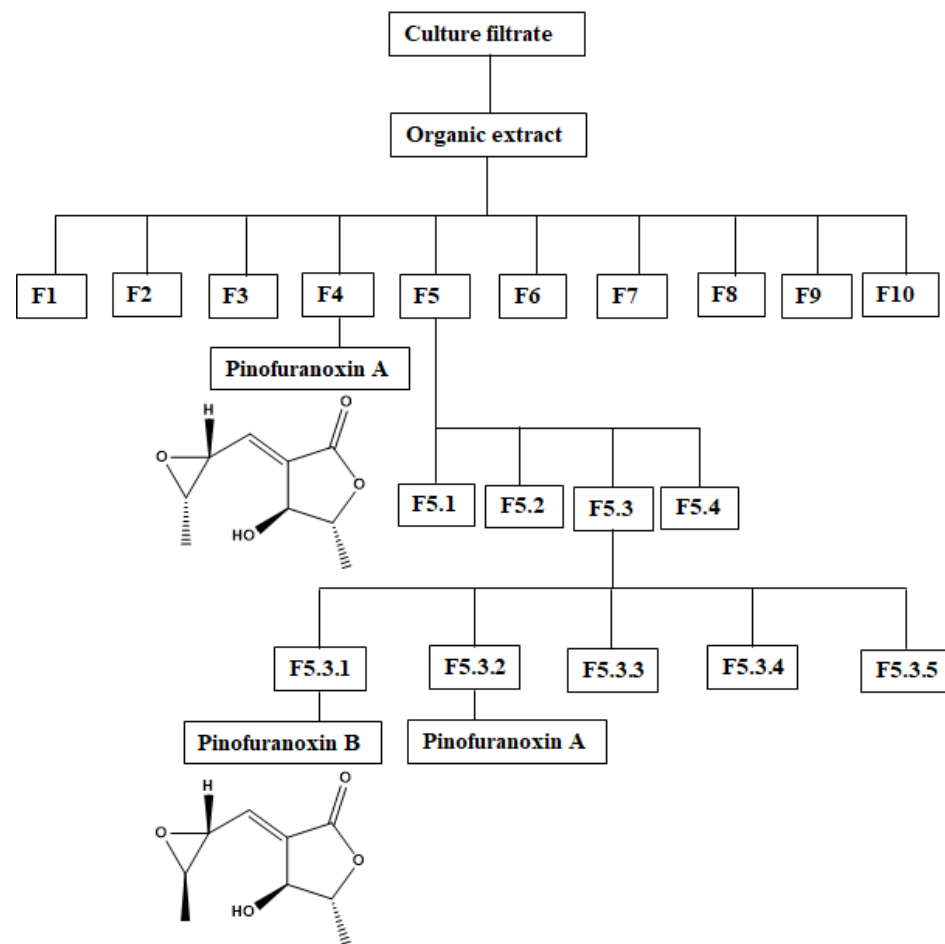
4.15 Leaf puncture assay of metabolites isolated from *A. argyroxiphii*

All compounds (**23–31**) were assayed at 1.0 mg/mL on young leaves of *Phaseolus vulgaris* L., *Hedera helix* L. and *Quercus ilex* L. Firstly the metabolites were dissolved in MeOH and then diluted distilled water to prepare a stock solution. A droplet (20 μL) of test solution was applied on the adaxial sides of leaves that had previously been needle punctured. MeOH in distilled water (4 %) were used as negative control. Each treatment was repeated three times. Leaves were observed daily and scored for

symptoms after 10 days, moreover the effect of the toxins on the leaves persisted up to 15 days. Lesions were estimated using APS Assess 2.0 software following the tutorials in the user's manual (Lamari 2002) and their size was expressed in mm².

4.16 Production, extraction and purification of secondary metabolites from *Diplodia sapinea* culture filtrates

Diplodia sapinea was grown on liquid medium (Czapek amended with 2% corn meal) at pH 5.7. The culture filtrates were extracted exhaustively with EtOAc, obtaining an oily brown residue (316 mg). The organic extract was fractionated by CC on silica gel eluted with CHCl₃/*iso*-PrOH (85:15), yielding 10 homogeneous fractions (F1-F10, Scheme 7). The residue (10.9 mg) of the F4 was purified by TLC eluted with *n*-hexane/EtOAc (1:1), affording an oily homogeneous compound named pinofuranoxin A (**32**, 3.4 mg, R_f 0.27). The residue (77.1 mg) of the F5 was further fractionated by TLC using *n*-hexane/CHCl₃/*iso*-PrOH (7:2:1), obtaining four fractions (F5.1-F5.4). The residue (33.5 mg) of F5.3 was fractionated by TLC using CHCl₃/*iso*-PrOH (98:2) as eluent, yielding five fractions (F5.3.1-F5.3.5). The residue of 5.3.1 was an oily homogeneous compound and was named pinofuranoxin B (**33**, 4.5 mg, R_f 0.14). The residue (15.6 mg) of F5.3.2 was purified by TLC eluted with *n*-hexane/EtOAc (1:1), affording a further amount of pinofuranoxin A (**32**, 12.5 for a total of 15.9 mg).



Scheme 7: Extraction and purification of *Diplodia sapinea* culture filtrate.

4.16.1 Pinofuranoxin A (31)

Pinofuranoxin A (Fig. 87, Page 147) was afforded as an amorphous solid and had: $[\alpha]_{25}^D +22.4$ (c 0.34, MeOH); UV λ_{\max} (log ϵ) 227 (4.1) nm; ECD (4.54×10^{-3} M, MeCN) λ_{\max} ($\Delta \epsilon$) 234 (+1.93), 263 (−0.39) nm; IR ν_{\max} 3393, 1725, 1654, 1266 cm^{-1} ; ^1H and ^{13}C NMR data are reported in Table 19; HRESIMS (+) spectrum m/z : 407.1111 $[2\text{M} + \text{K}]^+$, 391.1373 $[2\text{M} + \text{Na}]^+$, 373.1259 $[2\text{M} + \text{Na} - \text{H}_2\text{O}]^+$, 185.0823 $[\text{M} + \text{H}]^+$ (calcd for $\text{C}_9\text{H}_{13}\text{O}_4$ 185.0823), 167.0707 $[\text{M} + \text{H} - \text{H}_2\text{O}]^+$.

4.16.2 Pinofuranoxin B (32)

Pinofuranoxin B (Fig. 87, Page 147) was yielded as an amorphous solid and had: $[\alpha]_{25}^D +93.1$ (c 0.45, MeOH); UV λ_{\max} (log ϵ) 231 (4.3); ECD (4.37×10^{-3} M, MeCN) λ_{\max} ($\Delta \epsilon$) 231 (+4.36), 270 (−0.34) nm; IR ν_{\max} 3393, 1745, 1654, 1296 cm^{-1} ; ^1H and ^{13}C NMR data are reported in Table 19; HRESIMS (+) spectrum m/z : 407.1114 $[2\text{M} + \text{K}]^+$, 391.1369 $[2\text{M} + \text{Na}]^+$, 373.1260 $[2\text{M} + \text{Na} - \text{H}_2\text{O}]^+$, 185.0807 $[\text{M} + \text{H}]^+$ (calcd for $\text{C}_9\text{H}_{13}\text{O}_4$ 185.0823), 167.0712 $[\text{M} + \text{H} - \text{H}_2\text{O}]^+$.

4.17 Biological assays on metabolites produced by *D. sapinea*

4.17.1 Leaf Puncture Assay

Pinofuranoxins A and B (31 and 32) were assayed at 1.0, 0.5, and 0.1 mg/mL on young leaves of *Hedera helix* L., *Phaseolus vulgaris* L. and *Quercus ilex* L. The assay was performed using the procedure described by Andolfi *et al.* (2014b) and repeating the treatment three times. Leaves were observed daily and scored for symptoms after 5 days, even if the effect of the toxins persisted up to 10 days. Lesions were estimated using APS Assess 2.0 software following the tutorials in the user's manual (Lamari 2002) and the lesion size was expressed in mm^2 .

4.17.2 Antifungal Assays

Pinofuranoxins A and B (31 and 32) were preliminarily assayed on three plant pathogens, *Athelia rolfsii* (Curzi) C.C. Tu & Kimbr., *Diplodia corticola* A.J.L. Phillips, A. Alves & J. Luque, and *Phytophthora cambivora* (Petri) Buisman. The sensitivity of the three species to the compounds was evaluated, on carrot agar (CA) (*P. cambivora*) or PDA (*A. rolfsii* and *D. corticola*), as inhibitors of the mycelial radial growth. The assay was carried out as previously described (Masi *et al.*, 2016b), testing each metabolite at 200 and 100 $\mu\text{g}/\text{plug}$. MeOH was used as negative control. Metalaxyl-M (Mefenoxam; p.a. 43.88%; Syngenta), a synthetic fungicide for oomycetes, and PCNB for ascomycetes and basidiomycetes were used as positive controls. Each treatment consisted of three replicates and the experiment was repeated two times.

4.17.3 *Artemia salina* bioassays

The zootoxic effects of **31** and **32** were evaluated on brine shrimp larvae (*Artemia salina* L.), assaying the metabolites at 200, 100, and 50 µg/mL. The assay was performed in cell culture plates with 24 cells (Corning) as described by Favilla *et al.* (2006). The percentage (%) of larval mortality was evaluated after 36 h of incubation at 27 °C in the dark. Tests were carried out in quadruplicate.

5 RESULTS AND DISCUSSION

5.1 Structural identification of secondary metabolites isolated from *H. fraxineus* culture filtrates

The organic extract of *H. fraxineus* culture filtrate was purified as detailed in the Experimental section 4.1 (Scheme 1), obtaining five metabolites (1-5) that were isolated and characterized (Fig. 27). A new metabolite, named hyfraxinic acid (1), was isolated together with four known metabolites, 1-deoxyviridiol (2), viridiol (3), nodulisporiviridin M (4) and demethoxyviridiol (5). The already known metabolites were identified comparing their spectroscopic and specific optical data with those reported in literature: (Andersson *et al.*, 2012) for 1-deoxyviridiol (2), (Lumsden *et al.*, 1992) and (Del Bel *et al.*, 2017) for viridiol (3), (Wang *et al.*, 2018) for nodulisporiviridin M (4) and (Cole *et al.*, 1975) for demethoxyviridiol (5).

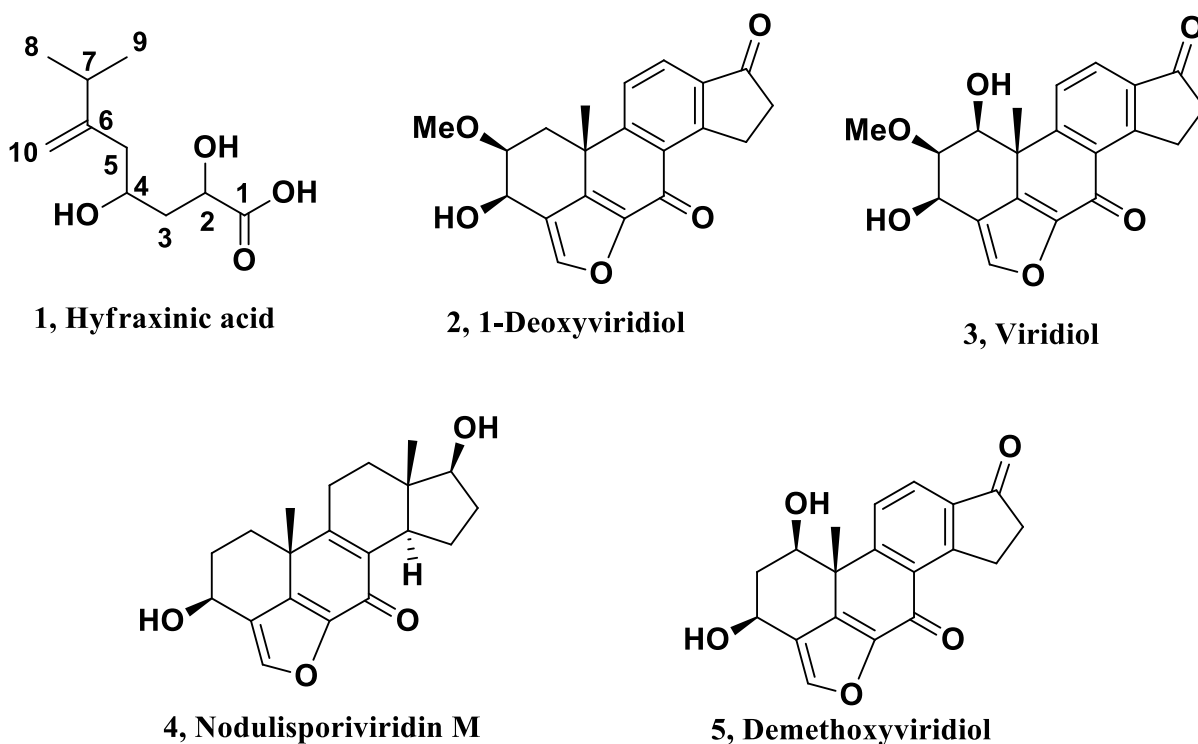


Figure 27: Secondary metabolites isolated from *Hymenoscyphus fraxineus*.

5.1.1 Structural determination of hyfraxinic acid

Hyfraxinic acid (**1**) has a molecular formula of $C_{10}H_{18}O_4$ as deduced from its HRESIMS and consistent with two hydrogen deficiencies. The IR spectrum presented the bands typical of hydroxyl, olefinic, and carboxy groups at ν_{\max} 3460, 1771, 1645 cm^{-1} (Nakanishi and Solomon, 1977). The UV spectrum showed only an end absorption (Pretsch *et al.*, 2000). The 1H NMR spectrum (Fig. 29, Table 1) presented two broad singlets at δ 4.95 and 4.84 typical of methylene olefinic protons (H₂-10), the typical signals of an isopropyl group as a doublet at δ 1.07, due to the overlapping of methyl group (Me-8 and Me-9, $J = 6.8$ Hz) signals, which, in the COSY spectrum (Fig. 30) (Berger and Braun, 2004), coupled with a septet at δ 2.26 (H-7, $J = 6.8$ Hz). The 1H spectrum (Fig. 29, Table 1) also showed two overlapped signals appearing as multiplets at δ 4.57, typical of secondary oxygenated carbons (H-4 and H-2). In the COSY spectrum (Fig. 30), one of these signals coupled with two double doublets at δ 2.62 and 2.37 ($J = 15.0$ and 7.1 Hz) of a methylene group (H₂-5), while the other one coupled with a doublet of double doublets at δ 2.74 ($J = 11.0, 8.3,$ and 5.2 Hz) and a double triplet at δ 1.93 ($J = 11.0$ and 9.7 Hz) which correspond to H-3A and H-3B, respectively (Pretsch *et al.*, 2000). Nine signals were present in the ^{13}C NMR spectrum (Fig. 31, Table 1), among them two appeared to be quaternary sp^2 carbons resonated at δ 177.1 and 150.0. The couplings observed in the HSQC spectrum (Fig. 32) (Berger and Braun, 2004) permitted to assign the signals resonating at δ 110.3, 76.8, 68.6, 40.1, 37.2, and 33.9 and the overlapped signals at δ 21.6 to the protonated carbons C-10, C-4, C-2, C-5, C-3, C-7, and Me-8 and Me-9, respectively. In the HMBC spectrum (Fig. 33, Table 1) (Berger and Braun, 2004) the long-range couplings observed between the carbon at δ 177.1 with H-2 and H₂-3 and the carbon at δ 150.0 with H₂-5 and H-7 allowed for the assignment of these signals at C-1 and C-6, respectively. Thus, all the chemical shifts were assigned to all carbons and corresponding protons as reported in Table 1 and hyfraxinic acid (**1**) was formulated as 2,4-dihydroxy-7-methyl-6-methyleneoctanoic acid.

Table 1: ^1H and ^{13}C NMR data of hyfraxinic acid (1**) and ^1H NMR data of its derivatives (**6** and **7**) recorded in $\text{CDCl}_3^{\text{a,b}}$**

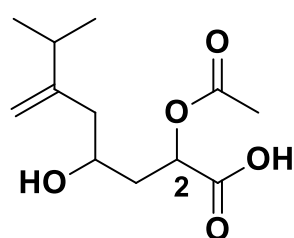
	1			6		7
Position	δ_{C}	δ_{H} (J in Hz)	HMBC	δ_{H} (J in Hz)	δ_{H} (J in Hz)	
1	177.1 s		H-2, H ₂ -3			
2	68.6 d	4.57 (2H) m ^c	H ₃ -3	5.51 (1H) dd (10.8, 8.6)	5.72 (1H) dd (10.6, 8.5)	
3	37.2 t	2.74 (1H) ddd (11.0, 8.3, 5.2) 1.93 (1H) dt (11.0, 9.7)	H ₂ -5	2.83 (1H) ddd (12.6, 8.6, 5.2) 1.94 (1H) dt (12.6, 10.8)	2.95 (1H) ddd (13.0, 8.5, 5.4) 2.08 (1H) dt (13.0, 10.6)	
4	76.8 d	4.57 (2H) m ^c	H ₂ -3, H ₂ -5	4.62 (2H) m	4.70 (2H) m	
5	40.1 t	2.62 (1H) dd (15.0, 7.1) 2.37 (1H) dd (15.0, 7.1)	H ₂ -3, H ₂ -10	2.66 (1H) dd (15.1, 6.6) 2.37 (1H) dd (15.1, 6.6)	2.71 (1H) dd (15.1, 6.6) 2.41 (1H) dd (15.1, 6.6)	
6	150.0 s		H ₂ -5, H-7			
7	33.9 d	2.26 (1H) septet (6.8)	H ₂ -5, H ₂ -10	2.26 (1H) septet (6.8)	2.28 (1H) septet (6.7)	
Me-8, Me-9 ^d	21.6 q	1.07 (6H) d (6.8)	H-7	1.07 (6H) d (6.8)	1.09 (6H) d (6.7)	
10	110.3 t	4.95 (1H) br s 4.84 (1H) br s	H ₂ -5, H-7	4.96 (1H) br s 4.83 (1H) br s	4.97 (1H) br s 4.85 (1H) br s	
COCH ₃				2.19 (3H) br s		
2', 6'					7.96 (2H) d (8.5)	
3', 5'					7.63 (2H) d (8.5)	

^aThe chemical shifts are in δ values (ppm) from TMS. ^b2D ^1H , ^1H (COSY) ^{13}C , ^1H (HSQC) NMR experiments delineated the correlations of all the protons and the corresponding carbons. ^cOverlapped signals. ^dOverlapped signals.

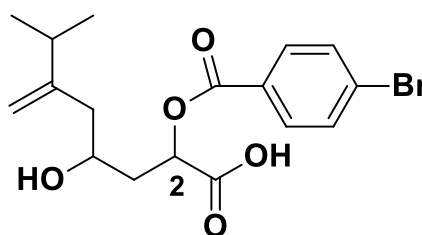
The different values observed for the coupling of H₂-3 with H-2 suggested a restricted freedom probably due to a hydrogen bond between the hydroxy group at C-4 and O=C-1. The ESIMS and HRESIMS data and all the couplings observed in the HMBC spectrum (Table 1) confirmed the structure assigned to compound **1**. In particular, the ESIMS spectrum showed the sodium dimer $[2\text{M} + \text{Na}]^+$ and the sodium cluster $[\text{M} + \text{Na}]^+$ at m/z 427 and 225, respectively; while the HRESIMS spectrum showed the pseudomolecular ion $[\text{M} + \text{H}]^+$ at m/z 203.1287.

The preparation of the corresponding 2-*O*-acetyl derivative (**6**; Fig. 28) and 2-*O-p*-bromobenzoyl derivative (**7**; Fig. 28) supported the structure assigned to compound **1**. In particular, in

the ^1H NMR spectrum of the acetyl derivative (Table 1) showed the expected downfield shifts ($\Delta\delta$ 0.94) of H-2 observed as a double doublet at δ 5.51 ($J = 10.8$ and 8.6 Hz) and the singlet of the acetyl group resonating at δ 2.19. Its ESIMS spectrum showed the pseudomolecular ion $[\text{M} + \text{H}]^+$ at m/z 245. In the ^1H NMR spectrum of the *p*-bromobenzoyl derivative (**7**; Table 1) a significant downfield shift of H-2 ($\Delta\delta$ 1.15), which resonated as a double doublet at δ 5.72 ($J = 11.0$ and 8.5 Hz), and a couple of doublets of the benzoyloxy residue at δ 7.96 and 7.63 ($J = 8.5$ Hz) were observed. The ESIMS spectrum showed the typical signals as a result of the presence of ^{81}Br and ^{79}Br isotopic peaks at m/z 387 $[\text{M} + 2 + \text{H}]^+$ and 385 $[\text{M} + \text{H}]^+$, respectively.



6, 2-*O*-Acetylhyfraxinic acid



7, 2-*O-p*-Bromobenzoyl ester of hyfraxinic acid

Figure 28: Structures of derivatives of hyfraxinic acid.

The acetylation and *p*-bromobenzoylation of HO-C2 (**6** and **7**) and not of HO-C4 confirmed the presence of the suggested hydrogen bond between HO-C4 and O=C-1.

All of the attempts carried out to assign the absolute configuration of **1** by either chiroptical (ECD) and computational methods or applying the advanced Mosher method (Cimmino *et al.*, 2017d) failed. Considering that the hydroxyl group at C-2 was acetylated and *p*-bromobenzoylated, probably the esters with both enantiomeric Mosher acids were not obtained due to the steric hindrance of the substituent linked to carbon α -located of Mosher's reagent.

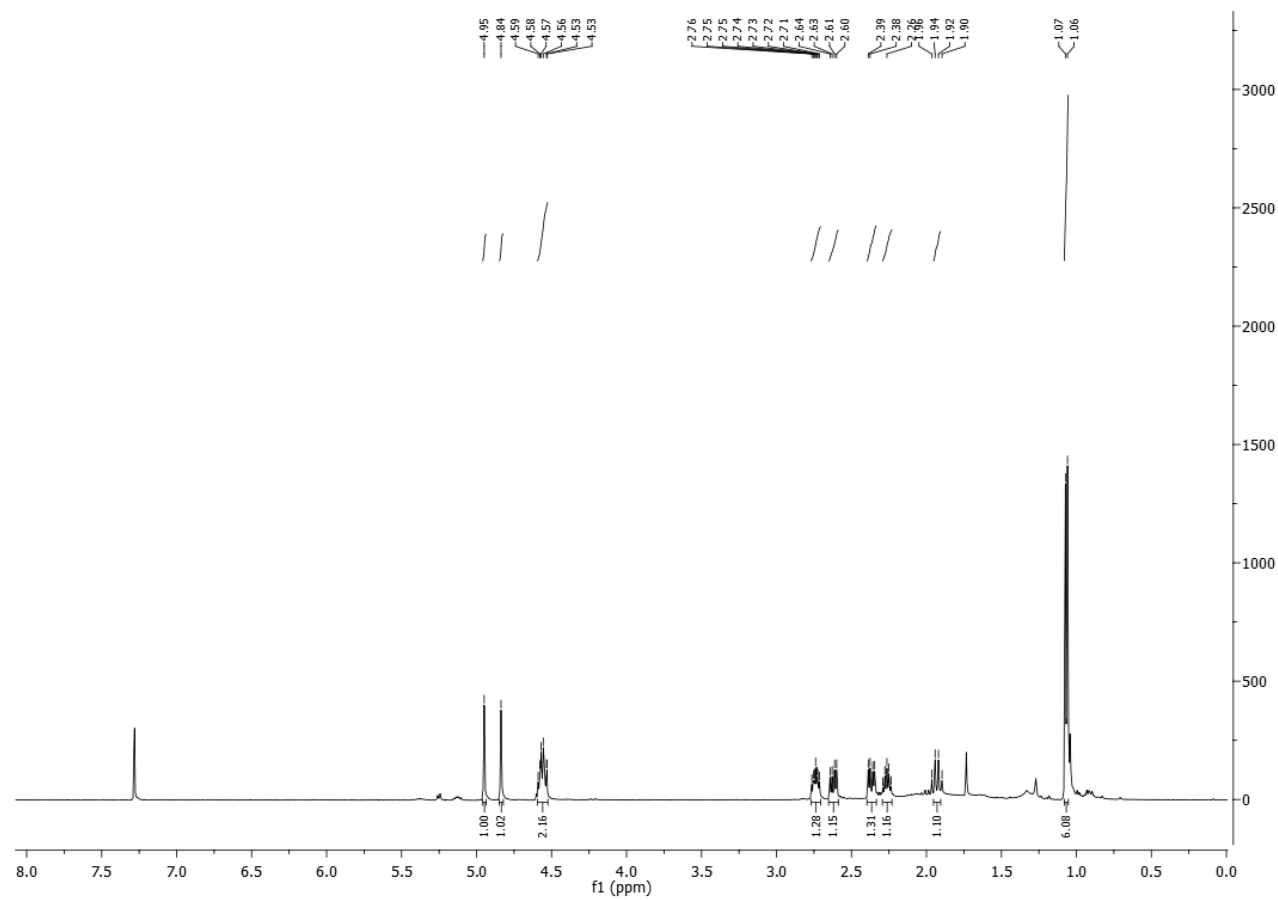


Figure 29: ^1H NMR spectrum of hyraxinic acid (1) (CDCl_3 , 500 MHz).

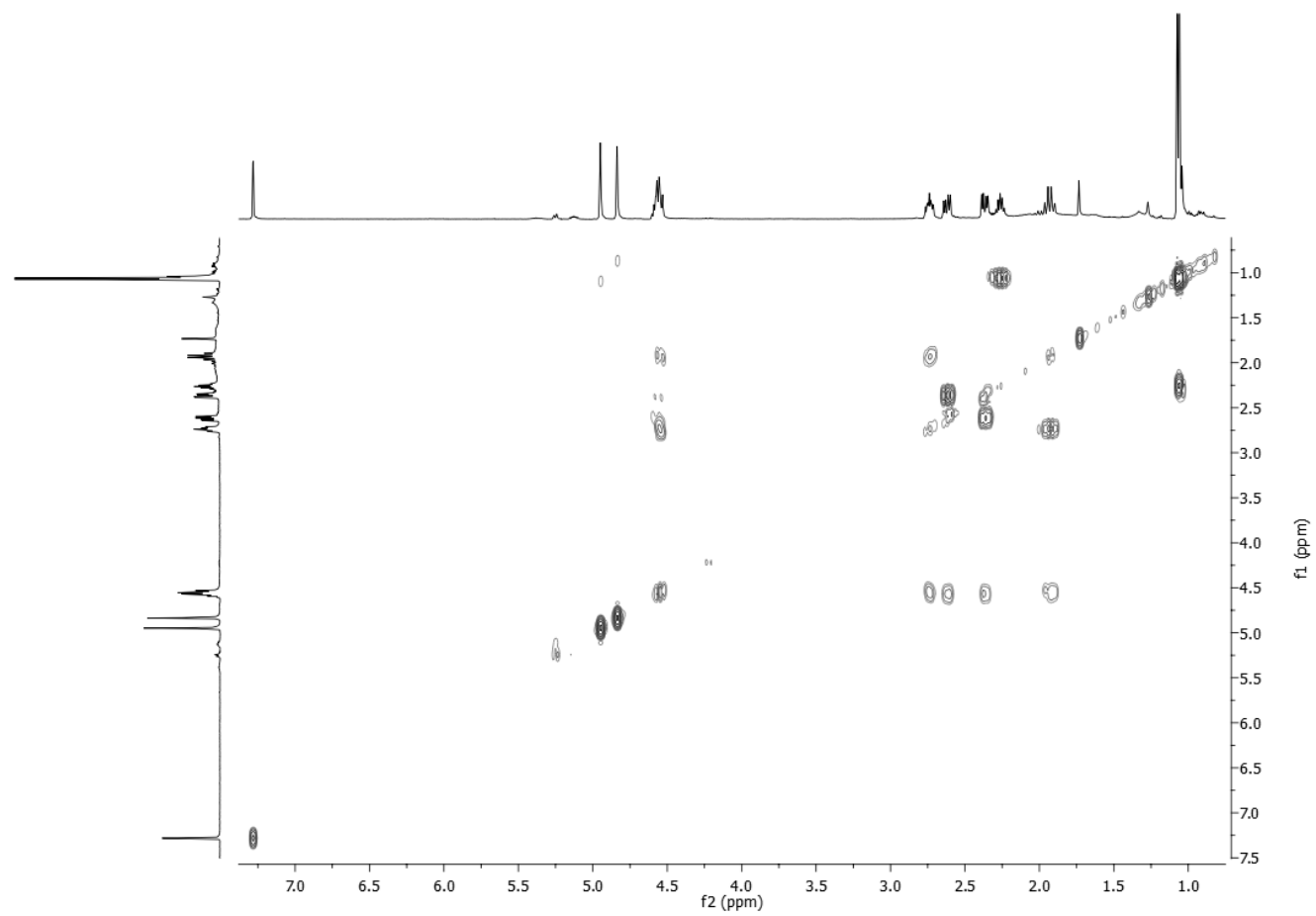


Figure 30: COSY spectrum of hyfraxinic acid (1) (CDCl₃, 500 MHz).

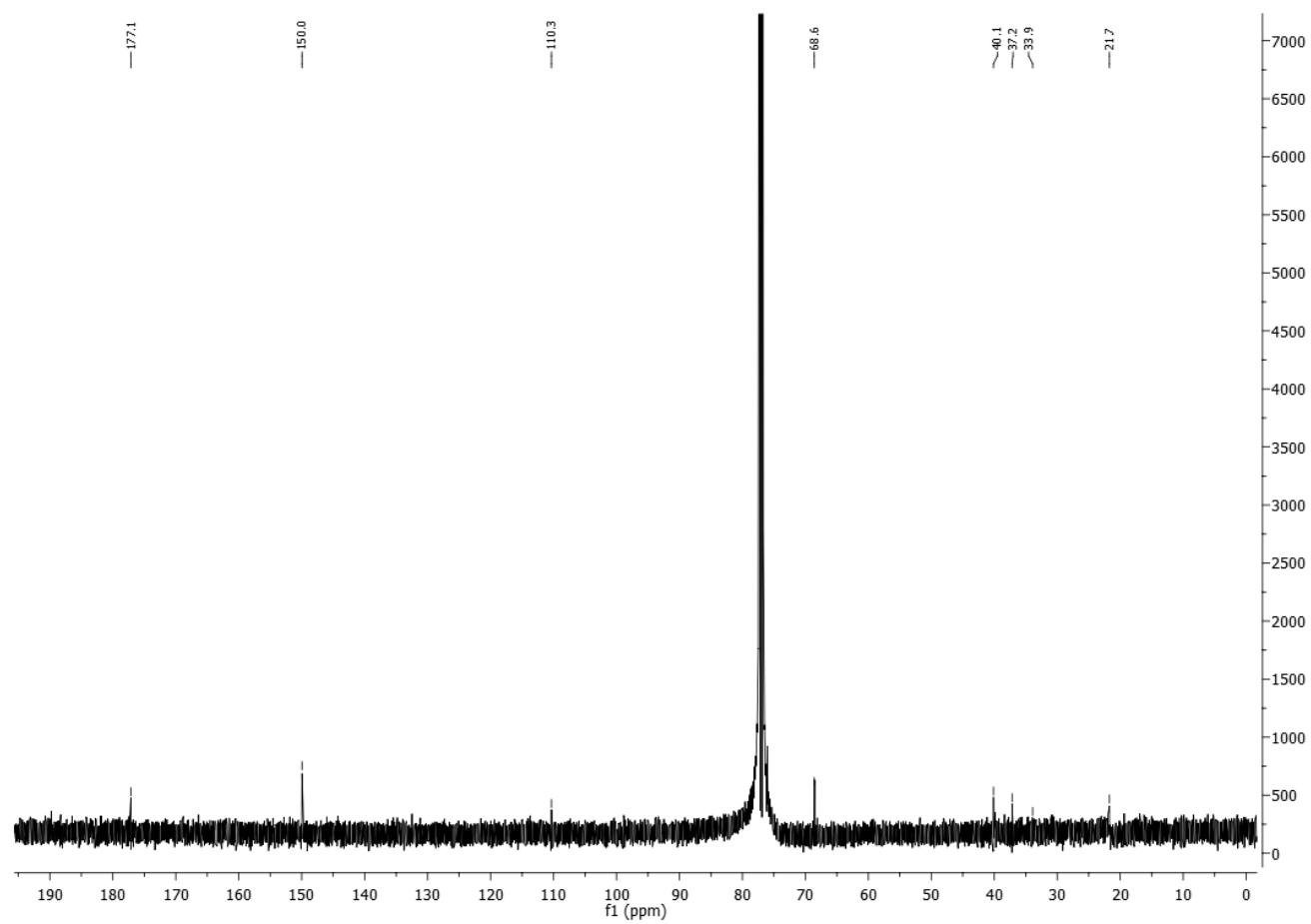


Figure 31: ^{13}C NMR spectrum of hyfraxinic acid (1) (CDCl_3 , 125 MHz).

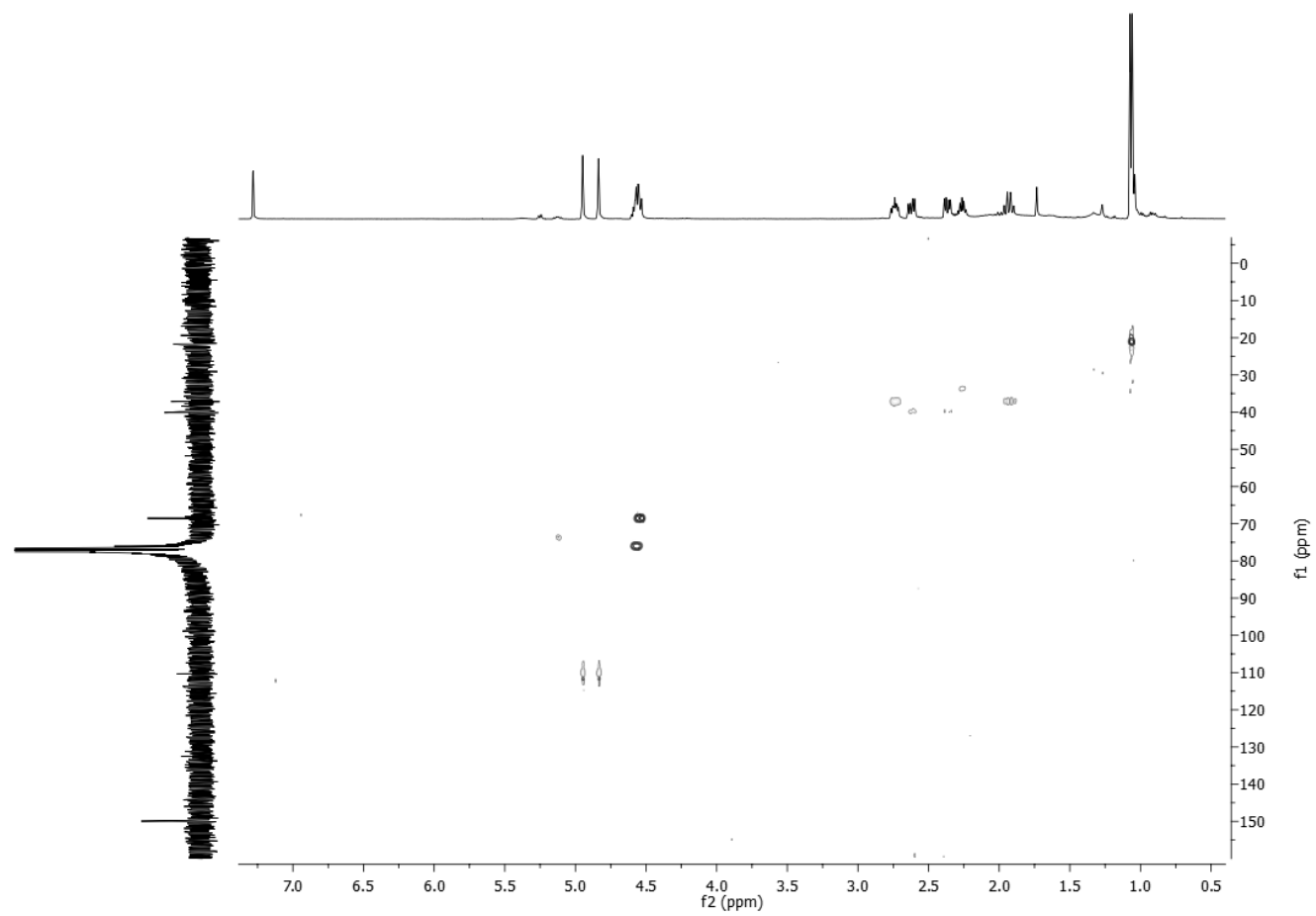


Figure 32: HSQC spectrum of hyfraxinic acid (1) (CDCl_3 , 500/125 MHz).

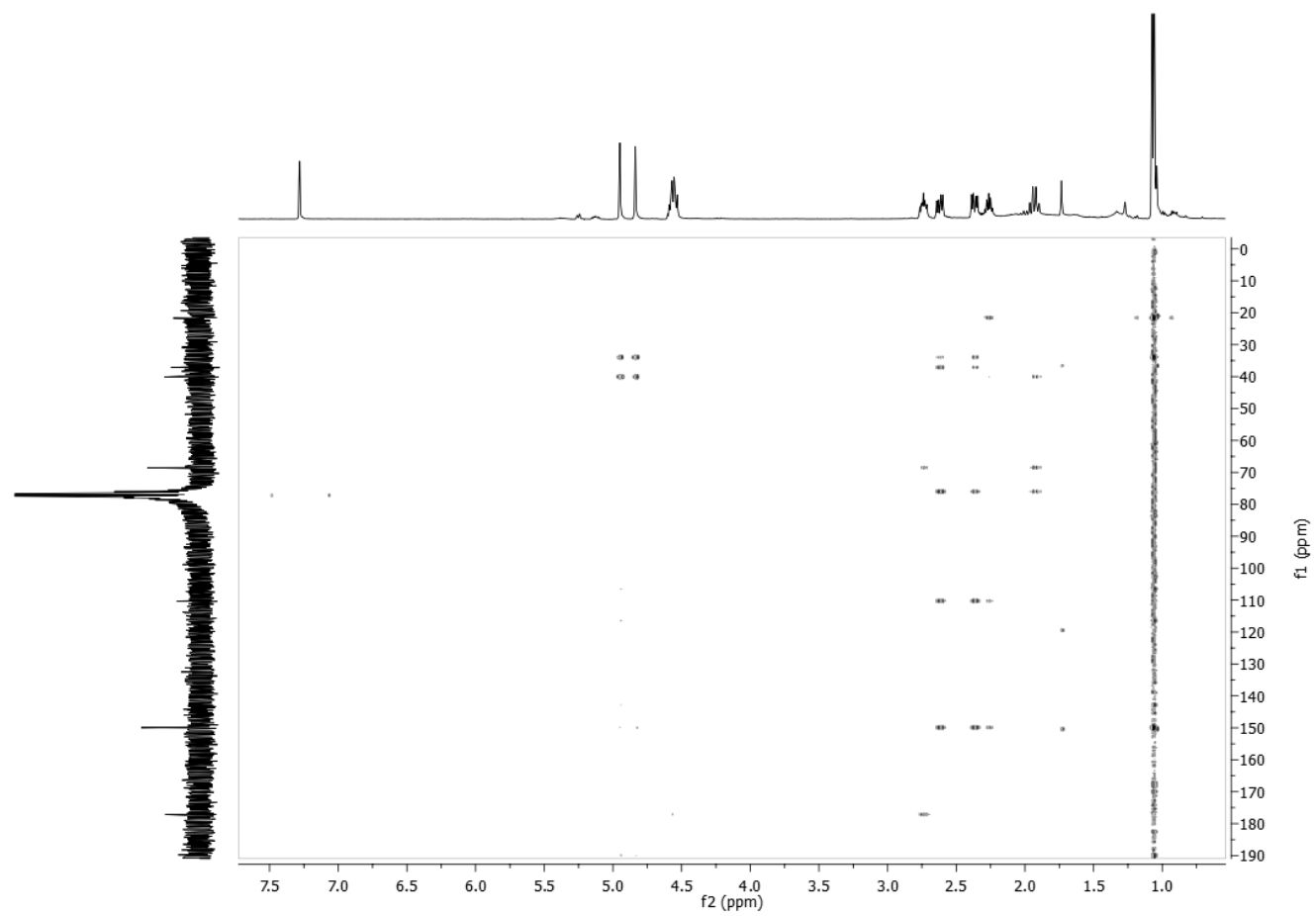


Figure 33: HMBC spectrum of hyfraxinic acid (1) (CDCl₃, 500/125 MHz).

5.1.2 Determination of relative and absolute configurations of 1-deoxyviridiol

1-Deoxyviridiol (**2**) is a known compound isolated from *H. pseudoalbidus* and its optical and spectroscopic data were similar to those reported in the literature (Andersson *et al.*, 2012). In the same article, its relative configuration was assigned by ROESY experiment and the absolute configuration was wrongly determined comparing the specific optical rotation to that of 1-deoxy-2-demethylviridiol. Thus, absolute configuration of **2** has not yet been determined.

Colorless block-shaped crystals of 1-deoxyviridiol (**2**) were obtained by slow evaporation of a EtOAc/MeOH (5:1) solution and they were analysed by X-ray diffraction confirming its structure and relative configuration. An ORTEP view **2** is shown in Figure 34. Crystal data and refinement details are reported in the Experimental section.

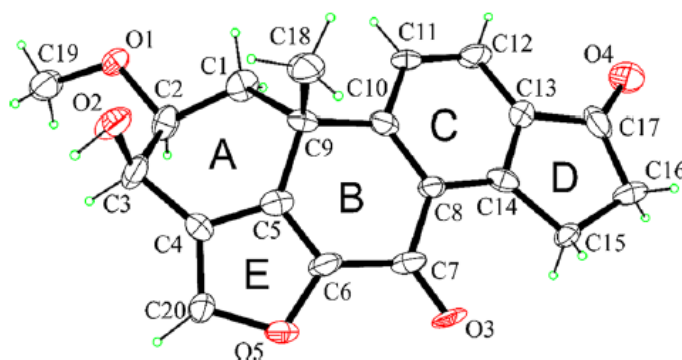


Figure 34: ORTEP view of the 1-deoxyviridiol (**2**) molecular structure, with ellipsoids drawn at the 30% probability level.

1-Deoxyviridiol crystallized in the P21 space group with 1 molecule in the independent unit. All bond lengths and angles were in the normal range and in agreement with similar compounds reported in literature (Neidle *et al.*, 1972; Aldridge *et al.*, 1975; Andersson *et al.*, 2013b). In the molecule, ring A presented the twist-boat conformation with methyl and hydroxy groups at the axial positions and methoxy group at the equatorial position. Ring B was in the envelope conformation with C-9 at the flap. Rings C and D were coplanar. Ring E was flat and quite coplanar with C-7/C-8/C-10 atoms of ring B. A nearly flat shape of the molecule was noted as a result of an approximately coplanarity of the condensed ring skeleton (Fig. 35).

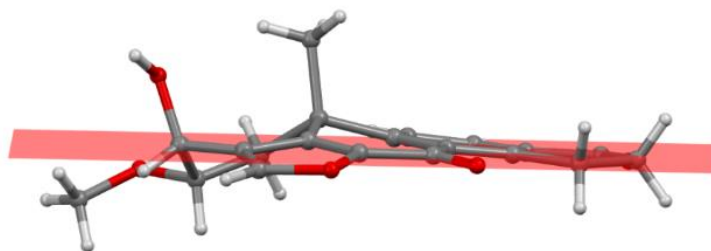


Figure 35: View of **2** showing the flat shape of the molecule with the mean plane of the condensed ring system shown as light-red plane.

The geometry of **2** was very similar to the known viridiol (Andersson *et al.*, 2013b), as shown by their superimposition in Figure 36, suggesting a high degree of rigidity in the condensed ring system of the molecule.



Figure 36: Superimposition of **2** (element color) molecule with viridiol (orange) molecule.

The crystal packing was dominated by strong intermolecular OH \cdots O-methoxy hydrogen bonds that form a monodimensional hydrogen-bonding pattern along the b axis direction. Weak CH \cdots O interactions contributed to stabilize the crystal packing (Fig. 37 and 38 and Table 2). Three stereogenic centers are present at C-2/C-3/C-9 carbon atoms with relative configuration 2*S**,3*R**,9*R**.

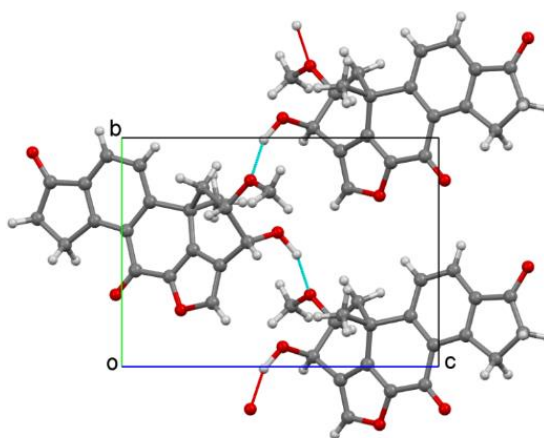


Figure 37: Partial packing of **2** with a chain of H-bonded molecules running parallel to the b axis direction. H-bonds are drawn as cyan dashed lines.

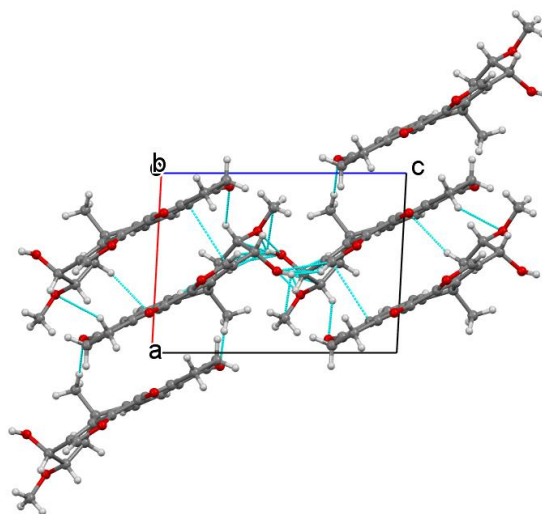


Figure 38: Crystal packing of **2** viewed along *b* axis. Contacts shorter than the sum of vdW radii are drawn as cyan dashed lines.

Table 2: Hydrogen bonds for **2** [Å and °]

D-H...A	d(D-H)	d(H...A)	d(D...A)	<(DHA)
C(1)-H(1B)...O(3)#1	0.97	2.60	3.493(19)	153.8
C(2)-H(2)...O(4)#2	0.98	2.61	3.37(2)	134.1
C(20)-H(20)...O(2)#3	0.93	2.27	3.052(19)	140.8
O(2)-H(2A)...O(1)#3	1.03(16)	1.81(16)	2.738(15)	147(13)

Symmetry transformations used to generate equivalent atoms:

#1 $-x+1, y+1/2, -z$ #2 $-x+1, y-1/2, -z$ #3 $-x+1, y-1/2, -z+1$

Considering the presence of a secondary hydroxyl group at C-3, its absolute configuration was determined applying the advanced Mosher method (Cimmino *et al.*, 2017d). Compound **2** was converted into the corresponding *S*-MTPA (**8**) and *R*-MTPA (**9**) monoesters at C-3 (Fig. 39) through the reaction with *R*-(-)- α -methoxy- α -trifluoromethyl- α -phenylacetyl (MTPA) and *S*-(+)-MTPA chlorides, respectively.

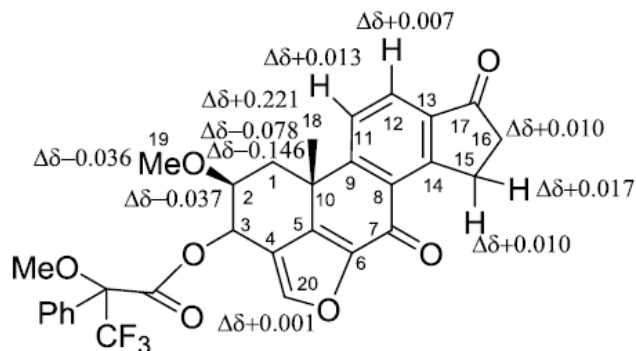


Figure 39: Structures of 3-*O*-*S*- and 3-*O*-*R*-MTPA of 1-deoxyviridol (8** and **9**, respectively), reporting the $\Delta\delta$ value obtained by comparison (**8** and **9**) of each proton system.**

The subtraction of the chemical shifts of the protons (Table 3) of compound **8** from those of compound **9** determined the $\Delta\delta$ values for all of the protons reported in Figure 30. According to the method (Cimmino *et al.*, 2017d), the negative $\Delta\delta$ values were located on the left-hand side and the positive values were located on the right-hand side of model A, this allowed to assign the *R* configuration at C-3. Thus, the absolute configuration of 1-deoxyviridol (**2**) was 2*S*,3*R*,9*R*.

Table 3: ¹H NMR data of 1-deoxyviridol (2**) and its derivatives (**8** and **9**) recorded in CDCl₃^a**

	2	8	9
Position	δ_{H} (<i>J</i> in Hz)	δ_{H} (<i>J</i> in Hz)	δ_{H} (<i>J</i> in Hz)
1	2.687 (1H) dd (14.1, 6.3) 2.431 (1H) dd (14.1, 6.3)	2.686 (1H) dd (14.1, 6.4) 2.234 (1H) dd (14.1, 6.4)	2.764 (1H) dd (14.2, 6.3) 2.380 (1H) dd (14.2, 6.3)
2	3.653 (1H) q (6.3)	3.476 (1H) q (6.4)	3.513 (1H) q (6.3)
3	5.044 (1H) br s	6.529 (1H) br s	6.407 (1H) br s
11	7.629 (1H) d (7.9)	7.560 (1H) d (7.8)	7.547 (1H) d (7.9)
12	7.981 (1H) d (7.9)	7.964 (1H) d (7.8)	7.957 (1H) d (7.9)
15	3.854 (1H) dt (19.9, 5.5) 3.713 (1H) dt (19.9, 5.5)	3.824 (1H) dt (19.9, 5.5) 3.686 (1H) dt (19.9, 5.5)	3.807 (1H) dt (19.9, 5.5) 3.676 (1H) dt (19.9, 5.5)
16	2.769 (2H) br s	2.780 (2H) br s	2.770 (2H) br s
18	1.800 (3H) br s	1.448 (3H) br s	1.227 (3H) br s
19	3.565 (3H) br s	3.435 (3H) br s	3.471 (3H) br s
20	7.805 (1H) br s	7.863 (1H) br s	7.862 (1H) br s
OH-3	3.095 (1H) br s		

^aThe chemical shifts are in δ values (ppm) from TMS.

5.1.3 Novel data for nodulisporiviridin M and demethoxyviridiol

Nodulisporiviridin M (**4**) was previously isolated from *Nodulisporium* sp. Its ^1H and ^{13}C spectra, HRESIMS and ECD data were in agreement with those reported in the literature (Wang *et al.*, 2018). Although, this is the first isolation from *H. fraxineus* and its optical rotation was reported for the first time as illustrated in the Experimental section.

Demethoxyviridiol (**5**) is an already known metabolite isolated from *Nodulisporium hinnuleum* and *H. fraxineus*. Its ^1H and ^{13}C spectra and HRESIMS data were in agreement with those reported in the literature (Aldridge *et al.*, 1975; Cole *et al.*, 1975; Andersson *et al.*, 2012). Its optical rotation was reported for the first time as illustrated in the Experimental section.

5.1.4 Leaf puncture assay

The phytotoxic activity of all isolated compounds (**1–5**) were tested by the leaf puncture bioassay on *C. australis* L., *Q. suber* L., *H. elix* L., *J. regia* L., and *F. angustifolia* L. young leaves. Viridiol (**3**) is a well-known phytotoxin and it was included in the assay to compare its activity to that of the other isolated metabolites. Compounds **2** and **4** were inactive in this bioassay at both concentrations used. The toxic effect of the other compounds (**1**, **3**, and **5**) are presented in Table 4. They induced necrotic lesions, sometimes surrounded by a chlorotic halo, at both concentrations tested.

Table 4: Phytotoxicity data for hyfraxinic acid (1), viridiol (3), and demethoxyviridiol (5).^a

Compound	Concentration (mg/mL)	<i>Juglans regia</i>	<i>Celtis australis</i>	<i>Hedera helix</i>	<i>Fraxinus angustifolia</i>	<i>Quercus suber</i>
1	1.0	296.9 ± 10.2	102.6 ± 29.4	117.4 ± 11.2	51.5 ± 51.5	42.7 ± 3.4
	0.5	67.7 ± 7.6	42.6 ± 5.3	46.0 ± 4.4	23.9 ± 5.6	19.3 ± 1.2
3	1.0	127.1 ± 26.2	69.5 ± 15.1	50.8 ± 5.2	20.1 ± 1.0	30.4 ± 6.1
	0.5	63.8 ± 12.6	20.6 ± 4.3	22.9 ± 4.6	16.4 ± 6.4	16.4 ± 2.0
5	1.0	210.5 ± 12.1	30.5 ± 1.8	54.4 ± 7.2	205.2 ± 46.2	20.9 ± 1.8
	0.5	25.9 ± 5.1	6.1 ± 0.3	22.1 ± 1.7	53.0 ± 6.4	14.5 ± 1.0

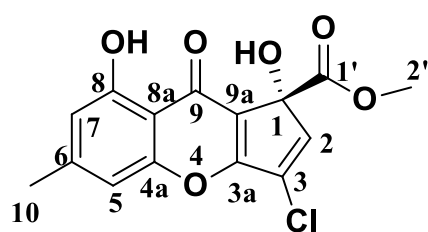
^aThe compounds were tested at concentrations of 1 and 0.5 mg/mL. Data are expressed as the median area lesions ± standard error (mm²).

Hyfraxinic acid (**1**) caused the most extensive necrosis on four of five plant species tested at 1.0 mg/mL. In particular, area lesion sizes ranged from 296.9 mm² on *J. regia*, to 117.4 mm² on *H. helix*, to 102.6 mm² on *C. australis*, to 51.5 mm² on *F. angustifolia*, and to 42.7 mm² on *Q. suber*. At this concentration, demethoxyviridiol (**5**) showed the most toxic effect on ash tree leaves. The same result was obtained at the lower concentration of 0.5 mg/mL. In addition, hyfraxinic acid exhibited similar activity to viridiol on *J. regia* (area lesion sizes of 67.7 and 63.8 mm², respectively).

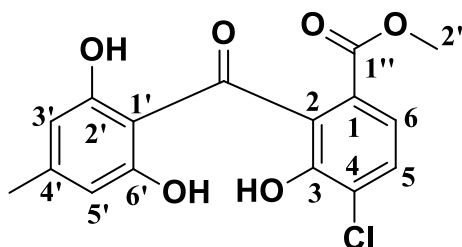
A structure-activity relationship (SAR) study was carried out. Considering these results, a central role for the phytotoxic activity was explained by the hydroxyl group present at C-1 in compounds **3** and **5**, in fact its absence in compounds **2** and **4** determined their complete inactivity in the leaf puncture assay. Whereas, the presence of a methoxy group at C-2 did not contribute to the phytotoxicity because it is present in the compounds **2** and **3**.

5.2 Structural identification of secondary metabolites isolated from *F. rabenhorstii* culture filtrates

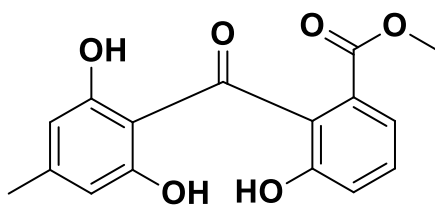
The EtOAc extract of *F. rabenhorstii* culture filtrates was fractionated and purified as detailed in the Experimental section 4.4 (Scheme 2), yielding four metabolites (**10-13**; Fig. 40) a new tetrasubstituted chromenone and a new hexasubstituted benzophenone, named rabenchromenone and rabenzophenone, respectively (**10** and **11**; Fig. 40) and two already known compounds, which were identified as moniliphenone and coniochaetone A (**12** and **13**; Fig. 40). The last two metabolites were identified comparing their specific optical properties and spectroscopic data with those previously reported in literature: (Kachi and Sassa; 1986) for moniliphenone (**12**) and (Wang *et al.*, 1995) for coniochaetone A (**13**).



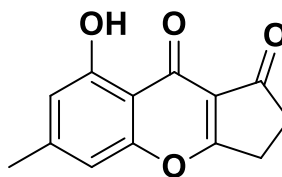
10, Rabenchromenone



11, Rabenzophenone



12, Moniliphenone



13, Coniochaetone A

Figure 40: Secondary metabolites isolated from *Fimetariella rabenhortstii*.

Moniliphenone (**12**) was isolated for the first time from *Monilia fructicola*, as an intermediate of chloromonilicin biosynthesis (Kachi and Sassa; 1986), and then from several other terrestrial and marine fungi, such as *Coniochaeta* sp. (Wang *et al.*, 2010), *Hypocreales* sp. (Ayers *et al.*, 2012),

Aspergillus sydowii (Song *et al.*, 2013), *Leptosphaeria* sp. (Lin *et al.*, 2017) and *Penicillium* spp (Guo *et al.*, 2020).

Coniochaetone A (**13**) was isolated for the first time together with coniochaetone B from *Coniochaeta saccardoi* (Wang *et al.*, 1995), as an antifungal metabolite, and successively it was produced by *Fimetariella* sp. (S207) together with the new cheniochaetones E–I and coniochaetone B (Deng *et al.*, 2013).

5.2.1 Structural determination of rabenchromenone

Rabenchromenone (**10**) has a molecular formula of C₁₅H₁₁ClO₆ as determined from its HRESIMS, consistent with 10 indices of hydrogen deficiencies. Its IR spectrum presented bands typical of aromatic, hydroxy, olefinic, and carbonyl groups at ν_{\max} 3423, 1742, 1654, 1618, 1596, 1462 cm⁻¹ (Nakanishi and Solomon, 1977). The UV spectrum showed absorption maxima at λ_{\max} (log ϵ), 341 (3.80), 272 (4.46) nm due to the presence of extended conjugated chromophores (Pretsch *et al.*, 2000). These results were in agreement with the initial investigation of its ¹H and ¹³C NMR data (Table 5). The ¹H NMR spectrum (Fig. 41, Table 5) and COSY spectrum (Fig. 42) showed a singlet typical of a hydrogen-bonded phenolic hydroxy group at δ 12.11, two broad singlets typical of two meta-coupled ($J < 1$ Hz) aromatic protons at δ 6.89 (H-7) and 6.70 (H-5), and two other singlets typical of a vinyl methyl (Me-10) and methoxy group at δ 2.43 and 3.79, respectively (Pretsch *et al.*, 2000). The ¹³C NMR spectrum (Fig. 43, Table 5) presented two carbonyls, one of a conjugated ketone and the other one of an ester group, three sp² methines, a vinyl methyl, a methoxy, seven quaternary sp² carbons, three of which appeared to be oxygenated, and one quaternary sp³ hydroxylated carbon. Hydrogenated carbons were assigned by the couplings observed in the HSQC spectrum (Fig. 44). The signals at δ 139.2, 113.7, 108.2, 54.1, and 22.2 were assigned to C-2, C-7, C-5, the methoxy group, and methyl (Me-10) at C-6 (Berger and Braun, 2004). Carbonyl signals at δ 176.4 and 170.5 were assigned to C-9 and C-1' by the long-range correlations observed in the HMBC spectrum (Fig. 45, Table 5) between C-1' and the methoxy group. The remaining quaternary carbons were assigned considering that in the HMBC spectrum (Fig. 45, Table 5), C-1, C-3, C-3a, and C-9a coupled with H-2, C-4a and C-8a coupled with H-7, and C-6 with H-10. Thus, the signals resonating at δ 164.7, 156.3, 147.1, 127.1, 119.3, 109.3, and 79.6 were assigned to C-3a, C-4a, C-6, C-3, C-9a, C-8a, and C-1. The quaternary signal at δ 161.0 was assigned to carbon C-8 linked to the phenolic hydroxy group (Breitmaier and Voelter, 1987). The benzyl methyl (Me-10) was positioned at C-6 due to the couplings between C-10 and H-5 and H-7. Consequently, the chlorine was located at C-3. Thus, all chemical shifts were assigned to all carbons and corresponding protons (Table 5) and rabenchromenone (**10**) was formulated as methyl-3-chloro-1,8-dihydroxy-6-methyl-9-oxo-1,9-dihydrocyclopenta[b]-chromene-1-carboxylate.

Table 5: ¹H and ¹³C NMR data of rabenchromenone (10)^{a,b}

position	δ_C^c	δ_H (<i>J</i> in Hz)	HMBC
1	79.9 s		H-2
2	139.3 d	6.65 s (1H)	
3	127.2 s		H-2
3a	164.8 s		H-2
4a	156.4 s		H-7
5	108.3 d	6.70 br s (1H)	H ₃ -10
6	147.2 s		H ₃ -10
7	113.8 d	6.89 br s (1H)	H ₃ -10
8	161.1 s		
8a	109.4 s		H-7
9	176.5 s		
9a	119.4 s		H-2
10	22.3 q	2.43 s (3H)	H-5, H-7
1'	170.6 s		H ₃ -2'
2'	54.1 q	3.79 s (3H)	
OH		12.08 s	

^aThe chemical shifts are in δ values (ppm) from TMS. ^b2D ¹H, ¹H (COSY) ¹³C, ¹H (HSQC) NMR experiments delineated the correlations of all the protons and the corresponding carbons. ^cMultiplicities were assigned by DEPT spectrum.

The structure of compound **10** was confirmed by the data of its HRESIMS spectrum, which showed the potassium [2M + K]⁺ and sodium [2M + Na]⁺ dimers, the sodium [M + Na]⁺ and the protonated [M + H]⁺ adducts ions at *m/z* 683.0139, 667.0417, 345.0155, and 323.0334, respectively. The same spectrum showed the typical isotopic peaks of ³⁷Cl at *m/z* 685.0119, 669.0384, 347.0126, and 325.0113.

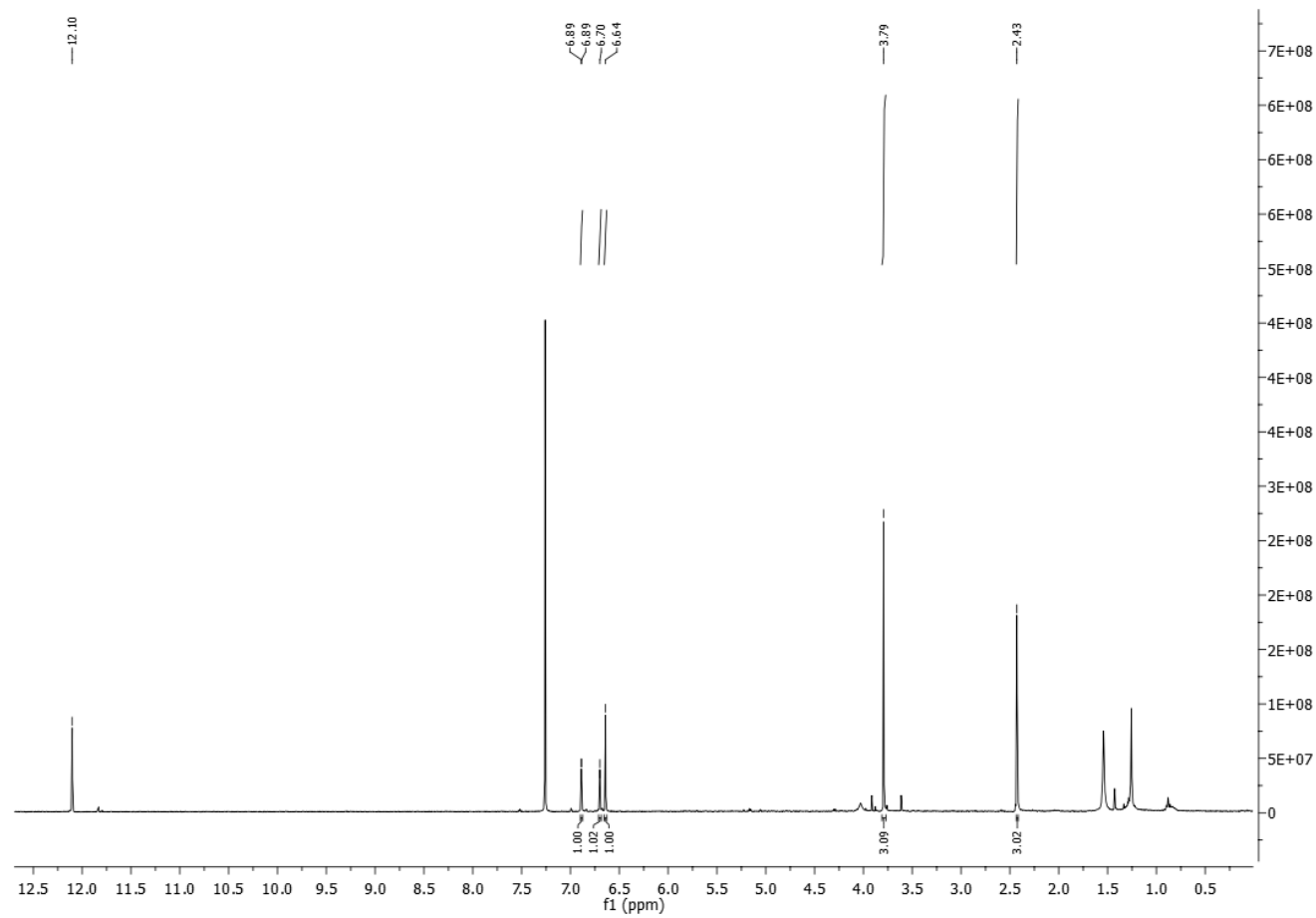


Figure 41: ^1H NMR spectrum of rabenchromenone (10) (CDCl_3 , 500 MHz).

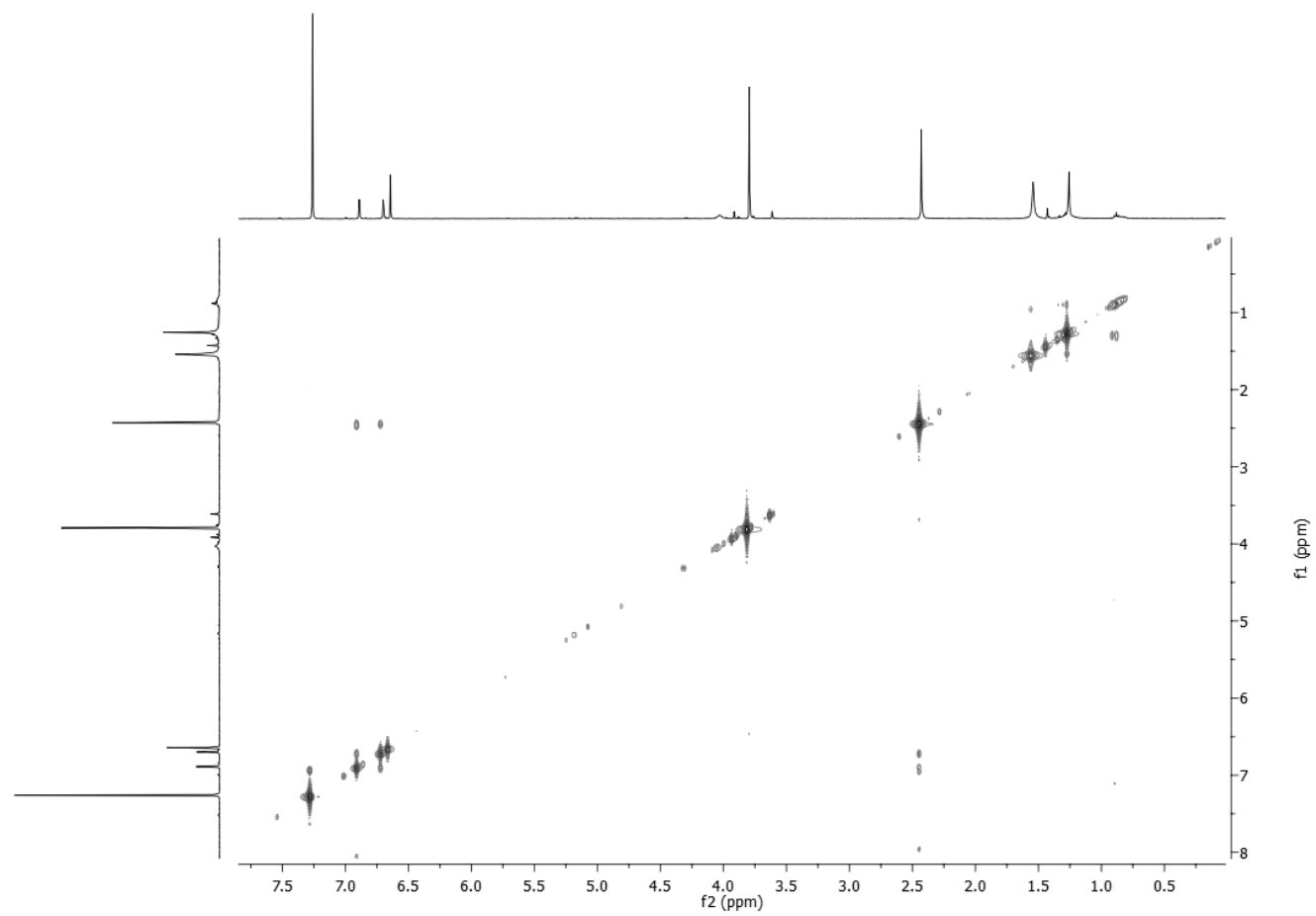


Figure 42: COSY spectrum of rabenchromenone (10) (CDCl₃, 500 MHz).

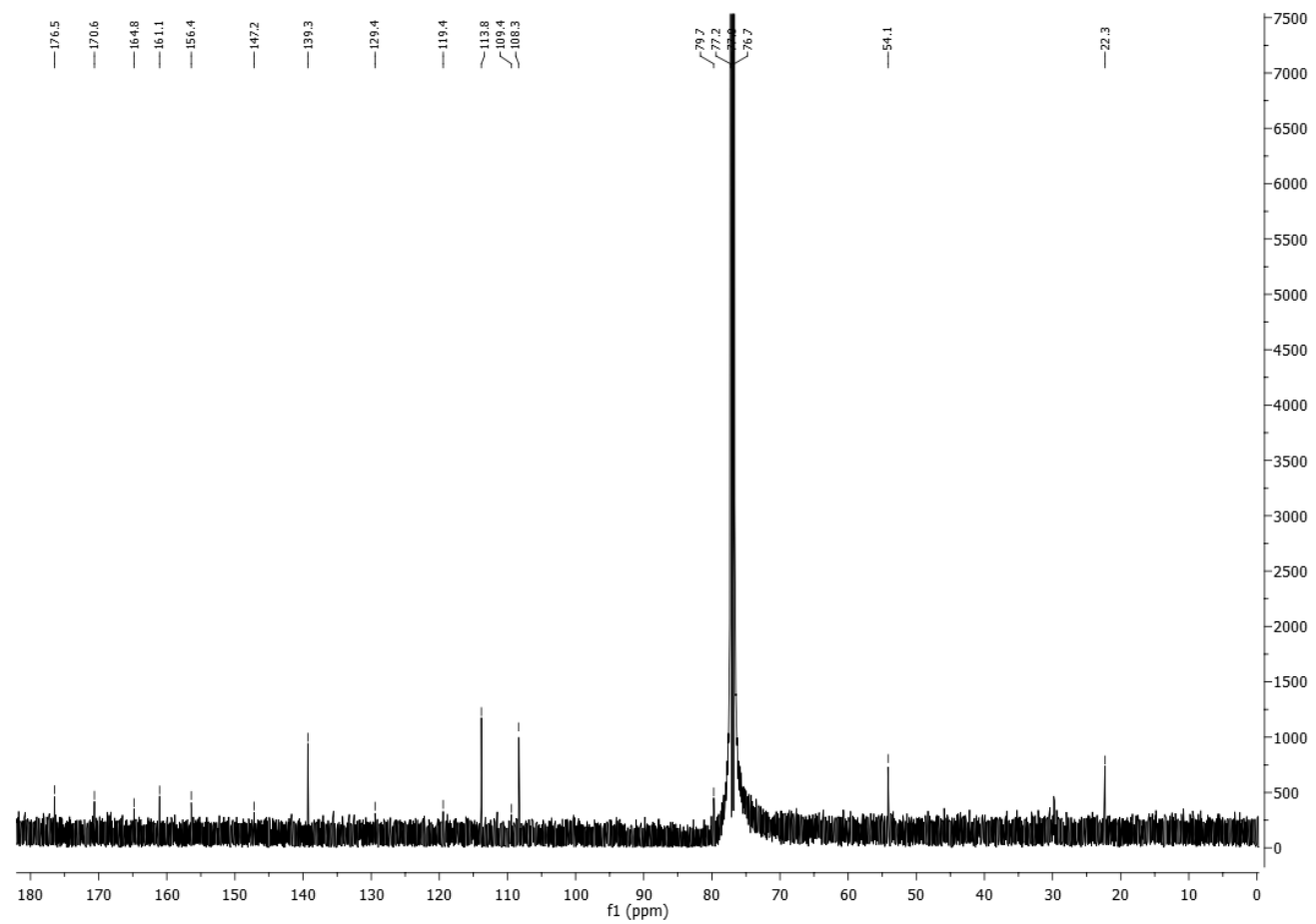


Figure 43: ^{13}C NMR spectrum of rabenchromenone (10) (CDCl_3 , 125 MHz).

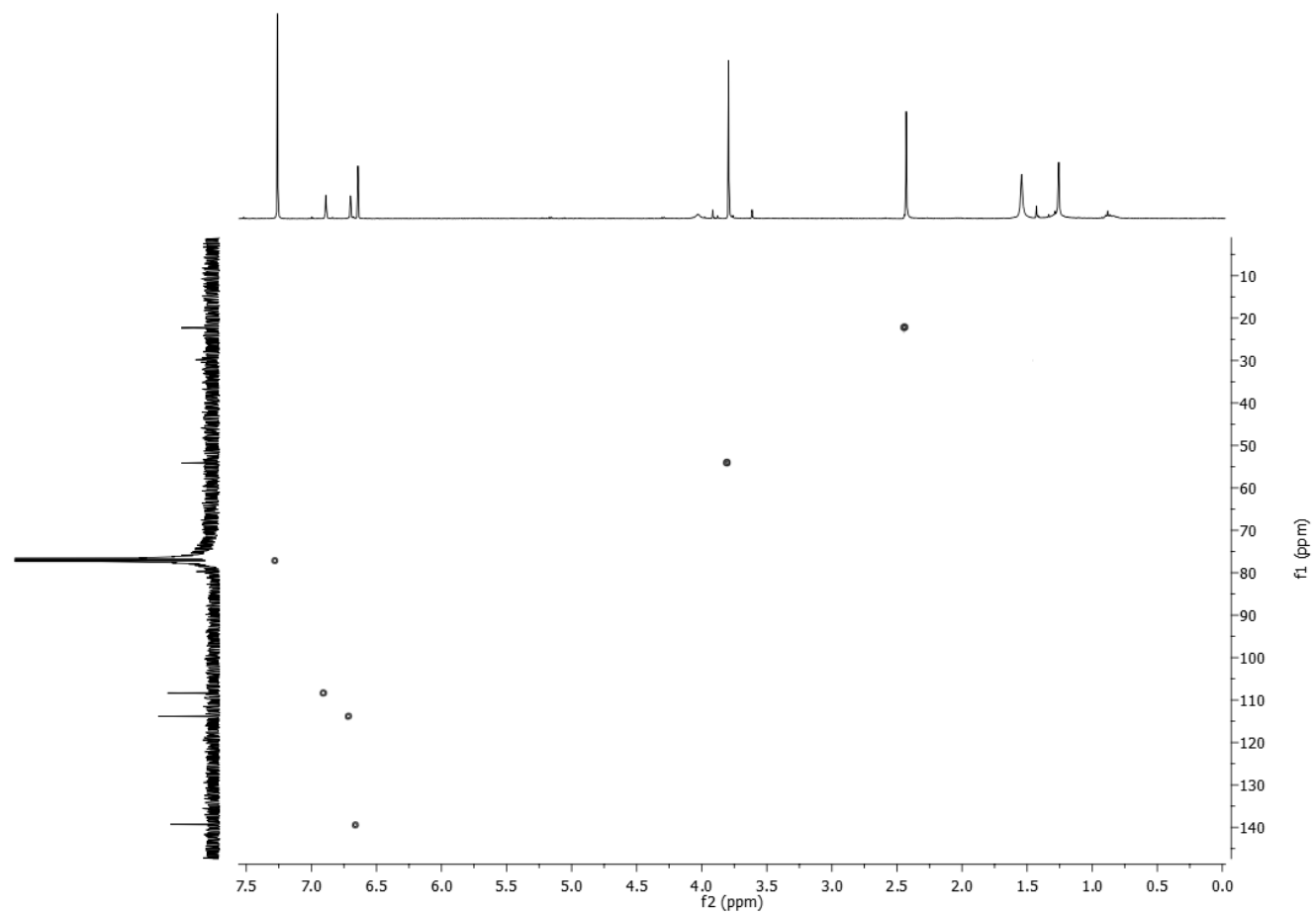


Figure 44: HSQC spectrum of rabenchromenone (10) (CDCl₃, 500/125 MHz).

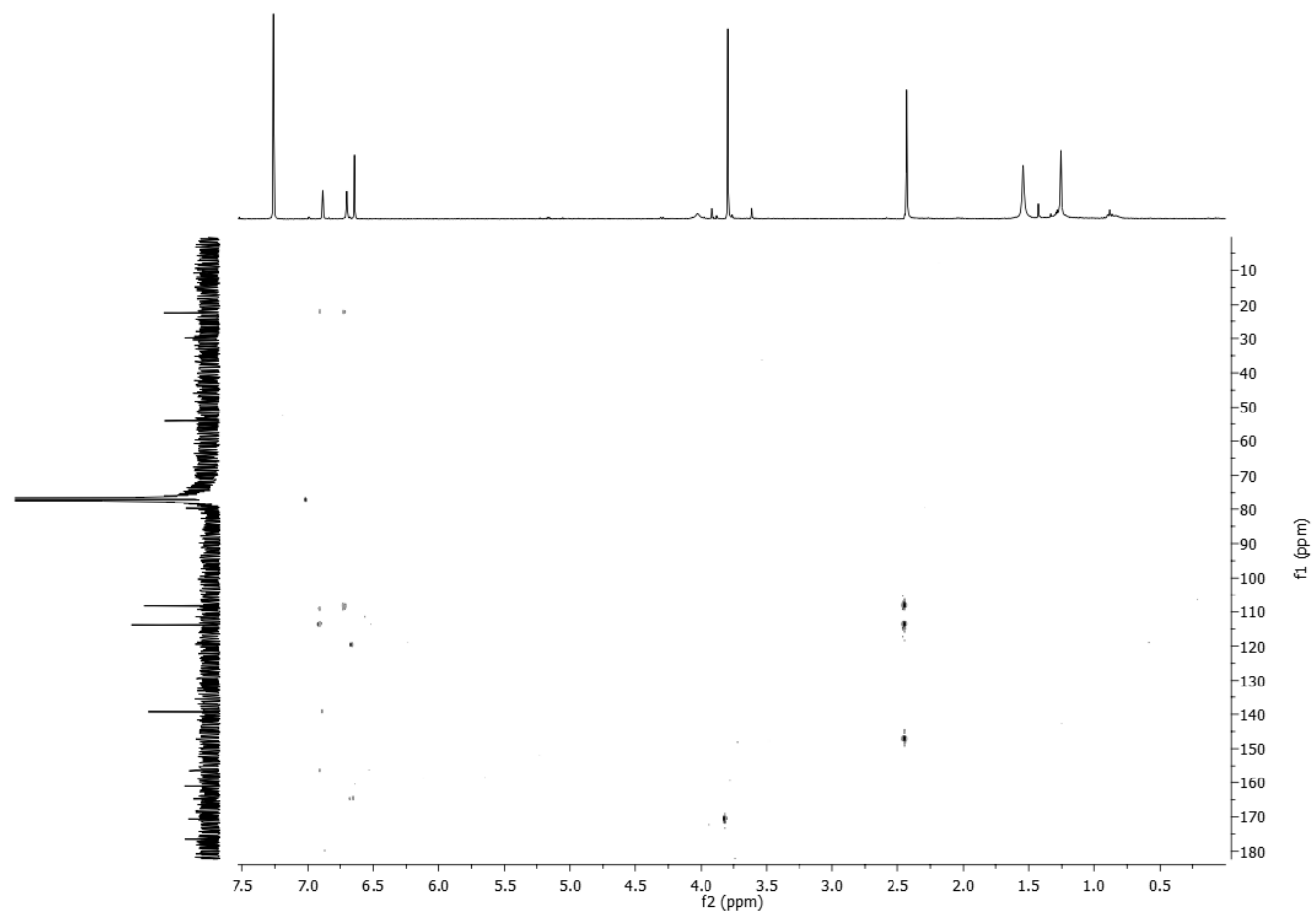


Figure 45: HMBC spectrum of rabenchromenone (10) (CDCl₃, 500/125 MHz).

5.2.2 Absolute configuration of rabenchromenone

The absolute configuration of rabenchromenone (**10**) was determined through electronic circular dichroism (ECD) spectroscopy and quantum mechanical calculations (Pescitelli and Bruhn, 2016; Superchi *et al.*, 2018). Rabenchromenone had a rigid structure and only two possible conformers were obtained by a molecular mechanics conformational search and density functional theory (DFT) geometry optimizations. The two conformers differed in the orientation of the ester group and to a smaller extent the C1–OH group; in the most stable conformation (Fig. 46) the ester C=O pointed toward O–H.

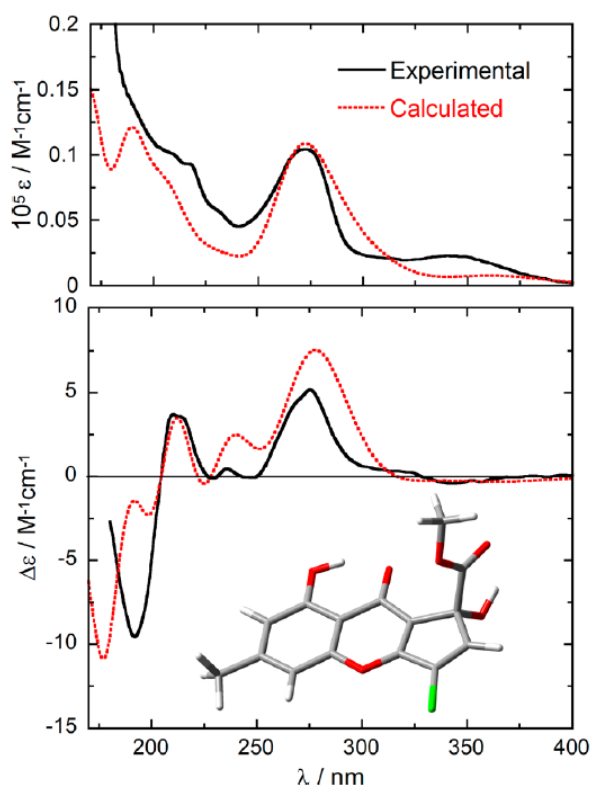


Figure 46: (Top) Ultraviolet–visible (UV–vis) absorption and (bottom) ECD spectra of compound **10** measured in CH₃CN (solid lines, 4.6 mM, 0.01 cm cell) compared to spectra calculated for (*R*)-**10** at the TD-B3LYP/def2-TZVP/PCM//ωB97X-D/6-311+G(d,p)/SMD level as the Boltzmann average of two conformers at 300 K (dotted lines). Calculated spectra were obtained as sums of Gaussian bands with 0.3 eV exponential half width, blue-shifted by 5 nm. The ECD spectrum was scaled by a factor of 0.3. The inset structure is the lowest energy conformer of compound **10**.

The UV and ECD spectra were measured in acetonitrile solutions and displayed several bands related to the extended conjugated chromophore (Fig. 46). The ECD spectrum calculated at the B3LYP/def2-TZVP/PCM level on the (*R*)-enantiomer of compound **10** matched in a satisfactory manner the experimental spectrum in terms of band signs, positions and intensities (Fig. 46). The results were in

agreement with other functionals (Experimental section 4.5). Thus, the absolute configuration of rabenchromenone (**10**) was determined as (*R*)-**10**.

5.2.3 Structural determination of rabenzophenone

Rabenzophenone (**11**) has a molecular formula of $C_{16}H_{13}ClO_6$ as determined from its HRESIMS, consistent with 10 indices of hydrogen deficiencies. The UV spectrum showed the absorption maxima at λ_{max} ($\log \epsilon$), 284 (2.50) nm for an extended conjugated system (Pretsch *et al.*, 2000). The IR spectrum presented bands typical of carbonyl, hydroxy, and aromatic groups at ν_{max} 3346, 1733, 1635, 1588, 1465 cm^{-1} (Nakanishi and Solomon, 1977). These findings were in agreement with the 1H and ^{13}C NMR data (Table 6). The 1H NMR spectrum (Fig. 47, Table 6) and COSY NMR spectrum (Fig. 48) showed two doublets at δ 7.56 (H-6) and 7.43 (H-5) ($J = 8.3$ Hz) due to two ortho-coupled aromatic protons and a broad singlet at δ 6.23 due to the overlapping of two aromatic meta-coupled protons (H-3' and H-5') typical of 1,2,4,6- and 1,2,3,4-tetrasubstituted benzene rings, respectively. The second ring appeared symmetrically substituted and this was supported also from the signals observed in the ^{13}C NMR spectrum (Fig. 49, Table 6). The 1H NMR spectrum (Fig. 47, Table 6) presented singlets for a benzyl methyl (Me-7') and a methoxy group at δ 2.25 and 3.77, respectively (Pretsch *et al.*, 2000). The ^{13}C NMR spectrum (Fig. 49, Table 6) showed two carbons typical of a ketone (C=O) and an ester carbonyl (C-1'') at δ 197.3 and 166.3, respectively. In the HMBC spectrum (Fig. 51, Table 6), the ketone (C=O) correlated with H-3',5', while the ester carbonyl (C-1'') correlated with H-6 and the methoxy group. The ^{13}C NMR spectrum (Fig. 49, Table 6) presented four protonated sp^2 carbons at δ 129.4, 123.2, and 109.9, which were assigned to C-5, C-6, and C-3',5' on the basis of the coupling observed in the HSQC spectrum (Fig. 50). In addition, the ^{13}C NMR spectrum (Fig. 49, Table 6) presented eight sp^2 quaternary carbons, three of which are oxygenated (C-2',6' and C-3) and two of them were equivalent (C-2',6'). These were assigned by the long-range correlations observed in the HMBC spectrum (Fig. 51, Table 6) between C-1 and C-4 and H-5 and H-6, between C-2 and C-3 and H-5, between C-1 and C-2',6' and H-3',5', and between C-4' and Me-7'. Thus, the signals at δ 160.9, 149.4, 148.2, 132.6, 128.0, 125.6, and 109.5 were assigned to C-2',6', C-4', C-3, C-4, C-2, C-1, and C-1' (Breitmaier and Voelter, 1987). The chemical shifts were assigned to all carbons and the corresponding protons (Table 6) and compound **11** was determined as methyl 4-chloro-2-(2,6-dihydroxy-4-methylbenzoyl)-3-hydroxybenzoate.

Table 6: ¹H and ¹³C NMR data of rabenzophenone (11)^{a,b}

position	δ_C^c	δ_H (<i>J</i> in Hz)	HMBC
1	125.1 s		H-5, H-6
2	127.5 s		H-5
3	147.9 s		H-5
4	132.1 s		H-5, H-6
5	129.2 d	7.43 (1H) d (8.3)	H-3, H-10
6	123.1 d	7.56 (1H) d (8.3)	H-5, H-7
1'	109.0 s		H-3', 5'
2', 6'	160.4 s		H-3', 5'
3', 5'	109.3 d	6.23 (2H) s	Me
4'	149.3 s		Me
CO	197.2 s		H-3', 5'
CO-C1	165.8 s		H-6, OMe
Me	22.3 q	2.25 (3H) s	H-3', 5'
OMe	52.8 q	3.76 (3H) s	
HO-2'			

^aThe chemical shifts are in δ values (ppm) from TMS. ^b2D ¹H, ¹H (COSY) ¹³C, ¹H (HSQC) NMR experiments delineated the correlations of all the protons and the corresponding carbons. ^cMultiplicities were assigned by DEPT spectrum.

The structure of rabenzophenone (**11**) was confirmed by the other couplings observed in the HMBC spectrum (Fig. 51, Table 6) and its HRESIMS spectrum, which showed a pseudomolecular ion [M + H]⁺ and typical isotopic peaks of ³⁷Cl at *m/z* 339.0458 and 337.0469 and the significant fragment-stable acyl ion of the benzoate moiety observed at *m/z* 216.003 and 214.0039, which came from the pseudo-molecular ion by the loss of a diphenoxy moiety.

Rabenzophenone (**11**) differed from moniliphenone (**12**) only by the presence of the chlorine atom at C-4.

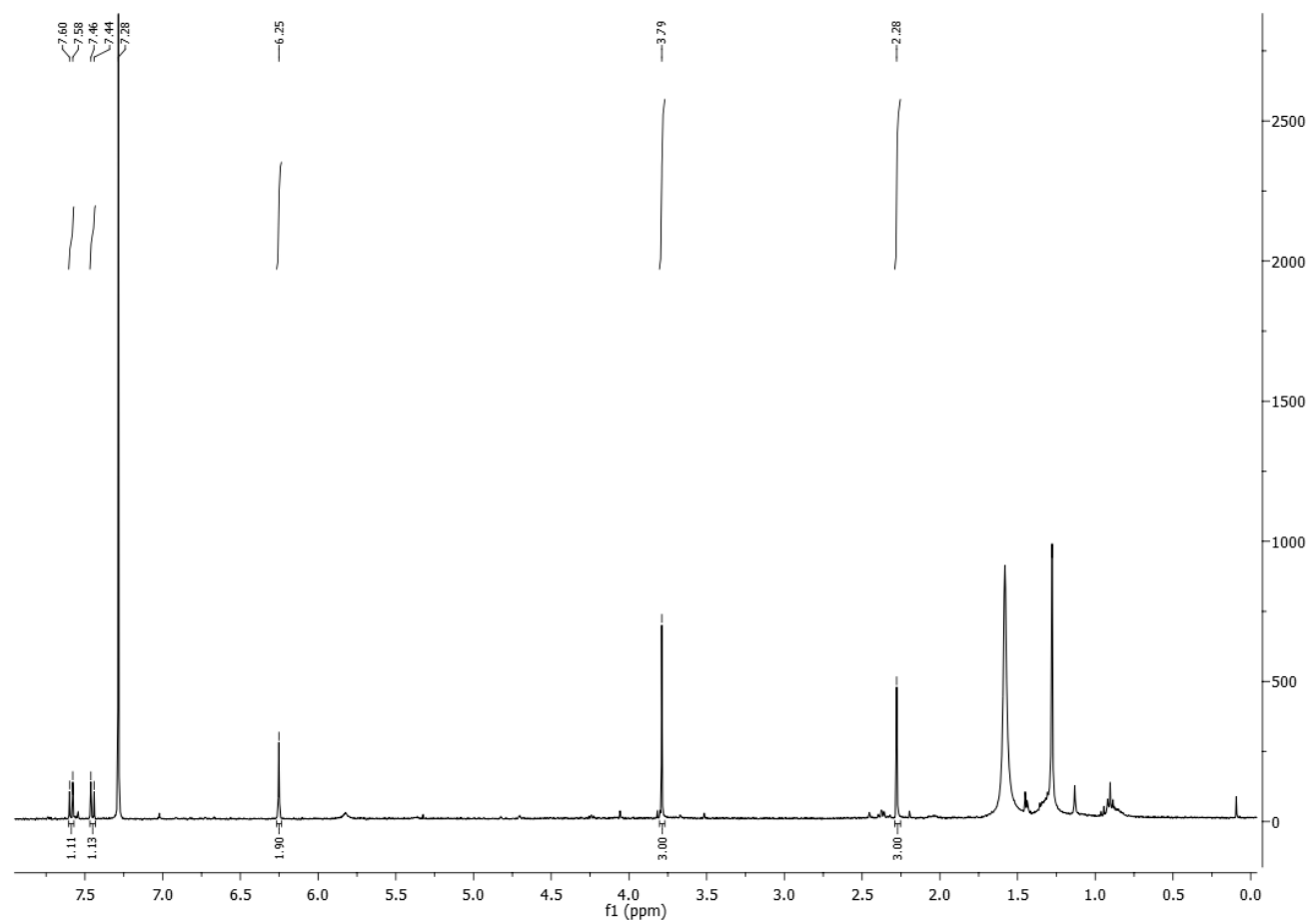


Figure 47: ^1H NMR spectrum of rabenzophenone (11) (CDCl_3 , 500 MHz).

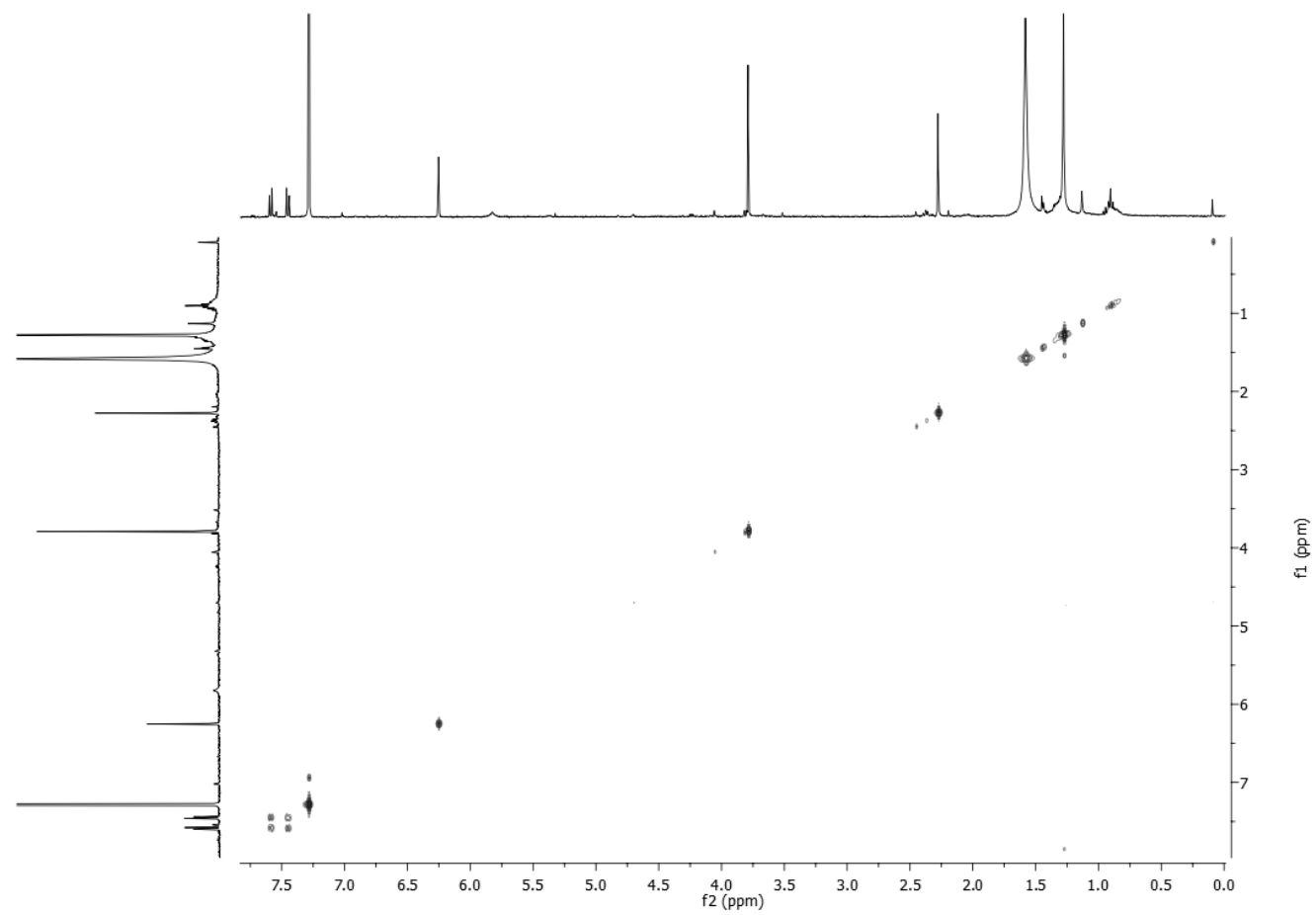


Figure 48: COSY spectrum of rabenzophenone (11) (CDCl₃, 500 MHz).

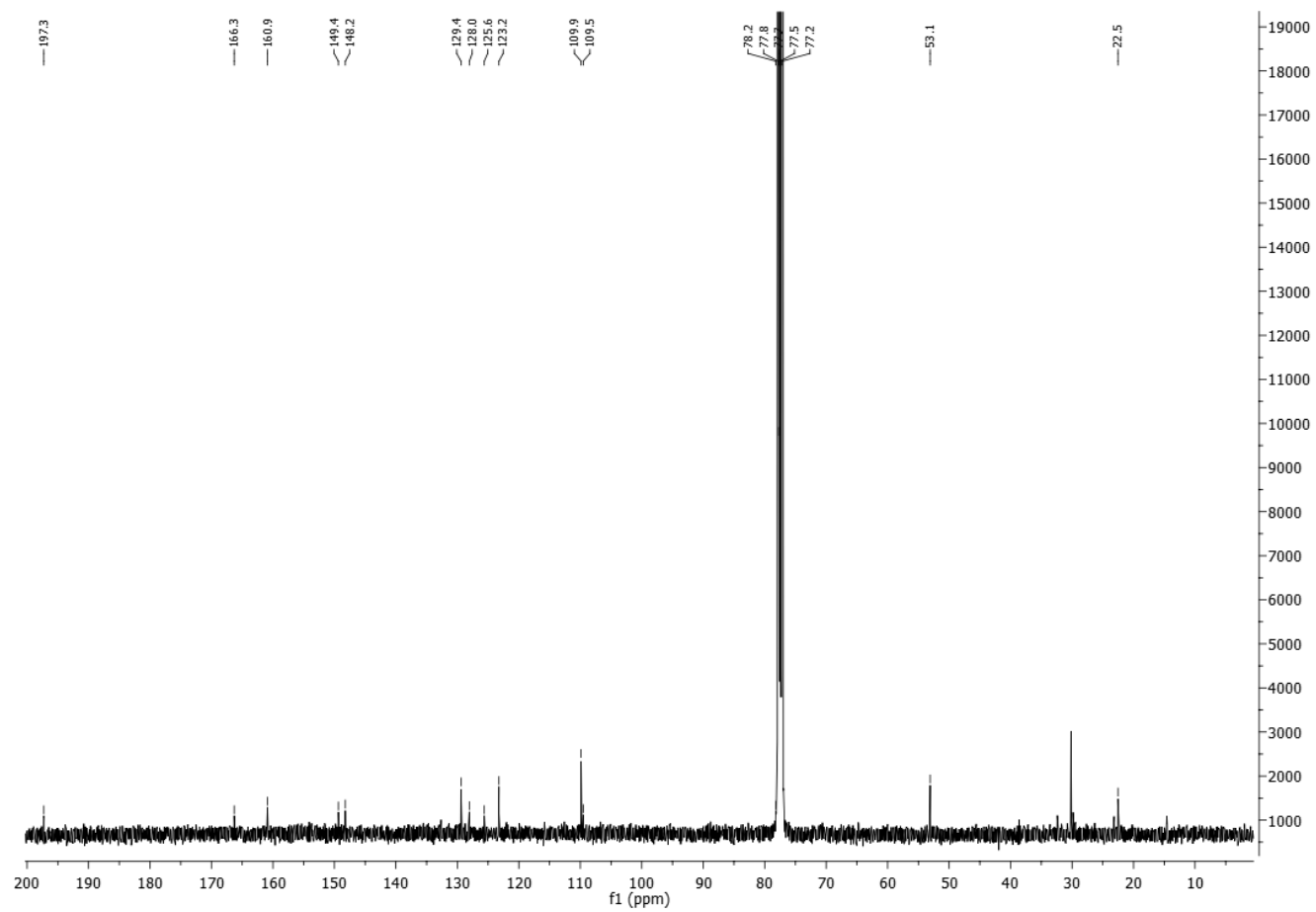


Figure 49: ^{13}C NMR spectrum of rabenzophenone (11) (CDCl_3 , 125 MHz).

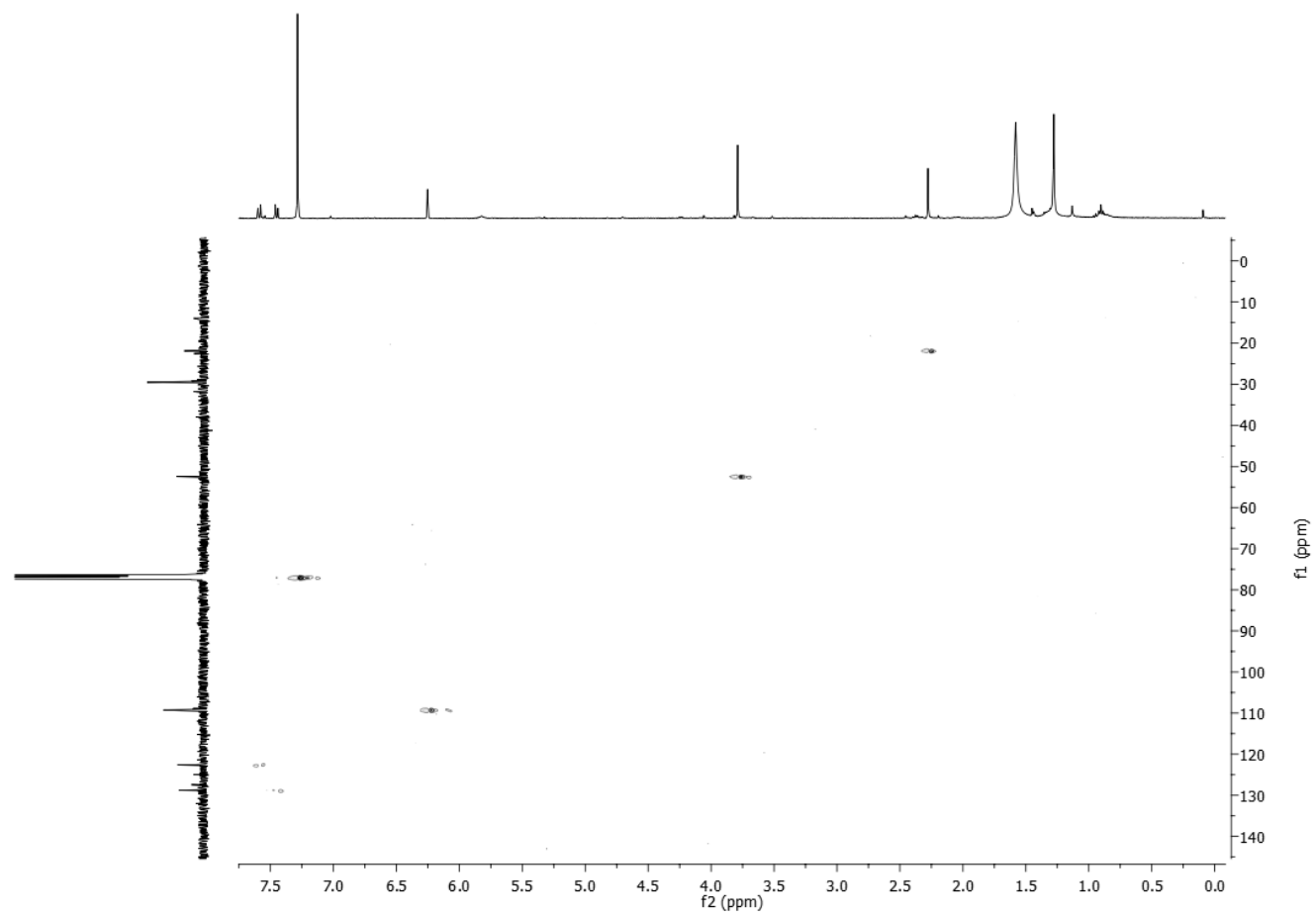


Figure 50: HSQC spectrum of rabenzophenone (11) (CDCl₃, 500/125 MHz).

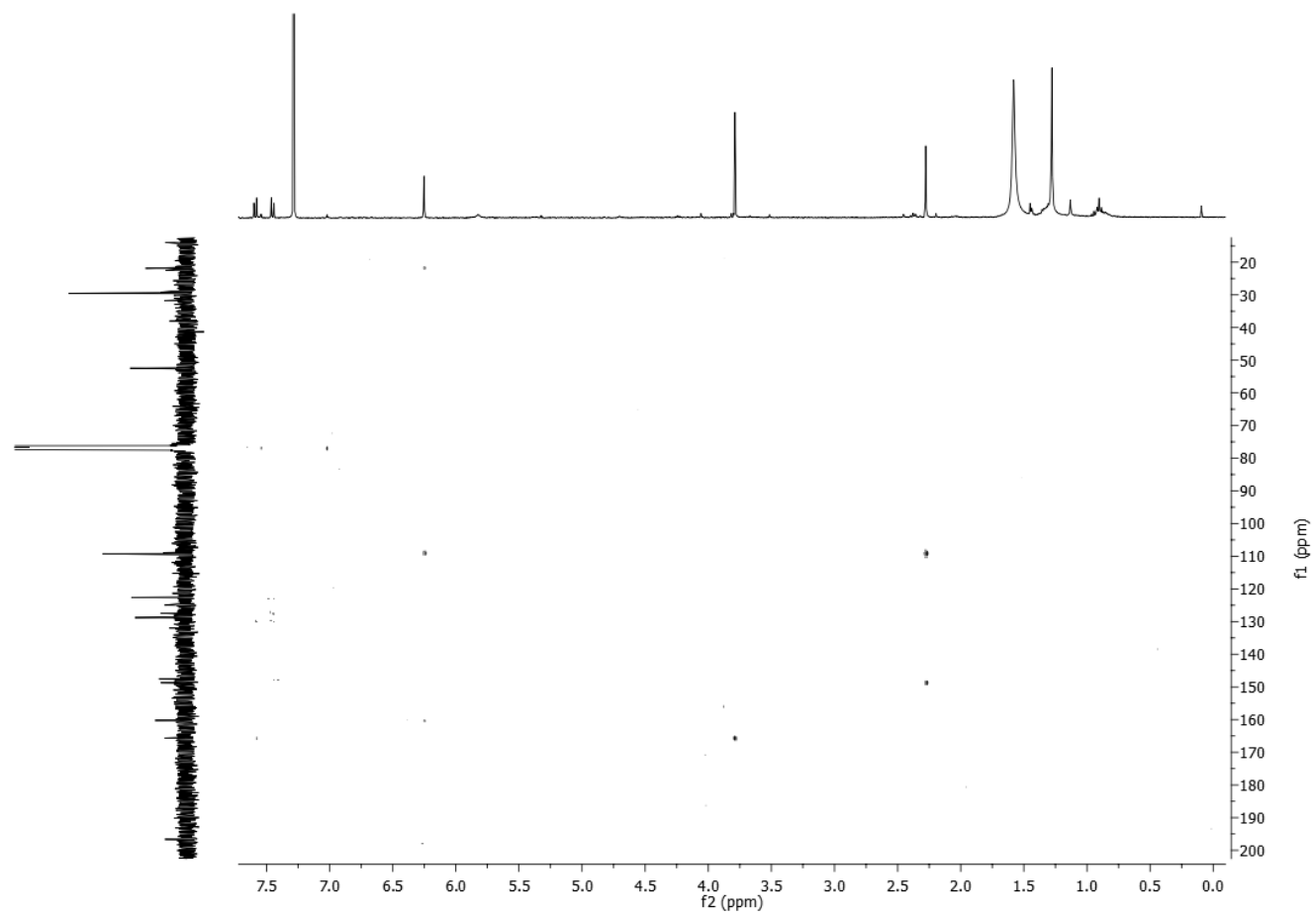


Figure 51: HMBC spectrum of rabenzophenone (11) (CDCl₃, 500/125 MHz).

5.2.4 Leaf puncture assay

The phytotoxicity of metabolites (**10-13**) was evaluated by a leaf puncture bioassay, on holm oak and tomato leaves (Table 7), at 1 mg/mL.

Table 7: Phytotoxic activity of 10-13 tested by leaf puncture assay at 1 mg/mL.^a

Compound	<i>Quercus brantii</i>	<i>Lycopersicon esculentum</i> L.
10	2	1
11	3	2
12	2	1
13	2	1

^aToxicity effects were expressed by using a visual scale from 0 (no symptoms) to 4 (wide necrosis up to 1 cm diameter).

All metabolites showed activity causing on both plants a necrosis diameter in the range between 0.2 and 0.5 cm. In particular, rabenzophenone (**11**) was the most phytotoxic compound on both plants causing significant necrosis (0.7 and 0.5 cm on holm oak and tomato leaves, respectively).

5.3 Structural identification of secondary metabolites isolated from *S. macrostoma* culture filtrates

The EtOAc extract of *S. macrostoma* culture filtrates was purified as detailed in the Experimental section 4.7 (Scheme 3), yielding three homogeneous compounds that were identified as 2,5-dihydroxymethylfuran, 5-hydroxymethyl-2-furaldehyde and tyrosol (**14-16**, Fig. 52). They were isolated for the first time from *S. macrostoma* and were identified comparing their spectroscopic data with those reported in literature: (Schneider *et al.*, 1996; Mancilla *et al.*, 2009) for 2,5-dihydroxymethylfuran (**14**), (Dohnal and Kisiel 2014; Li *et al.*, 2007; Guo *et al.*, 2016) for 5-hydroxymethyl-2-furaldehyde (**15**), (Cimmino *et al.*, 2017c; Masi *et al.*, 2020) for tyrosol (**16**).

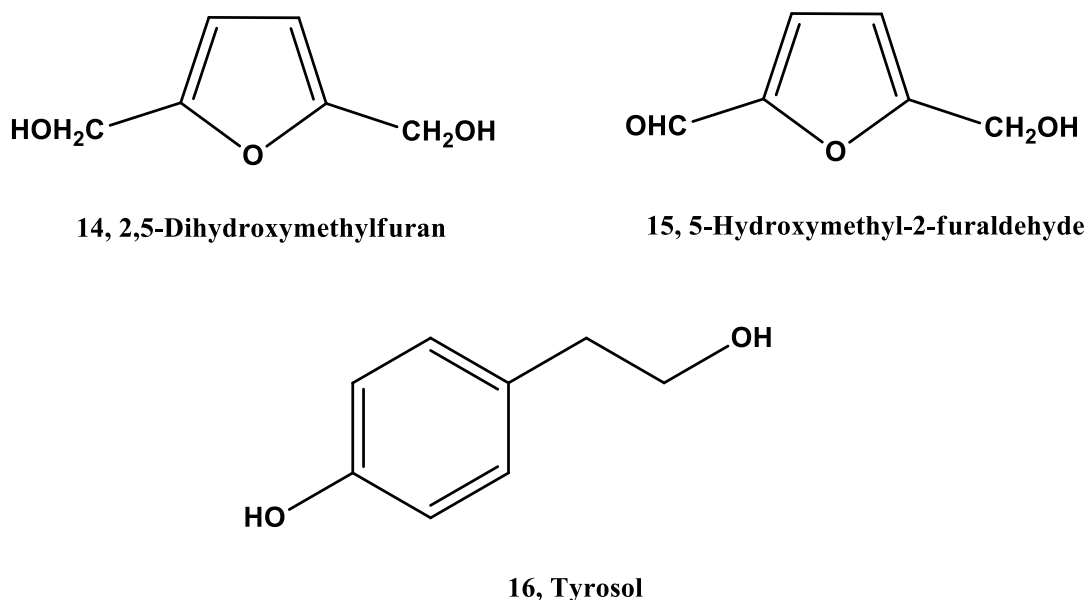


Figure 52: Secondary metabolites isolated from *Stilbocrea macrostoma*.

2,5-Dihydroxymethylfuran (**14**) was isolated for the first time from *Xylaria longipes*, an ascomycete with interesting biotechnological application (Schneider *et al.*, 1996), showing antifungal activity against *Nematospora coryli*. Successively, compound **14** was isolated from *Colletotrichum acutatum*, a fungus that caused anthracnose on a wide range of plants (Mancilla *et al.*, 2009), and *Lacrymaria velutina*, a fungus that possessed inhibitory activity against nitric oxide synthase (Ju *et al.*, 2010). Recently it was also isolated from *Paecilomyces* sp., a marine filamentous fungus, exhibiting antimicrobial activity (Mosadeghzad *et al.*, 2013).

5-Hydroxymethyl-2-furaldehyde (**15**) was isolated for the first time from *Tylophilus felleus* (Dohnal and Kisiel 2014), then from *Pleurotus ferulae*, showing nematocidal activity against

Bursaphelenchus xylophilus and *Pangrellus redivivus* (Li *et al.*, 2007). When compound **15** was isolated from *Penicillium chrysogenum* HGQ6, a marine derived fungus, it showed cytotoxic activity against BGC823 (Guo *et al.*, 2016). Recently, it was produced by *Bacillus subtilis*, showing *Candida albicans* antibiofilm growth and this effect was concentration dependent (Subramenium *et al.*, 2018).

Tyrosol (**16**) is a well-known phytotoxin produced by plant pathogens (Cimmino *et al.*, 2017c; 2018). Recently it was isolated from *Colletotrichum lupini*, the causal agent of lupin (*Lupinus albus* L.) anthracnose (Masi *et al.*, 2020).

5.3.1 X-ray analyses of 2,5-dihydroxymethylfuran

X-ray crystallographic analysis confirmed the structure assigned to 2,5-dihydroxymethylfuran (**14**). This metabolite crystallized in a one crystalline phase with two different crystal habitus: a rare snow-like habitus and a common rhombe-plate habitus (Fig. 53).

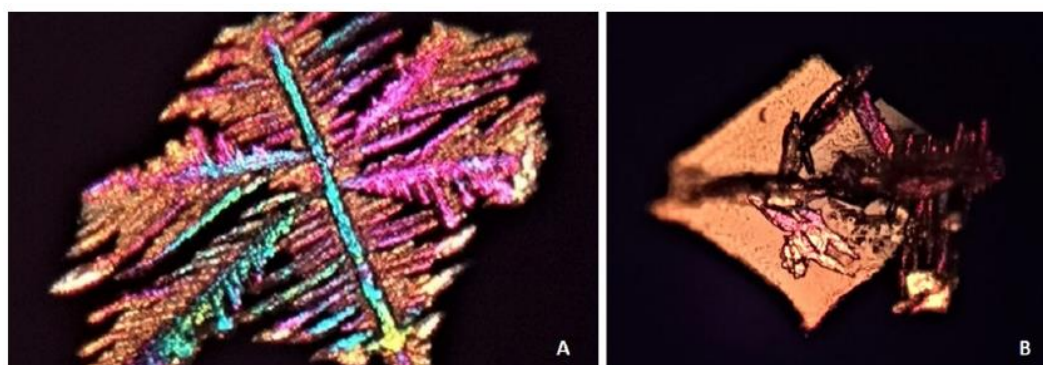


Figure 53: Two crystal habitus of **14**: A) Snow-like habitus; B) rhombeplate habitus (observation under polarized light at optical microscope).

The ORTEP view of 2,5-dihydroxymethylfuran (**14**) molecular structure is presented in Figure 54.

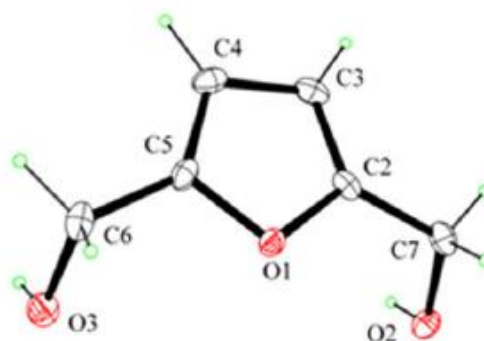


Figure 54: ORTEP view of **14** crystal obtained from a slow evaporation of CDCl_3 solution. Thermal ellipsoids were drawn at 30% probability level.

The crystal structure, previously reported by Glidewell *et al.* 1996, was redetermined at 173 K (Fig. 55, Tables 8–10).

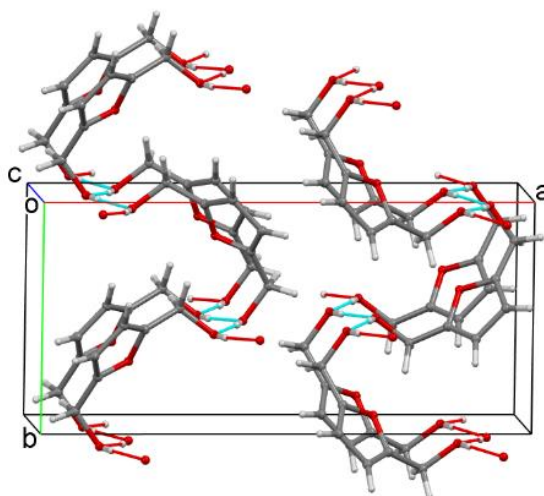


Figure 55: Crystal packing of 14 with hydrogen bonding pattern.

Table 8: Crystal data and structure refinement details for 2,5-dihydroxymethylfuran (14).

CCDC number	2005394	
Empirical formula	$C_6 H_8 O_3$	
Formula weight	128.12	
Temperature	173(2) K	
Wavelength	0.71073 Å	
Crystal system	Orthorhombic	
Space group	$P n a 2_1$	
Unit cell dimensions	$a = 16.2960(10)$ Å	$\alpha = 90^\circ$
	$b = 7.7050(11)$ Å	$\beta = 90^\circ$
	$c = 4.879(3)$ Å	$\gamma = 90^\circ$
Volume	$612.6(4)$ Å ³	
Z	4	
Calculated density	1.389 Mg/m ³	
Absorption coefficient	0.112 mm ⁻¹	
F(000)	272	
θ range	3.639° to 25.980°	
Reflections collected / unique	3164 / 1059 [$R_{int} = 0.0463$]	
Data / restraints / parameters	1059 / 1 / 88	
Goodness-of-fit on F^2	1.043	
Final R indices [$I > 2\sigma(I)$]	$R_1 = 0.0376$, $wR_2 = 0.0622$	
R indices (all data)	$R_1 = 0.0654$, $wR_2 = 0.0701$	
Largest diff. peak and hole	0.170 and -0.190 e.Å ⁻³	

Table 9: Bond lengths [Å] and angles [°] for 2,5-dihydroxymethylfuran (14).

C(2)-C(3)	1.346(4)
C(2)-O(1)	1.375(3)
C(2)-C(7)	1.479(4)
C(3)-C(4)	1.419(4)
C(4)-C(5)	1.333(5)
C(5)-O(1)	1.380(3)
C(5)-C(6)	1.484(4)
C(6)-O(3)	1.434(3)
C(7)-O(2)	1.433(3)

Table 10: Hydrogen bonds for 2,5-dihydroxymethylfuran (14) [Å and °].

D-H...A	d(D-H)	d(H...A)	d(D...A)	<(DHA)
C(6)-H(6B)...O(3)#1	0.99	2.61	3.565(4)	161.3
C(7)-H(7A)...O(1)#2	0.99	2.58	3.470(5)	148.9
O(2)-H(2A)...O(3)#2	0.82(3)	1.93(4)	2.740(4)	169(4)
O(3)-H(3A)...O(2)#3	0.82(4)	1.93(4)	2.739(4)	172(3)

Symmetry transformations used to generate equivalent atoms:

#1 -x+1,-y+1,z-1/2 #2 -x+1/2,y-1/2,z-1/2 #3 -x+1/2,y+1/2,z-1/2

5.3.2 Leaf puncture assay

All metabolites (**14-16**) were tested for their phytotoxic activity by the leaf puncture assay on holm oak (*Q. ilex* L.) and tomato (*L. esculentum* L.) leaves, at concentrations of 5.0, 1.0 and 0.1 mM. All compounds exhibited toxic effect on oak at all concentrations used, while they were low active on tomato leaves (Table 11).

Table 11: Phytotoxic activity of 14-16 tested by leaf puncture assay.^{a,b}

Compound	Concentration (mM)	<i>Quercus ilex</i> L.	<i>Lycopersicon esculentum</i> L.
14	5	4	1
	1	4	1
	0.1	2	1
15	5	4	1
	1	4	1
	0.1	3	1
16	5	3	1
	1	3	1
	0.1	3	1
Control	-	0	0

^aToxicity effects were expressed using a visual scale from 0 (no symptoms) to 4 (wide necrosis up to 1 cm in diameter); ^bWater solution with 4% of MeOH was used as negative control.

Compounds **14** and **15** determined significant necrosis on holm oak leaves at two concentrations (5.0 and 1.0 mM) (Fig. 56), but the phytotoxic effects were reduced for both compounds at the lower concentration with a significant reduction for **14**. Tyrosol (**16**) showed lower toxicity than the other two compounds, even independent from concentrations.

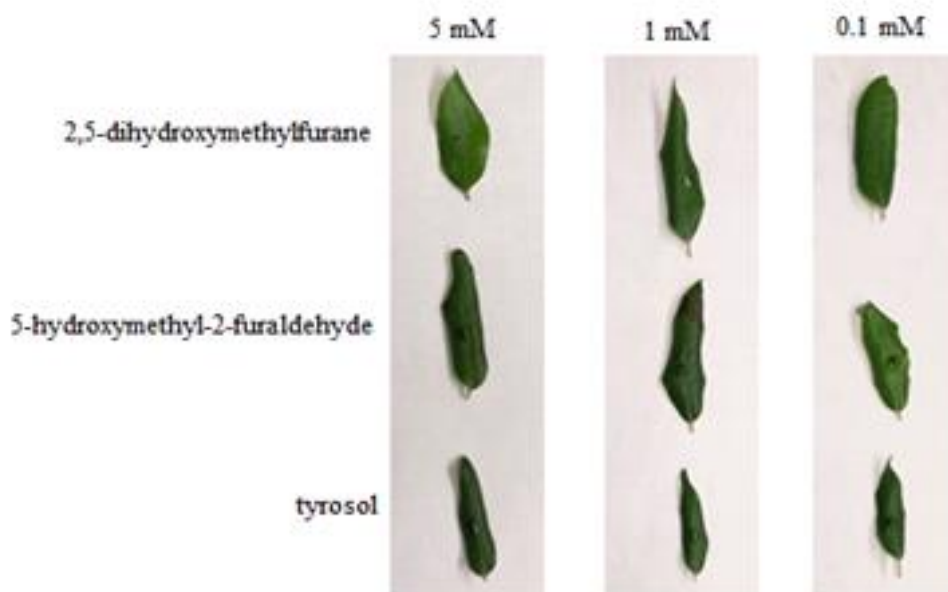


Figure 56: Leaf puncture assay on holm oak leaves of 14-16 at the three concentrations.

5.4 Structural identification of secondary metabolites isolated from *D. olivarum* culture filtrates

The organic extract of *D. olivarum* culture filtrates grown on Czapek medium was purified as detailed in the Experimental section 4.10 (Scheme 4), affording a new *nor*-diterpenoid cleistanthane (**17**, Fig. 57), named olicleistanone, together with two known pimarane diterpenoids, sphaeropsidins A and C (**18** and **19**, Fig. 57), and two known *nor*-pimarane diterpenoids, sphaeropsidin G and diplopimarane (**20** and **21**, Fig. 57). When *D. olivarum* was grown on mineral salt medium (Scheme 5), the fungus produced sphaeropsidin A, low amounts of sphaeropsidin G, diplopimarane and (-)-mellein (**18**, **20-22**, Fig. 57). The known compounds were identified comparing their specific optical rotation and spectroscopic data with those previously reported in literature: (Evidente *et al.*, 1996) for sphaeropsidin A (**18**), (Evidente *et al.*, 1997c) for sphaeropsidin C (**19**), (Cimmino *et al.*, 2016) for sphaeropsidin G (**20**), (Andolfi *et al.*, 2014b) for diplopimarane (**21**) and (Masi *et al.*, 2020) for (-)-mellein (**22**).

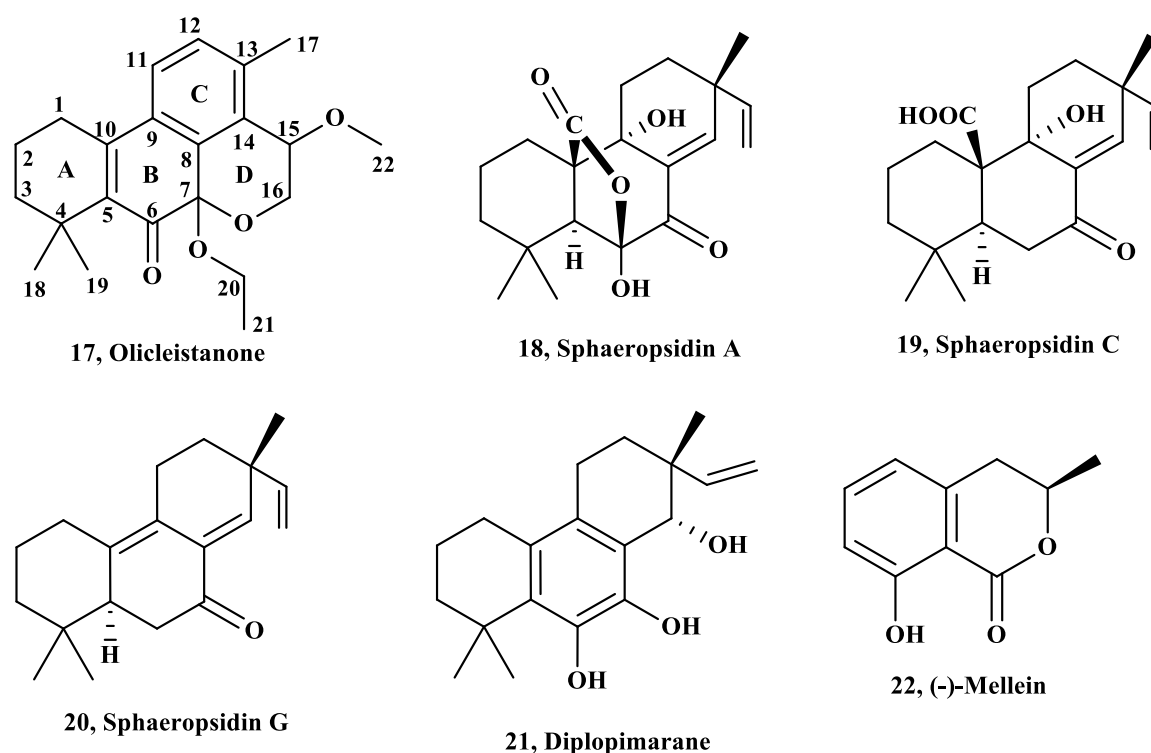


Figure 57: Secondary metabolites isolated from *Diplodia olivarum*.

Sphaeropsidins A, C and G (**18-20**) were previously isolated from *D. cupressi* (Evidente *et al.*, 1996; 1997), *D. mutila* (Sparapano *et al.*, 2004), and *D. corticola* (Masi *et al.*, 2018) and they are well-known fungus and plant metabolites. In deep study of sphaeropsidin A and its derivatives highlighted that sphaeropsidin A and its 6-*O*-acetyl derivative presented antimicrobial (Evidente *et al.*, 2011c) and anticancer activity (Lallemand *et al.*, 2012; Ingels *et al.*, 2017; Masi *et al.*, 2018).

(-)-Mellein (**22**) and the other 3,4-dihydroisocoumarins are well-known metabolites produced by many fungi, plants, insects and bacteria, showing phytotoxic, zootoxic and antifungal effects. (-)-Mellein was detected in symptomatic and asymptomatic grapevine wood samples and green shoots (Djoukeng *et al.*, 2009) from plants with *Botryosphaeria* dieback and leaf stripe, showing toxic effects on grapevine leaves and grapevine calli (Djoukeng *et al.*, 2009; Ramirez-Suero *et al.*, 2014, Masi *et al.*, 2018).

Recently, compound **22** has been isolated from *Lasiodiplodia euphorbiaceicola* during a screening of phytotoxic metabolites isolated from *Lasiodiplodia* spp. infecting grapevine in Brazil (Cimmino *et al.*, 2017c), and from *Sardiniella urbana*, a pathogen from declining European hackberry trees in Italy (Cimmino *et al.*, 2019).

5.4.1 Structural determination of olicleistanone

Olicleistanone (**17**) has a molecular formula of C₂₂H₂₈O₄ as determined from its HRESIMS, consistent with 9 hydrogen deficiencies. The IR spectrum showed the bands typical for carbonyl and aromatic groups at ν_{\max} 1725, 1610, 1592, 1560, 1458 cm⁻¹ (Nakanishi and Solomon, 1977). The UV spectrum presented absorption maxima at λ_{\max} (log ϵ) 333 (2.98), 241 (3.55) nm (Pretsch *et al.*, 2000). Preliminary investigation of its ¹H and ¹³C NMR spectra (Fig. 58 and 60, Table 12) revealed that the compound **17** was closely related to a tricyclic *nor*-diterpenoid, with aromatized and cyclohexadiene rings (C and B) joined to a dihydropyran ring (D) generated probably from a cleistanthane carbon skeleton (Devappa *et al.*, 2011).

The ¹H and COSY spectra (Fig. 58 and 59) of olicleistanone (**17**) presented the typical signals of two *ortho*-coupled protons of a 1,2,3,4-tetrasubstituted C benzene ring as two doublets at δ 7.31 (H-11) and 7.18 (H-12) ($J = 7.9$ Hz), and singlets of a methoxy group at δ 3.38 (CH₃-22), a vinyl methyl at δ 2.34 (CH₃-17) and two methyls at δ 1.23 and 1.36 (CH₃-19 and CH₃-18, respectively) bonded to a quaternary carbon (Berger and Braun, 2004). The two methyls represent the head of the geranylgeranyl biosynthetic precursor which generated the diterpenoid cleistanthane carbon skeleton.

The ¹H NMR spectrum (Fig. 58) presented the signal of an ethoxy group as two double quartets at δ 3.33 and 3.64 (H₂-20) ($J = 14.2, 7.0$ Hz) and a triplet at δ 1.14 (H₃-21) ($J = 7.0$ Hz). A signal pattern due to pyran moiety (ring D) of the benzohydropyran system (C and D rings) appeared as an ABC

system. The ^1H NMR spectrum (Fig. 58) also showed a signal typical of the three adjacent methylene groups, and of the A ring as a double triplet at δ 2.77 ($J = 18.8, 6.1$ Hz) and a double doublet of doublets at δ 2.47 ($J = 18.8, 12.2$ and 6.6 Hz) (CH_2 -1), as a multiplet at δ 1.80 (CH_2 -2) and as two multiplets at δ 1.62 and 1.49 (CH_2 -3) (Pretsch *et al.*, 2000). The same spectrum presented a doublet at δ 4.20 (CH -15) ($J = 3.3$ Hz) and a doublet at δ 4.41 ($J = 12.7$ Hz) and double doublet at δ 4.22 ($J = 12.7$ and 3.3 Hz) of a methylene group (CH_2 -16). All protonated carbons were identified as a result of the correlations observed in the HSQC spectrum (Fig. 61) (Berger and Braun, 2004). The quaternary carbons were identified by the long-range couplings observed in the HMBC spectrum (Fig. 62, Table 12). The signals at δ 34.0 correlated with H_2 -2, H_2 -3, H_3 -18 and H_3 -19 and, thus, were assigned to C-4, at 136.4 with H_2 -1, H_2 -3, H_3 -18 and H_3 -19 and assigned to C-5, at 195.5 with H_2 -1 and assigned to C-6, at 92.3 with H-15, H_2 -16 and H-20A and assigned to C-7, at 130.6 with H-12 and H_3 -17 and assigned to C-8, at 146.1 with H_2 -1, H_2 -2, H-11 and assigned to C-10, at 138.7 with H-11 and H_3 -17 and assigned to C-13, and finally at 130.2 with H-12, H-15 and H_2 -16 and assigned to C-14. The remaining signal at δ 132.9 was assigned to C-9 (Breitmaier and Voelter, 1987). The ethoxy group was located at C-7, due to the correlation between C-7 and H-20A, and consequently the methoxy group at C-15.

Table 12: ¹H and ¹³C NMR data of olicleistanone (17)^{a,b}

position	δ_C^c	δ_H (J in Hz)	HMBC
1	27.4 t	2.77 (1H) dt (18.8, 6.1) 2.47 (1H) ddd (18.8, 12.2, 6.6)	H ₂ -2, H ₂ -3
2	18.6 t	1.80 m (2H)	H ₂ -1
3	40.5 t	1.62 (1H) m 1.49 (1H) m	H ₂ -1, H ₂ -2, H ₃ -18, H ₃ -19
4	34.0 s		H ₂ -2, H ₂ -3, H ₃ -18, H ₃ -19
5	136.4 s		H ₂ -1, H ₂ -3, H ₃ -18, H ₃ -19
6	195.5 s		H ₂ -1
7	92.3 s		H-15, H ₂ -16, H-20A
8	130.6 s		H-12, H ₃ -17
9	132.9 s		
10	146.1 s		H ₂ -1, H ₂ -2, H-11
11	125.0 d	7.31 (1H) d (7.9)	
12	131.3 d	7.18 (1H) d (7.9)	
13	138.7 s		H-11, H ₃ -17
14	130.2 s		H-12, H-15, H ₂ -16
15	69.5 d	4.20 (1H) d (3.3) ^e	H ₂ -16, H ₃ -22
16	60.5 t	4.22 (1H) dd (12.7, 3.3) ^e 4.41 (1H) d (12.7)	H-15
17	18.4 q	2.34 (3H) s	H-12
18 ^d	27.7 q	1.23 (3H) s	H ₃ -19
19 ^d	29.7 q	1.36 (3H) s	H ₃ -18
20	59.0 t	3.33 (1H) dq (14.2, 7.0) 3.64 (1H) dq (14.2, 7.0)	H ₃ -21
21	15.4 q	1.14 (3H) t (7.0)	
22	55.7 q	3.38 (3H) s	H-15

^a2D ¹H, ¹H (COSY) and ¹³C, ¹H (HSQC) NMR experiments confirmed the correlations of all the protons and the corresponding carbons. ^bCoupling constants (J) are given in parenthesis. ^cMultiplicities were assigned with DEPT. ^dThese signals could be exchanged. ^eThese two signals are in part overlapped.

Ethoxy groups are relatively rare in natural products, as several ethoxy-containing ketals like **17** (Wang *et al.*, 2006; Lim *et al.*, 2013; Xiong *et al.*, 2015; Shen *et al.*, 2015; Zhang *et al.*, 2016).

Thus, the chemical shift were assigned to all carbons and corresponding protons (Table 12) and olicleistanone (**17**) was formulated as 4-ethoxy-6a-methoxy-3,8,8-trimethyl-4,5,8,9,10,11-hexahydrodibenzo[*de,g*]chromen-7(6aH)-one.

The structure of olicleistanone (**17**) was confirmed by the other HMBC couplings reported in Table 12 and by its ESIMS and HRESIMS spectra. The ESIMS spectrum presented the sodium dimer $[2M + Na]^+$ and the potassium adduct ion $[M + K]^+$ at m/z 735 and 395, respectively. The HRESIMS spectrum showed the sodium adduct ion $[M + Na]^+$ at m/z 379.1876. The significant ion $[M + H - CH_3CH_2OH]^+$ observed in the ESIMS spectrum at m/z 311 was probably generated from a pseudo-molecular ion by loss of ethanol.

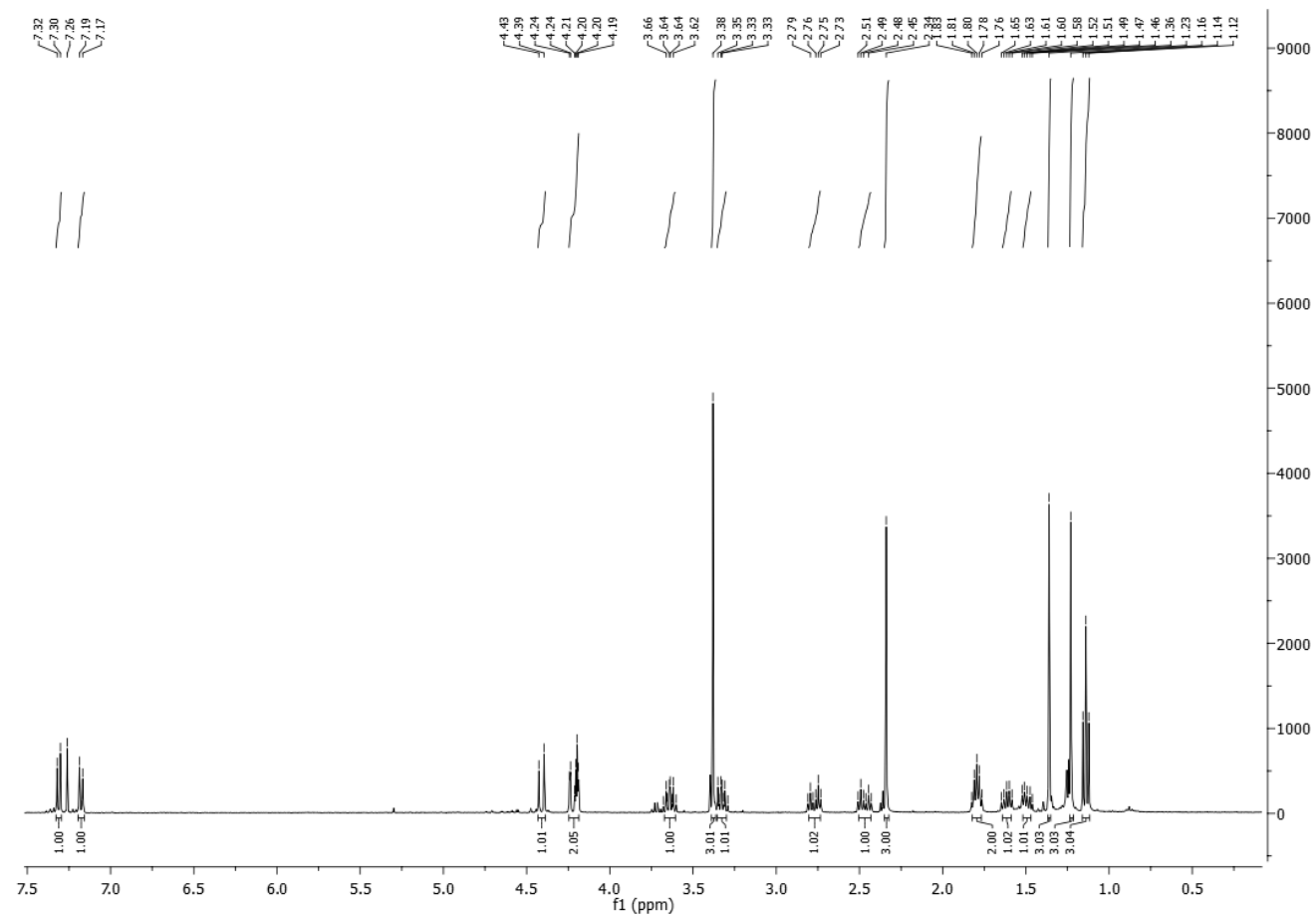


Figure 58: ¹H NMR spectrum of olicleistanone (17) (CDCl₃, 400 MHz).

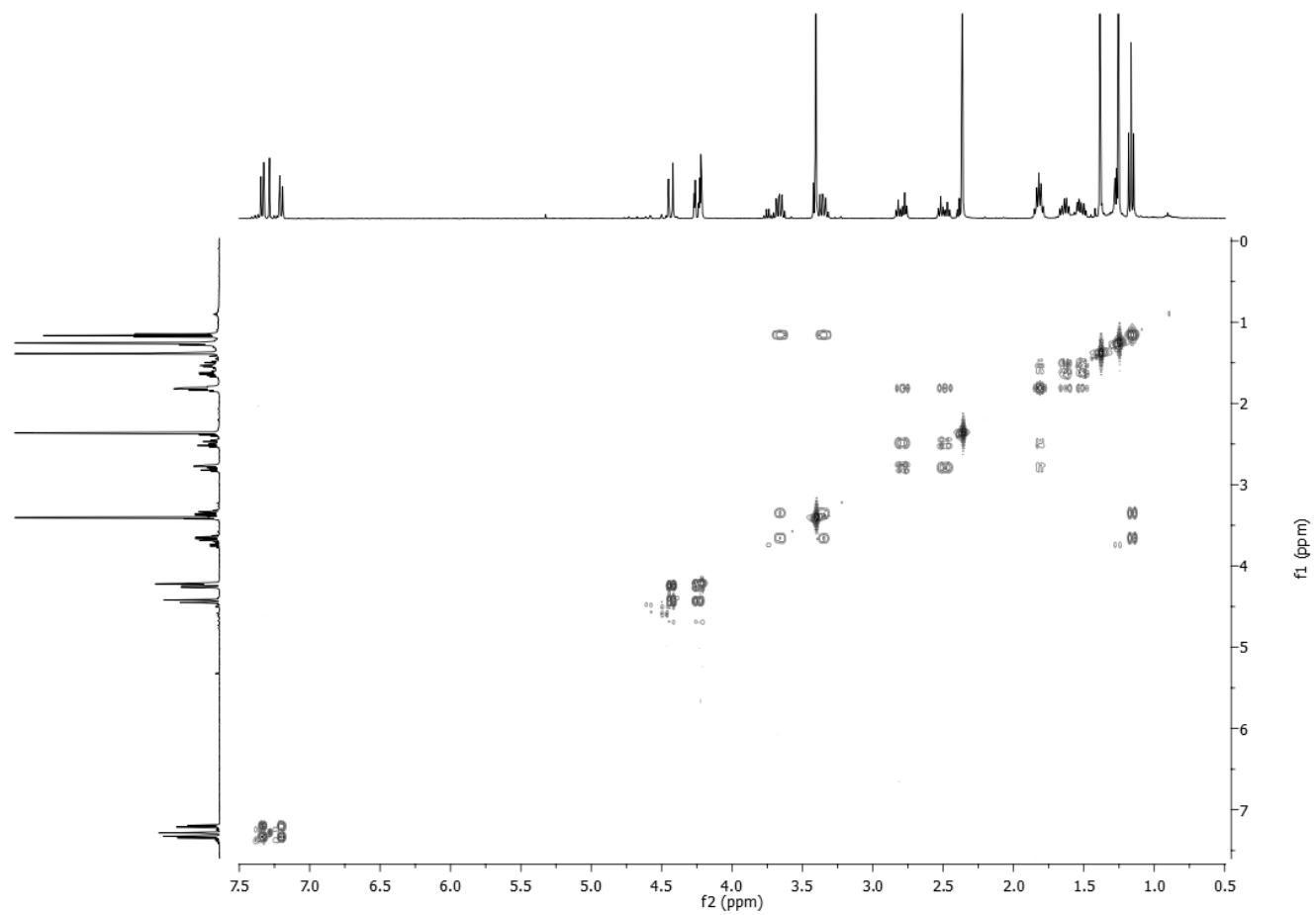


Figure 59: COSY spectrum of olicleistanone (17) (CDCl_3 , 400 MHz).

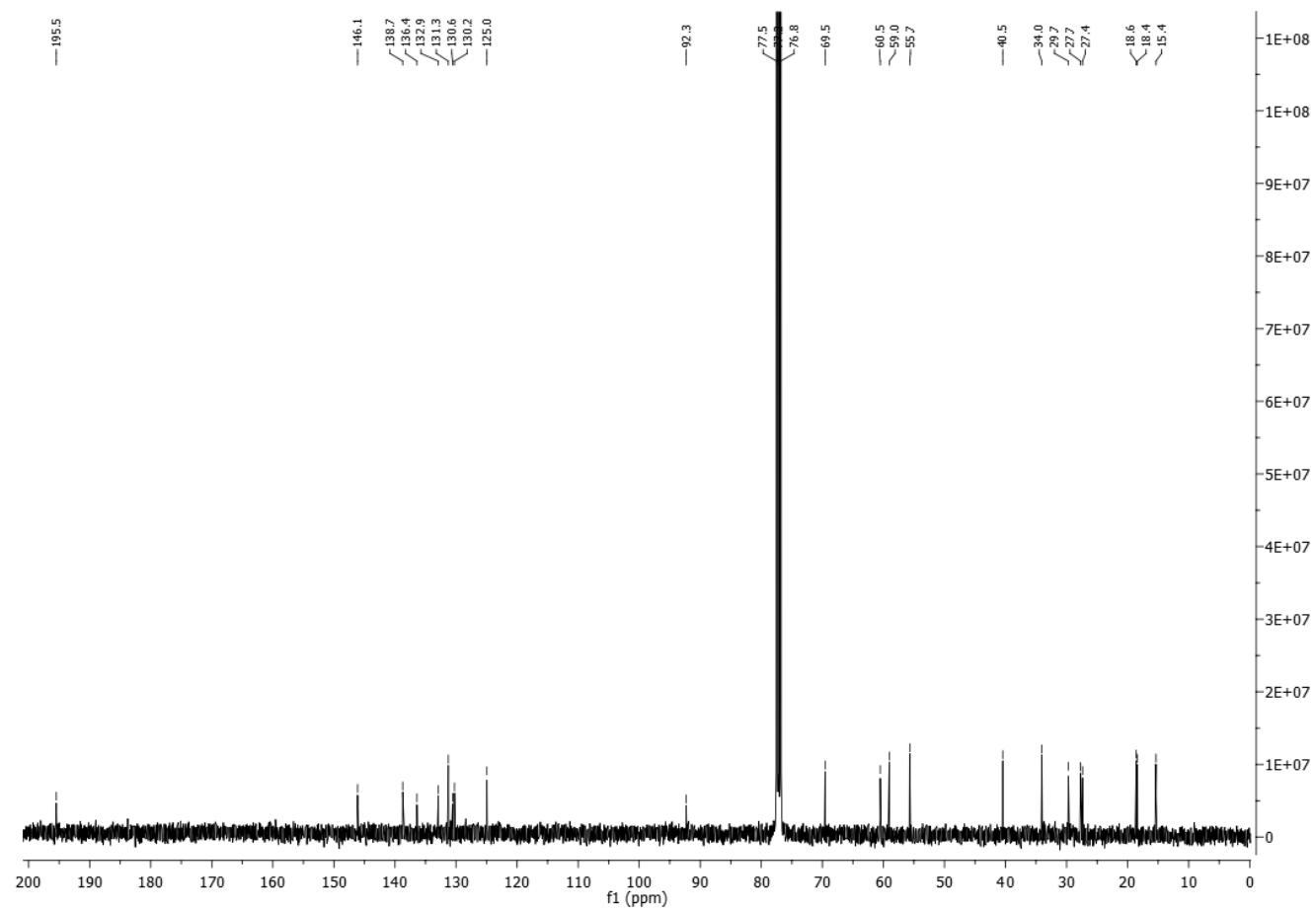


Figure 60: ^{13}C NMR spectrum of olicleistanone (17) (CDCl_3 , 100 MHz).

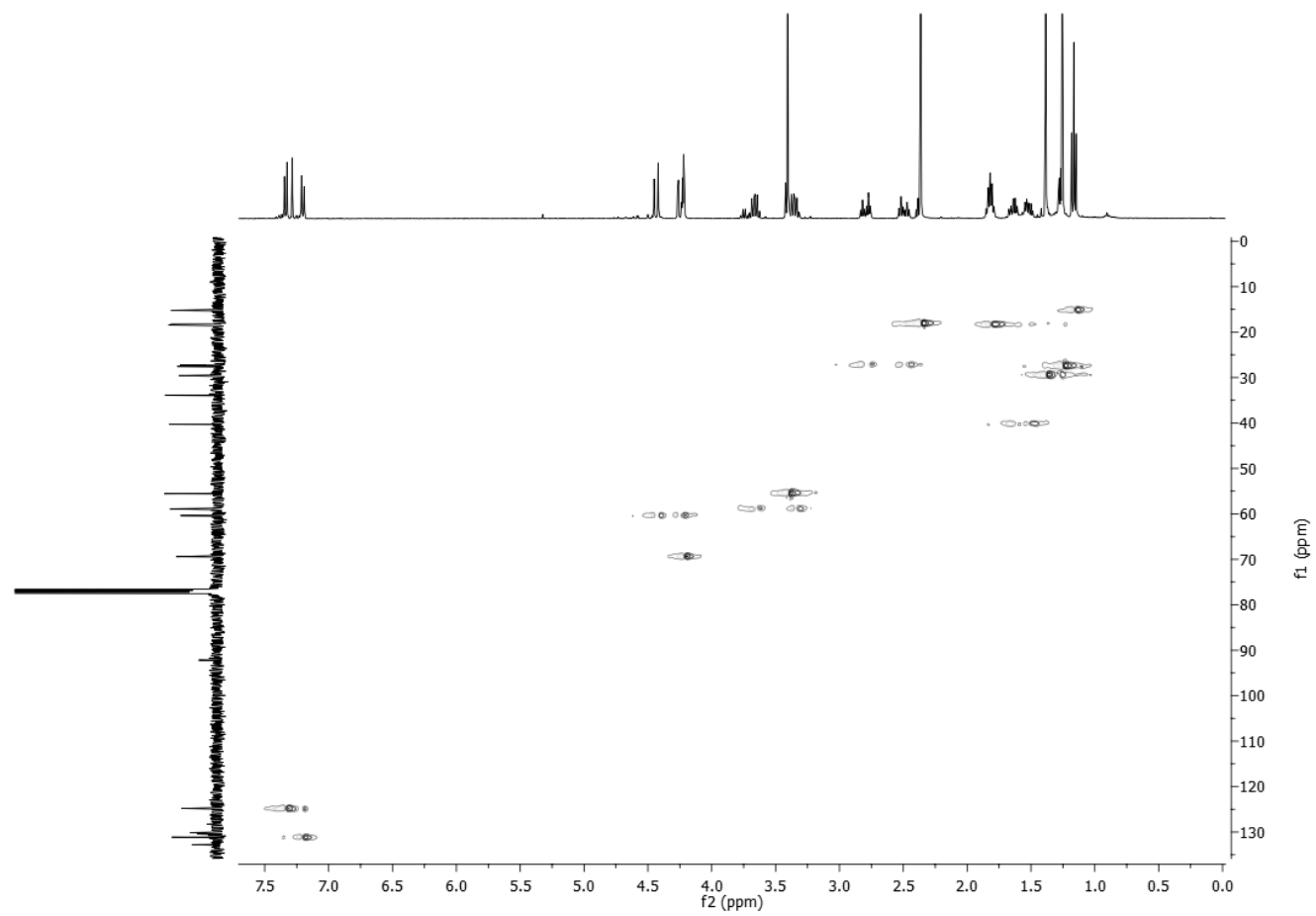


Figure 61: HSQC spectrum of olicleistanone (17) (CDCl₃, 400/100 MHz).

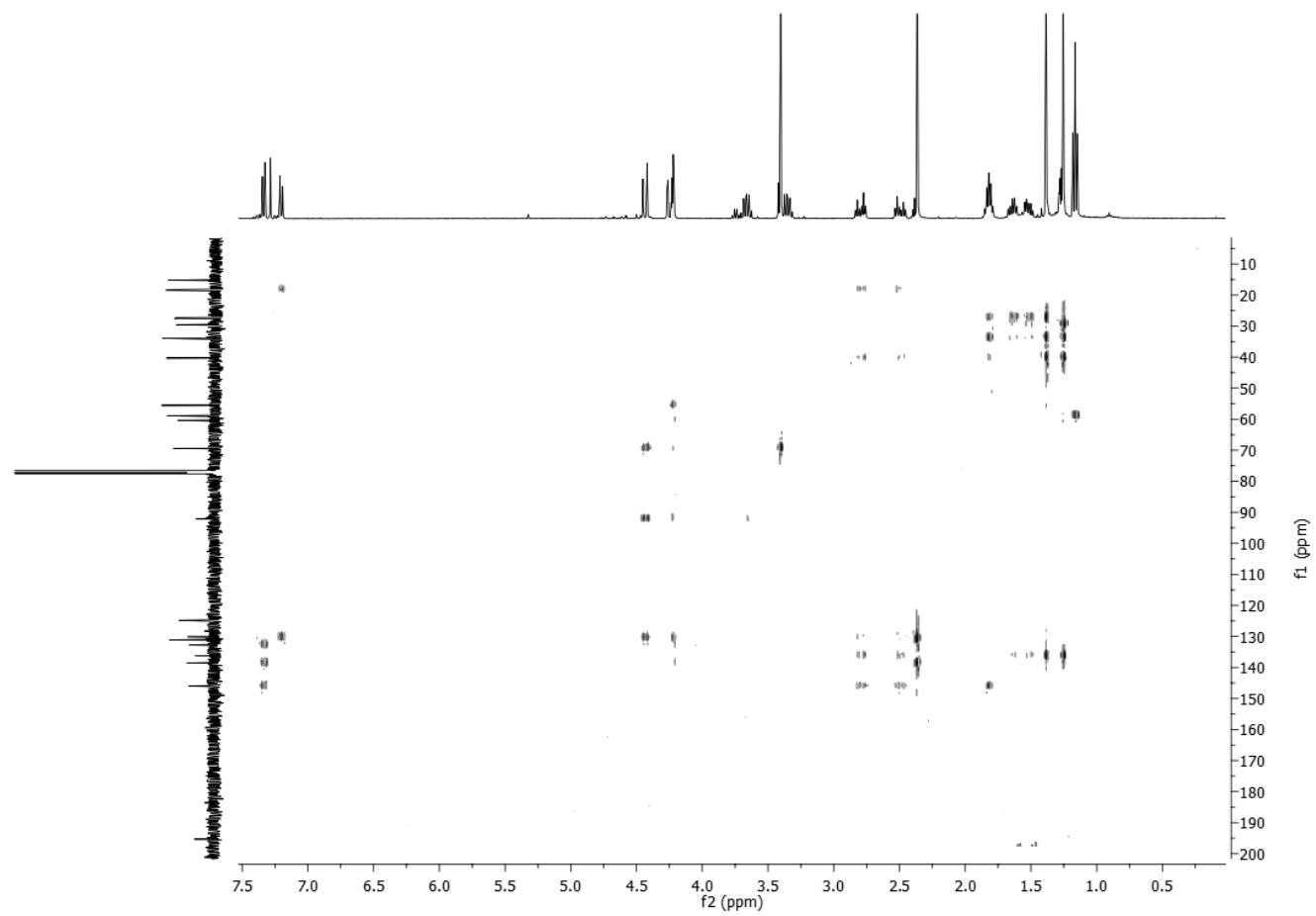


Figure 62: HMBC spectrum of olicleistanone (17) (CDCl₃, 400/100 MHz).

5.4.2 Relative and absolute configurations of olicleistanone

NOESY spectrum (Fig. 63, Table 13) was recorded to assign the relative configuration of **17**, but since there was no clear correlation between the protons of the methoxy and ethoxy groups, these data alone were not enough to determine the relative configuration of the two chiral centres (C-7 and C-15).

Table 13: NOESY data of olicleistanone (17)

Irradiated	Observed	Irradiated	Observed
H-11	H ₂ -1	H ₃ -21	H ₃ -17
H ₂ -20	H ₃ -21	H ₃ -18	H ₂ -20
H-15	H ₃ -17, H ₃ -21		

To better interpret NMR data, a molecular modelling study was undertaken. First, two diastereomeric structures (*7S,15S*)-**17** and (*7S,15R*)-**17** and their possible conformations were explored by means of a conformational search with molecular mechanics (Merck molecular force field, MMFF). Geometry optimizations were run with the density functional method (DFT) at the B97M-V/6-311+G(2df,2p)//B3LYP/6-31G(d) level, using the computational protocol for the prediction of ¹³C chemical shifts of flexible compounds (Hehre *et al.*, 2019). For the two diastereomers, six or ten conformers were found with detectable populations at room temperature, which differed in the conformation of the methoxy and ethoxy groups and in the puckering of ring A. A significant difference between the two diastereomers was the orientation of H-15, which was predominantly pseudo-equatorial in (*7S,15S*)-**17** and pseudoaxial (*7S,15R*)-**17**. Thus, the coupling constants between H-15 and H-16a/H-16b could be used to discriminate between the two isomers. Experimentally, H-15 appeared as a doublet with splitting of 3.3 Hz, meaning that one $J_{15/16}$ was small (3.3 Hz) and the other was negligible. This result suggested a pseudo-equatorial orientation. $^3J_{15/16}$ were then estimated with Karplus curve and spin-spin coupling calculations at B3LYP/pcJ-0 level (Table 14), supporting the assignment of **17** as (*7S**,*15S**)-**17**.

Table 14: Experimental and calculated $^3J_{\text{HH}}$ values (Hz) of olicleistanone.^a

	Experimental	Calculated	Calculated	Calculated	Calculated
		(Karplus)	(DFT)	(Karplus)	(DFT)
		<i>(7S,15S)</i> - 1		<i>(7S,15R)</i> - 1	
H-15/H-16a	3.3	3.14	4.05	7.24	9.26
H-15/H-16b	not detected	0.89	0.7	7.81	8.63

^a J values calculated either by a Karplus curve or by DFT at B3LYP/pcJ-0 level in vacuo, as Boltzmann average of all structures obtained by DFT geometry optimization (see text).

^{13}C NMR chemical shifts were calculated at the B3LYP/6-31G(d) level. The estimated root-mean-square (rms) error between experimental and calculated ^{13}C chemical shifts was acceptable (2.4-2.5) but similar for both isomers, thus this result did not give further information. Nevertheless, the argument based on J -couplings was accurate enough to assign the relative configuration.

For the absolute configuration, the ECD spectrum of a solution of **17** in acetonitrile (1 mM, 0.01 cm cell) was measured. The spectrum was not distinguishable from the baseline over the whole range (185-400 nm), despite the optimal absorption (0.3 to 0.8 for the absorption peaks), concluding that the isolated sample of **17** was a racemate.

Racemic natural products are rare and come from nonenzymatic reactions (Zask and Ellestad, 2018). Moreover, the chirality centre at C-7 of **17** was a tertiary benzylic carbon in α position to carbonyl group, which was easily subject to racemization. However, racemization of this centre did not occur in a post-synthetic step, otherwise two diastereomers would be obtained. On the other hand, the isolated (7*S*,15*S*)-**17** isomer was more stable than its (7*S*,15*R*) diastereomer by about 2 kcal mol⁻¹ at the present level of calculation. This suggested that if the chiral centre at C-15 was biosynthesized in a later step than C-7, its configuration would be dictated by that at C-7.

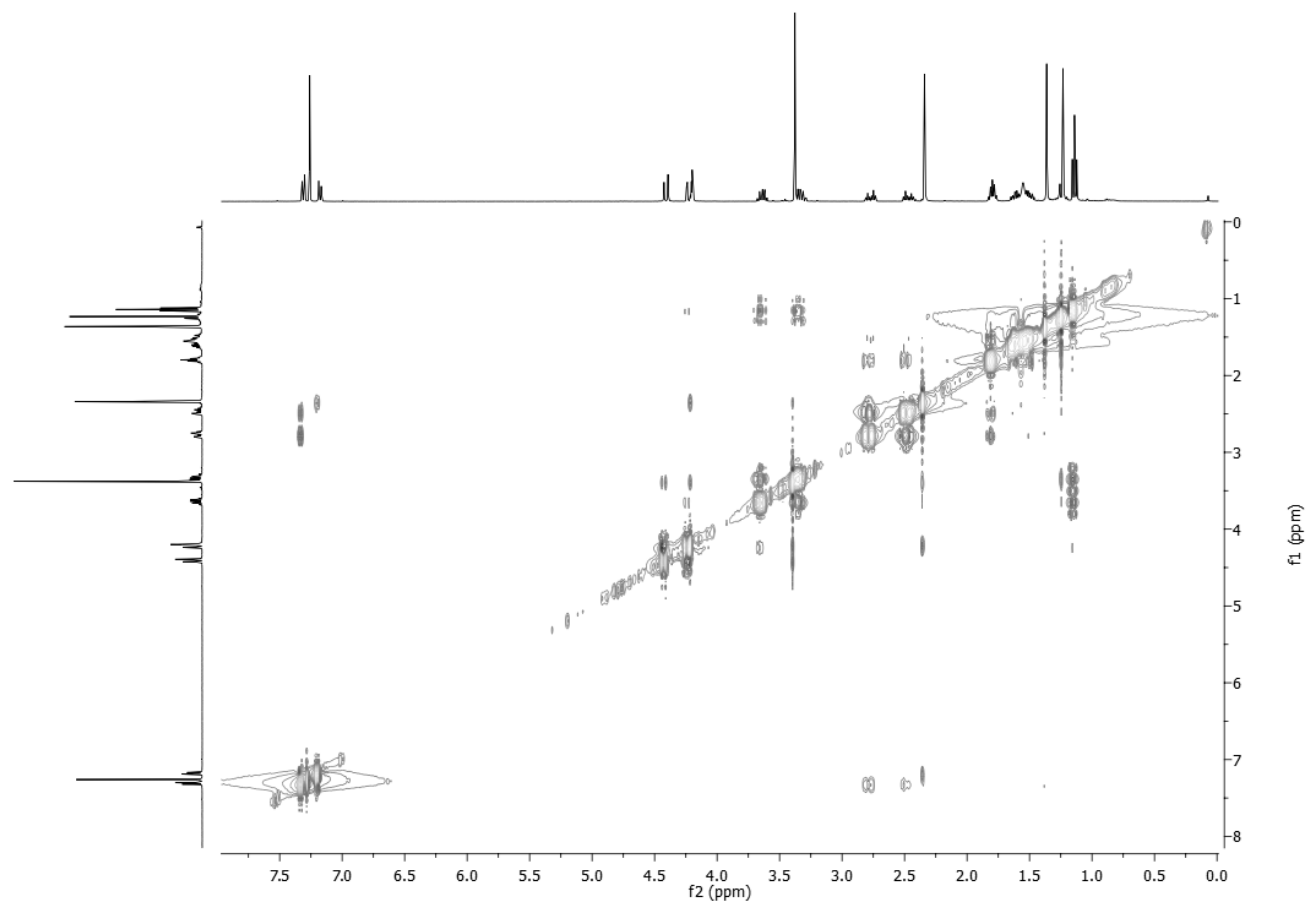


Figure 63: NOESY spectrum of olicleistanone (17) (CDCl₃, 400 MHz).

5.4.3 Biological assay

5.4.3.1 Leaf puncture assay

All metabolites (**17-22**) were tested for their phytotoxic activity at 1 mg/mL on *Phaseolus vulgaris* L., *Quercus suber* L., and *Juglans regia* L. young leaves. Only sphaeropsidin A (**18**) showed activity on tested plants, causing necrotic lesions with mean lesion sizes of 75.6 mm² on *P. vulgaris*, 163.3 mm² on *J. regia* and 15.1 mm² on *Q. suber*. While the other metabolites did not show phytotoxicity.

5.4.3.2 Antifungal assays

All compounds (**17-22**) were screened for their antifungal activity on two plant pathogens and two oomycetes (*Athelia rolfsii*, *Diplodia corticola*, *Phytophthora cambivora* and *P. lacustris*) at 200 µg per plug. Sphaeropsidin A (**18**) inhibited mycelium growth of tested fungi (100% inhibition rate). Diplopimarane (**21**) completely inhibited growth of *A. rolfsii* and partially inhibited growth of *D. corticola*, *P. cambivora* and *P. lacustris*, ranging from 56% to 75%. The other metabolites did not inhibit the growth of pathogens at the concentration used.

5.4.3.3 *Artemia salina* bioassay

All metabolites (**17-22**) were assayed at 100 mg/mL on brine shrimp (*Artemia salina*) larvae bioassay. This assay is widely used for toxicology and ecotoxicology studies. Olicleistanone (**17**), sphaeropsidin G (**20**) and (-)-mellein (**22**) caused 100% larval mortality, spaheropsidin A (**18**) caused 51% larval mortality, while sphaeropsidin C (**19**) and diplopimarane (**21**) were inactive.

5.5 Structural identification of secondary metabolites isolated from *A. argyroxiphii* culture filtrates

The organic extract of *A. argyroxiphii* culture filtrate was purified as reported in detail in the Experimental section 4.13 (Scheme 6), yielding 9 compounds. Three new compounds: a trisubstituted dihydroisobenzofuranone (**23**), a tetrasubstituted 2-hydroxyethylbenzamide (**24**) and a tetrasubstituted phenyl dihydroxybutyl ether (**25**), named argyrottoxins A-C, were isolated together with six already known phytotoxins, which were identified as porritoxinol (**26**), its closely related phthalide (**27**) and its carboxylic acid derivative (**28**), zinniol (**29**), alternariol (**30**) and its 4-methyl ether (**31**) (Fig. 64). The known compounds were identified comparing their specific optical rotation and spectroscopic data with those previously reported in literature: (Suemitsu *et al.*, 1994) for porritoxinol (**26**), (Suemitsu *et al.*, 1992) for phthalide (**27**), (Yang *et al.*, 2011) for phthalide derivative (**28**), (White and Starrat, 1967) for zinniol (**29**) and (Tan *et al.*, 2008) for alternariol (**30**) and its 4-methyl ether (**31**).

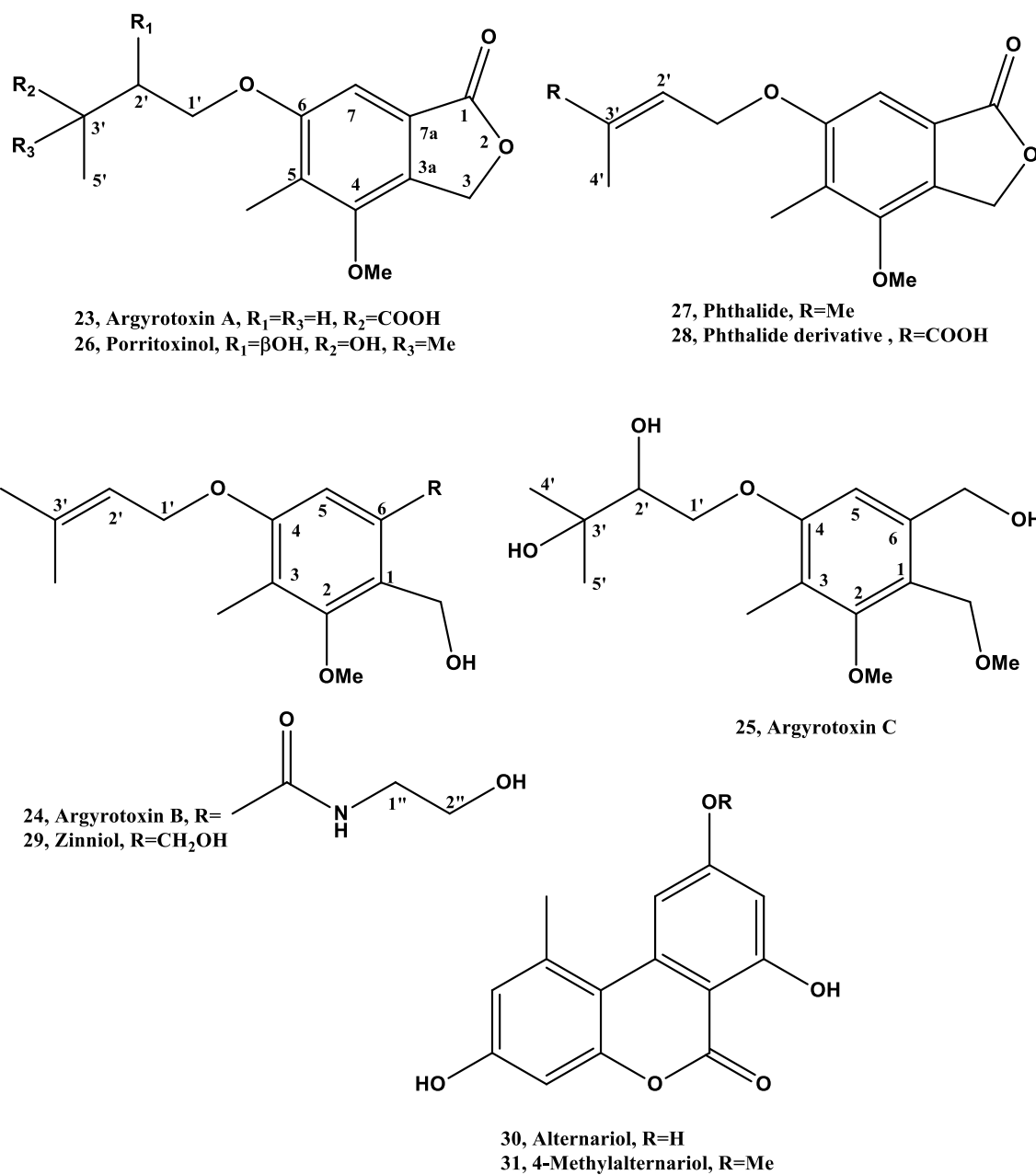


Figure 64: Secondary metabolites isolated from *Alternaria argyroxiphii*.

6-(3',3'-Dimethylallyloxy)-4-methoxy-5-methylphthalide was isolated from *Alternaria porri*, the causal fungus of black spot disease in the stone-leek and onion (Suemitsu *et al.*, 1992). Successively, from the same fungus porritoxinol (**26**) was isolated together with the known tentoxin,

porritoxin, and silvaticol (Suemitsu *et al.*, 1994). The phthalide derivative (**28**) was isolated from the endophytic fungus *Pestalotiopsis photiniae* Thüm (Yang *et al.*, 2011). Zinniol (**29**) was isolated for the first time from *Alternaria zinniae*, which caused leaf and stem blight on zinnia, sunflower, and marigold (White and Starrat, 1967). Then, it was isolated from *Phoma macdonaldii* Boerema, the causal agent of stem blight of sunflower (*Helianthus annuus* L.) (Sugawara and Strobel, 1986); successively, it was identified as the main metabolite from *Alternaria tagetica* S.K. Shome & Mustafee, the causal agent of early blight in marigold (*Tagetes erecta* L.) (Gamboa-Angulo *et al.*, 2000). Finally, it was a phytotoxin isolated from *Alternaria cirsinoxia* E.G. Simmons & K. Mort (Berestetskii *et al.*, 2010). Alternariol and its 4-methyl ether (**30** and **31**) were isolated from the mycelium of *Alternaria dauci* (J.G. Kühn) J.W. Groves & Skolko (Freeman, 1966) and, then, from the mangrove endophytic fungus GYT of No. 2240, obtained from the South China Sea Coast, together with a new alternariol derivative, 2240B and 4,10-dimethyl ether, showing strong anticancer activity against KB and KBv200 cells (Tan *et al.*, 2008). Compound **31** was previously isolated from an *Alternaria alternata* (Fr.) Keissl. strain isolated from grains of Linxian County, China, and it presented a strong mutagenic activity in *Escherichia coli* strain ND-160 (An *et al.*, 1989). The total synthesis of alternariol was also obtained in seven steps starting from orcinol and 3, 5-dimethoxybromobenzene (Koch *et al.*, 2005). Further study was also carried out on the mutagenicity of **30** and **31** in mammalian cells (Brugger *et al.*, 2006; Schrader *et al.*, 2006).

5.5.1 Structural determination of argyrotxin A

Argyrotxin A (**23**) had a molecular formula of $C_{15}H_{18}O_6$ as deduced from its HRESIMS, consistent with 7 hydrogen deficiencies. The IR spectrum showed the presence of bands typical of carboxylic, lactone, and aromatic groups at ν_{\max} 3400, 1754, 1700, 1618, 1466, 1423, 1125 cm^{-1} (Nakanishi and Solomon, 1977) and the UV spectrum had absorption maxima at λ_{\max} nm (log ϵ) 298 (3.2), 254 (3.6) indicating an extended conjugated system (Pretsch *et al.*, 2000).

Its 1H (Fig. 65, Table 15) and COSY NMR (Fig. 66) spectra presented two singlets at δ 7.07 and 5.37 typical of an aromatic proton (H-7) and of an oxygenated methylene (H_2C -3), probably involved in a lactone ring system. Two singlets at δ 3.88 and 2.19 due to a methoxy and a methyl groups were present together with the signals of a 3-substituted butyloxy side chain (Pretsch *et al.*, 2000). This latter was identified as a 3-carboxybutyloxy chain for the presence of a triplet at δ 4.09 ($J = 6.1$ Hz) (H_2C -1'), which in the COSY spectrum (Fig. 66) coupled with the two multiplets at δ 2.27 and 1.98 of the protons of the adjacent methylene group (H_2C -2'). The methylene group coupled with the proton resonating as a broad quartet at δ 2.78 ($J = 7.0$ Hz) of the adjacent methine group (HC-3'). This proton (HC-3') was also coupled with the protons of the adjacent methyl group (H_3C -5') appearing as a doublet at δ 1.30 ($J = 7.0$ Hz) (Pretsch *et al.*, 2000). The carboxyl group of this side chain resonated in

the ^{13}C NMR spectrum as a singlet at δ 180.6 (Breitmaier and Voelter, 1987) and coupled in the HMBC spectrum (Fig. 69, Table 15) with the protons of the next methine (HC-3'), methyl (H₃C-5') and methylene group (H₂C-2') (Berger and Braun, 2004). The long-range coupling observed in the HMBC spectrum (Fig. 69, Table 15) between C-6 and H₂C-1' allowed to locate the side chain at C-6 of the pentasubstituted benzene ring system. In the same way, the methoxy and the vinyl methyl were located at C-4 and C-5, respectively, of the same ring system due to the coupling observed in the same spectrum between OMe and C-4 and for those of the vinyl methyl group with C-3a and C-6. The ^{13}C NMR spectrum (Fig. 67, Table 15) presented another carbonyl (O= C-1) group as a singlet at δ 171.5 which belongs to a dihydrofuranone ring and coupled in the HMBC spectrum (Fig. 69, Table 15) with H₂C-3. In the HMBC spectrum (Fig. 69, Table 15), these protons (H₂C-3) also coupled with C-4 and C-5, while the carbonyl (C-1) coupled with HC-7. Thus, the junction between the trisubstituted benzene and the dihydrofuranone rings resulted to be between C-3a and C-7a. In the HMBC spectrum (Fig. 69, Table 15), these two tertiary sp² carbons coupled with HC-7, while C-7a also coupled with H₂C-3. The coupling observed in the HSQC spectrum (Fig. 68, Table 15) allowed to assign the chemical shifts to the protonated carbons. The signals observed at δ 101.6, 68.5, 66.5, 59.5, 36.4, 32.7, 17.3 and 9.8 were assigned to C-7, C-3, C-1', OMe, C-3', C-2', C-5' and MeC-5 (Breitmaier and Voelter, 1987). While the signals observed at δ 159.2, 153.0, 128.4, 125.7, and 125.0 were assigned to tertiary sp² carbons C-6, C-4, C-7a, C-3a and C-5 according to the coupling observed in the HMBC spectrum (Fig. 69, Table 15) (Breitmaier and Voelter, 1987).

Table 15: ¹H and ¹³C NMR data of argyrotxin A (23)^{a,b}

position	δ_C^c	δ_H (J in Hz)	HMBC
1	171.5 s		H ₂ -3, H-7
2			
3	68.5 t	5.37 s (2H)	
3a	125.7 s		Me, H-7
4	153.0 s		Me, Me, H ₂ -3, H-7
5	125.0 s		H ₂ -3
6	159.2 s		Me, H-7, H ₂ -1'
7	101.6 d	7.07 s	
7a	128.4 s		H ₂ -3, H-7
1'	66.5 t	4.09 t (6.1) (2H)	H ₂ -2'
2'	32.7 t	2.27 m 1.98 m	H ₂ -1', H-3', H ₃ -5'
3'	36.4 d	2.78 q (7.0)	H ₂ -1', H ₂ -2', H ₃ -5'
4'	180.6 s		H ₂ -2', H-3', H ₃ -5'
5'	17.3 q	1.30 d (7.0) (3H)	H ₂ -2', H-3'
OMe	59.5 q	3.88 s	
Me	9.8 q	2.19 s	

^aThe chemical shifts are in δ values (ppm) from TMS. ^b2D ¹H, ¹H (COSY) and ¹³C, ¹H (HSQC) NMR experiments confirmed the correlations of all the protons and the corresponding carbons.

^cMultiplicities were assigned with DEPT.

Thus, the chemical shifts were assigned to all carbons and corresponding protons (Table 15) and argyrotxin A (**23**) was formulated as 4-(7-methoxy-6-methyl-3-oxo-1, 3-dihydro-isobenzofuran-5-yloxy)-2-methyl-butyric acid.

The structure of **23** was supported from all the other couplings observed in the HMBC spectrum (Fig. 69, Table 15) and from its HRESIMS spectrum. This latter showed a sodium adduct ion $[M + Na]^+$ at m/z 317.1010. The ESIMS spectrum showed the same peak and the potassium $[M + K]^+$ and the protonated $[M + H]^+$ adduct ions at m/z 333 and 295. A significant fragmentation ion $[M + H - H_2O]^+$ was generated from the protonated adduct ion by loss of H₂O at m/z 277. The structure was also supported by the correlation observed in NOESY spectrum (Fig. 70) between MeO and H₂C-3 and Me and HC-7 and H₂C-1' (Berger and Braun, 2004).

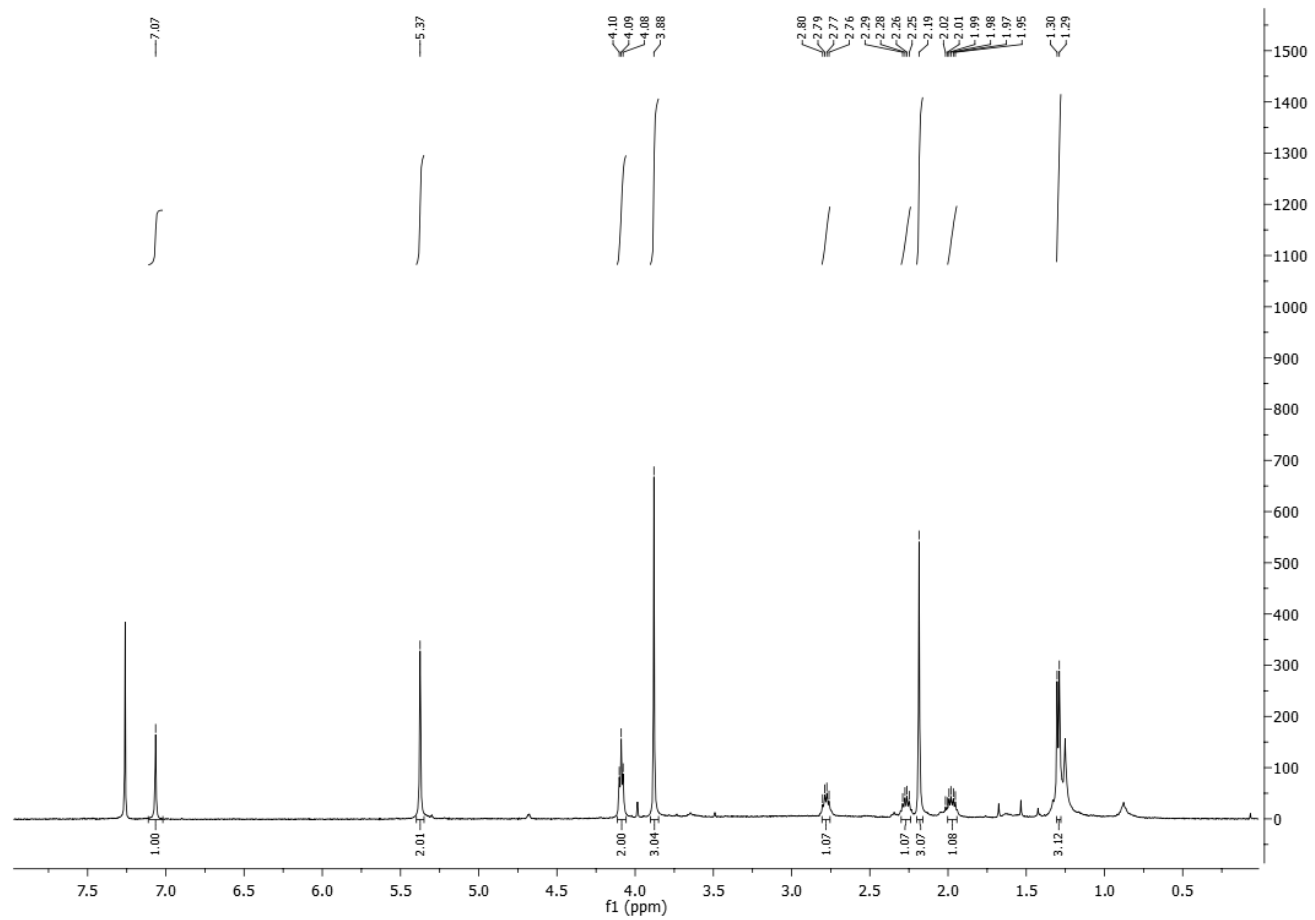


Figure 65: ^1H NMR spectrum of argyrotxin A (23) (CDCl_3 , 400 MHz).

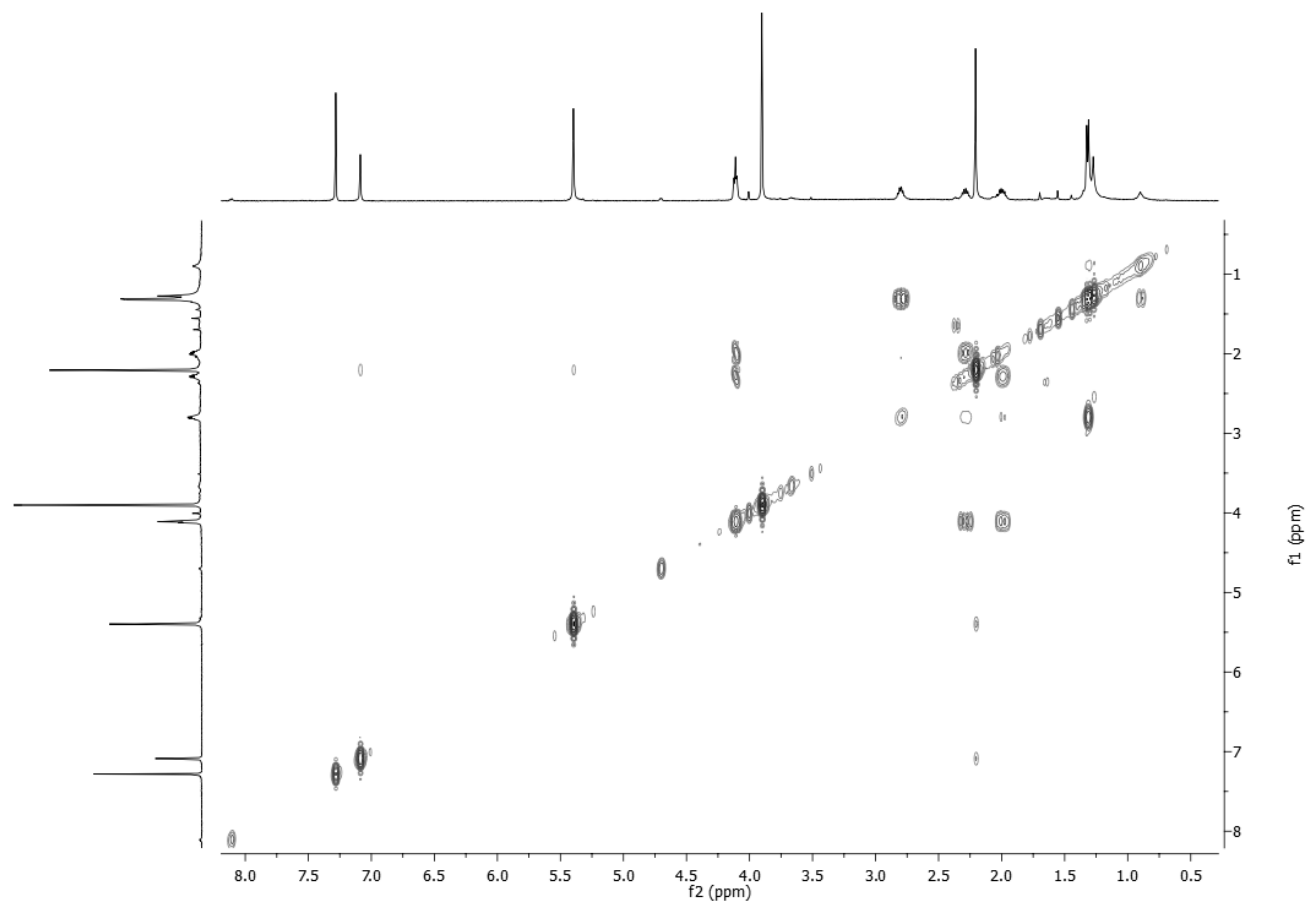


Figure 66: COSY spectrum of argyroxin A (23) (CDCl_3 , 400 MHz).

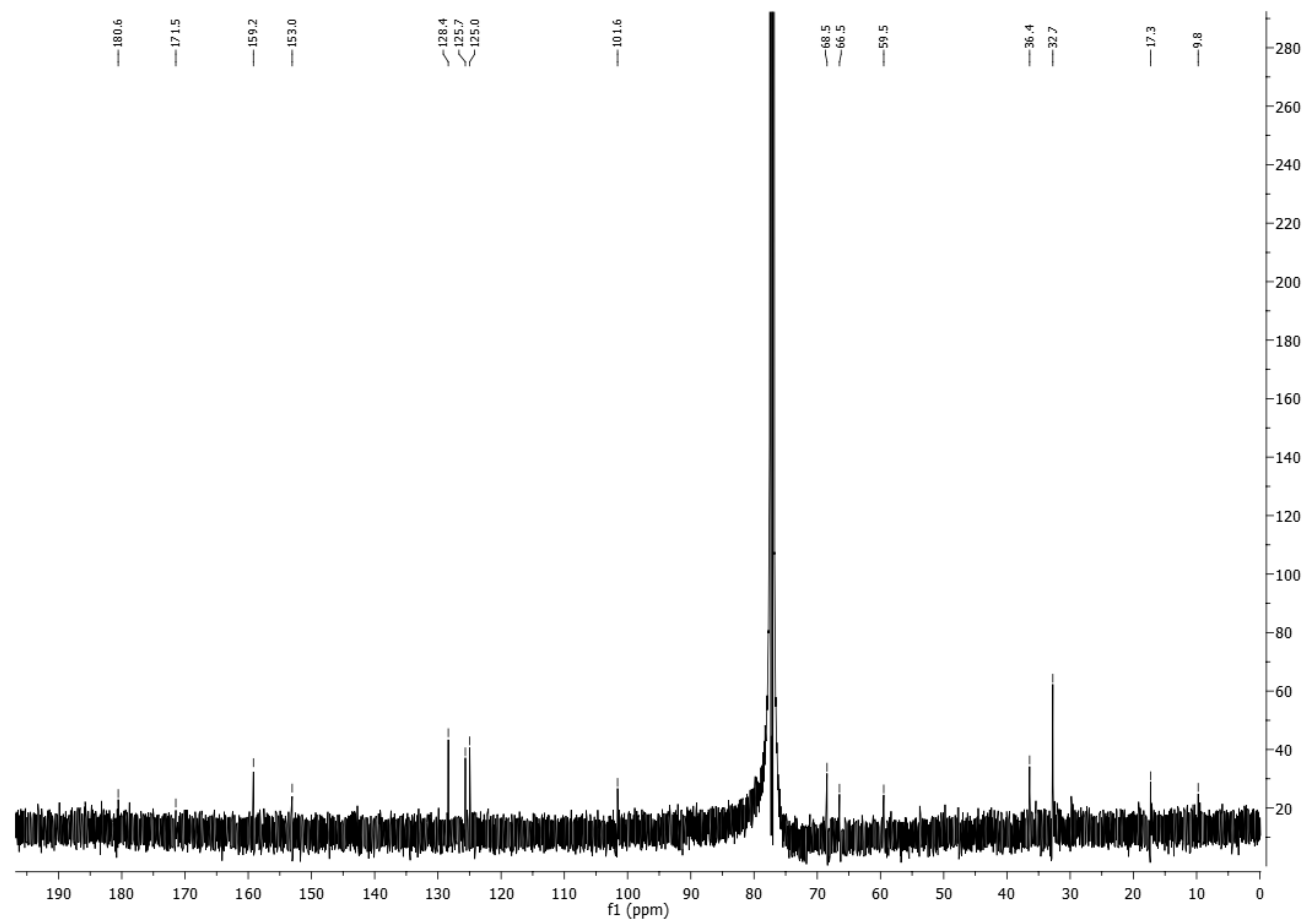


Figure 67: ^{13}C NMR spectrum of argyrotxin A (23) (CDCl_3 , 100 MHz).

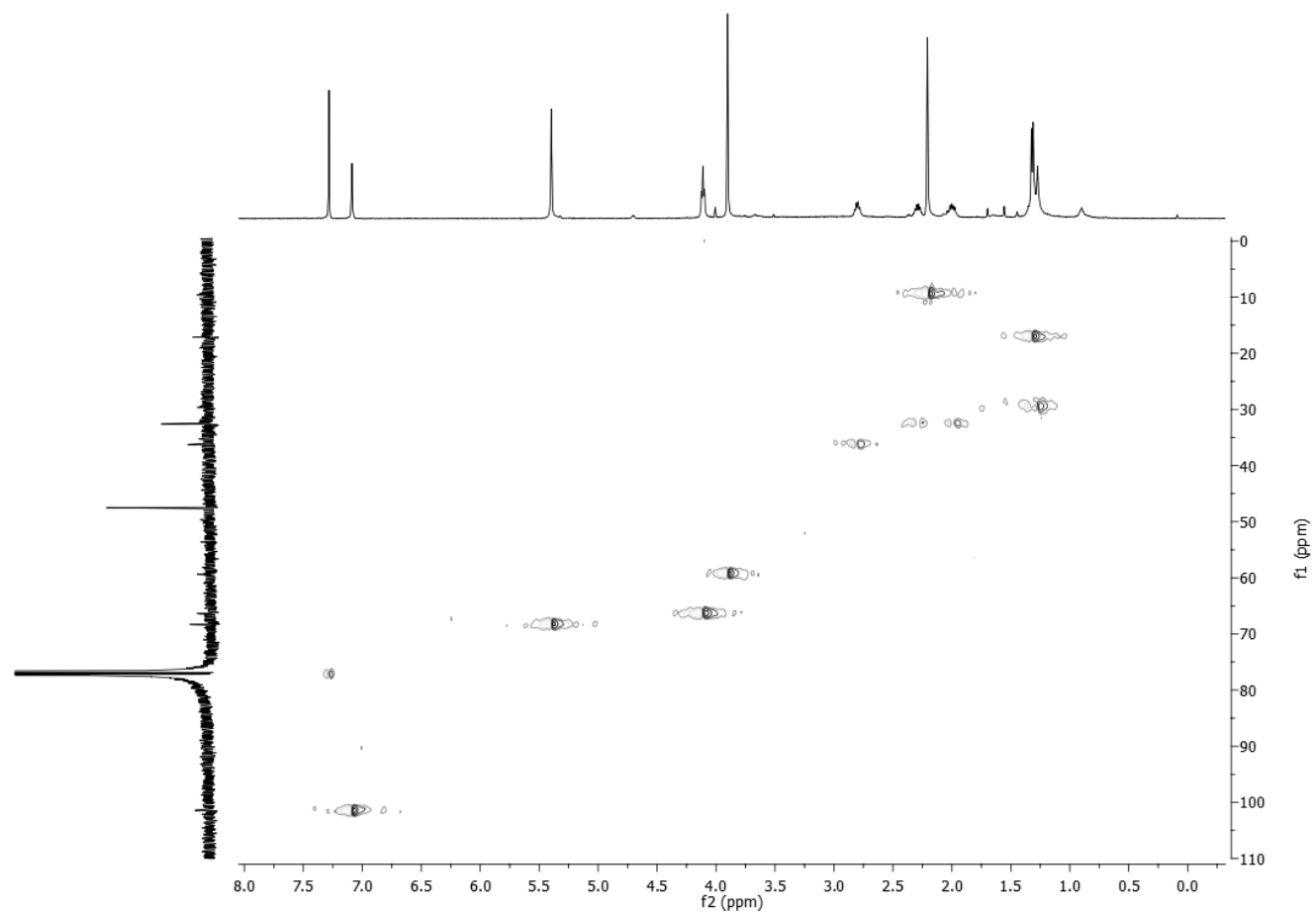


Figure 68: HSQC spectrum of argyrotxin A (23) (CDCl₃, 400/100 MHz).

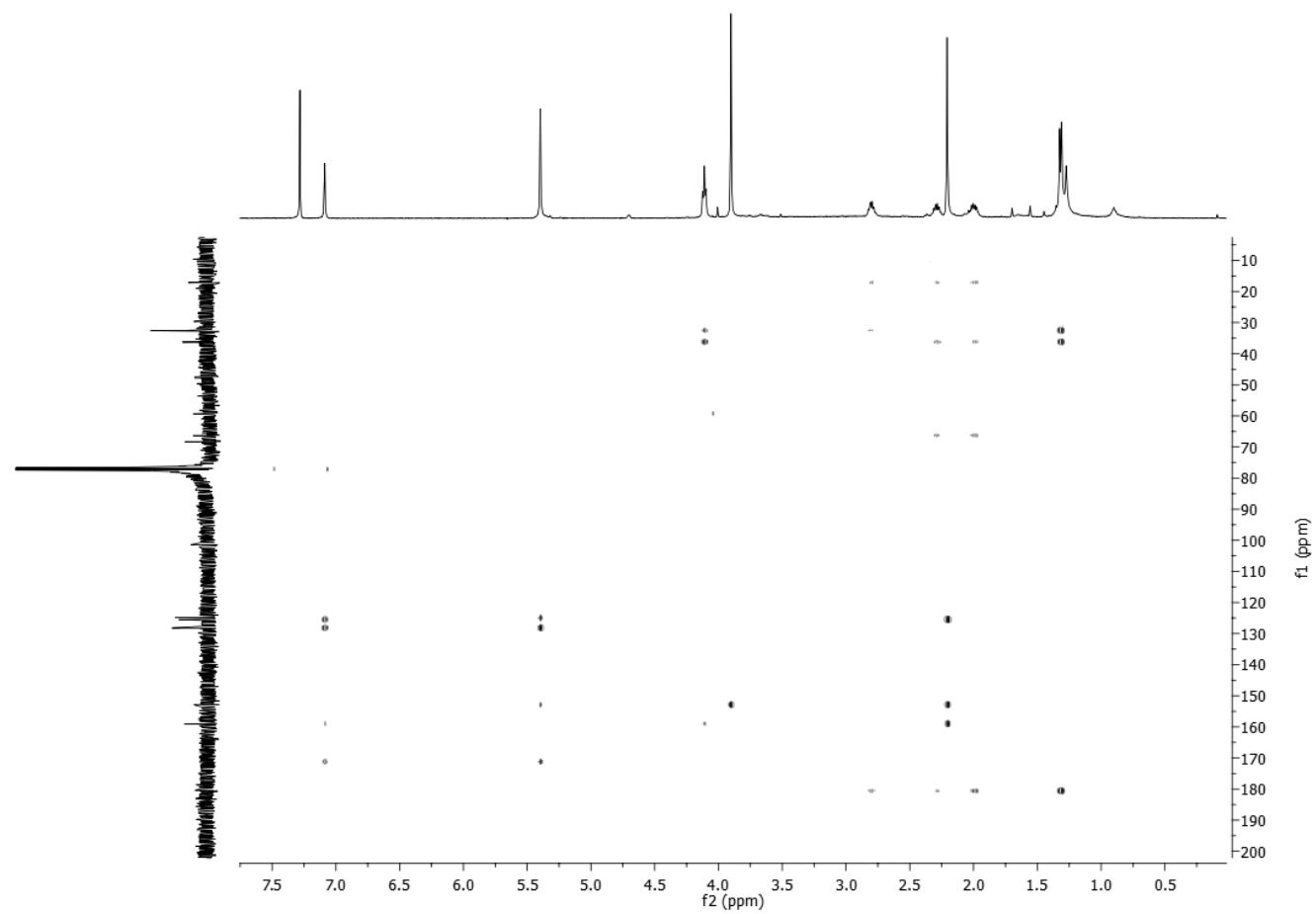


Figure 69: HMBC spectrum of argyrotxin A (23) (CDCl₃, 400/100 MHz).

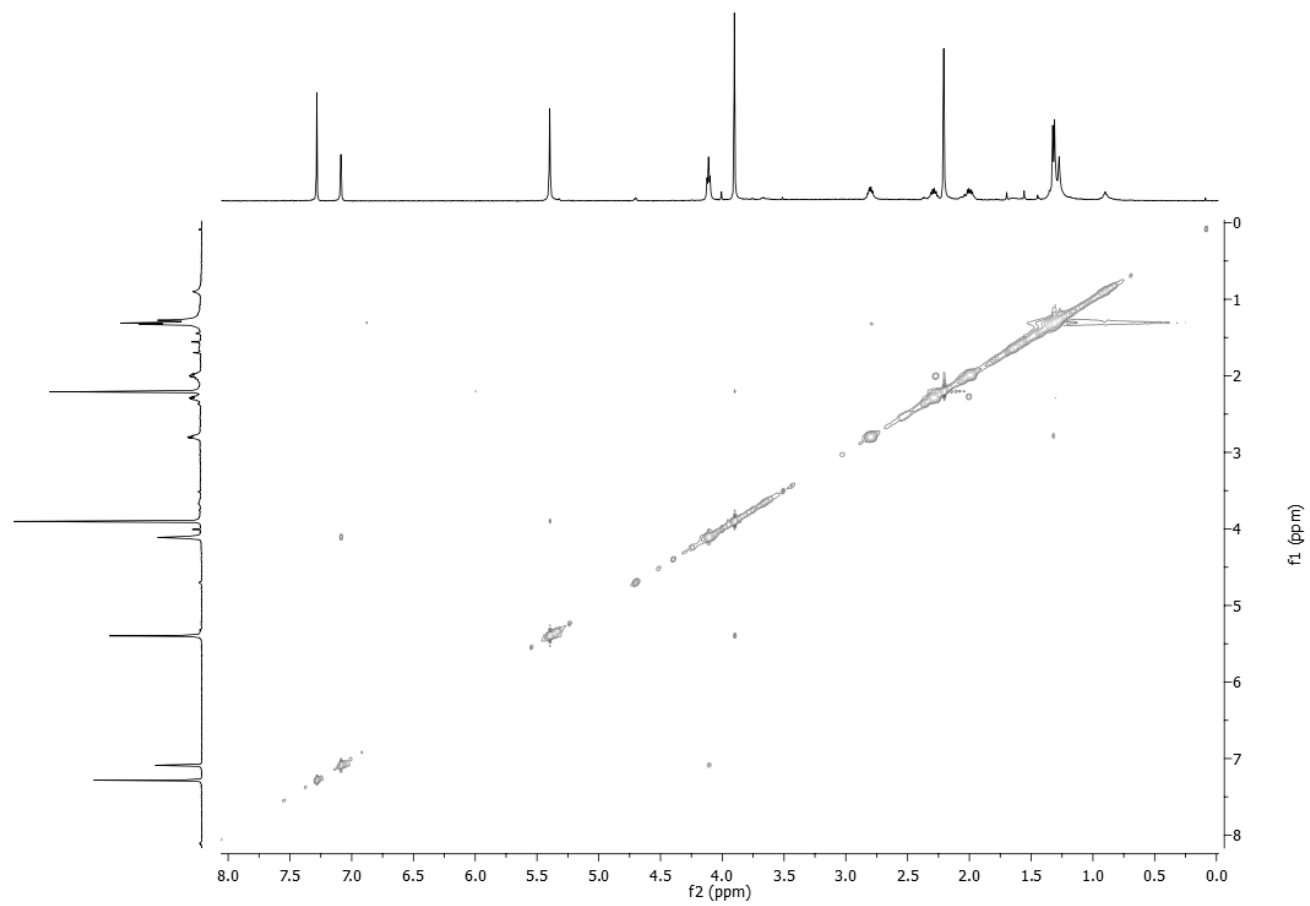


Figure 70: NOESY spectrum of argyrotxin A (23) (CDCl₃, 400 MHz).

5.5.2 Absolute configuration of argyrotxin A

The electronic circular dichroism (ECD) spectrum of **23** showed a single weak negative Cotton effect at about 190 nm, while above 210 nm, only very weak signals ($\Delta\epsilon < 0.01$) with a low signal to noise ratio were detected. This expecting result was due to the high distance between the stereogenic center and the aromatic chromophoric moiety. Moreover, a preliminary molecular mechanics conformational analysis of compound **23** provided about 100 populated conformers within a 10 kcal/mol energy range. Such high molecular flexibility and the very weak chiroptical response of compound **23** had necessitated the application of the so-called “chiroptical probes” for the absolute configuration assignment. In this method an achiral chromophoric moieties are linked to a chiral nonracemic substrate, give rise to diagnostic chiroptical signal(s), usually in ECD spectrum, from the sign of which the absolute configuration of the substrate can be determined without any computation. A very efficient type of chiroptical probes is constituted by the flexible 2,2'-bridged biphenyls, that have been extensively used for the absolute configuration assignment to chiral diols (Superchi *et al.*, 2001), carboxylic acids (Superchi *et al.*, 2006; Vergura *et al.*, 2019), primary amines (Vergura *et al.*, 2018), and recently applied to natural products (Santoro *et al.*, 2020) and chiral drugs (Vergura *et al.*, 2021). According to this method, 2-substituted carboxylic chiral acids, like argyrotxin A (**23**), are transformed in the corresponding biphenylamides (Fig. 71), affording a pair of diastereomeric amides with opposite biphenyl twist.

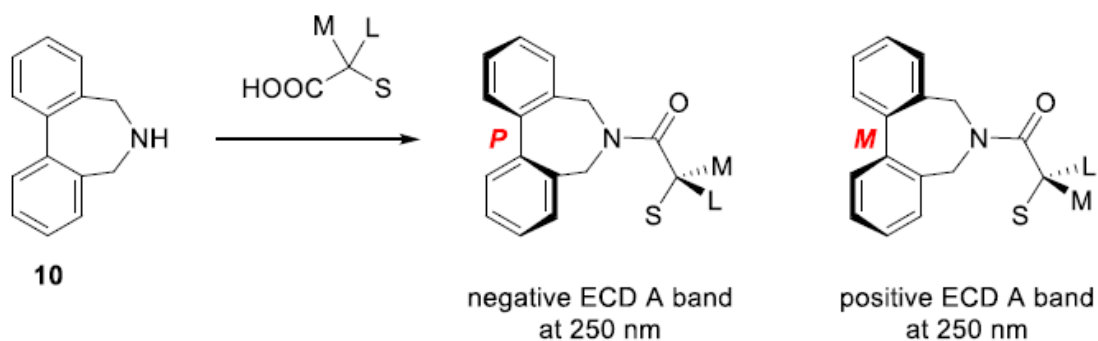


Figure 71: Biphenyl probes for the absolute configuration determination to chiral acids by ECD. L = largest group, M = medium size group, S = smallest group.

These diastereomers are in a thermodynamic equilibrium and the most stable atropisomer is also the major one. Moreover, the sense of the biphenyl twist can be detected by the sign of ECD Cotton effect at 250 nm (biphenyl A band) (Sagiv *et al.*, 1977), which is positive for a *M* torsion and negative for a *P* one (Mislow and Gordon, 1963). As depicted in Fig. 72, it was demonstrated that for the absolute configuration the diastereomer having *P* torsion is more stable (and thus more abundant) than the *M* twisted one (Superchi *et al.*, 2006).

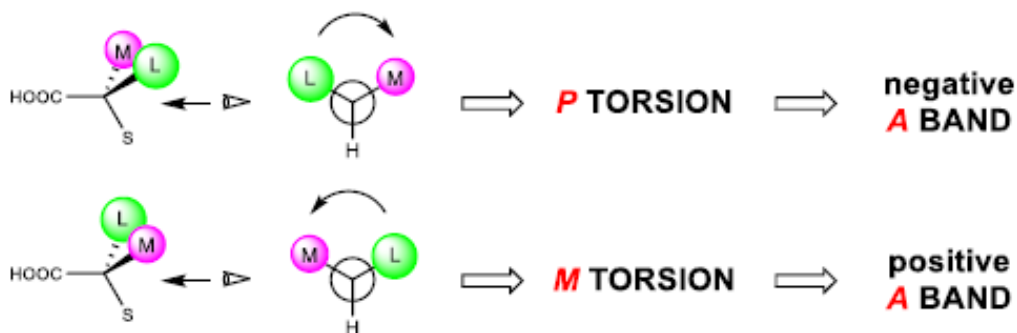


Figure 72: Mnemonic scheme relating the absolute configuration and the sign of the A band in the ECD spectrum of biphenylamides. L = largest group, M = medium size group, S = smallest group.

Thus, a non-empirical rule was found to determine the absolute configuration of chiral carboxylic acids by inspecting the sign of the biphenyl A band at ~250 nm in the ECD spectrum of their biphenylamides. According to such rule, a *P* biphenyl twist is preferred for 2-substituted aliphatic chiral carboxylic acids having absolute configuration such that a clockwise rotation leads from the largest to the smallest substituent on the acid moiety, and thus a negative A band is expected at around 250 nm in the ECD spectrum of the corresponding biphenyl derivatives. Instead, an *M* twist is preferred for a counterclockwise disposition of the substituents and a positive A band arises in the ECD spectrum (Fig. 72).

To apply this method, argyrotxin A (**23**) was converted to the corresponding biphenylamide **23a** by reaction with the biphenylazepine in the presence of EDC hydrochloride and *N,N'*-dimethylammino pyridine (DMAP) in CH_2Cl_2 (Fig. 73).

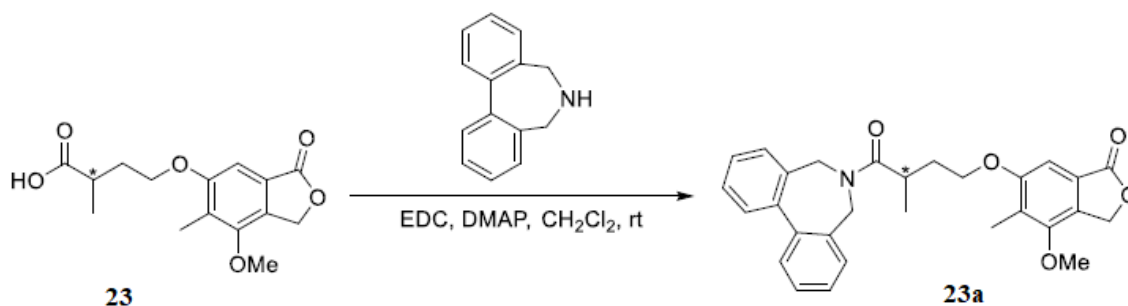


Figure 73: Synthesis of biphenylamide **23a** from argyrotxin A (**23**).

The UV and ECD spectra of biphenylamide **23a** were directly recorded on the crude (Fig. 74), because we did not expect significant ECD signal interference from not reacted argyrotxin A (**23**), while racemic amine was not ECD active as well. Therefore, the only ECD active compound was the biphenylamide derivative **23a**.

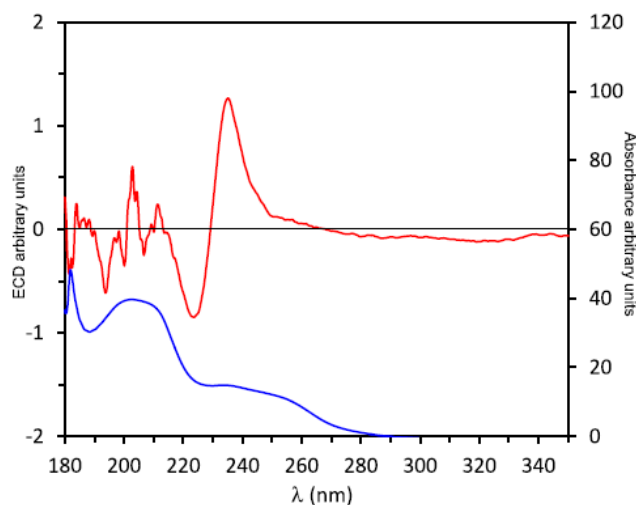


Figure 74: UV and ECD spectra (CH₃CN) of biphenylamide **23a. Being the spectra recorded on crude mixture, values on vertical axes are on arbitrary units.**

The UV spectrum of **23a** had the typical features of the biphenyl chromophore characterized by the A band at about 240 nm and the more intense C band at about 200 nm (Sagiv *et al.*, 1977). In the ECD spectrum, a positive Cotton effect was visible at 236 nm and a negative one at 224 nm. At shorter wavelength, the higher UV absorbance, due also to unreacted biphenylazepine, prevented detection of clear ECD signals. The positive Cotton effect in correspondence to the biphenyl A band revealed an *M* twist of the biphenyl moiety in **23a**, consequently the (*R*) absolute configuration to the C-3' stereocenter was assigned on the basis of the mnemonic rule (Fig. 72).

5.5.3 Structural determination of argyrotxin B

Argyrotxin B (**24**) had a molecular formula of C₁₇H₂₅NO₅ as deduced from its HRESIMS spectrum, consistent with 6 hydrogen deficiencies. Its IR showed the presence of bands typical of hydroxy, carbonyl, olefinic and aromatic residues at ν_{\max} 3409, 1660, 1620, 1561, 1453, 1424, 1124 cm⁻¹ (Nakanishi and Solomon, 1977), while the UV spectrum showed absorption maxima at λ_{\max} nm (log ϵ) 291 (3.3), 254 (3.7) typical for aromatic systems spectrum (Pretsch *et al.*, 2000). Its ¹H NMR (Fig. 75, Table 16) and COSY spectra (Fig. 76) showed a singlet at δ 7.08 typical of a pentasubstituted benzene ring proton (H-5), a singlet at δ 3.86 of a methoxy group, three singlets at δ 1.74, 1.79 and 2.20 of three methyl groups (Me-4', Me-5' and Me-3) and a singlet at δ 4.53 of the CH₂O bounded to C-1 (Pretsch *et al.*, 2000). Moreover, the signal systems of two side chains were also observed. The first was a 3-methylbut-2-enyloxy, as deduced from the doublet at δ 4.57 (*J* = 6.8 Hz) of an oxygenated methylene group (H₂C-1'), which coupled with the broad triplet at δ 5.50 (*J* = 6.8 Hz) of the adjacent proton (HC-2') of a trisubstituted olefinic group. The latter proton (HC-2') was also allylic coupled (*J* < 1 Hz) with the two methyl groups at δ 1.79 and 1.74 (Me-5' and Me-4') of the tail

(Pretsch *et al.*, 2000). The other side chain showed signal system typical of a 2-hydroxyethylcarboxamide, appearing as two coupled triplets at δ 3.92 (H₂C-2'') and 3.77 (H₂C-1'') (J = 4.8 Hz). The corresponding carbonyl group resonated in the ¹³C NMR spectrum (Fig. 77, Table 16) at δ 170.2 and coupled in the HMBC spectrum (Fig. 79, Table 16) with H₂C-2'', CH₂OH and H-5. The latter correlation allowed to locate the residue at C-6 of benzene ring. The coupling observed in the HMBC spectrum (Fig. 79, Table 16) between the OMe and C-4 and between Me and C-2, C-3, C-4 and C-6 allowed to locate these groups at C-2 and C-3, respectively. Consequently, the 3-methylbut-2-enyloxy residue resulted to be located at C-4. The coupling observed in the HSQC spectrum (Fig. 78) allowed to assign the protonated carbons. In particular, the signals observed at δ 119.8, 101.4, 65.9, 62.2, 59.9, 50.2, 46.7, 25.9, 18.4 and 9.7 were assigned to C-2', C-5, C-1', C-2'', OMe, CH₂OH, C-1'', C-4', C-5' and Me (Breitmaier and Voelter, 1987). The tertiary sp² olefinic carbon C-3' was assigned to the signal at δ 137.9 by its couplings observed in the HMBC spectrum (Fig. 79, Table 16) with H₂C-1', Me-4' and Me-5'. In the same spectrum, the five tertiary sp² aromatic carbons at δ 158.8, 153.5, 131.7, 124.1 and 123.5 coupled, respectively, with Me, OMe and Me, Me and CH₂OH, H-5, Me and CH₂OH, and Me and CH₂OH and, thus, were assigned to C-2, C-4, C-6, C-1 and C-3 (Breitmaier and Voelter, 1987).

Table 16: ¹H and ¹³C NMR data of argyrotaxin B (24)^{a,b}

position	δ_C^c	δ_H (J in Hz)	HMBC
1	124.1 s		H-5, Me, CH ₂ OH
2	158.8 s		Me
3	123.5 s		Me, CH ₂ OH
4	153.5 s		MeO, Me
5	101.4 d	7.08 s	
6	131.7 s		Me, CH ₂ OH
1'	65.9 t	4.57 d (6.8) (2H)	
2'	119.8 d	5.50 br t (6.8)	H ₂ -1', Me-4', Me-5'
3'	137.9 s		H ₂ -1', Me-4', Me-5'
Me-4' ^{td}	25.9 q	1.79 br s (3H)	Me-5'
Me-5' ^{td}	18.4 q	1.74 br s (3H)	Me-4'
1''	46.7 t	3.77 t (4.8) (2H)	H ₂ -2''
2''	62.2 t	3.92 t (4.8) (2H)	
OMe	59.9 q	3.86 s	
OCH ₂	50.2 t (2C)	4.53 s (2H)	
Me	9.7 q	2.20 s	
C=O	170.2 s		H-5, H ₂ -2'', CH ₂ OH

^aThe chemical shifts are in δ values (ppm) from TMS. ^b2D ¹H, ¹H (COSY) and ¹³C, ¹H (HSQC) NMR experiments confirmed the correlations of all the protons and the corresponding carbons.

^cMultiplicities were assigned with DEPT. ^dThese assignment could be reversed.

Thus, the chemical shifts were assigned to all the carbons and the corresponding protons (Table 16) and argyrotaxin B (**24**) was formulated as 5-but-2-enyloxy-*N*-(2-hydroxy-ethyl)-2-hydroxymethyl-3-methoxy-4-methyl-benzamide. The structure of **24** was supported by all the couplings observed in the HMBC spectrum (Fig. 79, Table 16) and by the data of its HRESIMS spectrum. This latter showed the peak generated from its sodium adduct ion by loss of H₂O [M + Na - H₂O]⁺ at *m/z* 328.1534. The ESIMS spectrum showed the same peak and the ions generated by loss of H₂O from the potassium and protonated adduct ions [M + K - H₂O]⁺ and [M + H - H₂O]⁺ at *m/z* 344 and 306, respectively. The structure was also confirmed by the correlations observed in the NOESY spectrum (Fig. 80) between

OMe and CH₂OH, this latter and H₂C-1", H-5 and H₂C-1', H₂-2' with both Me-4' and Me-5' and between these latter two methyl groups (Berger and Braun, 2004).

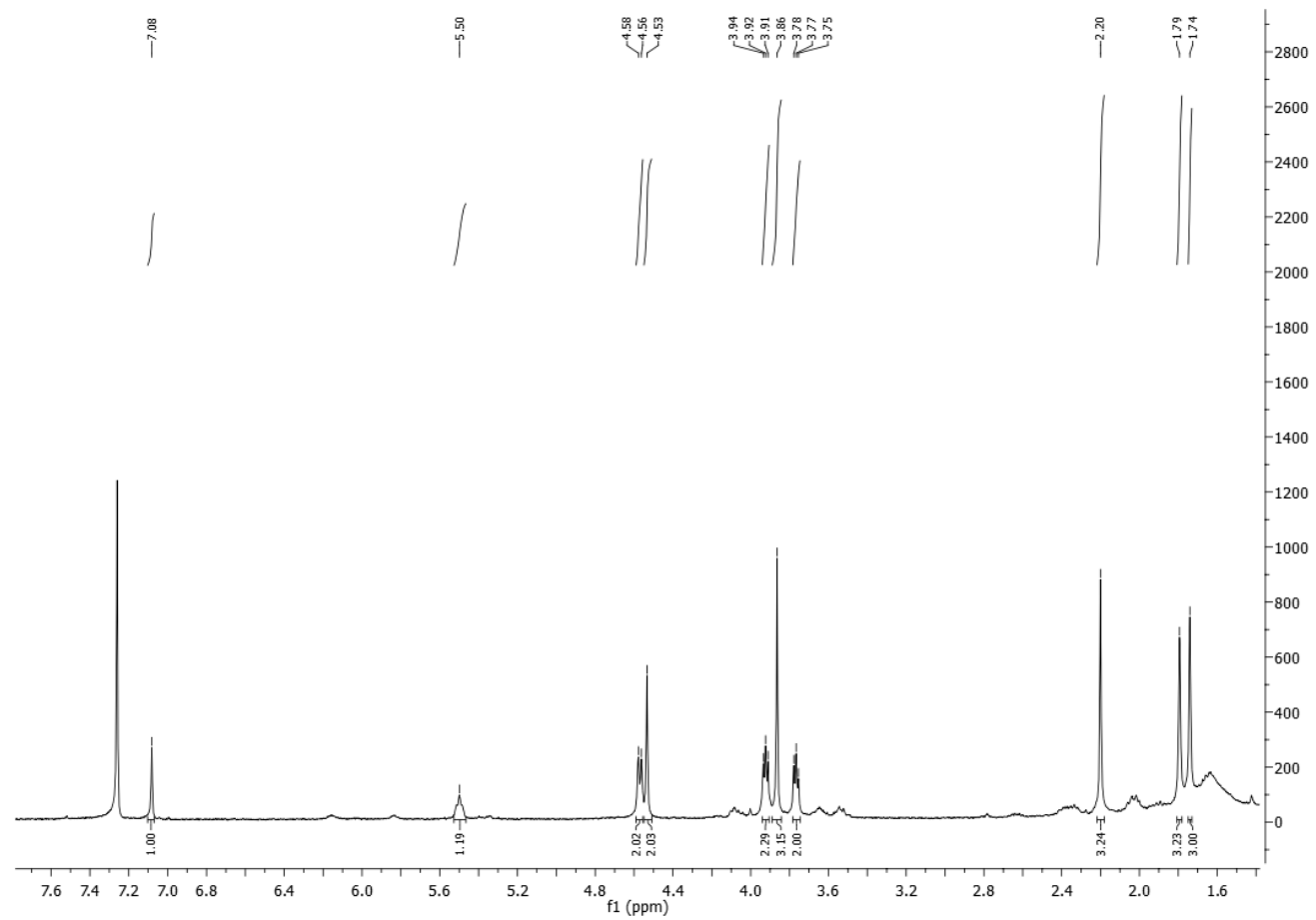


Figure 75: ^1H NMR spectrum of argyroxin B (24) (CDCl_3 , 400 MHz).

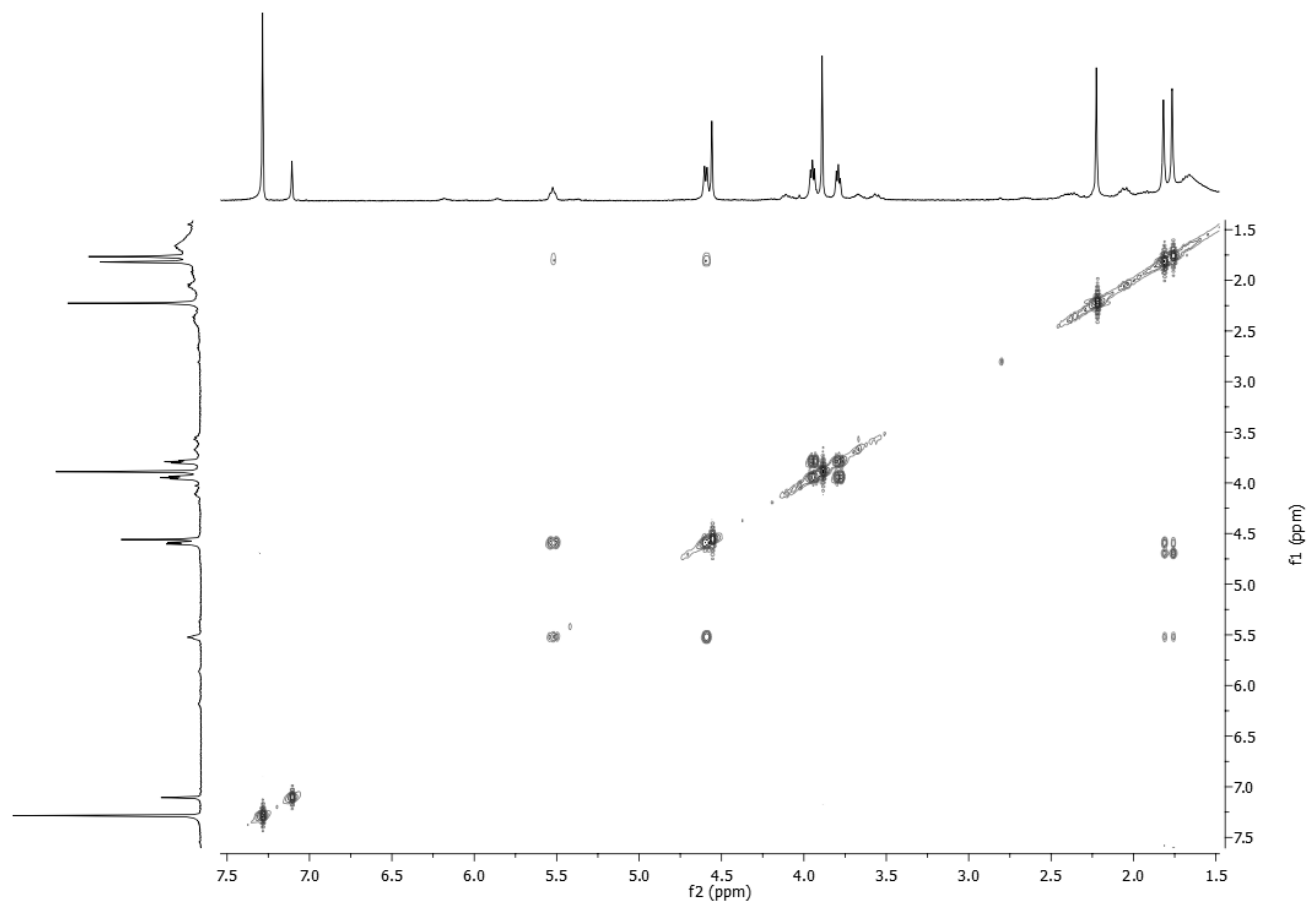


Figure 76: COSY spectrum of argyroxin B (24) (CDCl_3 , 400 MHz).

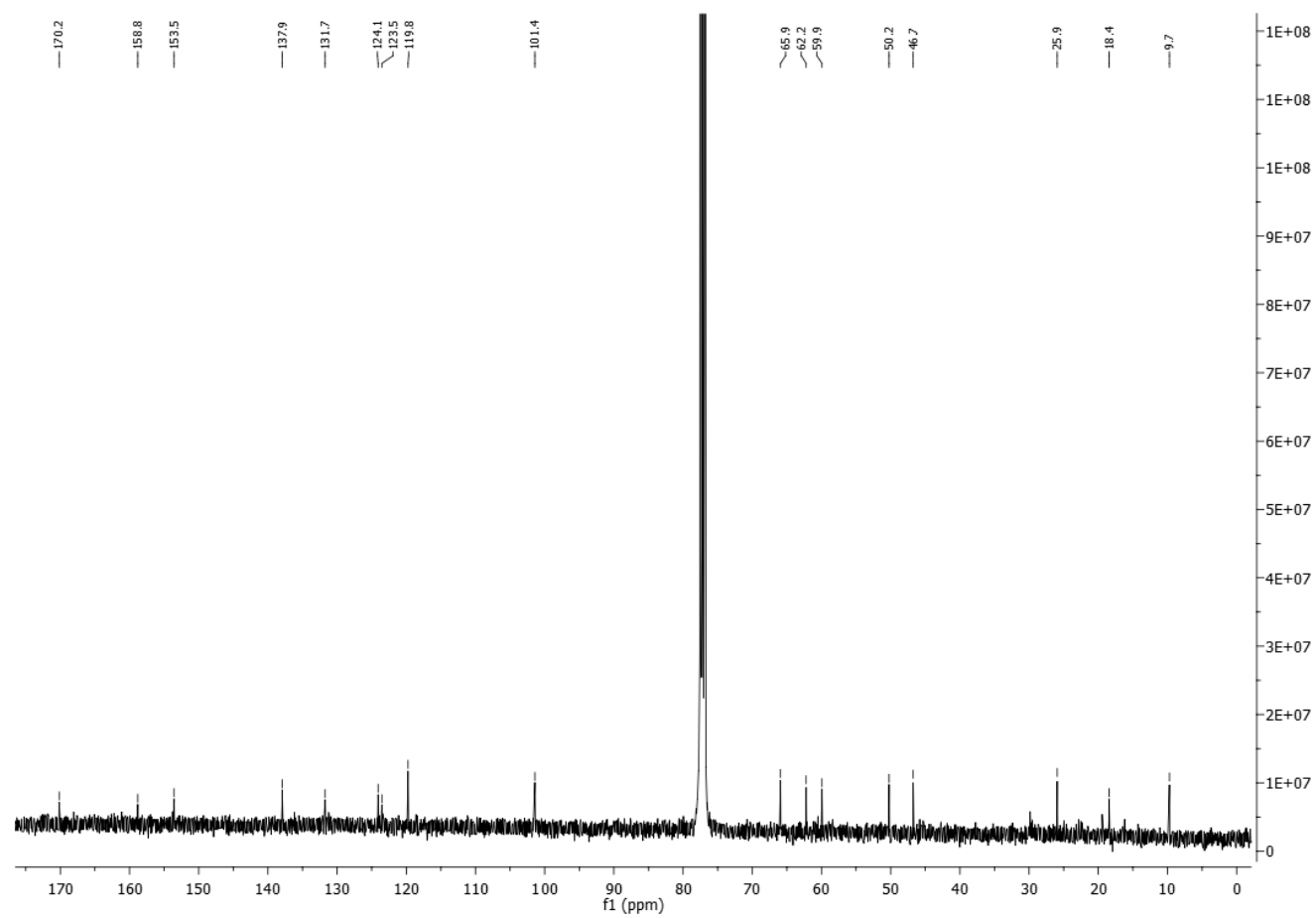


Figure 77: ^{13}C NMR spectrum of argyroxin B (24) (CDCl_3 , 100 MHz).

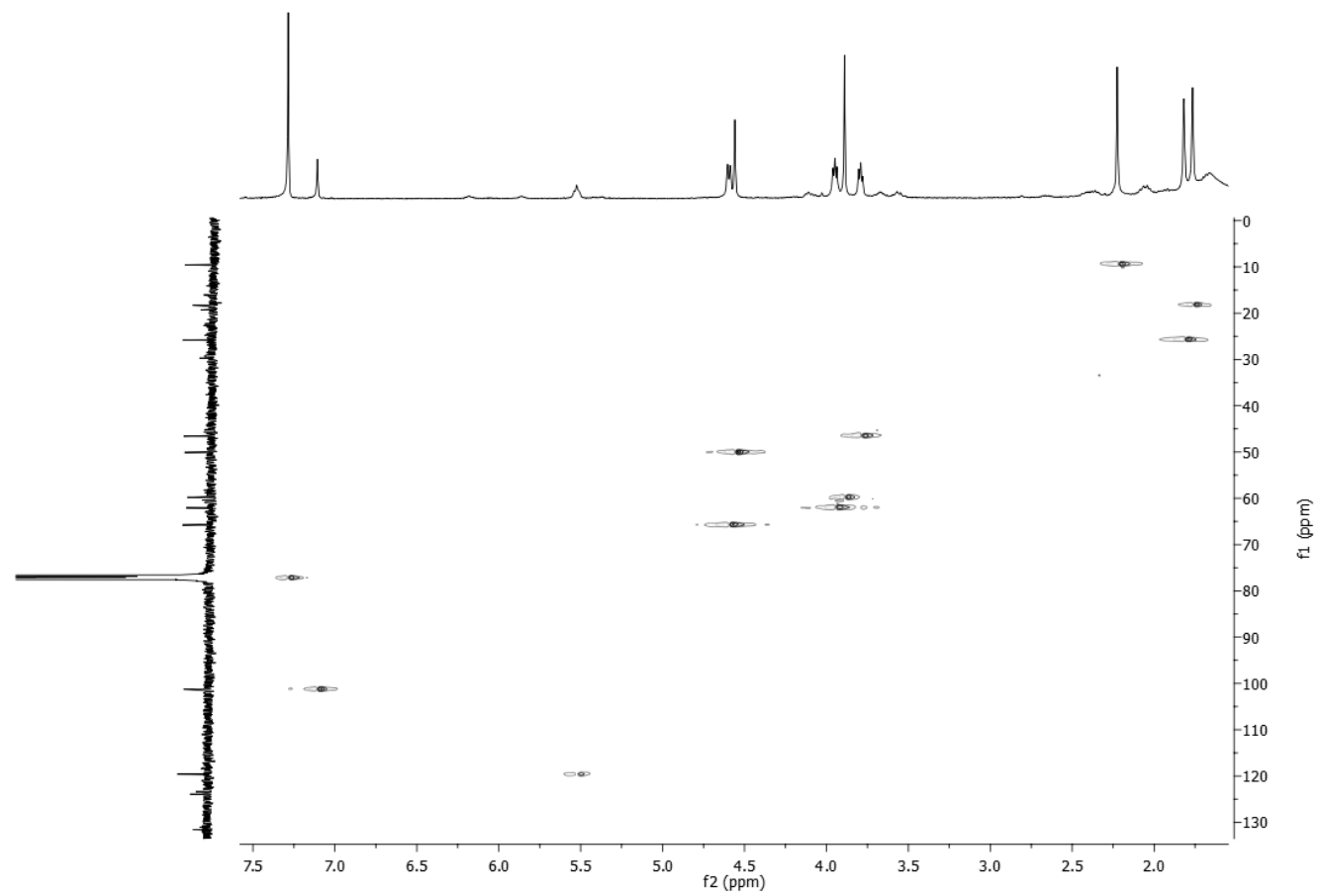


Figure 78: HSQC spectrum of argyrotxin B (24) (CDCl₃, 400/100 MHz).

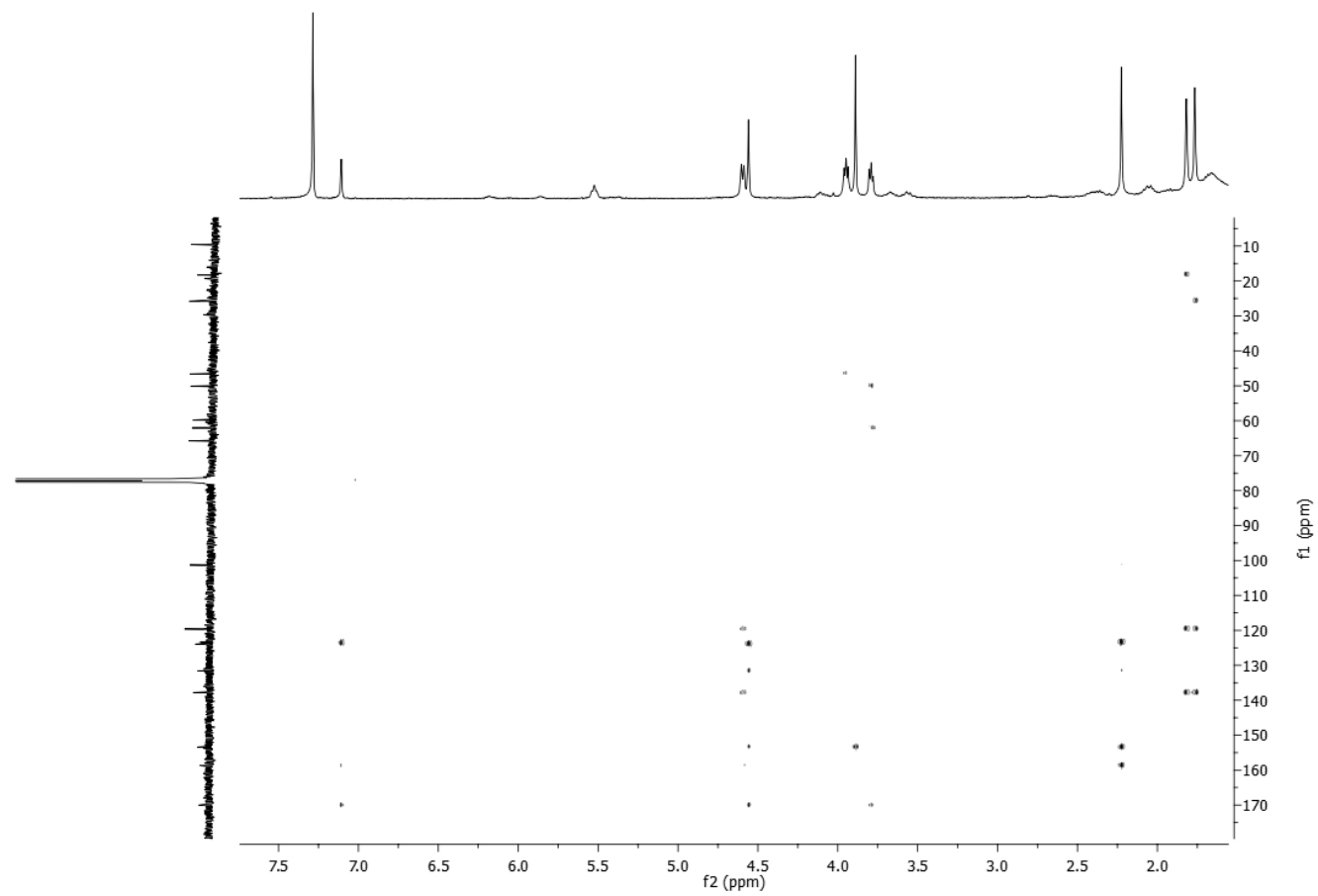


Figure 79: HMBC spectrum of argyrotxin B (24) (CDCl₃, 400/100 MHz).

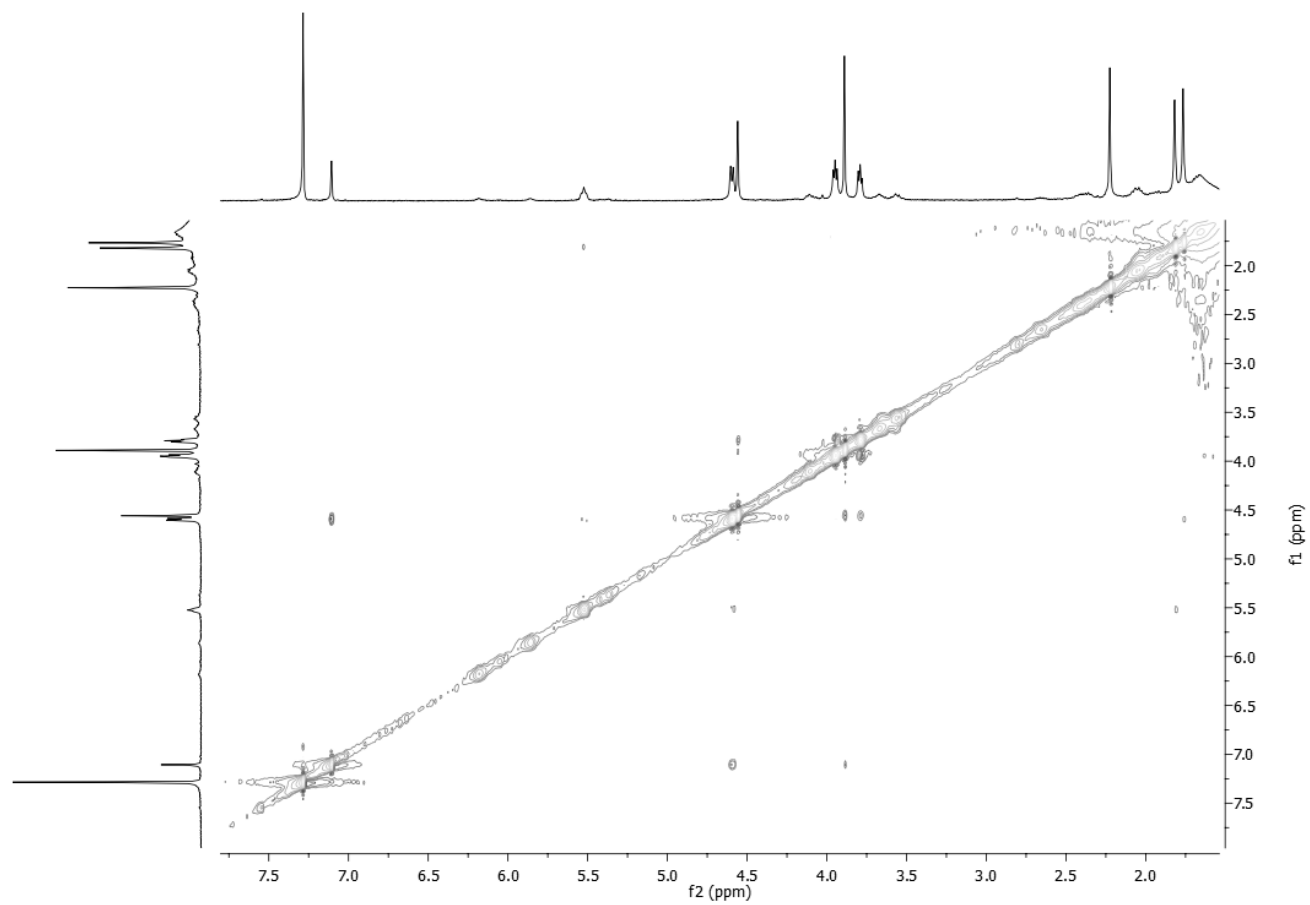


Figure 80: NOESY spectrum of argyrotxin B (24) (CDCl₃, 400 MHz).

5.5.4 Structural determination of argyrotxin C

Argyrotxin C (**25**) had a molecular formula of $C_{16}H_{26}O_6$ as deduced from its HRESIMS spectrum, consistent with 4 hydrogen deficiencies. Its IR spectrum had the bands typical of hydroxy and aromatic groups at ν_{\max} 3369, 1605, 1582, 1456, cm^{-1} (Nakanishi and Solomon, 1977); the UV spectrum showed absorption maxima at λ_{\max} nm ($\log \epsilon$) 273 (3.2) typical for aromatic systems (Pretsch et al., 2000). The preliminary investigation of its 1H and ^{13}C NMR spectra highlighted that it was close to both zinniol (**29**) and agyrotxin B (**24**), having a tetrasubstituted anisole moiety as those compounds. However, argyrotxin C (**25**) differed from zinniol (**29**) for the presence of a methoxymethylene group and of the side chains attached to C-1, C-4 and C-6. In fact, its 1H (Fig. 81, Table 17) and COSY (Fig. 82) presented a singlet typical of another methoxy group at δ 3.39 linked, on the basis of the coupling observed in the HMBC (Fig. 85, Table 17), to the benzylic methylene at C-1, which appeared as singlet at δ 4.53 in the 1H NMR spectrum (Fig. 81, Table 17). This spectrum had the singlet of the other benzyl hydroxymethylene group at δ 4.68 linked at C-6, as derived from the coupling observed in the HMBC (Fig. 85, Table 17). Furthermore, the side chain located to C-4 was a 2,3-dihydroxy-3-methylbutyloxy, while in compound **29** was a 3-methylbut-2-enyloxy. In fact, the 1H and COSY spectra showed the presence of three doublet doublets typical of an ABC system resonated at δ 4.29 and 3.98 and 3.78 ($J = 9.8$ and 3.3 and $J = 9.8$ and 8.0 Hz and $J = 8.0$ and 3.3) for the signal of H_2C-1' and $HC-2'$, respectively (Sternhell, 1969). The two terminal methyl groups (Me-4' and Me-5') resonated as two singlets at δ 1.29 and 1.26 and were linked at C-3' by their couplings observed in the HMBC spectrum (Fig. 85, Table 17). The same carbon also coupled in the HMBC spectrum with the proton of the adjacent hydroxylated methine $HC-2'$, which resonated in the ^{13}C NMR spectrum (Fig. 83, Table 17) at δ 72.8 (Breitmaier and Voelter 1987). The coupling observed in the HSQC (Fig. 84) and the HMBC spectra allowed to assign the chemical shifts to all the carbons and the corresponding protons as reported in Table 17.

Table 17: ¹H and ¹³C NMR data of argyrotxin C (25).^{a,b}

position	δ_C^c	δ_H (J in Hz)	HMBC
1	121.7 s		OCH ₂ , <u>CH₂OMe</u> , H-5
2	159.7 s		OMe, Me, <u>CH₂OMe</u>
3	119.5 s		Me, H-5
4	159.5 s		Me, H-5
5	108.1 d	6.91 s	OCH ₂
6	141.7 s		OCH ₂ , <u>CH₂OMe</u>
1'	70.8 t	4.29 dd (9.8, 3.3) 3.98 dd (9.8, 8.0)	
2'	77.7 d	3.78 dd (8.0, 3.3)	Me-4', Me-5', H-1'B
3'	72.8 s		H-2', Me-4', Me-5'
Me-4' ^d	26.7 q	1.29 s (3H)	Me-5'
Me-5' ^d	25.0 q	1.26 s (3H)	H-2', Me-4'
OMe	62.3 q	3.73 s	
OCH ₂	62.6 t	4.68 s	H-5
<u>CH₂OMe</u>	58.2 t	3.39 s	<u>CH₂OMe</u>
<u>CH₂OMe</u>	66.7 q	4.53 s	<u>CH₂OMe</u>
Me	9.4 q	2.18	
C=O			

^aThe chemical shifts are in δ values (ppm) from TMS. ^b2D ¹H, ¹H (COSY) and ¹³C, ¹H (HSQC) NMR experiments confirmed the correlations of all the protons and the corresponding carbons.

^cMultiplicities were assigned with DEPT. ^dThese assignment could be reversed.

Thus, argyrotxin C (**3**) was formulated as 1-(5-(hydroxymethyl)-3-methoxy-4-(methoxymethyl)-2-methyl-phenoxy)-3-methylbutane-2,3- diol. Its structure was confirmed from its NOESY (Fig. 86) and HRESIMS spectra, which showed the sodium adduct ion $[M + Na]^+$ at m/z 337.1635. The ESIMS had the same peak, the dimer potassium adduct ion $[2M + K]^+$ at m/z 353 and a fragmentation ion generated by the protonated adduct ion by loss of MeOH $[M + H - MeOH]^+$ at m/z 283.

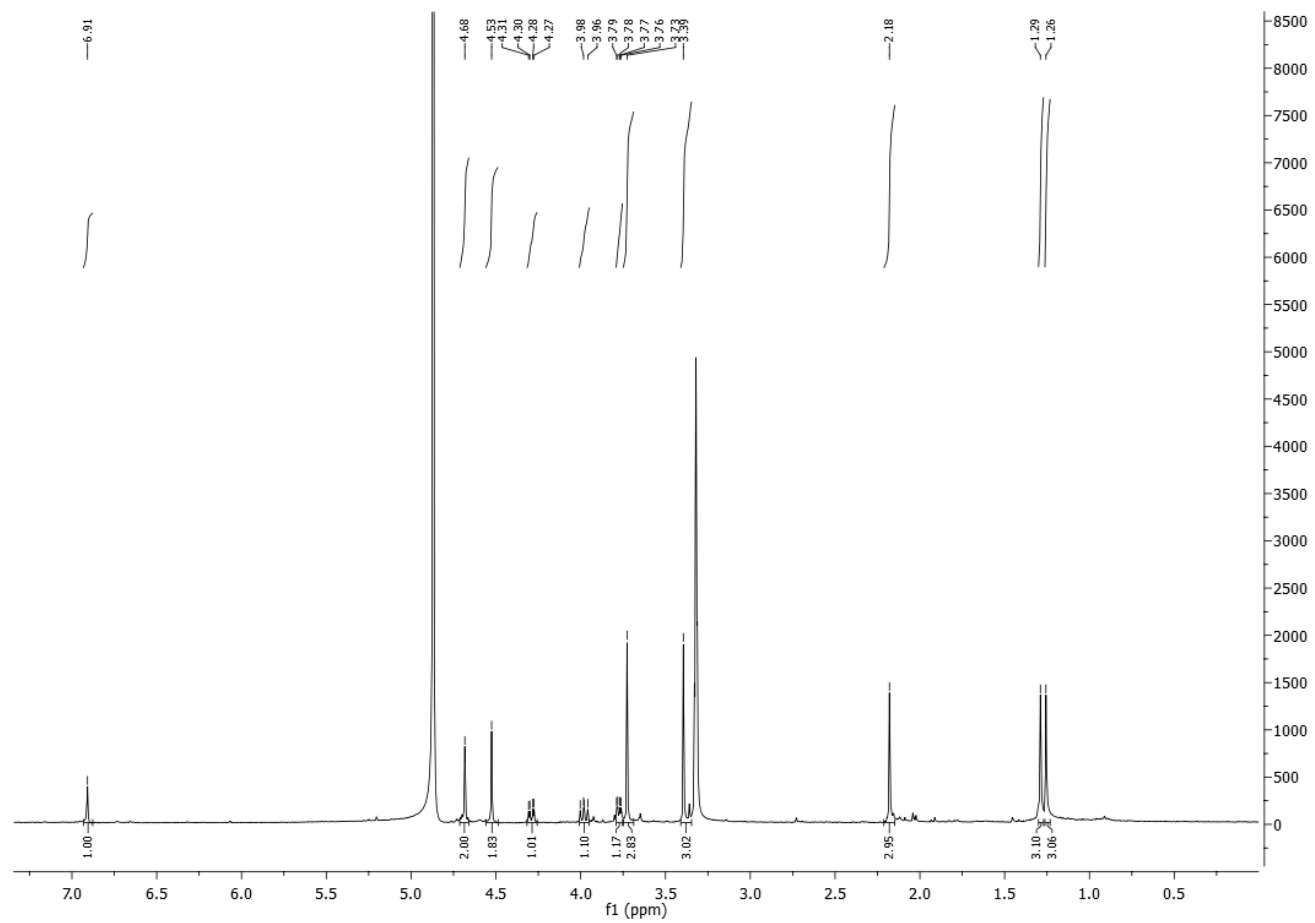


Figure 81: ^1H NMR spectrum of argyrotxin C (25) (CD_3OD , 400 MHz).

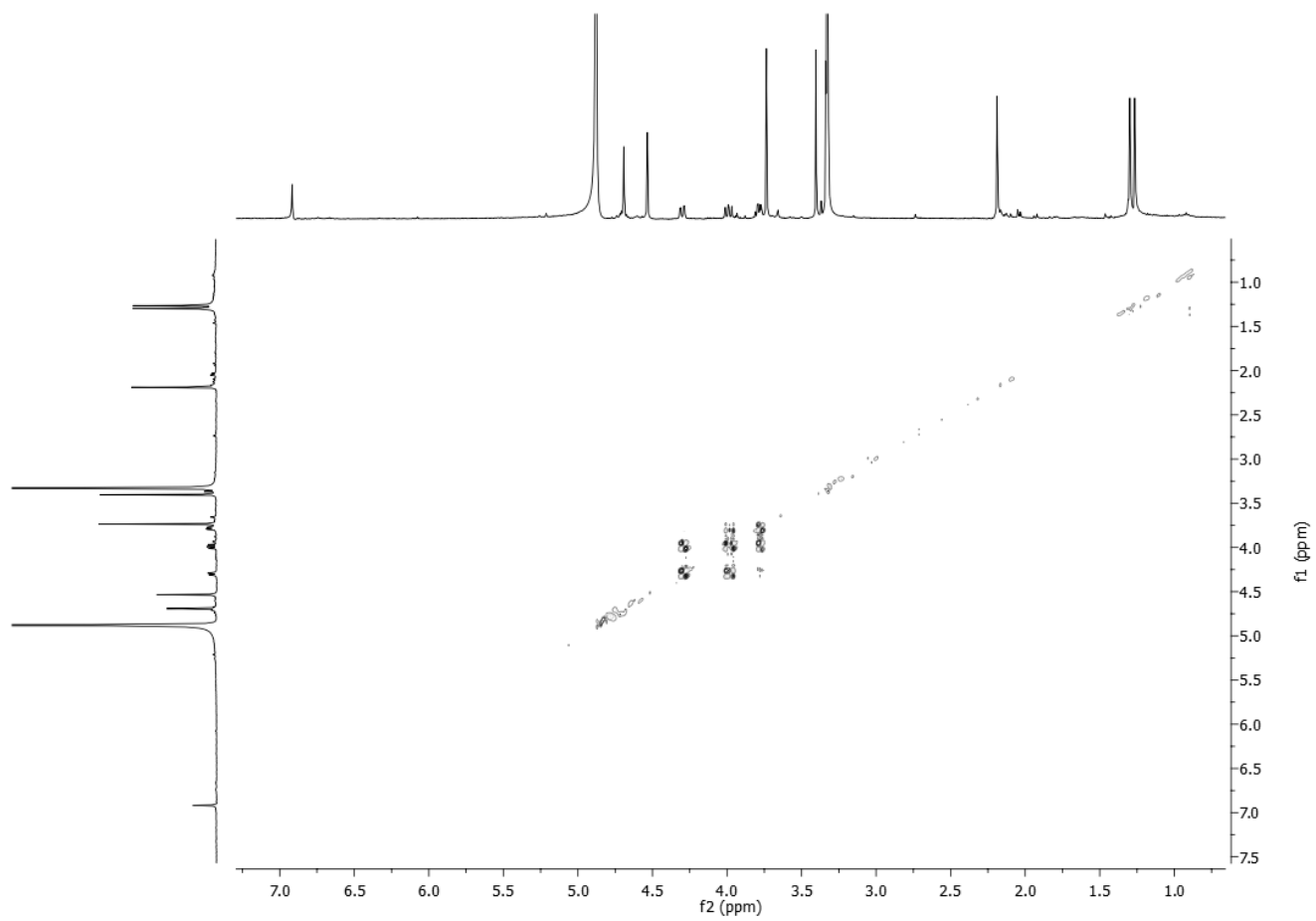


Figure 82: COSY spectrum of argyrotxin C (25) (CD₃OD, 400 MHz).

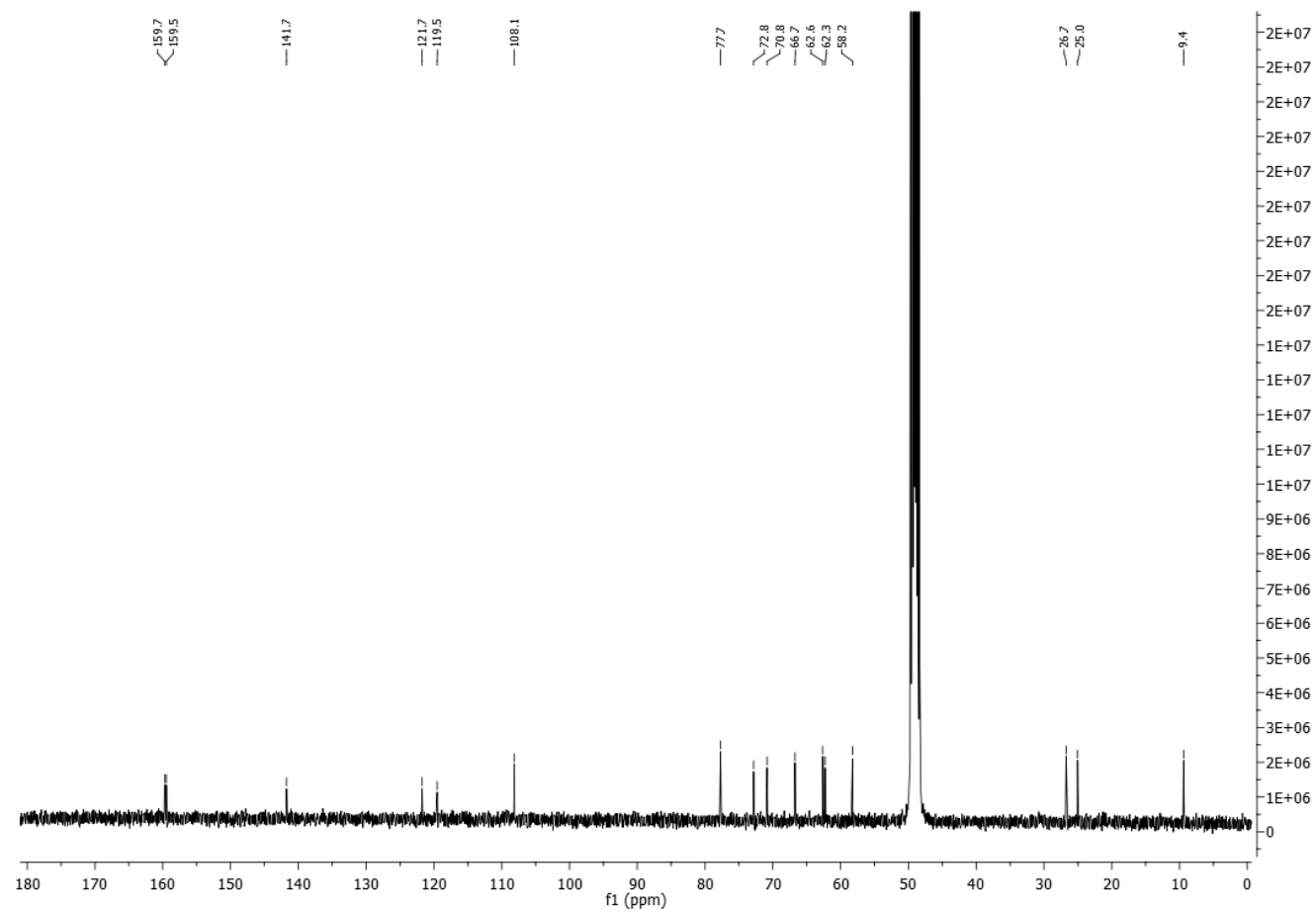


Figure 83: ^{13}C NMR spectrum of argyrotxin C (25) (CD_3OD , 100 MHz).

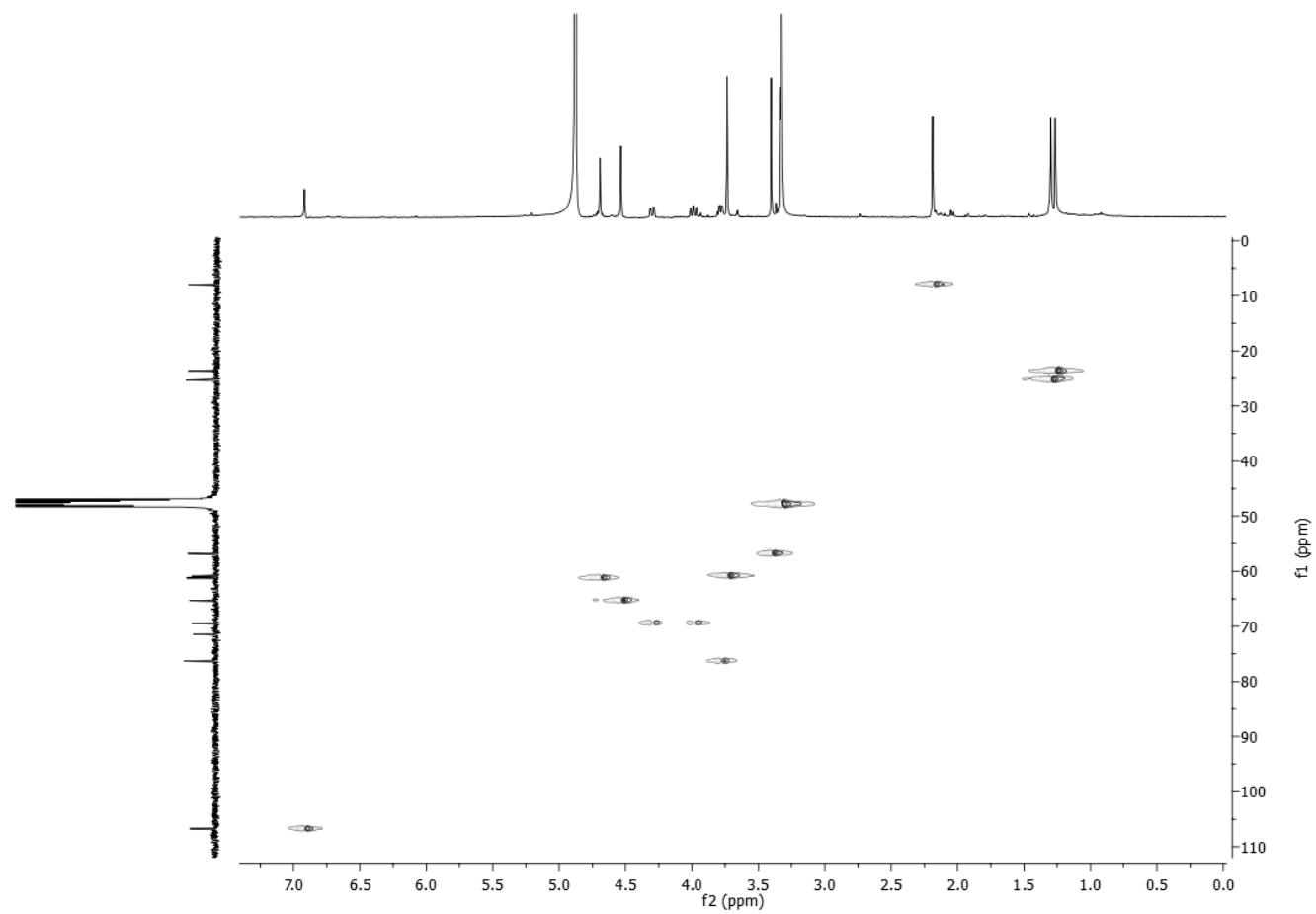


Figure 84: HSQC spectrum of argyroxin C (25) (CD_3OD , 400/100 MHz).

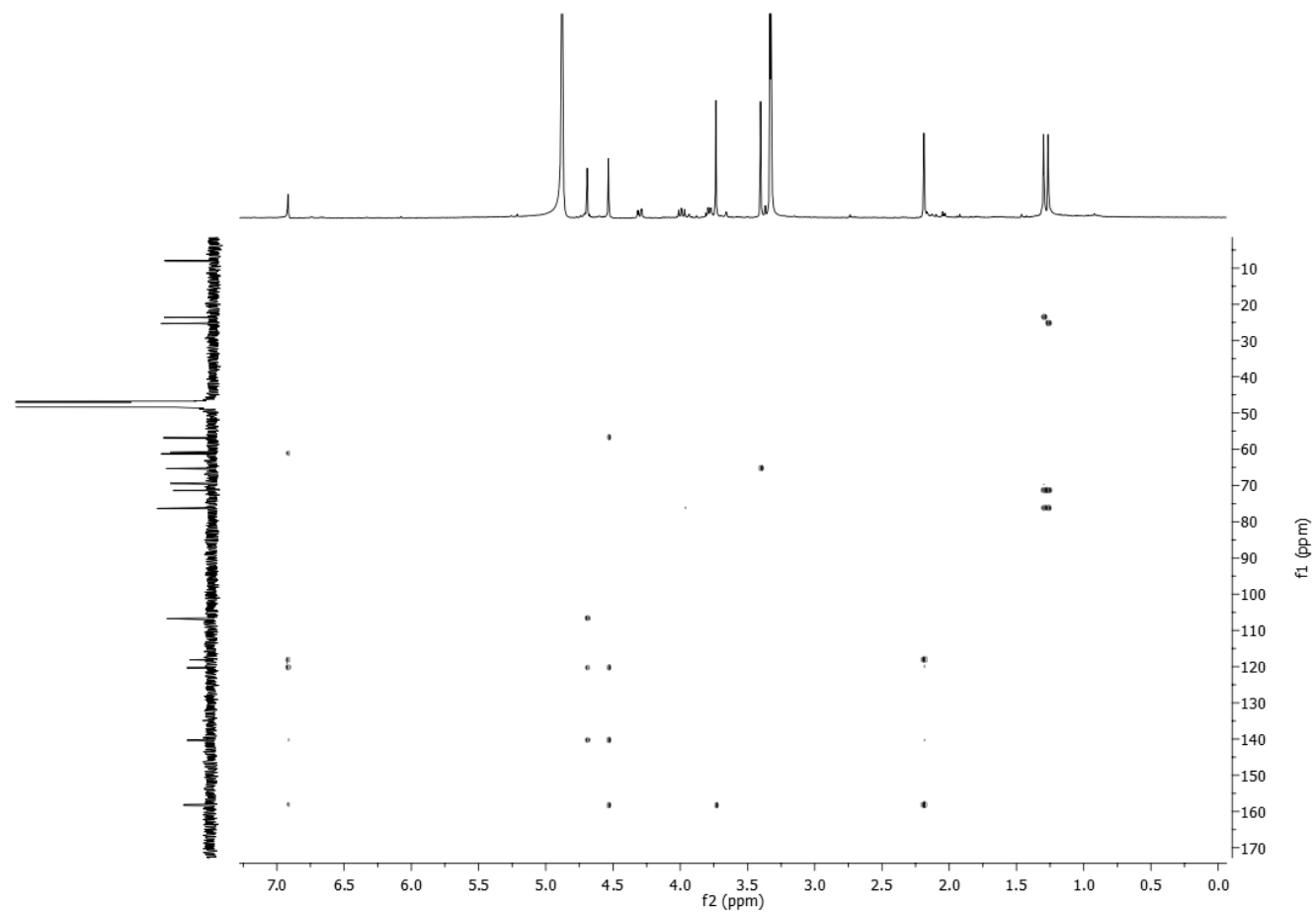


Figure 85: HMBC spectrum of argyroxin C (25) (CD₃OD, 400/100 MHz).

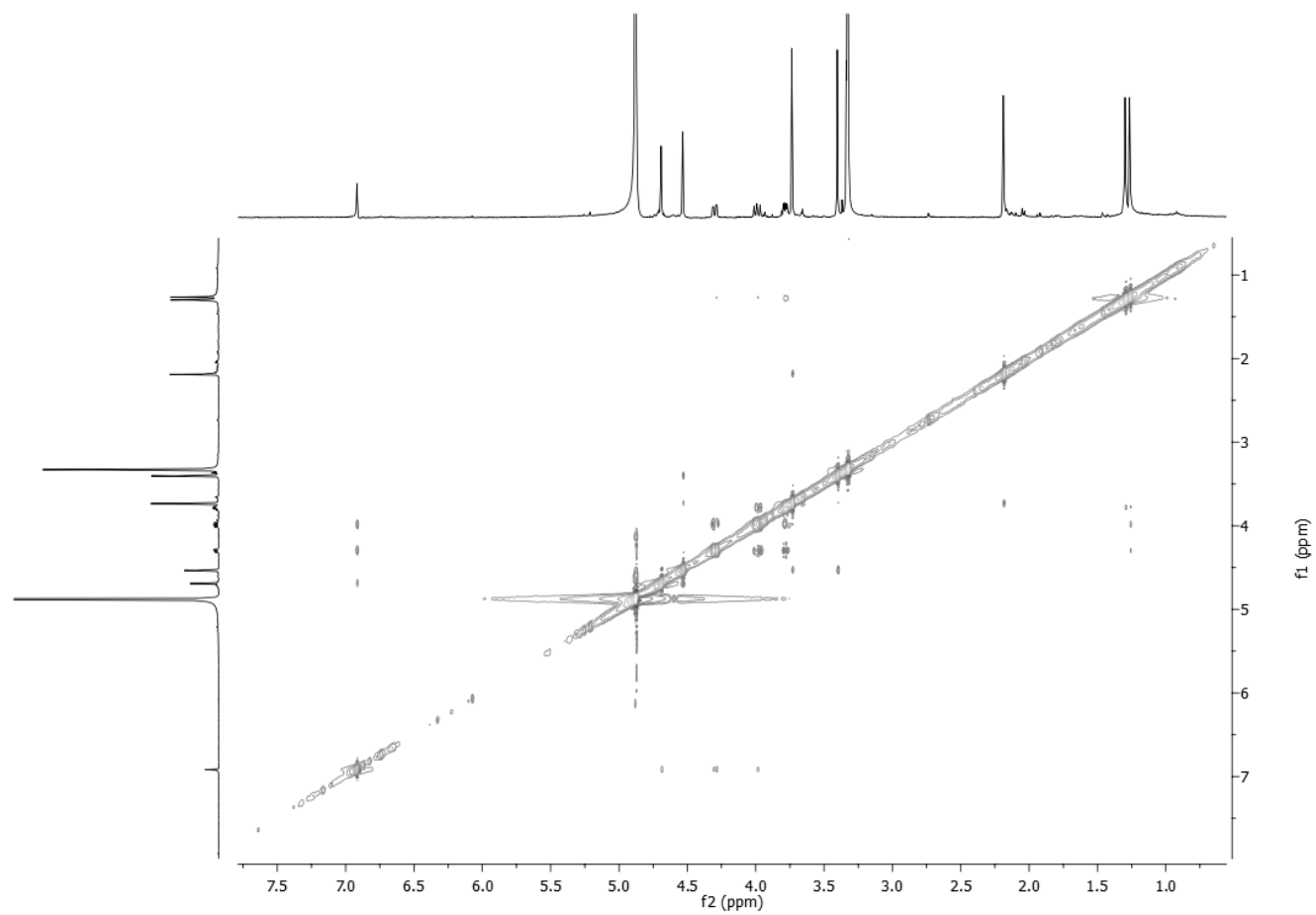


Figure 86: NOESY spectrum of argyrotxin C (25) (CD_3OD , 400 MHz).

5.5.5 Leaf puncture assay

The phytotoxic activity of all isolated metabolites (**23-31**) was assayed on young leaves of *Hedera helix* L., *Phaseolus vulgaris* L. and *Quercus ilex* L., using a solution 1.0 mg/mL of each compound.

Among them, zinniol (**29**) appeared to be the most active metabolite (Table 18), causing necrotic lesions (necrosis area ranging from 7.1 to 77.5 mm²) to leaves of all species tested.

Table 18: Phytotoxicity data for 23-31 produced by *A. argyroxiphii* tested at 1 mg/mL.^a

Compound	<i>Phaseolus vulgaris</i> L.	<i>Hedera helix</i> L.	<i>Quercus ilex</i> L.
23	6.7 ± 1.1	na ^b	na
24	7.7 ± 1.1	na	na
25	na	na	na
26	na	na	16.7 ± 3.2
27	na	na	na
28	na	na	na
29	77.5 ± 6.4	12.9 ± 1.5	7.1 ± 0.6
30	na	na	na
31	na	na	na

^a Data are expressed as median area lesion ± error standard (mm²). ^b na = inactive.

Argyrotxin A (**23**) and B (**24**) showed phytotoxicity only on leaves of bean, while porritoxinol (**26**) was active only on holm oak leaves. The other metabolites (**25**, **27**, **28**, **30** and **31**) were inactive on all species plants tested. This could also be dependent from the different plant sensitivity.

A structure-activity relationships (SAR) study was carried out. The substituents of the benzene ring of zinniol (**29**) seemed to be important features for the activity. When the hydroxymethylene at C-6 was oxidized to a carboxylic group and this, in turn, converted into the corresponding 2-hydroxyethylamide as in argyrotxin B (**24**), the phytotoxicity decreased. But also, the 3-methylbut-2-enyloxy chain at C-4 was important for the activity, because its modification determined the inactivity in argyrotxin C (**25**).

In the porritoxinol group of metabolites (**23**, **26-28**) the two *ortho*-hydroxymethylene groups were converted in the furanone ring. This conversion imparted selectivity to porritoxinol (**26**) and argyrotxin A (**23**), which were the only toxic compounds but on two different tested plants, holm oak and bean respectively. This could depend from the butyloxy side chain at C-6, which, although was equally flexible, showed different functionalization in **26** in respect to **23**. When the same residue at C-6 was converted into but-2-enyloxy differently functionalized in 6-(3',3'-dimethylallyloxy)-4-methoxy-5-methylphthalide (**27**) and phthalide carboxylic acid derivative (**28**), it caused the loss of activity. The two tetrasubstituted benzochromenones, alternariol (**30**) and alternariol methyl ether (**31**), did not

present structural correlation with either zinniol (**29**) or porritoxinol (**26**) and were completely inactive.

5.6 Structural identification of secondary metabolites isolated from *D. sapinea* culture filtrates

The organic extract of *D. sapinea* culture filtrate was purified as reported in detail in the Experimental section 4.16 (Scheme 7), yielding two new trisubstituted furanones, named pinofuranoxins A (**31**) and B (**32**) (Fig. 87).

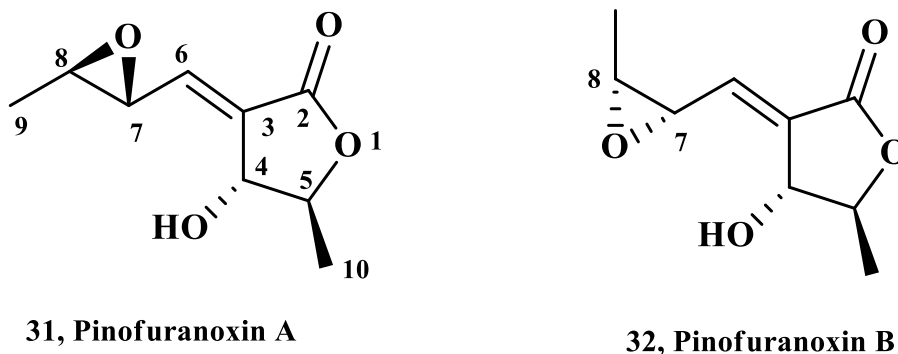


Figure 87: Secondary metabolites isolated from *Diplodia sapinea*.

5.6.1 Structural determination of pinofuranoxins A and B

The preliminary ^1H and ^{13}C NMR investigation of the two new metabolites (**31** and **32**) showed that they were probably diastereomers. This was confirmed by their HRESIMS since they shared the same molecular formula of $\text{C}_9\text{H}_{12}\text{O}_4$, consistent with the 4 indices of hydrogen deficiencies. In addition, their IR and UV spectra showed, in agreement with NMR data, the presence of a conjugated ester carbonyl and a hydroxy group.

The ^1H (Fig. 88, Table 19) and COSY NMR (Fig. 89) spectra of pinofuranoxin A (**31**) presented a doublet of doublets at δ 6.89 ($J = 4.1$ and 2.1 Hz) (H-6) of an olefinic proton and a broad singlet at δ 4.68 (H-4) of the proton of a secondary hydroxylated carbon. H-6 coupled in the COSY spectrum (Fig. 89) with the multiplet at δ 3.52 of the proton (H-7) of the adjacent epoxide methine and H-7 coupled with the double quartet at δ 3.06 ($J = 5.2$ and 2.1 Hz) of the other adjacent epoxide proton (H-8). The latter was also coupled in the COSY spectrum (Fig. 89) with a doublet at δ 1.45 ($J = 5.2$ Hz) of the geminal methyl (Me-9). H-4 allylic coupled ($J = 2.1$ Hz) with H-6 and with a double quartet at δ 4.44 ($J = 6.7$ and 3.8 Hz) of the proton (H-5) of the adjacent oxygenated secondary carbon (C-5). The latter also coupled with a doublet at δ 1.42 ($J = 6.7$ Hz) of the geminal methyl (Me-10). Finally, the ^1H NMR spectrum (Fig. 88, Table 19) showed the presence of a the multiplet at δ 3.52 due to a partial overlapping of signals of the hydroxy group at C-4 and the H-7 signal. The ^{13}C NMR spectrum of pinofuranoxin A (**31**) (Fig. 90, Table 19) presented the signals of a carbonyl, five methines, two sp^3

carbons, one of which was oxygenated, one sp^2 carbon, and two carbons, probably attributable to an oxirane ring, a tertiary sp^2 carbon, and two methyls. The ester carbonyl group resonated at δ 169.0 in the ^{13}C NMR spectrum (Fig. 90, Table 19) and in the HMBC spectrum (Fig. 92, Table 19) coupled with H-5 and H-6. In the ^{13}C NMR spectrum (Fig. 90, Table 19) the signal resonating at δ 72.5 was assigned, according to the coupling observed in the HSQC spectrum (Fig. 91), to C-4 and coupled in the HMBC spectrum with H-5, H-6 and Me-10. The signal resonating at δ 81.4 was assigned at C-5 and coupled in the HMBC spectrum (Fig. 92, Table 19) with Me-10. The couplings observed in the HMBC spectrum (Fig. 92, Table 19) between C-3 with H-6 and HO-C4, allowed to locate the 3,4-oxirane-1-pentenyl side chain at tertiary sp^2 C-3. The coupling observed in the HSQC (Fig. 91) and the HMBC spectra allowed to assign the chemical shifts to all the carbons and corresponding protons as reported in Table 19.

Table 19: ¹H and ¹³C NMR data of pinofuranoxins A and B (31 and 32).^{a,b}

position	31			32		
	δ_C^c	δ_H (<i>J</i> in Hz)	HMBC	δ_C^c	δ_H (<i>J</i> in Hz)	HMBC
2	169.0 s		H-5, H-6	168.8 s		H-4, H-5, H-6
3	133.2 s		H-7, HO-4, H-6	135.3 s		H-6, H-7
4	72.5 d	4.68 (1H) br s	H-5, H-6, H ₃ -10	72.4 d	4.70 (1H) br s	H-5, H-6, H ₃ -10
5	81.4 d	4.44 (1H) dq (6.7, 3.8)	H ₃ -10	81.5 d	4.49 (1H) dq (6.5, 3.4)	H-4, H ₃ -10
6	139.4 d	6.89 (1H) dd (4.1, 2.1)	H-7, HO-4	137.0 d	6.93 (1H) dd (3.1, 2.2)	H-7, H-8
7	57.4 d	3.52 (1H) m ^d	H ₃ -9	55.9 d	3.85 (1H) dd (5.5, 3.1)	H-6, H-8, H ₃ -9
8	57.3 d	3.06 (1H) dq (5.2, 2.1)	H-6, H-7, H ₃ -9	54.7 d	3.39 (1H) quint (5.5)	H-7, H ₃ -9
9	17.6 q	1.45 (3H) d (5.2)	H-7, H-8	13.5 q	1.34 (3H) d (5.5)	H-8
10	19.9 q	1.42 (3H) d (6.7)		20.0 q	1.42 (3H) d (6.5)	H-4
HO-4		3.52 m ^d			3.64	

^a2D ¹H, ¹H (COSY) and ¹³C, ¹H (HSQC) NMR experiments confirmed the correlations of all the protons and the corresponding carbons. ^bCoupling constants (*J*) are given in parenthesis. ^cMultiplicities were assigned with DEPT.

^dThese two signals are in part overlapped.

Thus, pinofuranoxin A (**31**) was formulated as 4-hydroxy-5-methyl-3-((3-methyloxiran-2-yl)-methylene)dihydrofuran-2(3*H*)-one.

Pinofuranoxin B (**32**) had the same molecular formula and structural features as **31**, suggesting their diastereomeric relationship. Compound **32** showed NMR (Fig. 93-97, Table 19) and HRESIMS data very similar to those of compound **31**.

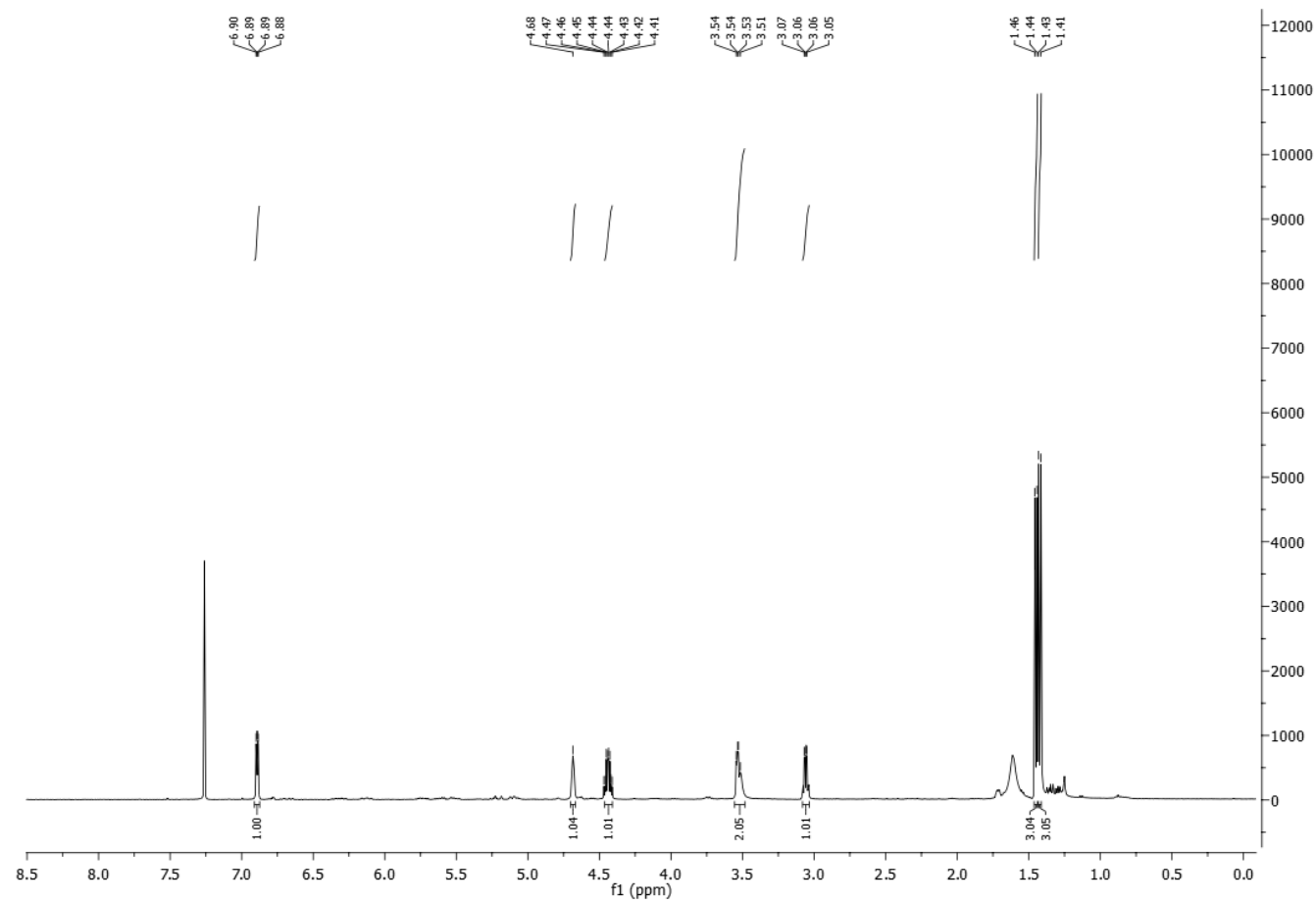


Figure 88: ^1H NMR spectrum of pinofuranoxin A (31) (CDCl_3 , 400 MHz).

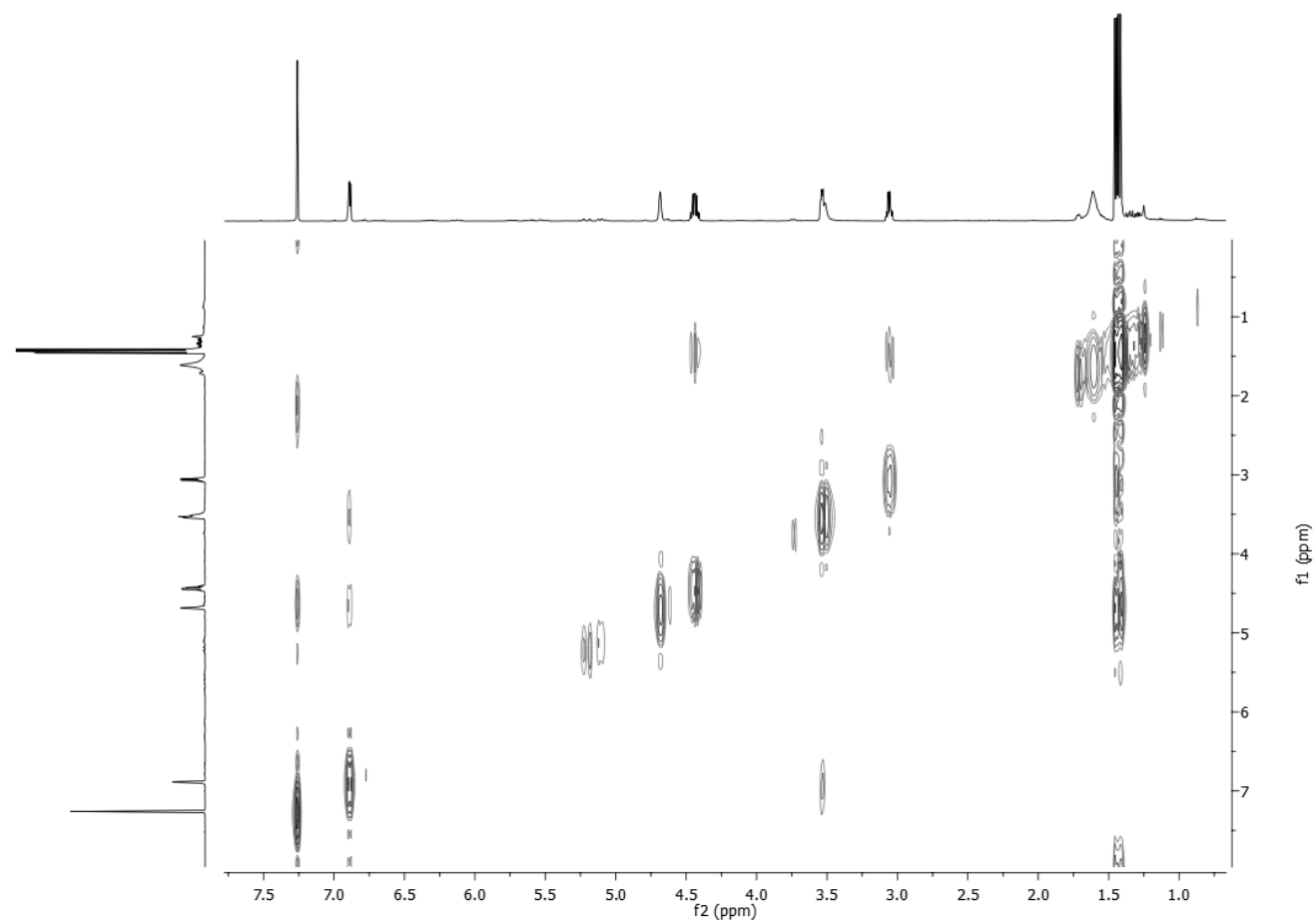


Figure 89: COSY spectrum of pinofuranoxin A (31) (CDCl₃, 400 MHz).

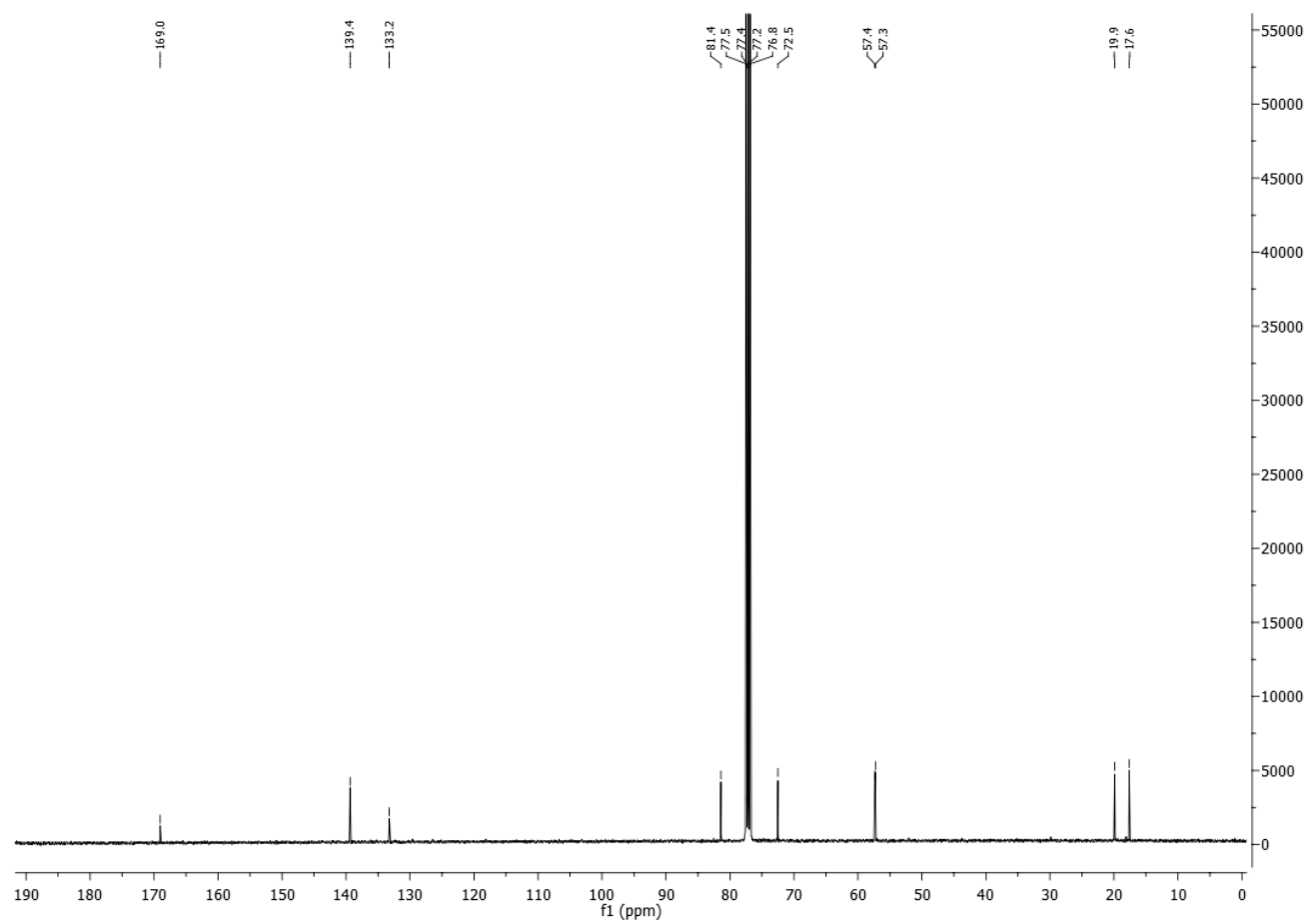


Figure 90: ^{13}C NMR spectrum of pinofuranoxin A (31) (CDCl_3 , 100 MHz).

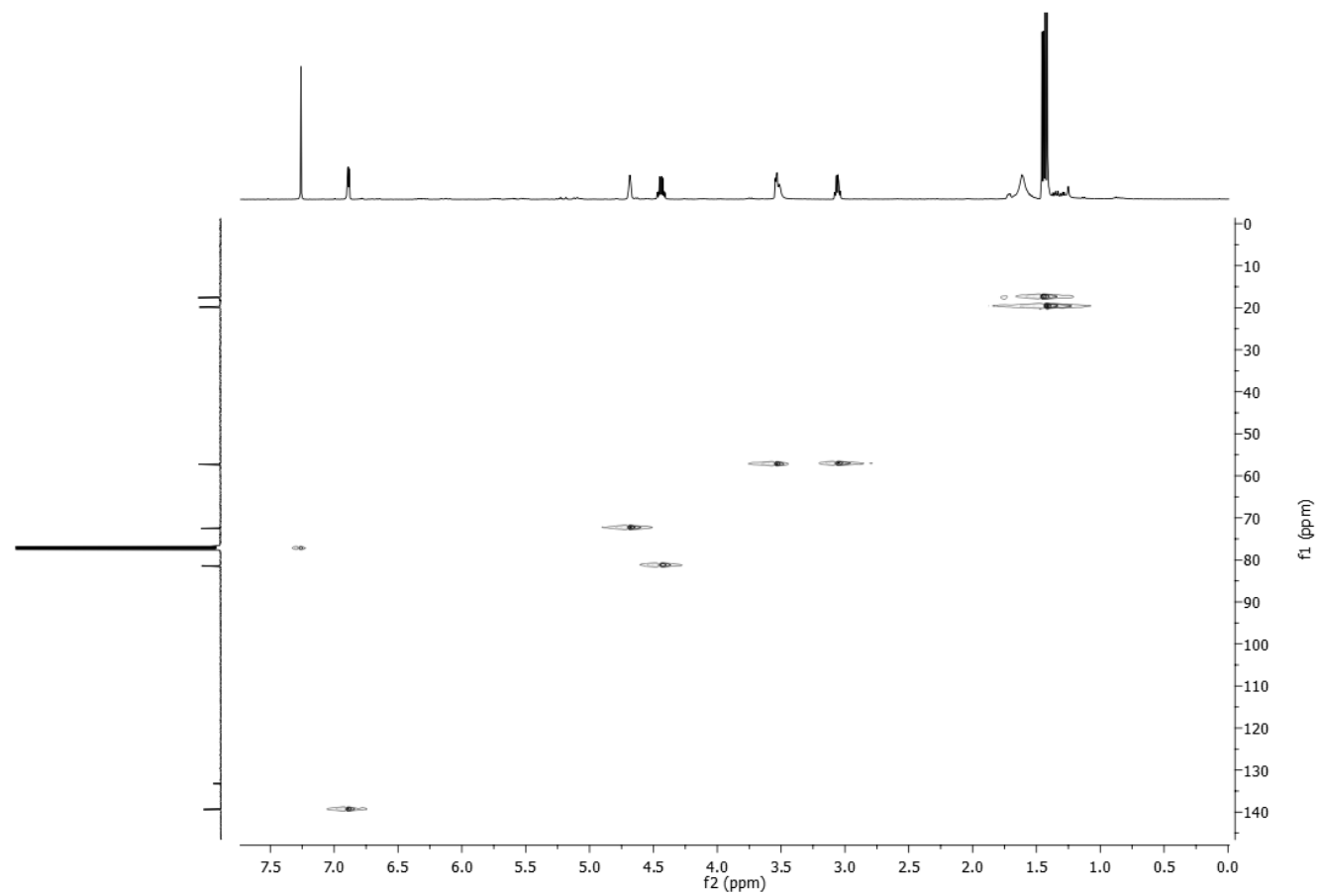


Figure 91: HSQC spectrum of pinofuranoxin A (31) (CDCl₃, 400/100 MHz).

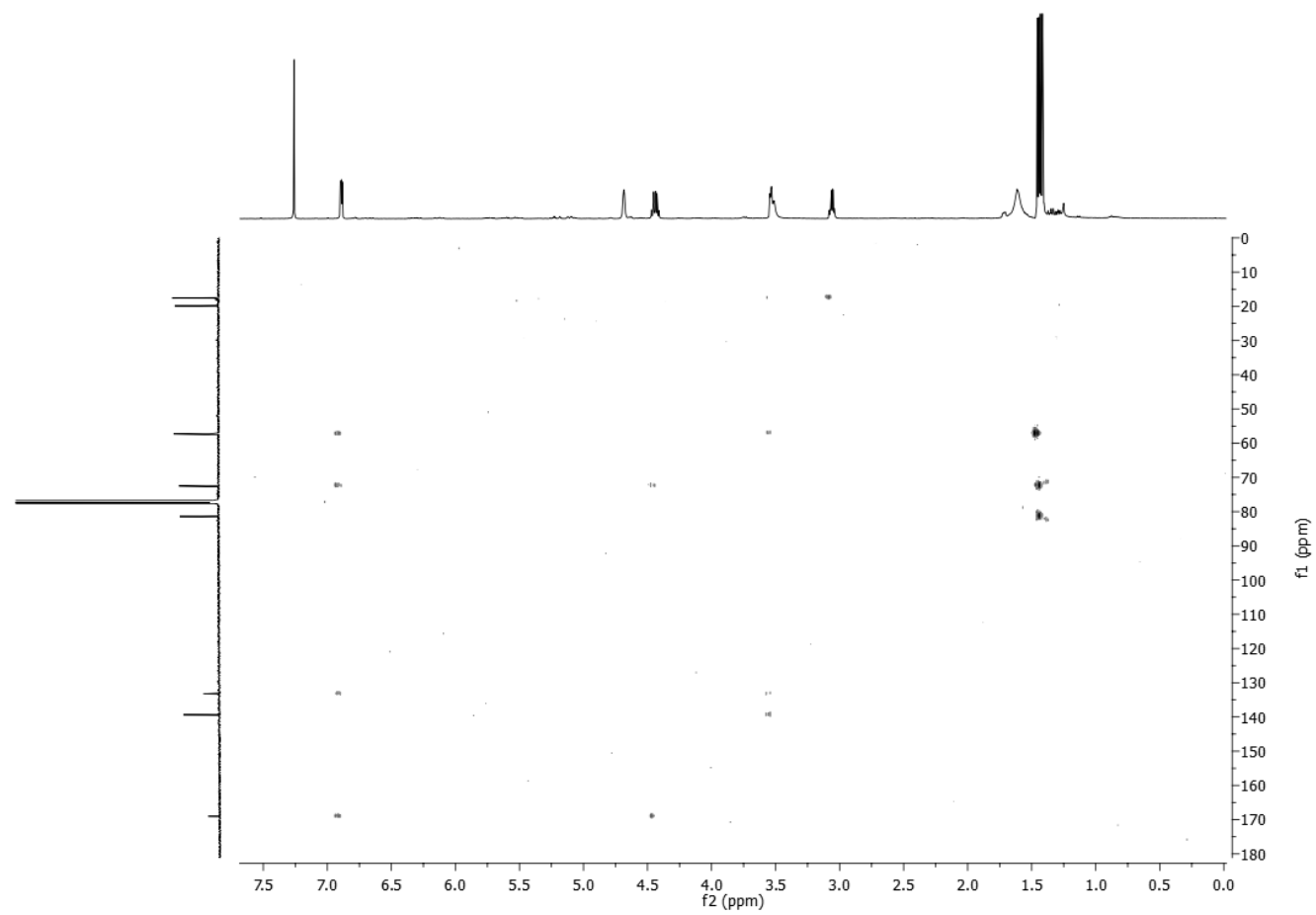


Figure 92: HMBC spectrum of pinofuranoxin A (31) (CDCl_3 , 400/100 MHz).

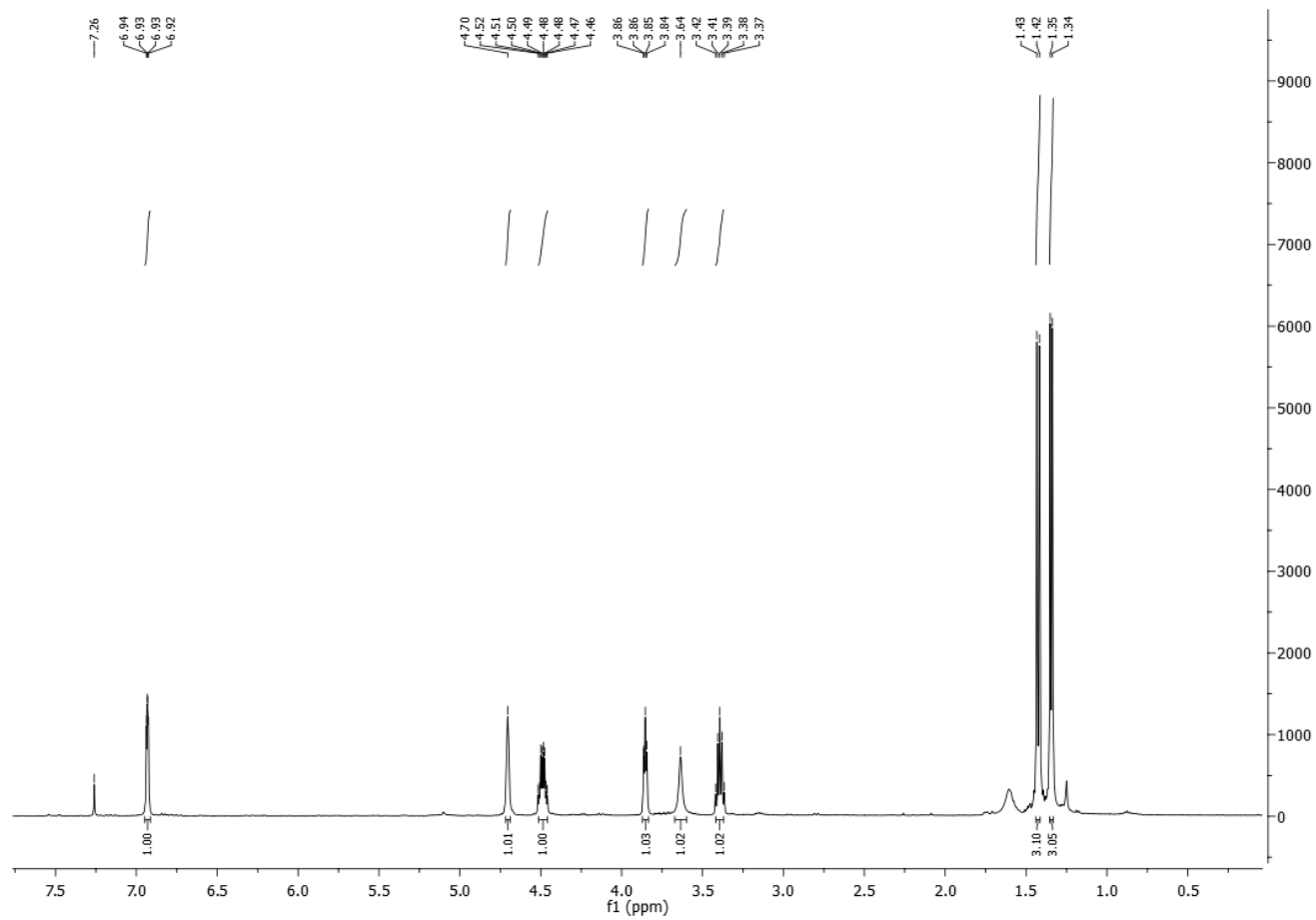


Figure 93: ¹H NMR spectrum of pinofuranoxin B (32) (CDCl₃, 400 MHz).

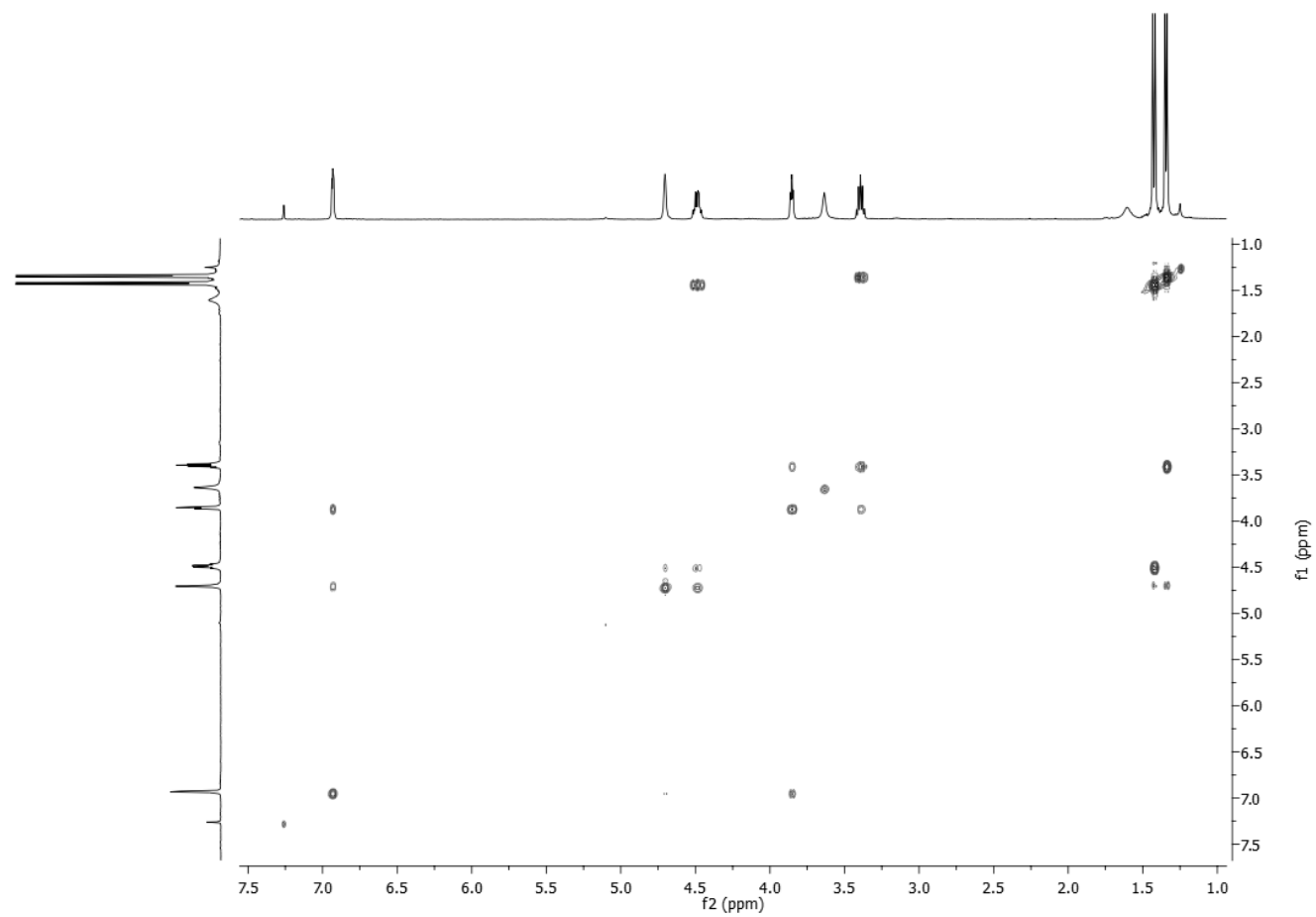


Figure 94: COSY spectrum of pinofuranoxin B (32) (CDCl₃, 400 MHz).

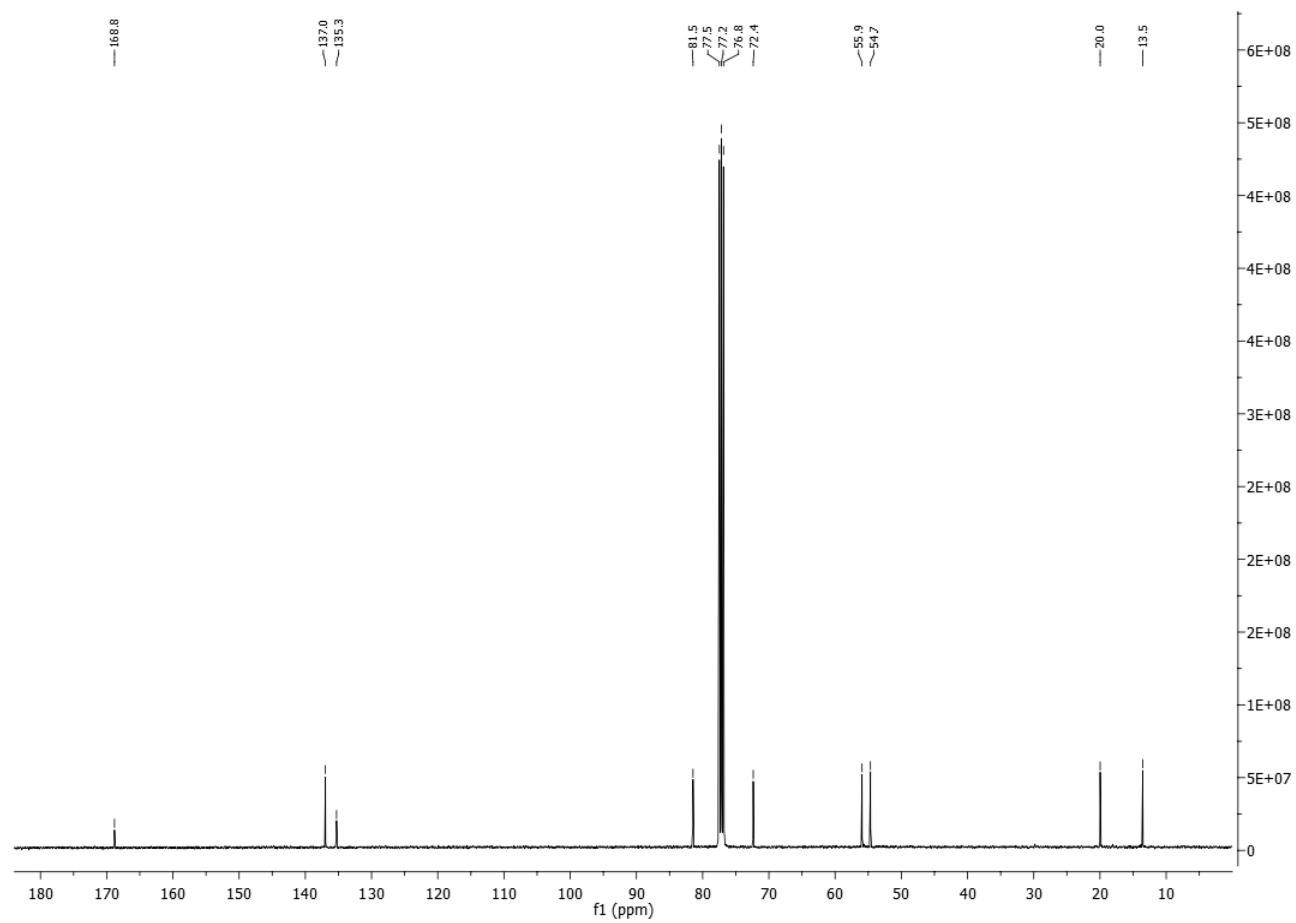


Figure 95: ¹³C NMR spectrum of pinofuranoxin B (32) (CDCl₃, 100 MHz).

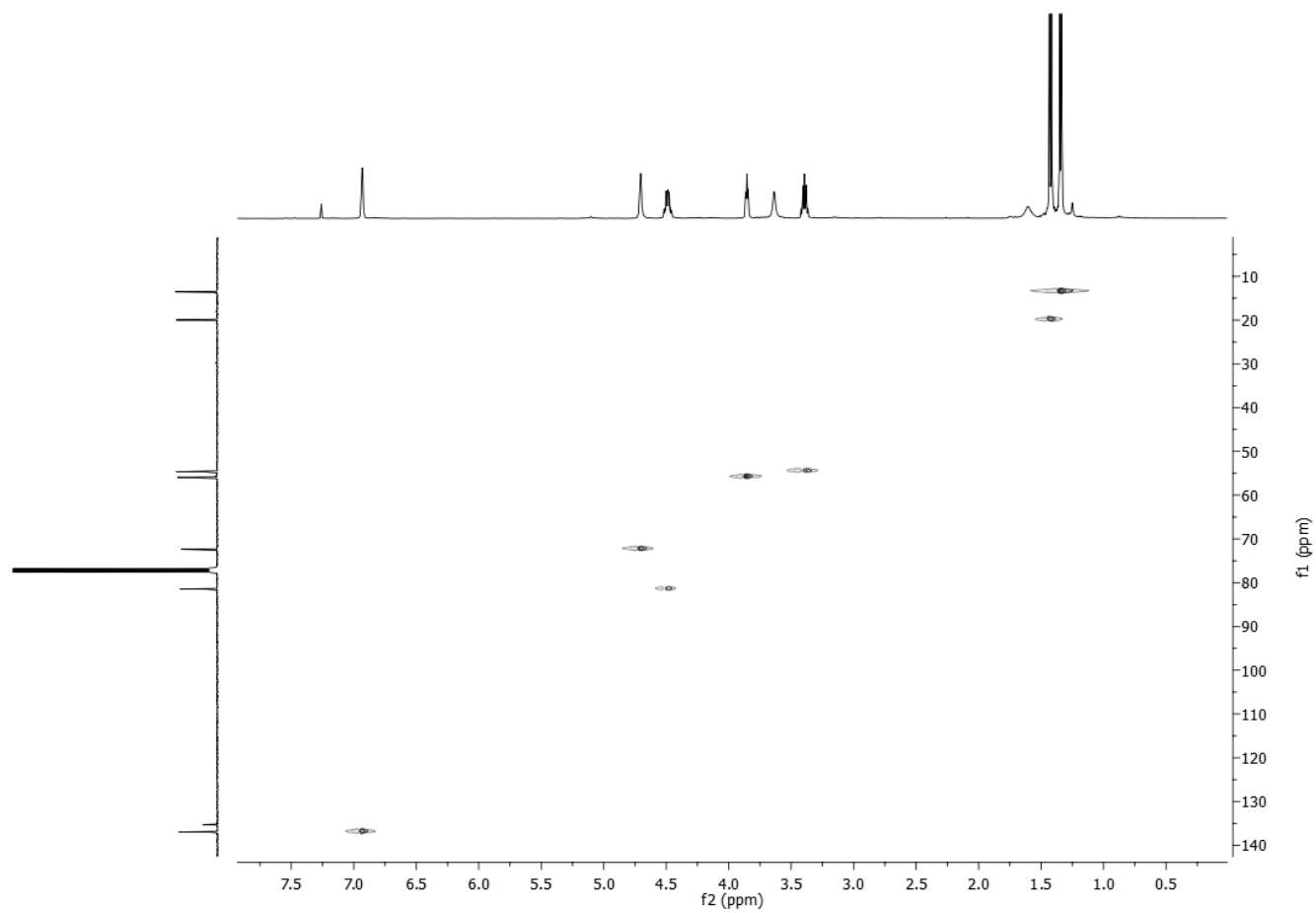


Figure 96: HSQC spectrum of pinofuranoxin B (32) (CDCl₃, 400/100 MHz).

5.6.2 Relative configurations of pinofuranoxins A and B

The pinofuranoxins A and B (**31** and **32**) differed in the correlations observed in their NOESY spectra (Fig. 98), allowing to discriminate their relative configurations.

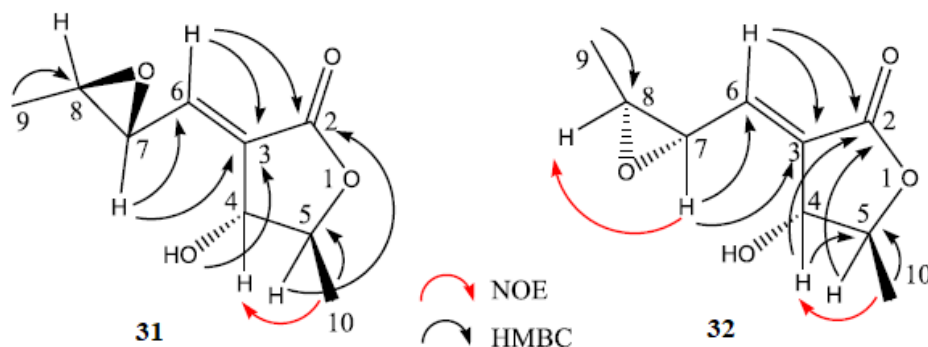


Figure 98: Most significant HMBC (black arrows) and NOE (red arrows) correlations for **31** and **32**.

The correlations between H-4 and Me-10 and the lack of one between H-4 and H-5 supported a *trans*-substitution of the dihydrofuranone ring of both compounds (**31** and **32**) (Fig. 99 and 100, Table 20). The correlation observed only in pinofuranoxin B (**32**) between H-7 and H-8 allowed to assigned a *cis*-substitution of the oxirane ring in **32** and a *trans*-substitution in **31** (Fig. 99 and 100, Table 20).

Table 20: NOESY data of pinofuranoxins A and B (**31** and **32**).

31		32	
Irradiated	Observed	Irradiated	Observed
H-8	Me-9	H-5	Me-10
H-4	Me-10	H-4	Me-10
H-5	Me-10	H-8	Me-9
		H-7	H-8

The configuration of the double bond for both compounds (**31** and **32**) was derived from the absence of coupling in the NOESY spectra (Fig. 99 and 100) between H-6 and H-4. Moreover, the chemical shifts of H-6 and C-6 were very similar to those of protons and carbons of some natural furanones having an α *E*-disubstituted vinyl group, which were significantly different from those having a *Z*-vinyl group (Cheng *et al.*, 2009; Tedeka *et al.*, 1972). Thus, pinofuranoxin B (**32**) was a diastereomer of pinofuranoxin A (**31**) by inversion of the configuration on the oxirane ring.

The two metabolites consist of a unique combination of functional groups. In fact, some 2-alkylidene-3-hydroxy-4-methyl-butanolides were identified as bioactive metabolites of *Lauraceae* plants (Tedeka *et al.*, 1972) and only a single compound of this family was isolated from a fungus of marine sponges (Abrell *et al.*, 1996). Nevertheless, this is the case in which there is an epoxy moiety in such structures.

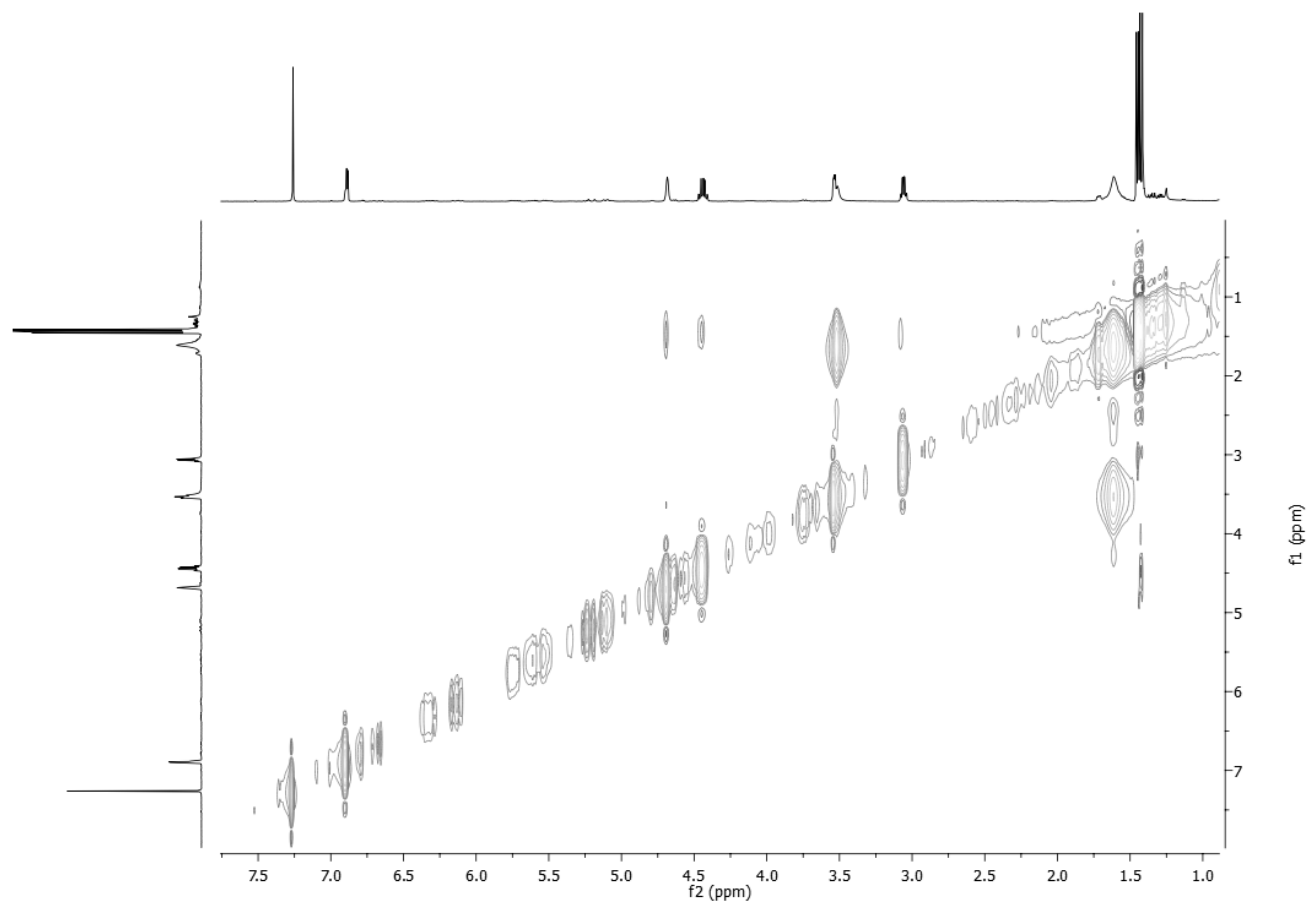


Figure 99: NOESY spectrum of pinofuranoxin A (31) (CDCl₃, 400 MHz).

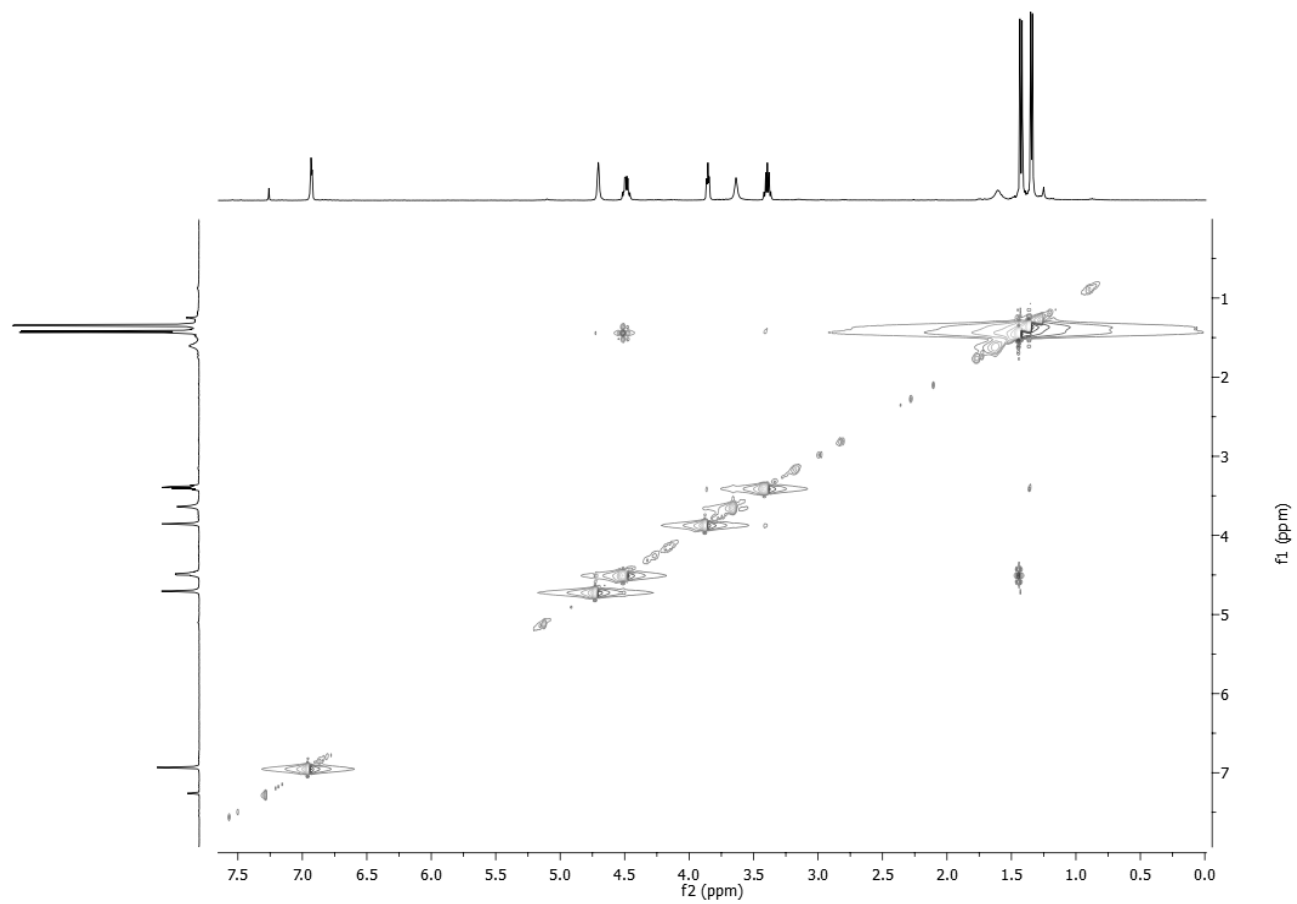


Figure 100: NOESY spectrum of pinofuranoxin B (32) (CDCl_3 , 400 MHz).

5.6.3 Absolute configurations of pinofuranoxins A and B

The absolute configuration (AC) of compounds **31** and **32** were assigned by computational analysis of their electronic circular dichroism (ECD) spectra, which were recorded in MeCN in the 200–340 nm range. The ECD spectrum of (+)-**31** (Fig. 101) showed a weak broad negative Cotton effect (CE) centered at about 263 nm ($\Delta\epsilon -0.39$) and a more intense positive one at 234 nm ($\Delta\epsilon +1.93$), while that of (+)-**32** (Fig. 102) had two oppositely signed CEs: a weaker negative one at 270 nm ($\Delta\epsilon -0.34$) and a more intense positive band at 231 nm ($\Delta\epsilon +4.36$).

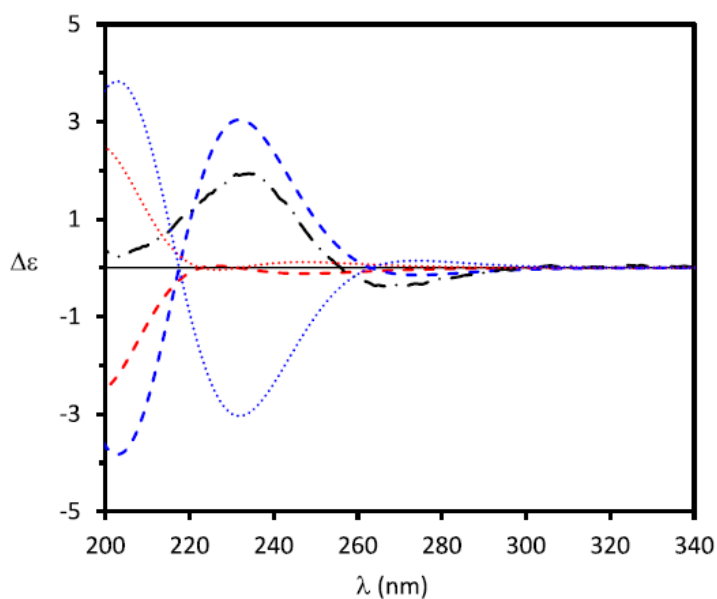


Figure 101: Comparison between experimental ECD spectra (dashed-dotted black line) of (+)-**31** with calculated [TDDFT/CAM-B3LYP/aug-cc-pVDZ/IEFPCM(MeCN)] ones. Computed ECD spectrum for (4*S*,5*R*,7*R*,8*R*)-**31a** (dotted red line), (4*R*,5*S*,7*S*,8*S*)-*ent*-**31a** (dashed red line), (4*S*,5*R*,7*S*,8*S*)-**31b** (dotted blue line), and (4*R*,5*S*,7*R*,8*R*)-*ent*-**31b** (dashed blue line).

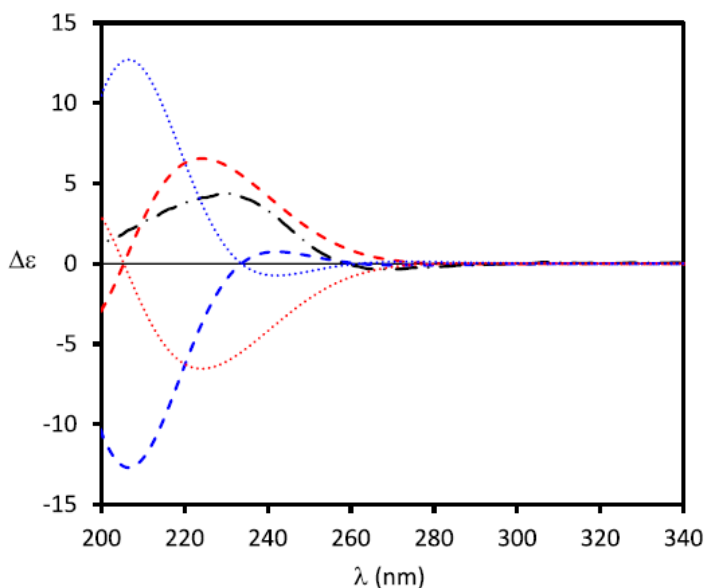


Figure 102: Comparison between experimental ECD spectra (dashed-dotted black line) of (+)-**32** with calculated [TDDFT/CAM-B3LYP/ aug-cc-pVDZ/IEFPCM(MeCN)] ones. Computed ECD spectrum for (4*S*,5*R*,7*R*,8*S*)-**32a** (dotted red line), (4*R*,5*S*,7*S*,8*R*)-*ent*-**32a** (dashed red line), (4*S*,5*R*,7*S*,8*R*)-**32b** (dotted blue line), and (4*R*,5*S*,7*R*,8*S*)-*ent*-**32b** (dashed blue line).

A computational analysis of these chiroptical data was carried out by DFT. The NOESY NMR studies gave information about the relative configurations of some stereocenters. In particular, both compounds (**31** and **32**) had a *trans* (4*S*^{*},5*R*^{*}) relative configuration to the two stereocenters of the lactone ring. Regarding the oxirane ring, compound **31** presented a *trans*-configuration, which could be either a (7*R*,8*R*) or (7*S*,8*S*) AC of the two C-7 and C-8 stereocenters, while compound **32** had a *cis*-oxirane ring, thus the two stereocenters could be either a (7*R*,8*S*) or a (7*S*,8*R*) AC. These results allowed to perform the computational analysis on the (4*S*^{*},5*R*^{*},7*R*^{*},8*R*^{*}) and (4*S*^{*},5*R*^{*},7*S*^{*},8*S*^{*}) diastereomers for the *trans* compound **31** and on the (4*S*^{*},5*R*^{*},7*R*^{*},8*S*^{*}) and (4*S*^{*},5*R*^{*},7*S*^{*},8*R*^{*}) diastereomers for the *cis* compound **32**. Since enantiomeric diastereomers had mirror-image ECD spectra, for each compound it was possible to predict the chiroptical properties for only one enantiomer of the possible diastereomers. In the case of **31**, conformational analysis on the arbitrarily chosen stereoisomers (4*S*,5*R*,7*R*,8*R*)-**31a** and (4*S*,5*R*,7*S*,8*S*)-**31b** afforded four appreciably populated conformers for both (Fig. 103 and 104; Table 21 and 22).

Table 21: Conformers Boltzmann distribution of (4*S*,5*R*,7*R*,8*R*)-31a.

DFT/B3LYP/6-311++G(2d,2p)/(IEFPCM(CH₃CN))

Conformers	ΔG (Kcal/mol)	% Pop
C1	0.000000	39.3
C2	0.212553	27.4
C3	0.491568	17.1
C4	0.526053	16.2

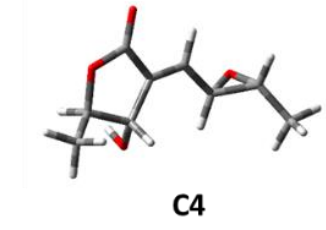
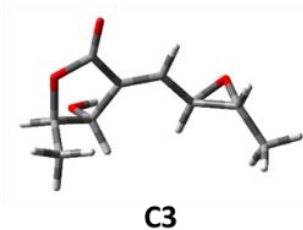
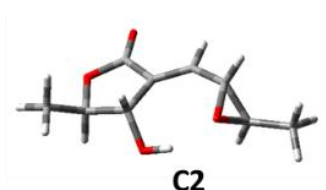
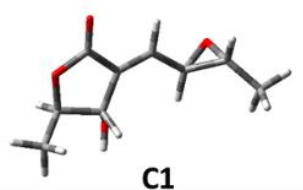


Figure 103: Minimum energy conformers of (4*S*,5*R*,7*R*,8*R*)-31a computed at DFT/B3LYP/6-311++G(2d,2p)/IEFPCM(CH₃CN) level.

Table 22: Conformers Boltzmann distribution of (4*S*,5*R*,7*S*,8*S*)-31b.

DFT/B3LYP/6-311++G(2d,2p)/(IEFPCM(CH₃CN))

Conformers	ΔG (Kcal/mol)	% Pop
C1	0.000000	41.4
C2	0.299079	25.0
C3	0.493449	18.0
C4	0.581229	15.5

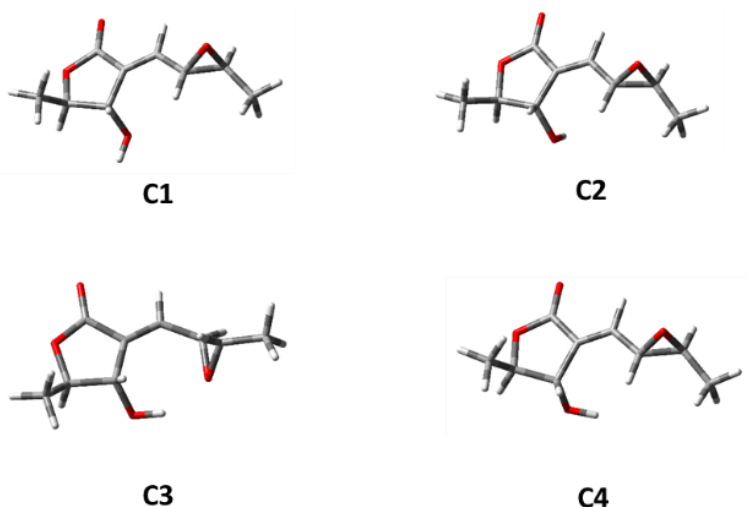


Figure 104: Minimum energy conformers of (4*S*,5*R*,7*S*,8*S*)-**31b** computed at DFT/B3LYP/6-311++G(2d,2p)/IEFPCM(CH₃CN) level.

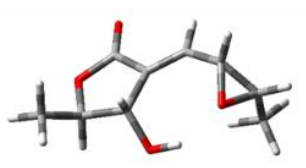
The two most abundant conformers of **31a** and **31b** (70% and 46% of the overall population, respectively) presented the methyl and hydroxy substituents of the lactone ring in equatorial arrangement. Investigation of the conformer ensemble revealed that in the second most populated conformer of **31a** and in the third most populated conformer of **31b** hydrogen bonding happened between the hydroxy moiety and oxirane ring. The polarized continuum solvation model (PCM) was employed in these computations to mimic bulk solvent effects, but it was not suitable to describe the ability of the solvent to directly participate as a hydrogen-bond acceptor. For this reason, the intramolecular H-bonded conformers provided by PCM computations in MeCN was considered as computational artifacts (Iwahana *et al.*, 2014). Therefore, the conformers displaying an intramolecular H-bonding in the Boltzmann averaging of the computed ECD spectra were discarded. The ECD spectra of **31a** and **31b** diastereomers were then calculated for each chosen conformer and Boltzmann averaged over the conformers' populations. Comparing the ECD experimental spectrum with the computed ones of **31a** and **31b** and the mirror-image spectra of their enantiomers (4*R*,5*S*,7*S*,8*S*)-*ent*-**31a** and (4*R*,5*S*,7*R*,8*R*)-*ent*-**31b** (Fig. 101), a quite good agreement was obtained between the experimental and the spectrum of the *ent*-**31b** stereoisomer. Thus, the (4*R*,5*S*,7*R*,8*R*) AC was assigned to (+)-pinofuranoxin A ((+)-**31**). The same result was also derived taking into account all the possible conformers, including H-bonded ones, or by simulating the solvent effects by an explicit approach.

The same analysis was carried out for (+)-pinofuranoxin B ((+)-**32**). The computational conformational analysis performed on the arbitrarily chosen diastereoisomers (4*S*,5*R*,7*R*,8*S*)-**32a** and (4*S*,5*R*,7*S*,8*R*)-**32b** gave four and five populated conformers for **32a** and **32b**, respectively (Fig. 105 and 106, Table 23 and 24).

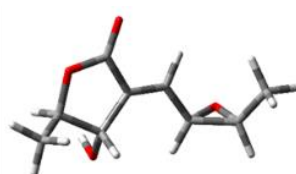
Table 23: Conformers Boltzmann distribution of (4*S*,5*R*,7*R*,8*S*)-32a.

DFT/B3LYP/6-311++G(2d,2p)/(IEFPCM(CH₃CN))

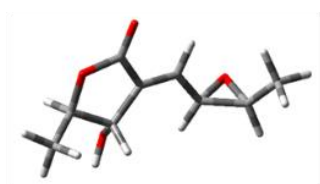
Conformers	ΔG (Kcal/mol)	% Pop
C1	0.000000	59.9
C2	0.795663	15.6
C3	0.800679	15.5
C4	1.131108	8.9



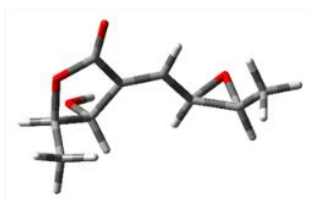
C1



C2



C3



C4

Figure 105: Structures of conformers found of (4*S*,5*R*,7*R*,8*S*)-32a computed at DFT/B3LYP/6-311++G(2d,2p)/IEFPCM(CH₃CN) level.

Table 24: Conformers Boltzmann distribution of (4*S*,5*R*,7*S*,8*R*)-32b.

DFT/B3LYP/6-311++G(2d,2p)/(IEFPCM(CH₃CN))

Conformers	ΔG (Kcal/mol)	% Pop
C1	0.000000	35.8
C2	0.282777	22.2
C3	0.426360	17.4
C4	0.537339	14.4
C5	0.741741	10.2

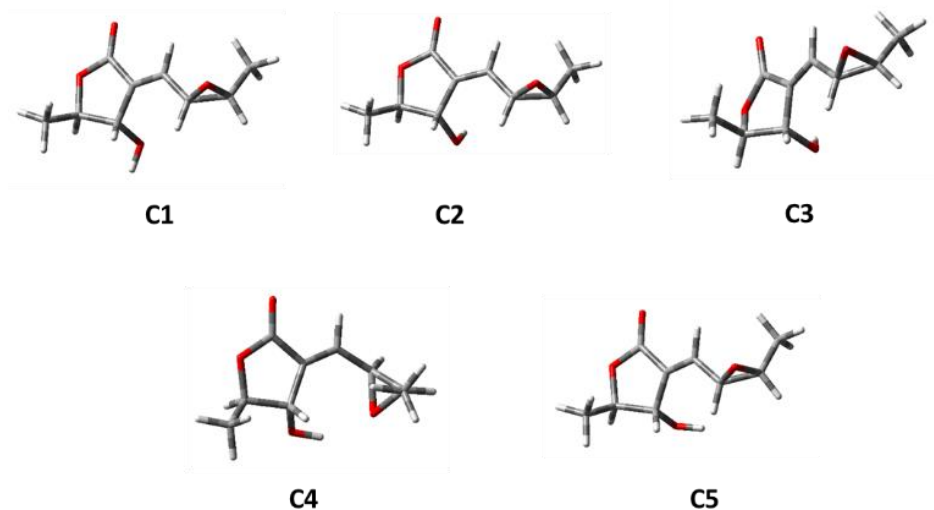


Figure 106: Structures of conformers found of (4*S*,5*R*,7*S*,8*R*)-32b** computed at DFT/B3LYP/6-311++G(2d,2p)/IEFPCM(CH₃CN) level.**

It was performed the same consideration did for pinofuranoxin A ((+)-**32**). Comparing the ECD experimental spectrum with the computed ones for **32a** and **32b** and of their enantiomers (4*R*,5*S*,7*S*,8*R*)-*ent*-**32a** and (4*R*,5*S*,7*R*,8*S*)-*ent*-**32b** (Fig. 102), the quite good agreement was obtained between the experimental spectrum and that of the *ent*-**32a** stereoisomer. Thus, the (4*R*,5*S*,7*S*,8*R*) AC was assigned to (+)-pinofuranoxin B ((+)-**32**).

5.6.4 Biological assay

5.6.4.1 Leaf puncture assay

The phytotoxicity of both compounds (**31** and **32**) was tested at three concentrations by leaf puncture assay on *Hedera helix* L., *Phaseolus vulgaris* L. and *Quercus ilex* L. Pinofuranoxins A (**31**) and B (**32**) at a concentration of 1 mg/ mL caused necrotic lesions on English ivy, bean, and holm oak leaves, with area lesion sizes of 112, 46, and 61 mm² and 79, 55, and 50 mm², respectively. Compound **31** showed phytotoxic effects at the other concentrations also, while compound **32** was inactive at the lowest concentration (Table 25).

Table 25: Phytotoxicity data for pinofuranoxins A (31) and B (32).^a

Compound	Concentration (mg/mL)	<i>Hedera helix</i> L.	<i>Phaseolus vulgaris</i> L.	<i>Quercus ilex</i> L.
31	1.0	112 ± 14	46 ± 5	61 ± 10
	0.5	49 ± 5	40 ± 2	36 ± 7
	0.1	5 ± 1	7 ± 1	1 ± 0
32	1.0	79 ± 3	55 ± 10	50 ± 2
	0.5	14 ± 3	27 ± 3	23 ± 2
	0.1	na	na	na

^aData are expressed as median area lesion ± error standard (mm²); na = inactive.

5.6.4.2 Antifungal assays

Both compounds (**31** and **32**) were also tested against two plant pathogenic fungi (*Athelia rolfsii* and *Diplodia corticola*) and the oomycete *Phytophthora cambivora* at 200 and 100 µg/plug. Pentachloronitrobenzene (PCNB) and metalaxyl-M were used as positive controls for ascomycetes and oomycetes, respectively. Pinofuranoxin A (**31**) completely inhibited the mycelial growth of *P. cambivora* and *A. rolfsii* at both concentrations used, while it showed low antifungal activity against *D. corticola*. Pinofuranoxin B (**32**) completely inhibited *P. cambivora* at both concentrations, whereas it was inactive against *A. rolfsii* and *D. corticola* (Table 26).

Table 26: Inhibitory activity of pinofuranoxins A (31) and B (32) against fungal pathogens.

Compound	Concentration (mg/plug)	<i>Athelia rolfsii</i>	<i>Diplodia corticola</i>	<i>Phytophthora cambivora</i>
31	0.2	100	38	100
	0.1	100	21	100
32	0.2	na ^a	na	100
	0.1	na	na	100
PCNB	0.2	81	72	nt ^b
	0.1	76	69	nt
metalaxyl-M	0.2	nt	nt	100
	0.1	nt	nt	100

^ana = inactive. ^bnt = not tested.

5.6.4.3 *Artemia salina* bioassay

Pinofuranoxins A and B (**31** and **32**) were tested for their zootoxic activity by *Artemia salina* bioassay at 200, 100 and 50 µg/mL. Both compounds determined 96% and 51% of larval mortality in a brine shrimp (*Artemia salina* L.) assay at 200 µg/mL (Rajabi *et al.*, 2015). At the other two concentrations (100 and 50 µg/mL) compound **31** caused a larval mortality less than 20%, while compound **32** was inactive.

6 CONCLUSIONS

This thesis project has been focused on the isolation and chemical and biological characterization of different phytotoxins produced by pathogenic fungi involved in forest plant diseases:

- *Hymenoscyphus fraxineus* has been identified as the main causes of “ash dieback”, causing a significative reduction of *Fraxinus excelsior* L. population across Europe. From its culture filtrate a new metabolite, named hyfraxinic acid (**1**, Fig. 27) has been isolated and characterized by spectroscopic techniques as 2,4-dihydroxy-7-methyl-6-methyleneoctanoic acid.

Other four known metabolites were isolated and identified as 1-deoxyviridiol, viridiol, nodulisporiviridin M and demethoxyviridiol (**2-5**, Fig. 6). Moreover, the relative and the absolute configurations of 1-deoxyviridiol (**2**, Fig. 6), which were not assigned correctly in literature, have been determine by X-ray analysis and by applying the advanced Mosher’s method, respectively.

The phytotoxicity of all isolated metabolites (**1-5**, Fig. 6) has been tested by leaf puncture assay, yielding that hyfraxinic acid has caused the most extensive necrosis on four of five plant species tested, although ash tree leaves have been more susceptible to the demethoxyviridiol.

- *Fimetariella rabenhorstii* has been recently detected as the causal agent of *Quercus brantii* decline in Iran. From its organic extract two new metabolites, named rabenchromenone and rabenzophenone (**10** and **11**, Fig. 40), have been isolated and characterized together with two related, known compounds moniliphenone and coniochaetone A (**12** and **13**, Fig. 40). Rabenchromenone and rabenzophenone (**10** and **11**, Fig. 40) have been formulated as methyl-3-chloro-1,8-dihydroxy-6-methyl-9-oxo-1,9-dihydrocyclopenta[b]-chromene-1-carboxylate and 4-chloro-2-(2,6-dihydroxy-4-methylbenzoyl)-3-hydroxybenzoate, respectively. Furthermore, the absolute configuration of rabenchromenone (**10**, Fig. 40) has been assigned by quantum chemical calculations and electronic circular dichroism experiments.

In the leaf puncture bioassay, all metabolites (**10-13**, Fig. 40) have been showed a stronger activity on holm oak leaves than on tomato leaves. In addition, rabenzophenone (**11**, Fig. 40) has been the most phytotoxic compound.

- *Stilbocrea macrostoma* has been identified as virulent fungus from *Q. brantii* branches, causing wood necrosis. Three well-known metabolites have been isolated and characterized from its organic extract, 2,5-dihydroxymethylfuran, 5-hydroxymethyl-2-furaldehyde and tyrosol (**14-16**, Fig. 52). The structure assigned to 2,5-dihydroxymethylfuran (**14**, Fig. 52) was supported by its X-ray crystallographic analysis.

In the phytotoxic assay, the two furan derivatives (**14** and **15**, Fig. 52) have been determined significant necrosis on both plants tested and their activity has been concentration-dependent; while tyrosol (**16**, Fig. 52) has been showed a lower activity than the other two metabolites.

- *Diplodia olivarum* has been identified as the canker agent of many plants in Italy, as carob tree, lentisk and wild olive. From its culture filtrates a new metabolite, named olicleistanone (**17**, Fig. 57) has been isolated and characterized by spectroscopic techniques as 4-ethoxy-6a-methoxy-3,8,8-trimethyl-4,5,8,9,10,11-hexahydrodibenzo[*de,g*]chromen-7(6a*H*)-one. Other five well-known phytotoxins have been identified as sphaeropsidins A, C and G, diplopimarane and (-)-mellein (**18-22**, Fig. 57). Moreover, the relative configuration of olicleistanone (**17**, Fig. 57) has been determined by NOESY correlations; while all attempts to assigned the absolute configuration have been proved that olicleistanone has been a racemate.

All metabolites (**17-22**, Fig. 57) have been tested for their phytotoxic, antifungal and zootoxic activities. Olicleistanone (**17**, Fig. 57) has exhibited strong activity against the insect *Artemia salina* L., but not phytotoxic and antifungal activities.

- *Alternaria argyroxiphii* has been detected as the causal agent of leaf spot of African mahogany. From its organic extract three new metabolites, named argyrottoxins A-C (**23-25**, Fig. 64), have been isolated and characterized as 4-(7-methoxy-6-methyl-3-oxo-1,3-dihydroisobenzofuran-5-yloxy)-2-methyl-butyrac acid, 5-but-2-enyloxy-*N*-(2-hydroxy-ethyl)-2-hydroxymethyl-3-methoxy-4-methyl-benzamide and 1-(5-(hydroxymethyl)-3-methoxy-4-(methoxymethyl)-2-methyl-phenoxy)-3-methylbutane-2,3-diol, respectively. The absolute configuration of argyrottoxin A (**23**, Fig. 64) has been assigned through ECD by applying the biphenyl chiroptical probe approach.

Other six metabolites have been identified as porritoxinol, phthalide, phthalide carboxylic acid derivative, zinniol, alternariol and 4-methylalternariol (**26-31**, Fig. 64).

In the leaf puncture assay, argyrottoxin A and B (**23** and **24**, Fig. 64) have been active on leaves of bean, porritoxinol (**26**, Fig. 64) has been showed phytotoxicity on holm oak leaves only, while zinniol (**29**, Fig., 64) has been phytotoxic on all plants tested.

- *Diplodia sapinea* has been recently associated to canker and dieback of *Pinus pinaster* in Tunisia. From its culture filtrate two new metabolites, pinofuranoxins A and B (**31** and **32**, Fig. 87), have been isolated and characterized by spectroscopic techniques as 4-hydroxy-5-methyl-3-((3-methyloxiran-2-yl)-methylene)dihydrofuran-2(3*H*)-ones. Their relative configurations have been determined by NOESY correlations, resulting that pinofuranoxins A and B are two diastereomers with opposite configurations of the oxirane rings. Their absolute configurations have been assigned by computational and ECD analyses.

When tested for the biological activity, using different bioassays, the new compounds (**31** and **32**, Fig. 87) have presented interesting activities. In particular, in the phytotoxic assay pinofuranoxin A has induced necrosis at all concentrations used, while pinofuranoxin B has been toxic at the higher concentration only. In the antifungal bioassay, pinofuranoxin A has inhibited the mycelial growth of all the tested pathogens, while pinofuranoxin B has inhibited the growth of *P. cambivora* only. Both compounds have been caused larval mortality of *Artemia salina* L. at the higher concentration tested.

7 REFERENCES

- Abdollahzadeh, J., Goltapeh, E.M., Javadi, A., Shams-Bakhsh, M., Zare, R., Phillips, A.J.L. (2009). *Barriopsis iraniana* and *Phaeobotryon cupressi*: two new species of the *Botryosphaeriaceae* from trees in Iran. *Persoonia*, 23,1–9.
- Abrell, L.M., Borgeson, B., Crews, P. (1996). Chloro polyketides from the cultured fungus (*Aspergillus*) separated from a marine sponge. *Tetrahedron Lett.* 37, 2331–2334.
- Ahn, J.W., Lee, M.K., Choi, S.U., Lee, C.O., Kim, B.S. (1998). Cytotoxic ophiobolins produced by *Bipolaris* sp. *J. Microbiol. Biotechnol.* 8, 406–408.
- Aldridge, D.C., Turner, W.B., Geddes, A.J., Sheldrick, B. (1975). Demethoxyviridin and demethoxyviridiol: New fungal metabolites. *J. Chem. Soc., Perkin Trans. 1*, 1, 943–945.
- Alidadi, A., Kowsari, M., Javan-Nikkhah, M., Jouzani, G.S., Rastaghi, M.E. (2019). New pathogenic and endophytic fungal species associated with Persian oak in Iran. *Eur. J. Plant Pathol.* 155, 1017–1032.
- Allwood, J.W., Ellis, D.I., Goodacre, R. (2008). Metabolomic technologies and their application to the study of plants and plant–host interactions. *Physiol. Plant.* 132, 117–135.
- Altomare, A., Burla, M.C., Camalli, M., Cascarano, G.L., Giacovazzo, C., Guagliardi, A., Moliterni, A.G., Polidori, G., Spagna, R. (1999). SIR97: A new tool for crystal structure determination and refinement. *J. Appl. Crystallogr.* 32, 115–119.
- Alves, A., Correia, A., Phillips, A.J. (2006). Multi-gene genealogies and morphological data support *Diplodia cupressi* sp. nov., previously recognized as *D. pinea* f. sp. *cupressi*, as a distinct species. *Fungal Divers.* 23, 1–15.
- An, Y., Zhao, T., Miao, J., Liu, G., Zheng, Y., Xu, Y., Van Etten, R.L. (1989). Isolation, identification, and mutagenicity of alternariol monomethyl ether. *J. Agric. Food Chem.* 37, 1341–1343.

- Andersson, P.F., Bengtsson, S., Stenlid, J., Broberg, A. (2012). B-norsteroids from *Hymenoscyphus pseudoalbidus*. *Molecules*, *17*, 7769–7781.
- Andersson, P.F., Bengtsson, S., Cleary, M., Stenlid, J., Broberg, A. (2013a). Viridin-like steroids from *Hymenoscyphus pseudoalbidus*. *Phytochemistry*, *86*, 195–200.
- Andersson, P.F., Broberg, A., Lundberg, D. (2013b). The furanosteroid viridiol. *Acta Crystallogr., Sect. E: Struct. Rep. Online*, *69*, o467–o468.
- Andolfi, A., Cimmino, A., Evidente, A., Iannaccone, M., Capparelli, R., Mugnai, L., Surico, G. (2009). A new flow cytometry technique to identify *Phaeoconiella chlamydospora* exopolysaccharides and study mechanisms of esca grapevine foliar symptoms. *Plant Dis.* *93*, 680–684.
- Andolfi, A., Maddau, L., Linaldeddu, B.T., Scanu, B., Cimmino, A., Basso, S., Evidente, A. (2014a). Bioactivity studies of oxysporone and several derivatives. *Phytochem. Lett.* *10*, 40–45.
- Andolfi, A., Maddau, L., Basso, S., Linaldeddu, B.T., Cimmino, A., Scanu, B., Deidda, A., Tuzi, A., Evidente, A. (2014b). Diplopimarane, a 20-nor-ent-pimarane produced by the oak pathogen *Diplodia quercivora*. *J. Nat. Prod.* *77*, 2352–2360.
- Atanasov, A.G., Zotchev, S.B., Dirsch, V.M., Supuran, C.T. (2021). Natural products in drug discovery: Advances and opportunities. *Nat. Rev. Drug Discov.* *20*, 200–216.
- Au, T.K., Chick, W.S.H., Leung, P.C. (2000). The biology of ophiobolins. *Life Sci.* *67*, 733–742.
- Ayers, S., Graf, T.N., Adcock, A.F., Kroll, D.J., Shen, Q., Swanson, S.M., Matthew, S., de Blanco, E.J.C., Wani, M.C., Darveaux, B.A., Pearce, C.J., Oberlies, N.H. (2012). Cytotoxic xanthone–anthraquinone heterodimers from an unidentified fungus of the order Hypocreales (MSX 17022). *J. Antibiot.* *65*, 3–8.
- Bajsa, J., Singh, K., Nanayakkara, D., Duke, S.O., Rimando, A.M., Evidente, A., Tekwani, B.L. (2007). A survey of synthetic and natural phytotoxic compounds and phytoalexins as potential antimalarial compounds. *Biol. Pharm. Bull.* *30*, 1740–1744.

- Bakys, R., Vasaitis, R., Barklund, P., Thomsen, I.M., Stenlid, J. (2009). Occurrence and pathogenicity of fungi in necrotic and non-symptomatic shoots of declining common ash (*Fraxinus excelsior*) in Sweden. *Eur. J. For. Res.* *128*, 51–60.
- Balde, E.S., Andolfi, A., Bruyère, C., Cimmino, A., Lamoral-Theys, D., Vurro, M., Damme, M. Van, Altomare, C., Mathieu, V., Kiss, R. (2010). Investigations of fungal secondary metabolites with potential anticancer activity. *J. Nat. Prod.* *73*, 969–971.
- Bani, M., Cimmino, A., Evidente, A., Rubiales, D., Rispaill, N. (2018). Pisatin involvement in the variation of inhibition of *Fusarium oxysporum* f. sp. *pisi* spore germination by root exudates of *Pisum* spp. germplasm. *Plant Pathol.* *67*, 1046–1054.
- Baral, H.O., Queloz, V., Hosoya, T. (2014). *Hymenoscyphus fraxineus*, the correct scientific name for the fungus causing ash dieback in Europe. *IMA Fungus*, *5*, 79–80.
- Barilli, E., Cimmino, A., Masi, M., Evidente, M., Rubiales, D., Evidente, A. (2016). Inhibition of spore germination and appressorium formation of rust species by plant and fungal metabolites. *Nat. Prod. Commun.* *11*, 1343–1347.
- Barilli, E., Cimmino, A., Masi, M., Evidente, M., Rubiales, D., Evidente, A. (2017). Inhibition of early development stages of rust fungi by the two fungal metabolites cyclopaldic acid and epi-epoformin. *Pest Manag. Sci.* *73*, 1161–1168.
- Barilli, E., González-Bernal, M.J., Cimmino, A., Agudo-Jurado, F.J., Masi, M., Rubiales, D., Evidente, A. (2019). Impact of fungal and plant metabolites application on early development stages of pea powdery mildew. *Pest Manag. Sci.* *75*, 2464–2473.
- Ben Jamaa, M.L., Lieutier, F., Yart, A., Jerraya, A., Khouja, M.L. (2007). The virulence of phytopathogenic fungi associated with the bark beetles *Tomicus piniperda* and *Orthotomicus erosus* in Tunisia. *For. Pathol.* *37*, 51–63.
- Bérdy, J. (1980). *Handbook of antibiotic compounds* (Florida: Crc Press).
- Berestetskiy, A.O. (2008). A review of fungal phytotoxins: from basic studies to practical use. *Appl. Biochem. Microbiol.* *44*, 453–465.

- Berestetskii, A.O., Yuzikhin, O.S., Katkova, A.S., Dobrodumov, A.V., Sivogrivov, D.E., Kolombet, L.V. (2010). Isolation, identification, and characteristics of the phytotoxin produced by the fungus *Alternaria cirsinoxia*. *Appl. Biochem. Microbiol.* *46*, 75–79.
- Berger, S., and Braun, S. 200 and More Basic NMR Experiments: A Practical Course, 1st ed.; Wiley-VCH: Weinheim, Germany, 2004.
- Bhuiyan, M.N.I., Begum, J., Bhuiyan, M.N.H. (2009) Analysis of essential oil of eaglewood tree (*Aquilaria agallocha* Roxb.) by gas chromatography mass spectrometry. *Bangladesh J. Pharmacol.* *4*, 24–28.
- Brandwagt, B.F., Kneppers, T.J.A., Van der Weerden, G.M., Nijkamp, H.J.J., Hille, J. (2001). Most AAL toxin-sensitive *Nicotiana* species are resistant to the tomato fungal pathogen *Alternaria alternata* f. sp. *lycopersici*. *Mol. Plant-Microbe Interact.* *14*, 460–470.
- Brase, S., Encinas, A., Keck, J., Nising, C.F. (2009). Chemistry and biology of mycotoxins and related fungal metabolites. *Chem. Rev.* *109*, 3903–3990.
- Breitmaier, E., and Voelter, W. (1987). Carbon-13 NMR Spectroscopy; VCH: Weinheim, Germany, 183–280.
- Bruhn, T., Schaumlöffel, A., Hemberger, Y., Pescitelli, G. (2017). SpecDis, Version 1.70; Berlin, Germany.
- Brugger, E.M., Wagner, J., Schumacher, D.M., Koch, K., Podlech, J., Metzler, M., Lehmann, L. (2006). Mutagenicity of the mycotoxin alternariol in cultured mammalian cells. *Toxicol. Lett.* *164*, 221–230.
- Bury, M., Girault, A., Megalizzi, V., Spiegl-Kreinecker, S., Mathieu, V., Berger, W., Evidente, A., Kornienko, A., Gailly, P., Vandier, C. (2013). Ophiobolin A induces paraptosis-like cell death in human glioblastoma cells by decreasing BKCa channel activity. *Cell Death Dis.* *4*, e561.
- Byrd, A.L., and Segre, J. A. (2016). Adapting Koch's postulates. *Science*, *351*, 224–226.

- Cabras, A., Mannoni, M.A., Serra, S., Andolfi, A., Fiore, M., Evidente, A. (2006). Occurrence, isolation and biological activity of phytotoxic metabolites produced *in vitro* by *Sphaeropsis sapinea*, pathogenic fungus of *Pinus radiata*. *Eur. J. Plant Pathol.* *115*, 187–193.
- Capasso, R., Cristinzio, G., Evidente, A., Scognamiglio, F. (1992). Isolation, spectroscopy and selective phytotoxic effects of polyphenols from vegetable waste waters. *Phytochemistry*, *31*, 4125–4128.
- Cheng, W., Zhu, C., Xu, W., Fan, X., Yang, Y., Li, Y., Chen, X., Wang, W., Shi, J. (2009). Chemical constituents of the bark of *Machilus wangchiana* and their biological activities. *J. Nat. Prod.* *72*, 2145–2152.
- Chidley, C., Trauger, S.A., Birsoy, K., O’Shea, E.K. (2016). The anticancer natural product ophiobolin A induces cytotoxicity by covalent modification of phosphatidylethanolamine. *Elife*, *5*, e14601.
- Cimmino, A., Andolfi, A., Avolio, F., Ali, A., Tabanca, N., Khan, I.A., Evidente, A. (2013). Cyclopaldic acid, seiridin, and sphaeropsidin A as fungal phytotoxins, and larvicidal and biting deterrents against *Aedes aegypti* (Diptera: Culicidae): Structure-activity relationships. *Chem. Biodivers.* *10*, 1239–1251.
- Cimmino, A., Fernández-Aparicio, M., Andolfi, A., Basso, S., Rubiales, D., Evidente, A. (2014). Effect of fungal and plant metabolites on broomrapes (*Orobancha* and *Phelipanche* spp.) seed germination and radicle growth. *J. Agric. Food Chem.* *62*, 10485–10492.
- Cimmino, A., Masi, M., Evidente, M., Superchi, S., Evidente, A. (2015). Fungal phytotoxins with potential herbicidal activity: chemical and biological characterization. *Nat. Prod. Rep.* *32*, 1629–1653.
- Cimmino, A., Maddau, L., Masi, M., Evidente, M., Linaldeddu, B.T., Evidente, A. (2016). Further secondary metabolites produced by *Diplodia corticola*, a fungal pathogen involved in cork oak decline. *Tetrahedron*, *72*, 6788–6793.
- Cimmino, A., Iannaccone, M., Petriccione, M., Masi, M., Evidente, M., Capparelli, R., Scortichini, M., Evidente, A. (2017a). An ELISA method to identify the phytotoxic *Pseudomonas syringae*

pv. *actinidiae* exopolysaccharides: A tool for rapid immunochemical detection of kiwifruit bacterial canker. *Phytochem. Lett.* *19*, 136–140.

Cimmino, A., Maddau, L., Masi, M., Linaldeddu, B.T., Pescitelli, G., Evidente, A. (2017b). Fraxitoxin, a new isochromanone isolated from *Diplodia fraxini*. *Chem. Biodivers.* *14*, e1700325.

Cimmino, A., Cinelli, T., Masi, M., Reveglia, P., da Silva, M.A., Mugnai, L., Michereff, S.J., Surico, G., Evidente, A. (2017c). Phytotoxic lipophilic metabolites produced by grapevine strains of *Lasiodiplodia* species in Brazil. *J. Agric. Food Chem.* *65*, 1102–1107.

Cimmino, A., Masi, M., Evidente, M., Superchi, S., Evidente, A. (2017d). Application of Mosher's method for absolute configuration assignment to bioactive plants and fungi metabolites. *J. Pharm. Biomed. Anal.* *144*, 59–89.

Cimmino, A., Nocera, P., Linaldeddu, B.T., Masi, M., Gorecki, M., Pescitelli, G., Montecchio, L., Maddau, L., Evidente, A. (2018). Phytotoxic metabolites produced by *Diaportheella cryptica*, the causal agent of hazelnut branch canker. *J. Agric. Food Chem.* *66*, 3435–3442.

Cimmino, A., Maddau, L., Masi, M., Linaldeddu, B.T., Evidente, A. (2019). Secondary metabolites produced by *Sardiniella urbana*, a new emerging pathogen on European hackberry. *Nat. Prod. Res.* *33*, 1862–1869.

Citron, C.A., Junker, C., Schulz, B., Dickschat, J.S. (2014). A volatile lactone of *Hymenoscyphus pseudoalbidus*, pathogen of European ash dieback, inhibits host germination. *Angew. Chem. Int. Ed.* *53*, 4346–4349.

Clark, M.F., and Adams, A.N. (1977). Characteristics of the microplate method of enzyme-linked immunosorbent assay for the detection of plant viruses. *J. Gen. Virol.* *34*, 475–483.

Cleary, M.R., Daniel, G., Stenlid, J. (2013). Light and scanning electron microscopy studies of the early infection stages of *Hymenoscyphus pseudoalbidus* on *Fraxinus excelsior*. *Plant Pathol.* *62*, 1294–1301.

- Cleary, M.R., Andersson, P.F., Broberg, A., Elfstrand, M., Daniel, G., Stenlid, J. (2014). Genotypes of *Fraxinus excelsior* with different susceptibility to the ash dieback pathogen *Hymenoscyphus pseudoalbidus* and their response to the phytotoxin viridiol–A metabolomic and microscopic study. *Phytochemistry*, *102*, 115–125.
- Cole, R.J., Kirksey, J.W., Springer, J.P., Clardy, J., Cutler, H.G., Garren, K.H. (1975). Desmethoxyviridiol, a new toxin from *Nodulisporium hinnuleum*. *Phytochemistry* *14*, 1429–1432.
- Couto, J.M.F., Otoni, W.C., Pinheiro, A.L., Fonseca, E.P. (2004). Desinfestação e germinação in vitro de sementes de mogno (*Swietenia macrophylla* King). *Rev. Árvore* *28*, 633–642.
- Damm, U., Crous, P.W., Fourie, P.H. (2007). Botryosphaeriaceae as potential pathogens of prunus species in South Africa, with descriptions of *Diplodia africana* and *Lasiodiplodia plurivora* sp. nov. *Mycologia*, *99*, 664–680.
- Dar, A.S., Nisar, A.D., Mudasir, A.B., Mudasir, H.B. (2014) Prospects, utilization and challenges of botanical pesticides in sustainable agriculture. *Int. J. Mol. Biol. Biochem.* *13*, 2858–2872.
- Dasari, R., Masi, M., Lisy, R., Ferdérin, M., English, L.R., Cimmino, A., Mathieu, V., Brenner, A.J., Kuhn, J.G., Whitten, S.T. (2015a). Fungal metabolite ophiobolin A as a promising anti-glioma agent: In vivo evaluation, structure–activity relationship and unique pyrrolylation of primary amines. *Bioorg. Med. Chem. Lett.* *25*, 4544–4548.
- Dasari, R., De Carvalho, A., Medellin, D.C., Middleton, K.N., Hague, F., Volmar, M.N.M., Frolova, L.V., Rossato, M.F., Jorge, J., Dybdal-Hargreaves, N.F. (2015b). Wittig derivatization of sesquiterpenoid polygodial leads to cytostatic agents with activity against drug resistant cancer cells and capable of pyrrolylation of primary amines. *Eur. J. Med. Chem.* *103*, 226–237.
- Del Bel, M.; Abela, A.R.; Ng, J.D.; Guerrero, C.A. (2017). Enantioselective chemical syntheses of the furanosteroids (–)-viridin and (–)-viridiol. *J. Am. Chem. Soc.* *139*, 6819–6822.
- Del Sorbo, G., Evidente, A., Scala, F. (1994). Production of polyclonal antibodies for cyclopaldic acid, a major phytotoxic metabolite produced by the plant pathogen *Seiridium cupressi*. *Nat. Toxins* *2*, 136–140.

- Deng, L., Niu, S., Liu, X., Che, Y., Li, E. (2013). Coniochaetones E–I, new 4H-chromen-4-one derivatives from the *Cordyceps*-colonizing fungus *Fimetariella* sp. *Fitoterapia*, 89, 8–14.
- Devappa, R.K., Makkar, H.P., Becker K. (2011). *Jatropha* diterpenes: a review. *J. Am. Oil Chem. Soc.* 88, 301–322.
- Dewick, P.M. (2009a). The shikimate pathway: aromatic amino acids and phenylpropanoids. *Med. Nat. Prod.* 137, 86.
- Dewick, P.M. (2009b). The mevalonate and methylerythritol phosphate pathways: terpenoids and steroids. *Medicinal natural products: a biosynthetic approach*. Wiley, 187–310.
- Djoukeng, J.D., Polli, S., Larignon, P., Abou-Mansour, E. (2009). Identification of phytotoxins from *Botryosphaeria obtusa*, a pathogen of 525 black dead arm disease of grapevine. *Eur. J. Plant Pathol.* 124, 303–308.
- Dohnal, B., and Kisiel, W. (2014). The effect of a fungal preparation on the tissue cultures of *Holarrhena anfidysenterica* (Roxb.) Wall. *Acta Soc. Bot. Pol.* 62, 43–45.
- Durbin, R.D. (1983). The biochemistry of fungal and bacterial toxins and their modes of action. *Biochem. Plant Pathol* 47, 137–162.
- Evidente, A., Sparapano, L., Motta, A., Giordano, F., Fierro, O., Frisullo, S. (1996). A phytotoxic pimarane diterpene of *Sphaeropsis sapinea* f. sp. *cupressi*, the pathogen of a canker disease of cypress. *Phytochemistry*, 42, 1541–1546.
- Evidente, A. (1997a). Bioactive metabolites from phytopathogenic fungi and bacteria. *Recent Research Developments in Phytochemistry*. Trivandrum, India, Research Signpost, 255–292.
- Evidente, A., Andolfi, A., D'Apice, L., Iannelli, D., Scala, F. (1997b). Identification by flow cytometry of seiridin, one of the main phytotoxins produced by three *Seiridium* species pathogenic to cypress. *Nat. Toxins* 5, 14–19.

- Evidente, A., Sparapano, L., Fierro, O., Bruno, G., Giordano, F., Motta, A. (1997c). Sphaeropsidins B and C, phytotoxic pimarane diterpenes from *Sphaeropsis sapinea* f. sp. *cupressi* and *Diplodia mutila*. *Phytochemistry*, *45*, 705–713.
- Evidente, A., Sparapano, L., Fierro, O., Bruno, G., Giordano, F., Motta, A. (1998). Sphaeropsidone and episphaeropsidone, phytotoxic dimedone methyl ethers by *Sphaeropsis sapinea* f. sp. *cupressi* grown in liquid culture. *Phytochemistry*, *48*, 1139–1143.
- Evidente, A., Sparapano, L., Fierro, O., Bruno, G., Motta, A. (1999). Sapinofuranones A and B, two new 2(3H)-dihydrofuranones produced by *Sphaeropsis sapinea*, a common pathogen of conifers. *J. Nat. Prod.* *62*, 253–256.
- Evidente, A., Sparapano, L., Andolfi, A., Bruno, G., Giordano, F., Motta, A. (2000). Chlorosphaeropsidone and epichlorosphaeropsidone, two new chlorinated dimedone methyl ethers isolated from liquid cultures of *Sphaeropsis sapinea* f. sp. *cupressi*. *Phytopathol. Mediterr.* *39*, 299–309.
- Evidente, A. and Motta, A. (2001). Phytotoxins from fungi pathogenic for agrarian, forestal and weedy plants. *Bioactive Compounds from Natural Sources*. (London, UK: Taylor and Francis) *12*, 473–525.
- Evidente, A. and Motta, A. (2002). Bioactive metabolites from phytopathogenic bacteria and plants. *Studies in Natural Products Chemistry*. Amsterdam, Elsevier Science, *26*, 581–628.
- Evidente, A., Sparapano, L., Bruno, G., Motta, A. (2002). Sphaeropsidins D and E, two other pimarane diterpenes, produced in vitro by the plant pathogenic fungus *Sphaeropsis sapinea* f. sp. *cupressi*. *Phytochemistry*, *59*, 817–823.
- Evidente, A., Sparapano, L., Andolfi, A., Bruno, G., Motta, A. (2003). Sphaeropsidin F, a new pimarane diterpene produced in vitro by the cypress pathogen *Sphaeropsis sapinea* f. sp. *cupressi*. *Aust. J. Chem.* *56*, 615–619.
- Evidente, A., Fiore, M., Bruno, G., Sparapano, L., Motta, A. (2006). Chemical and biological characterisation of sapinopyridione, a phytotoxic 3,3,6-trisubstituted-2,4-pyridione produced by

Sphaeropsis sapinea, a toxigenic pathogen of native and exotic conifers, and its derivatives. *Phytochemistry*, *67*, 1019–1028.

Evidente, A., Abouzeid, A.M., Andolfi, A., Cimmino, A. (2011a). Recent achievements in the bio-control of *Orobanche* infesting important crops in the Mediterranean basin. *J. Agric. Sci. Technol. A* *1*, 461–483.

Evidente, A., Andolfi, A., Cimmino, A. (2011b). Relationships between the stereochemistry and biological activity of fungal phytotoxins. *Chirality*, *23*, 674–693.

Evidente, A., Venturi, V., Masi, M., Degrassi, G., Cimmino, A., Maddau, L., Andolfi, A. (2011c). *In vitro* antibacterial activity of sphaeropsidins and chemical derivatives toward *Xanthomonas oryzae* pv. *oryzae*, the causal agent of rice bacterial blight. *J. Nat. Prod.* *74*, 2520–2525.

Evidente, A., Maddau, L., Scanu, B., Andolfi, A., Masi, M., Motta, A., Tuzi, A. (2011d). Sphaeropsidones, phytotoxic dimedone methyl ethers produced by *Diplodia cupressi*: A structure-activity relationship study. *J. Nat. Prod.* *74*, 757–763.

Evidente, A., Masi, M., Linaldeddu, B.T., Franceschini, A., Scanu, B., Cimmino, A., Andolfi, A., Motta, A., Maddau, L. (2012). Afritoxinones A and B, dihydrofuropyran-2-ones produced by *Diplodia africana* the causal agent of branch dieback on *Juniperus phoenicea*. *Phytochemistry*, *77*, 245–250.

Evidente, A., Kornienko, A., Cimmino, A., Andolfi, A., Lefranc, F., Mathieu, V., Kiss, R. (2014). Fungal metabolites with anticancer activity. *Nat. Prod. Rep.* *31*, 617–627.

Fabre, B., Piou, D., Desprez-Loustau, M.L., Marçais, B. (2011). Can the emergence of pine *Diplodia* shoot blight in France be explained by changes in pathogen pressure linked to climate change?. *Glob. Change Biol.* *17*, 3218–3227.

Falesi, I.C., and Baena, A.R.C. (1999). Mogno-africano *Khaya ivorensis* A. Chev. em sistema silvipastoril com leguminosa e revestimento natural do solo. Embrapa Amazônia Oriental, Belém, 52.

Farrugia, L.J. (2012). WinGX and ORTEP for Windows: An Update. *J. Appl. Crystallogr.* *45*, 849–854.

- Favilla, M., Macchia, L., Gallo, A., Altomare, C. (2006). Toxicity assessment of metabolites of fungal biocontrol agents using two different (*Artemia salina* and *Daphnia magna*) invertebrate bioassays. *Food Chem. Toxicol.* *44*, 1922–1931.
- Fernández-Aparicio, M., Cimmino, A., Evidente, A., Rubiales, D. (2013). Inhibition of *Orobancha crenata* seed germination and radicle growth by allelochemicals identified in cereals. *J. Agric. Food Chem.* *61*, 9797–9803.
- Fernández-Aparicio, M., Masi, M., Maddau, L., Cimmino, A., Evidente, M., Rubiales, D., Evidente, A. (2016). Induction of haustorium development by sphaeropsidones in radicles of the parasitic weeds *Striga* and *Orobancha*. A structure-activity relationship study. *J. Agric. Food Chem.* *64*, 5188–5196.
- Freeman, G.G. (1966). Isolation of alternariol and alternariol monomethyl ether from *Alternaria dauci* (kühn) groves and skolko. *Phytochemistry*, *5*, 719–725.
- Frisch, M.J., Trucks, G.W., Schlegel, H.B., Scuseria, G.E., Robb, M.A., Cheeseman, J.R., Scalmani, G., Barone, V., Petersson, G.A., Nakatsuji, H., Li, X., Caricato, M., Marenich, A.V., Bloino, J., Janesko, B.G., Gomperts, R., Mennucci, B., Hratchian, H.P., Ortiz, J.V., Izmaylov, A.F., Sonnemborg, J.L., Williams-Young, D., Ding, F., Lipparini, F., Egidi, F., Goings, J., Peng, B., Petrone, A., Henderson, T., Ranasinghe, D., Zakrzewski, V.G., Gao, J., Rega, N., Zheng, G., Liang, W., Hada, M., Ehara, M., Toyota, K., Fukuda, R., Hasegawa, J., Ishida, M., Nakajima, T., Honda, Y., Kitao, O., Nakai, H., Vreven, T., Throssell, K., Montgomery, J.A.Jr., Peralta, J.E., Ogliaro, F., Bearpark, M., Heyd, J.J., Brothers, E., Kudin, K.N., Staroverov, V.N., Keith, T.A., Kobayashi, R., Normand, J., Raghavachari, K., Rendell, A., Burant, J.C., Iyengar, S.S., Tomasi, J., Cossi, M., Millam, J.M., Klene, M., Adamo, C., Cammi, R., Ochterski, J.W., Martin, R.L., Morokuma, K., Farkas, O., Foresman, J.B., Fox, D.J. (2016). Gaussian 16, Revision A.03; Gaussian, Inc.: Wallingford, CT.
- Gadgil, P.D. (2005). Fungi on Trees and Shrubs in New Zealand. *Fungi New Zealand*, *4*.
- Gamboa-Angulo, M.M., Alejos-González, F., Escalante-Erosa, F., García-Sosa, K., Delgado-Lamas, G., Peña-Rodríguez, L.M. (2000). Novel dimeric metabolites from *Alternaria tagetica*. *J. Nat. Prod.* *63*, 1117–1120.

- Gasparotto, L., Hanada, R.E., Albuquerque, F.C., Duarte, M.L.R. (2001). Mancha areolada causada por *Thanatephorus cucumeris* em mogno-africano. *Fitopatol. Bras.* 26, 660–661.
- Gea-Izquierdo, G., Ferriz, M., García-Garrido, S., Aguín, O., Elvira-Recuenco, M., Hernandez-Escribano, L., Martin-Benito, D., Raposo, R. (2019). Synergistic abiotic and biotic stressors explain widespread decline of *Pinus pinaster* in a mixed forest. *Sci. Total Environ.* 685, 963–975.
- Glidewell, C., Zakaria, C.M., Ferguson, G. (1996). Multiple hydrogen-bonding modes in furan-2,5-dimethanol and furan-2,5-diylbis (diphenylmethanol). *Acta Crystallogr. C Cryst. Struct. Commun.* 52,1305–1309.
- Granata, G., Faedda, R., Sidoti, A. (2011). First report of canker caused by *Diplodia olivarum* on carob tree in Italy. *Plant Dis.* 100, 2483–2491.
- Graniti, A. (1991). Phytotoxins and their involvement in plant diseases. *Experientia* 47, 751–755.
- Gross, A., Holdenrieder, O., Pautasso, M., Queloz, V., Sieber, T.N. (2014). *Hymenoscyphus pseudoalbidus*, the causal agent of European ash dieback. *Mol. Plant Pathol.* 15, 5–21.
- Guo, L., Huang, T., Hu, B., Wang, C. (2016). Bioactivity-guided isolation and characterization of antitumor active compound from marine-derived fungus *Penicillium chrysogenum* HGQ6. *Adv. J. Food Sci. Technol.* 10, 353–355.
- Guo, C., Lin, X.P., Liao, S.R., Yang, B., Zhou, X.F., Yang, X.W., Tian, X.P.; Wang, J.F.; Liu, Y.H. (2020). Two new aromatic polyketides from a deep-sea fungus *Penicillium* sp. SCSIO 06720. *Nat. Prod. Res.* 34, 1197–1205.
- Halecker, S., Surup, F., Kuhnert, E., Mohr, K.I., Brock, N.L., Dickschat, J.S., Corina Junker, C., Schulz, B., Stadler, M. (2014). Hymenosetin, a 3-decalinoyltetramic acid antibiotic from cultures of the ash dieback pathogen, *Hymenoscyphus pseudoalbidus*. *Phytochemistry*, 100, 86–91.

- Hehre, W., Klunzinger, P., Deppmeier, B., Driessen, A., Uchida, N., Hashimoto, M., Fukushi, E., Takata, Y. (2019). Efficient protocol for accurately calculating ^{13}C chemical shifts of conformationally flexible natural products: scope, assessment, and limitations. *J. Nat. Prod.* 82, 2299–2306.
- Hlaiem, S., Zouaoui Boutiti, M., Yangui, I., Ben Jamaa, M.L. (2020). Identification and pathogenicity of *Diplodia seriata* and *Diplodia africana* related to lentisk dieback in Tunisia. *Arch. Phytopathol. Plant Prot.* 53, 99–111.
- Hohn, T.M. (1997). Fungal phytotoxins: biosynthesis and activity. *Plant Relationships*. (Heidelberg, Berlin: Springer), 129–144.
- Ingels, A., Dinhof, C., Garg, A. D., Maddau, L., Masi, M., Evidente, A., Berger, W., Dejaegher, B., Mathieu, V. (2017). Computed determination of the in vitro optimal chemocombinations of sphaeropsidin A with chemotherapeutic agents to combat melanomas. *Cancer Chemother. Pharmacol.* 79, 971.
- John, J.E. (2009). Natural products-based drug discovery: some bottlenecks and considerations. *Curr. Sci.* 96, 753–754.
- Ishida, T., and Wada, K. (1975). A steroid hydroxylase inhibitor, diplodialide A from *Diplodia pinea*. *J. Chem. Soc., Chem. Comm.* 6, 209–210.
- Ishihara, M., Tsuneya, T., Uneyama, K. (1991) Guaiane sesquiterpenes from agarwood. *Phytochemistry*, 30, 3343–3347.
- Iwahana, S., Iida, H., Yashima, E., Pescitelli, G., Di Bari, L., Petrovic, A.G., Berova, N. (2014). Absolute stereochemistry of a 4 a-hydroxyriboflavin analogue of the key intermediate of the FAD-monooxygenase cycle. *Chem. Eur. J.* 20, 4386–4395.
- Jain, T.C., and Bhattacharyya, S.C. (1959) Structure, stereochemistry and absolute configuration of agarol, a new sesquiterpene alcohol from agarwood oil. *Tetrahedron Lett.* 1, 13–17.
- Ju Y.M., Wang G.J., Chen C.Y., Tsau Y.J., Chou C.H., Lee T.H. (2010). Chemical constituents from fermented broth and mycelium of the basidiomycete *Lacrymaria velutina*. *Bot. Stud.* 51, 311–315.

- Junker, C., Mandey, F., Pais, A., Ebel, R., Schulz, B. (2014). *Hymenoscyphus pseudoalbidus* and *Hymenoscyphus albidus*: viridiol concentration and virulence do not correlate. *For. Pathol.* *44*, 39–44.
- Kachhawa, D. (2017) Microorganisms as a biopesticides. *J. Entomol. Zool. Stud.* *3*, 468–473.
- Kachi, H., and Sassa, T. (1986). Isolation of moniliphenone, a key intermediate in xanthone biosynthesis from *Monilinia fructicola*. *Agric. Biol. Chem.* *50*, 1669–1671.
- Kale, S., and Bennett, J.W. (1992). Strain instability in filamentous fungi. *Handb. Appl. Mycol* *5*, 311–331.
- Keller, N.P. (2019). Fungal secondary metabolism: regulation, function and drug discovery. *Nat. Rev. Microbiol.* *17*, 167–180.
- Khan, V.A., Gatilov, Y.V., Dubovenko, Z.V., Pentegova, V.A. (1979) Crystal structure of koraiol-a sesquiterpene alcohol with a new type of carbon skeleton from the oleoresin of *Pinus koraiensis*. *Chem. Nat. Compd.* *15*, 572–576.
- Kimura, Y., and Tamura, S. (1973). Isolation of L- β -phenyllactic acid and tyrosol as plant growth regulators from *Gloeosporium laeticolor*. *Agric. Biol. Chem.* *37*, 2925.
- Koch, K., Podlech, J., Pfeiffer, E., Metzler, M. (2005). Total synthesis of alternariol. *J. Org. Chem.* *70*, 3275–3276.
- Konishi, T., Iwagoe, K., Sugimoto, A., Kiyosawa, S., Fujiwara, Y., Shimada, Y. (1991) Studies on agarwood (Jinko). Structures of 2-(2-phenylethyl)chromone derivatives. *Chem. Pharm. Bull.* *39*, 207–209.
- Konishi, T., Konoshima, T., Shimada, Y., Kiyosawa, S. (2002) Six new 2-(2-phenylethyl)chromones from agarwood. *Chem. Pharm. Bull.* *50*, 419–422.
- Kowalski, T. (2006). *Chalara fraxinea* sp. Nov. associated with dieback of ash (*Fraxinus excelsior*) in Poland. *For. Pathol.* *36*, 264–270.

- Lahlou, M. (2007). Screening of natural products for drug discovery. *Expert Opin. Drug Discov.* 2, 697–705.
- Lallemand, B., Masi, M., Maddau, L., De Lorenzi, M., Dam, R., Cimmino, A., Laetitia, M.Y.B., Andolfi, A., Kiss, R., Mathieu, V., Evidente, A. (2012). Evaluation of in vitro anticancer activity of sphaeropsidins A-C, fungal rearranged pimarane diterpenes, and semisynthetic derivatives. *Phytochem. Lett.* 5, 770–775.
- Lamari, L. (2002). *Assess: image analysis software for plant disease quantification*. APS press.
- Lazzizzera, C., Frisullo, S., Alves, A., Lopes, J., Phillips, A.J.L. (2008). Phylogeny and morphology of *Diplodia* species on olives in southern Italy and description of *Diplodia olivarum* sp. nov. *Fungal Divers.* 31, 63–71.
- Lengai, G., and Muthomi, J.W. (2018) Biopesticides and their role in sustainable agricultural production. *J. Biosci. Med.* 6, 7–41.
- Li, G., Wang, X., Zheng, L., Li, L., Huang, R., Zhang, K. (2007). Nematicidal metabolites from the fungus *Pleurotus ferulae* Lenzi. *Ann. Microbiol.* 57, 527–529.
- Lim, S.H., Low, Y.Y., Subramaniam, G., Abdullah, Z., Thomas, N.F., Kam, T.S. (2013). Lumusidines A–D and villalstonidine F, macrolin-macrolin and macrolin-pleiocarpamine bisindole alkaloids from *Alstonia macrophylla*. *Phytochemistry*, 87, 148–156.
- Lin, J., Wang, R., Xu, G., Ding, Z., Zhu, X., Li, E., Liu, L. (2017). Two new polyketides from the ascomycete fungus *Leptosphaeria* sp. *J. Antibiot.* 70, 743–746.
- Linaldeddu, B.T., Hasnaoui, F., Franceschini, A. (2008). First report of shoot blight and dieback caused by *Diplodia pinea* on *Pinus pinaster* and *P. radiata* trees in Tunisia. *Phytopathol. Mediterr.* 47, 258–261.
- Linaldeddu, B.T., Scanu, B., Maddau, L., Franceschini, A. (2011). *Diplodia africana* causing dieback disease on *Juniperus phoenicea*: A new host and first report in the northern hemisphere. *Phytopathol. Mediterr.* 50, 473–477.

- Linaldeddu, B.T., Maddau, L., Franceschini, A., Alves, A., Phillips, A.J.L. (2016a). Botryosphaeriaceae species associated with lentisk dieback in Italy and description of *Diplodia insularis* sp. nov. *Mycosphere*, 7, 962–977.
- Linaldeddu, B.T., Alves, A., Phillips, A.J.L. (2016b). *Sardiniella urbana* gen. et sp. nov., a new member of the *Botryosphaeriaceae* isolated from declining *Celtis australis* trees in Sardinian streetscapes. *Mycosphere*, 7, 893–905.
- Lopes, A., Linaldeddu, B.T., Phillips, A.J.L., Alves, A. (2018). Mating type gene analyses in the genus *Diplodia*: from cryptic sex to cryptic species. *Fungal Biol.* 122, 629–638.
- Lou, J., Fu, L., Peng, Y., Zhou, L. (2013). Metabolites from *Alternaria* fungi and their bioactivities. *Molecules*, 18, 5891–5935.
- Lucas, G.B., Campbell, C.L., Lucas, L.T. (1992). Introduction to plant diseases: identification and management. Springer Science & Business Media.
- Lumsden, R.D., Ridout, C.J., Vendemia, M.E., Harrison, D.J., Waters, R.M., Walter, J.F. (1992). Characterization of major secondary metabolites produced in soilless mix by a formulated strain of the biocontrol fungus *Gliocladium virens*. *Can. J. Microbiol.* 38, 1274–1280.
- Macrae, C.F., Bruno, I.J., Chisholm, J.A., Edgington, P.R., McCabe, P., Pidcock, E., Rodriguez-Monge, L., Taylor, R., van de Streek, J., Wood, P.A. (2008). Mercury CSD 2.0—New features for the visualization and investigation of crystal structures. *J. Appl. Crystallogr.* 41, 466–470.
- Manca, D., Bregant, C., Maddau, L., Pinna, C., Montecchio, L., Linaldeddu, B.T., (2020). First report of canker and dieback caused by *Neofusicoccum parvum* and *Diplodia olivarum* on oleaster in Italy. *Ital. J. Mycol.* 49, 85–91.
- Mancilla, G., Jiménez-Teja, D., Femenía-Ríos, M., Macías-Sánchez, A.J., Collado, I.G., Hernández-Galán, R. (2009). Novel macrolide from wild strains of the phytopathogen fungus *Colletotrichum acutatum*. *Nat. Prod. Comm.* 4, 1934578X0900400316.

- Mansfield, J., Brown, I., Papp-Rupar, M. (2019). Life at the edge-The cytology and physiology of the biotroph to necrotroph transition in *Hymenoscyphus fraxineus* during lesion formation in ash. *Plant Pathol.* 68, 908–920.
- Mansoura, A.B., Garchi, S., Daly, H. (2001). Analyzing forest users' destructive behaviour in Northern Tunisia. *Land Use Policy* 18, 153–163.
- Marrone, P.G. (2019). Pesticidal natural products—status and future potential. *Pest Manag. Sci.* 75, 2325–2340.
- Masi, M., Cimmino, A., Maddau, L., Kornienko, A., Tuzi, A., Evidente, A. (2016a). Crystal structure and absolute configuration of sphaeropsidin A and its 6-*O-p*-bromobenzoate. *Tetrahedron Lett.* 57, 4592–4594.
- Masi, M., Maddau, L., Linaldeddu, B.T.; Cimmino, A., D'Amico, W., Scanu, B., Evidente, M., Tuzi, A., Evidente, A. (2016b). Bioactive secondary metabolites produced by the oak pathogen *Diplodia corticola*. *J. Agric. Food Chem.* 64, 217–225.
- Masi, M., Maddau, L., Linaldeddu, B.T., Scanu, B., Evidente, A., Cimmino, A. (2018). Bioactive metabolites from pathogenic and endophytic fungi of forest trees. *Curr. Med. Chem.* 25, 208–252.
- Masi, M., Dasari, R., Evidente, A., Mathieu, V., Kornienko, A. (2019). Chemistry and biology of ophiobolin A and its congeners. *Bioorg. Med. Chem. Lett.* 29, 859–869.
- Masi, M., Nocera, P., Boari, A., Zonno, M.C., Pescitelli, G., Sarrocco, S., Baroncelli, R., Vannacci, G., Vurro, M., Evidente, A. (2020). Secondary metabolites produced by *Colletotrichum lupini*, the causal agent of anthracnose of lupin (*Lupinus* spp.). *Mycologia*, 112, 533–542.
- Mathieu, V., Chantôme, A., Lefranc, F., Cimmino, A., Miklos, W., Paulitschke, V., Mohr, T., Maddau, L., Kornienko, A., Berger, W., Vandier, C., Evidente, A., Delpire, E., Kiss, R. (2015). Sphaeropsidin A shows promising activity against drug-resistant cancer cells by targeting regulatory volume increase. *Cell Mol. Life Sci.* 72, 3731–3746.

- Maslivetc, V., Laguera, B., Chandra, S., Dasari, R., Olivier, W.J., Smith, J.A., Bissember, A.C., Masi, M., Evidente, A., Mathieu, V., Kornienko, A. (2021). Polygodial and ophiobolin A analogues for covalent crosslinking of anticancer targets. *Int. J. Mol. Sci.* 22, 11256.
- Mazzeo, G., Santoro, E., Andolfi, A., Cimmino, A., Troselj, P., Petrovic, A.G., Superchi, S., Evidente, A., Berova, N. (2013). Absolute configurations of fungal and plant metabolites by chiroptical methods. ORD, ECD, and VCD studies on phyllostin, scytolide, and oxysporone. *J. Nat. Prod.* 76, 588–599.
- Mennucci, B., Claps, M., Evidente, A., Rosini, C. (2007). Absolute configuration of natural cyclohexene oxides by time dependent density functional theory calculation of the optical rotation: The absolute configuration of (-)-sphaeropsidone and (-)-episphaeropsidone revised. *J. Org. Chem.* 72, 6680–6691.
- Mesbah, L.A., Van der Weerden, G.M., Nijkamp, H.J.J., Hille, J. (2000). Sensitivity among species of Solanaceae to AAL toxins produced by *Alternaria alternata* f. sp. *lycopersici*. *Plant Pathol.* 49, 734–741.
- Misaghi, I.J. (1982). The role of pathogen-produced toxins in pathogenesis. *Physiology and Biochemistry of plant-pathogen interactions*, (Boston, MA, Springer, 35–61.
- Mislow, K., and Gordon, A.J. (1963). Photoracemization of biphenyls. *J. Am. Chem. Soc.* 85, 3521–3521.
- Möbius, N., and Hertweck, C. (2009). Fungal phytotoxins as mediators of virulence. *Curr. Opin. Plant Biol.* 12, 390–398.
- Moises, S.S., and Schäferling, M. (2009). Toxin immunosensors and sensor arrays for food quality control. *Bioanal. Rev.* 1, 73–104.
- Moreno-Fernández, D., Montes, F., Sánchez-González, M., Gordo, F.J., Cañellas, I. (2018). Regeneration dynamics of mixed stands of *Pinus pinaster* Ait. and *Pinus pinea* L. in Central Spain. *Eur. J. For. Res.* 137, 17–27.

- Mosadeghzad, Z., Zuriati, Z., Asmat, A., Gires, U., Wickneswari, R., Pittayakhajonwut, P., Farahani, G. (2013). Chemical components and bioactivity of the marine-derived fungus *Paecilomyces* sp. collected from Tinggi Island, Malaysia. *Chem. Nat. Compd.* 49, 621–625.
- Müller, M.M., Hantula, J., Wingfield, M., Drenkhan, R. (2019). *Diplodia sapinea* found on Scots pine in Finland. *For. Pathol.* 49, e12483.
- Nakanishi, K., and Solomon, P. H. (1977). *Infrared Absorption Spectroscopy*, 2nd ed., Holden Day, Oakland, CA, 17–44.
- Neidle, S., Rogers, D., Hursthouse, M.B. (1972). Crystal and molecular structure of viridin. *J. Chem. Soc., Perkin Trans. 2*, 2, 760–766.
- Newman, D.J., and Cragg, G.M. (2020). Natural products as sources of new drugs over the nearly four decades from 01/1981 to 09/2019. *J. Nat. Prod.* 83, 770–803.
- Nozoe, S., Morisaki, M., Tsuda, K., Iitaka, Y., Takahashi, N., Tamura, S., Ishibashi, K., Shirasaka, M. (1965). The structure of ophiobolin, a C₂₅ terpenoid having a novel skeleton. *J. Am. Chem. Soc.* 87, 4968–4970.
- O'Brien, H.E., Parrent, J.L., Jackson, J.A., Moncalvo, J.M., Vilgalys, R. (2005). Fungal community analysis by large-scale sequencing of environmental samples. *Appl. Environ. Microbiol.* 71, 5544–5550.
- Ohtani, I., Kusumi, T., Kashman, Y., Kaksawa, H. (1991). Highfield FT NMR application of Mosher's method. The absolute configurations of marine terpenoids. *J. Am. Chem. Soc.* 113, 4092–4096.
- Okudera, Y., and Ito, M. (2009) Production of agarwood fragrant constituents in *Aquilaria calli* and cell suspension cultures. *Plant Biotechnol.* 26, 307–315.
- Otani, H., Kohmoto, K., Kodama, M. (1995). Alternaria toxins and their effects on host plants. *Can. J. Bot.* 73, 453–458.
- Palmer, M.A., Stewart, E.L., Wingfield, M.J. (1987). Variation among isolates of *Sphaeropsis sapinea* in the North Central United States. *Phytopathology*, 77, 944–948.

- Pautasso, M., Aas, G., Queloz, V., Holdenrieder, O. (2013). European ash (*Fraxinus excelsior*) dieback – A conservation biology challenge. *Biol. Conserv.* *158*, 37–49.
- Perez-Vera, O.A., Cibrian-Tovar, D., T-Hanlin, R. (2017). First description of *Sclerotium coffeicola* on African mahogany in Mexico. *Rev. Argent. Microbiolo.* *50*, 202–205.
- Pescitelli, G., and Bruhn, T. (2016). Good computational practice in the assignment of absolute configurations by TDDFT calculations of ECD spectra. *Chirality*, *28*, 466–474.
- Phatik, T., Paran, B., Subhan, N., Piet, L. (2005) Essential oil of eaglewood tree: a product of pathogenesis. *J. Essent. Oil Res.* *17*, 601–604.
- Phillips, A.J.L., Alves, A., Abdollahzadeh, J., Slippers, B., Wingfield, M.J., Groenewald, J.Z., Crous, P.W. (2013). The Botryosphaeriaceae: genera and species known from culture. *Stud. Mycol.* *76*, 51–167.
- Pinheiro, A.L., Couto, L., Pinheiro, D.T., Brunetta, J.M.F.C. (2001). Ecologia, silvicultura e tecnologia de utilização dos mognos-africanos. (*Khaya* spp.). Viçosa, UFV, 102.
- Pinkerton, F., and Strobel, G. (1976). Serinol as an activator of toxin production in attenuated cultures of *Helminthosporium sacchari*. *PNAS*, *73*, 4007–4011.
- Pontes, J.G.D.M., Fernandes, L.S., dos Santos, R.V., Tasic, L., Fill, T.P. (2020). Virulence factors in the phytopathogen–host interactions: an overview. *J. Agric. Food Chem.* *68*, 7555–7570.
- Pretsch, E.; Buhlmann, P.; Affolter, C. (2000). ¹H NMR Spectroscopy. Structure Determination of Organic Compounds, 3rd ed.; Springer-Verlag: Berlin, Germany, 161–243.
- Prieto-Recio, C., Martín-García, J., Bravo, F., Diez, J.J. (2015). Unravelling the associations between climate, soil properties and forest management in *Pinus pinaster* decline in the Iberian Peninsula. *For. Ecol. Manag.* *15*, 74–83.
- Przybył, K. (2002). Fungi associated with necrotic apical parts of *Fraxinus excelsior* shoots. *For. Pathol.* *32*, 387–394.

- Pusztahelyi, T., Holb, I.J., Pócsi, I. (2015). Secondary metabolites in fungus-plant interactions. *Front. Plant Sci.* 6, 573.
- Qi, S.Y., He, M.L., Lin, L.D., Zhang, C.H., Hu, L.J., Zhang, H.Z. (2005) Production of 2-(2-phenylethyl)chromones in cell suspension cultures of *Aquilaria sinensis*. *Plant Cell, Tissue Organ Cult.* 83, 217–221.
- Queloz, V., Grünig, C.R., Berndt, R., Kowalski, T., Sieber, T.N., Holdenrieder, O. (2011). Cryptic speciation in *Hymenoscyphus albidus*. *For. Pathol.* 41, 133–142.
- Rahman, H.U., Yue, X., Yu, Q., Xie, H., Zhang, W., Zhang, Q., Li, P. (2019). Specific antigen-based and emerging detection technologies of mycotoxins. *J. Sci. Food Agric.* 99, 4869–4877.
- Rajabi, S., Ramazani, A., Hamidi, M., Naji, T. (2015). *Artemia salina* as a model organism in toxicity assessment of nanoparticles. *DARU J. Pharm. Sci.* 23, 1–6.
- Ramirez-Suero, M., Benard-Gellon, M., Chong, J., Lalou, H., Stempien, E., Abou-Mansour, E., Fontaine, F., Larignon, P., Mazet-Kieffer, F., Farine, S., Bertsch, C. (2014). Extracellular compounds produced by fungi associated with *Botryosphaeria dieback* induce differential defence gene expression patterns and necrosis in *Vitis vinifera* cv. Chardonnay cells. *Protoplasma*, 251, 1417–1426.
- Rodríguez-García, A., Martín, J.A., López, R., Sanz, A., Gil, L. (2016). Effect of four tapping methods on anatomical traits and resin yield in Maritime pine (*Pinus pinaster* Ait.). *Ind. Crop. Prod.* 86, 143–154.
- Sagiv, J., Yogev, A., Mazur, Y. (1977). Application of linear dichroism to the analysis of electronic absorption spectra of biphenyl, fluorene, 9,9'-spirobifluorene, and [6.6] vespirene. Interpretation of the circular dichroism spectrum of [6.6] vespirene. *J. Am. Chem. Soc.* 99, 6861–6869.
- Sanchez, M.S., Bills, G.F., Zabalgogezcoa I. (2008) Diversity and structure of the fungal endophytic assemblages from two sympatric coastal grasses. *Fungal Divers.* 33, 87–100.

- Santoro, E., Vergura, S., Scafato, P., Belviso, S., Masi, M., Evidente, A., Superchi, S. (2020). Absolute configuration assignment to chiral natural products by biphenyl chiroptical probes: the case of the phytotoxins colletochlorin A and agropyrenol. *J. Nat. Prod.* *83*, 1061–1068.
- Sarrocco, S., Diquattro, S., Avolio, F., Cimmino, A., Puntoni, G., Doveri, F., Evidente, A., Vannacci, G. (2015). Bioactive metabolites from new or rare fimicolous fungi with antifungal activity against plant pathogenic fungi. *Eur. J. Plant Pathol.* *142*, 61–71.
- Schneider, G, Anke, H, Sterner, O. (1996). Xylaramide, a new antifungal compound, and other secondary metabolites from *Xylaria longipes*. *Z. Naturforsch. C.* *51*, 802-806.
- Schrader, T.J., Cherry, W., Soper, K., Langlois, I. (2006). Further examination of the effects of nitrosylation on *Alternaria alternata* mycotoxin mutagenicity in vitro. *Mutat. Res. Genet. Toxicol. Environ. Mutagen* *606*, 61–71.
- Schrader, K.K., Andolfi, A., Cantrell, C.L., Cimmino, A., Duke, S.O., Osbrink, W., Wedge, D.E., Evidente, A. (2010). A survey of phytotoxic microbial and plant metabolites as potential natural products for pest management. *Chem. Biodivers.* *7*, 2261–2280.
- Sheldrick, G.M. (2015). Crystal structure refinement with SHELXL. *Acta Crystallogr., Sect. C, Struct. Chem.* *71*, 3–8.
- Shen, C.P., Luo, J.G., Yang, M.H., Kong, L.Y. (2015). A pair of novel 2,3-seco cafestol-type diterpenoid epimers from the twigs of *Tricalysia fruticosa*. *Tetrahedron Lett.* *56*, 1328–1331.
- Simmons, E.G. (2007). *Alternaria: an identification manual*. CBS Fungal Biodiversity Centre, Utrecht, Netherlands.
- Singh, D.D., and Datta, M. (2020). A promising source of anticancer drug from fungal secondary metabolite. *New and Future Developments in Microbial Biotechnology and Bioengineering.*, Elsevier, 95–101.
- Song, X.Q., Zhang, X., Han, Q.J., Li, X.B., Li, G., Li, R.J., Jiao, Y., Zhou, J.C., Lou, H.X. (2013). Xanthone derivatives from *Aspergillus sydowii*, an endophytic fungus from the liverwort *Scapania ciliata* S. Lac and their immunosuppressive activities. *Phytochem. Lett.* *6*, 318–321.

- Sparapano, L., Bruno, G., Fierro, O., Evidente, A. (2004). Studies on structure-activity relationship of sphaeropsidins A-F, phytotoxins produced by *Sphaeropsis sapinea* f. sp. *cupressi*. *Phytochemistry*, *65*, 189–198.
- Strobel, G.A. (1982). Phytotoxins. *Annu. Rev. Biochem* *51*, 309–333.
- Subramenium, G.A., Swetha, T.K., Iyer, P.M., Balamurugan, K., Pandian, S.K. (2018). 5-hydroxymethyl-2-furaldehyde from marine bacterium *Bacillus subtilis* inhibits biofilm and virulence of *Candida albicans*. *Microbiol. Res.* *207*, 19–32.
- Suemitsu, R., Ohnishi, K., Horiuchi, M., Morikawa, Y. (1992). Isolation and identification of 6-(3',3'-dimethylallyloxy)-4-methoxy-5-methylphthalide from *Alternaria porri*. *Biosci. Biotechnol. Biochem.* *56*, 986–986.
- Suemitsu, R., Ohnishi, K., Morikawa, Y., Ideguchi, I., Uno, H. (1994). Porritoxinol, a phytotoxin of *Alternaria porri*. *Phytochemistry*, *35*, 603–605.
- Sugawara, F., and Strobel, G. (1986). Zinniol, a phytotoxin, is produced by *Phoma macdonaldii*. *Plant Sci.* *43*, 19–23.
- Superchi, S., Casarini, D., Laurita, A., Bavoso, A., Rosini, C. (2001). Induction of a preferred twist in a biphenyl core by stereogenic centers: a novel approach to the absolute configuration of 1,2- and 1,3-diols. *Angew. Chem. Int. Ed.* *40*, 451–454.
- Superchi, S., Bisaccia, R., Casarini, D., Laurita, A., Rosini, C. (2006). Flexible biphenyl chromophore as a circular dichroism probe for assignment of the absolute configuration of carboxylic acids. *J. Am. Chem. Soc.* *128*, 6893–6902.
- Superchi, S., Scafato, P., Gorecki, M., Pescitelli, G. (2018). Absolute configuration determination by quantum mechanical calculation of chiroptical spectra: basics and applications to fungal metabolites. *Curr. Med. Chem.* *25*, 287–320.

- Surup, F., Halecker, S., Nimtz, M., Rodrigo, S., Schulz, B., Steinert, M., Stadler, M. (2018). Hyfraxins A and B, cytotoxic ergostane-type steroid and lanostane triterpenoid glycosides from the invasive ash dieback ascomycete *Hymenoscyphus fraxineus*. *Steroids*, *135*, 92–97.
- Sternhell, S. (1969). Correlation of interproton spin–spin coupling constants with structure. *Q. Rev., Chem. Soc.* *23*, 236–270.
- Švábová, L., and Lebeda, A. (2005). In vitro selection for improved plant resistance to toxin-producing pathogens. *J. Phytopathol.* *153*, 52–64.
- Tan, N., Tao, Y., Pan, J., Wang, S., Xu, F., She, Z., Jones, E.G. (2008). Isolation, structure elucidation, and mutagenicity of four alternariol derivatives produced by the mangrove endophytic fungus No. 2240. *Chem. Nat. Compd.* *44*, 296–300.
- Tao, M.H., Yan, J., Wei, X.Y., Li, D.L., Zhang, W.M., Tan, J.W. (2011). A novel sesquiterpene alcohol from *Fimetariella rabenhorstii*, an endophytic fungus of *Aquilaria sinensis*. *Nat. Prod. Commun.* *6*, 763–766.
- Teixeira, L.P., Soares, T.D.P.F., Oliveira, L.S.S., Mathioni, S., Ferreira, M.A. (2017). First report of leaf spot caused by *Alternaria argyroxiphii* on African mahogany trees (*Khaya senegalensis*). *Phytopathol. Mediterr.* *56*, 502–510.
- Thomma, B.P.H.J. (2003). *Alternaria* spp.: From general saprophyte to specific parasite. *Mol. Plant Pathol.* *4*, 225–236.
- Tsuge, T., Harimoto, Y., Akimitsu, K., Ohtani, K., Kodama, M., Akagi, Y., Egusa, M., Yamamoto, M., Otani, H. (2013). Host-selective toxins produced by the plant pathogenic fungus *Alternaria alternata*. *FEMS Microbiol. Rev.* *37*, 44–66.
- Tuzi, A., Andolfi, A., Maddau, L., Masi, M., Evidente, A. (2012). Structure and stereochemical assignment of spheropsidone, a phytotoxin from *Diplodia cupressi*. *J. Struct. Chem.* *53*, 786–792.

- Vergura, S., Pisani, L., Scafato, P., Casarini, D., Superchi, S. (2018). Central-to-axial chirality induction in biphenyl chiroptical probes for the stereochemical characterization of chiral primary amines. *Org. Biomol. Chem.* *16*, 555–565.
- Vergura, S., Scafato, P., Belviso, S., Superchi, S. (2019). Absolute configuration assignment from optical rotation data by means of biphenyl chiroptical probes. *Chem. Eur. J.* *25*, 5682–5690.
- Vergura, S., Orlando, S., Scafato, P., Belviso, S., Superchi, S. (2021). Absolute configuration sensing of chiral aryl- and aryloxy-propionic acids by biphenyl chiroptical probes. *Chemosensors*, *9*, 154.
- Verma, V.C., Kharwar, R.N., Strobel, G.A. (2009) Chemical and functional diversity of natural products from plant associated endophytic fungi. *Nat. Prod. Commun.* *4*, 1511–1532.
- Vilgalys, R., and Hester, M. (1990). Rapid genetic identification and mapping of enzymatically amplified ribosomal DNA from several *Cryptococcus* species. *J. Bacteriol.* *172*, 4238–4246.
- Voglmayr, H., and Jaklitsch, W.M. (2019). *Stilbocrea walteri* sp. Nov., an unusual species of Bionectriaceae. *Mycol Prog.* *18*, 91–105.
- Wada, K., and Ishida, T. (1979). A steroid hydroxylase inhibitor, diplodialide-A, and related metabolites from *Diplodia pinea*. *J. Chem. Soc., Perkin Trans. I*, 1154–1158.
- Walton, J.D. (1996). Host-selective toxins: agents of compatibility. *Plant Cell* *8*, 1723–1733.
- Wang, H.J., Gloer, J.B., Scott, J.A., Malloch, D. (1995). Coniochaetones A and B: new antifungal benzopyranones from the coprophilous fungus *Coniochaeta saccardoi*. *Tetrahedron Lett.* *36*, 5847–5850.
- Wang, H., Wu, F.H., Xiong, F., W J.J., Zhang, L.Y., Ye, W.C., Li, P., Zhao, S.X. (2006). Iridoids from *Neopicrorhiza scrophulariiflora* and their hepatoprotective activities *in vitro*. *Chem. Pharm. Bull.* *54*, 1144–1149.
- Wang, L., Zhang, W.M., Pan, Q.L., Li, H.H., Tao, M.H., Gao, X.X. (2009) Isolation and molecular identification of endophytic fungi from *Aquilaria sinensis*. *J. Fungal Res.* *7*, 37–42.

- Wang, Y., Zheng, Z., Liu, S., Zhang, H., Li, E., Guo, L., Che, Y. (2010). Oxepinochromenones, furochromenone, and their putative precursors from the endolichenic fungus *Coniochaeta* sp. J. Nat. Prod. 73, 920–924.
- Wang, G.Q., Chen, G.D., Qin, S.Y., Hu, D., Awakawa, T., Li, S.Y., Lv, J.M., Wang, C.X., Yao, X.S., Abe, I., Gao, H. (2018). Biosynthetic pathway for furanosteroid demethoxyviridin and identification of an unusual pregnane side-chain cleavage. Nat. Commun. 9, 1–13.
- Weyerstahl, P., Schneider, S., Marschall, H. (1996) Constituents of the Brazilian *Cangerana* oil. Flavour Fragr. J. 11, 81–94.
- Whipps, J.M., and Lumsden, R.D. (2001). Commercial use of fungi as plant disease biological control agents: status and prospects. Fungal Biocontrol Agents Progress, Probl. Potential 9–22.
- White, G.A., and Starrat, A.N. (1967). The production of a phytotoxic substance by *Alternaria zinniae*. Can. J. Bot. 45, 2087–2090.
- Woudenberg, J.H.C., Groenewald, J.Z., Binder, M., Crous, P.W. (2013). *Alternaria* redefined. Stud. Mycol. 75, 171–212.
- Xiong, L., Zhou, Q.M., Zou, Y., Chen, M.H., Guo, L., Hu, G.Y., Liu, Z.H., Peng C. (2015). Leonuketol, a spiroketal diterpenoid from *Leonurus japonicus*. Org. Lett. 17, 6238–6241.
- Yang, J.S., and Chen, Y.W. (1986) Studies on the chemical constituents of *Aquilaria sinensis* (Lour.) Gilg. II. Isolation and structure of baimuxinol and dehydrobaimuxinol. Acta Pharm. Sin. 21, 516–520.
- Yang, X.L., Zhang, S., Hu, Q.B., Luo, D.Q., Zhang, Y. (2011). Phthalide derivatives with antifungal activities against the plant pathogens isolated from the liquid culture of *Pestalotiopsis photiniae*. J. Antibiot. 64, 723–727.
- Yousefshahi, B., Bazgir, M., Jamali, S., Kakhki, F.V. (2020). Morphological and molecular identification of ectomycorrhizal fungi associated with Persian oak (*Quercus brantii* Lindl.) tree. J. For. Sci. 66, 244–251.

- Zask, A., and Ellestad, G. (2018). Biomimetic syntheses of racemic natural products. *Chirality*, *30*, 157–164.
- Zhang, D., Fukuzawa, S., Satake, M., Li, X., Kuranaga, T., Niitsu, A., Yoshizawa, K., Tachibana, K. (2012). Ophiobolin O and 6-epi-ophiobolin O, two new cytotoxic sesterterpenes from the marine derived fungus *Aspergillus* sp. *Nat. Prod. Commun.* *7*, 1411–1414.
- Zhang, P., Tang, C., Yao, S., Ke, C., Lin, G., Hua, H.M., Ye, Y. (2016). Cassane diterpenoids from the pericarps of *Caesalpinia bonduc*. *J. Nat. Prod.* *79*, 24–29.
- Zheng, M.Z., Richard, J.L., Binder, J. (2006). A review of rapid methods for the analysis of mycotoxins. *Mycopathologia*, *161*, 261–273.

8 APPENDIX A

Introduction

During a six months stage in Kiel (Germany) under the supervision of Prof. Christian Zidorn, the PhD work has been focused on the isolation and characterization of secondary metabolites produced from the roots of *Leontodon tenuiflorus*.

Leontodon tenuiflorus (Gaudin) Rchb. [synonym: *Leontodon incanus* Schrank subsp. *tenuiflorus* (Gaudin) Schinz & R.Keller] is an herb of 10 to 40 centimeters height, which grows at the Southern margins of the Alps, from the Swiss canton of Ticino to Monte Baldo and in the alpine foothills of Friuli (Zidorn, 2012).

Previously, a comparative study on the phenolics of flowering heads of various taxa of the genus *Leontodon* s.l. was carried out (Sareedenchai and Zidorn, 2010; Enke *et al.*, 2012). In this study, ten flavonoids were detected in flowering heads of *L. tenuiflorus* from the Province of Trento (Italy) and were identified as aesculin, chlorogenic acid, 3,5-*O*-dicaffeoylquinic acid, caffeoyltartaric acid, cichoric acid, luteolin, luteolin 7-*O*-glucoside, luteolin 7-*O*-gentiobioside, luteolin 7-*O*-glucuronide, and luteolin 4'-*O*-glucoside.

Experimental

L. tenuiflorus seeds were collected in the wild near Borno, between the Rifugio Laeng and the Pizzo Camino, (N 45°58'49.3'', E 10°11'14.2'', alt.: 1870 m a.m.s.l., Brescia, Lombardia, Italy; CZ-20170814D-1) and grown in the Botanical Garden of the Department of Pharmaceutical Biology (N 54°19'59.9", E 10°06'57.5"; 35 m a.m.s.l.), University of Kiel, Germany. The plants were identified following the keys and characters provided by Zidorn (2012). *L. tenuiflorus*, present in the garden of the Pharmaceutical Institute, were harvested in September, 2018 and a voucher specimen was deposited in the Herbarium of Kiel University (CZ-20180917A-1, KIEL0005013).

The dried roots of *L. tenuiflorus* were macerated with acetone and then with a mixture of Me₂CO/MeOH/H₂O (3:1:1) at room temperature and extracted with EtOAc, yielding 7.55 g and 1.50 g of residues, respectively. Having the same TLC profiles, the two organic extracts were combined and analyzed by reverse phase HPLC system (instrument: Hitachi ChromasterUltra Rs; column: Luna Omega 1.6 μm C₁₈; 100 × 2.1 mm: injection volume 5.0 μl; flow rate: 0.300 ml/min; oven temperature: 30°C; detection wave lengths: 210 nm, 254 nm, 280 nm and 360 nm; solvent A: H₂O, solvent B: MeCN; linear gradient (% B): from 5 % to 95 % in 45 min, 60 min: 95 %), yielding the chromatogram at 210 nm reported in Fig. 107. The combined organic extract was fractionated by medium pressure silica gel (Büchi PrepChrom C-700) using a gradient of CH₂Cl₂/MeOH as eluent, obtaining nine homogeneous fractions (F1-F9). The residue (1.44 g) of F3 was fractionated by

medium pressure silica gel (Büchi PrepChrom C-700) eluted with a gradient of *n*-hexane/EtOAc/MeOH, obtaining twelve homogeneous fractions (F3.1-F3.12). The residue (132.5 mg) of F3.5 was further purified with a Sephadex LH-20 chromatography eluted with Me₂CO and then a preparative medium pressure liquid chromatography (MPLC) using as eluent H₂O (A) and MeCN (B) with a flow rate of 2.0 mL min⁻¹, column temperature of 30°C and the following gradient: 50% B to 95% B in 10 min, isolating two metabolites identified as linolenic acid (**4a**, 2.6 mg) and linoleic acid (**5a**, 8.8 mg). The residue (65.3 mg) of F3.7 was purified by MPLC using the same method, yielding other amounts of linolenic acid (**4a**, 5.2 mg, for a total amount of 7.8 mg) and linoleic acid (**5a**, 1.3 mg, for a total amount of 10.1 mg). The residue (58.1 mg) of F5 was purified by MPLC eluted with H₂O (A) and MeCN (B), with a flow rate of 2.0 mL min⁻¹, column temperature of 35°C and the following gradient: 30% B to 45% B in 20 min, and to 95% B in 10 min, affording three pure metabolites identified as ixeriside D (**1a**, 1.0 mg) and sonchuside A (**2a**, 1.2 mg) and an unknown compound (**3a**, 1.4 mg). The residue (142.2 mg) of F6 was fractionated with a Sephadex LH-20 chromatography eluted with MeOH and, then, purified by MPLC using the same method used for F5, obtaining further amounts of ixeriside D (**1a**, 2.6 mg, for a total amount of 3.6 mg), sonchuside A (**2a**, 0.9 mg, for a total amount of 2.1 mg) and the unknown compound (**3a**, 2.5 mg, for a total amount of 3.9 mg).

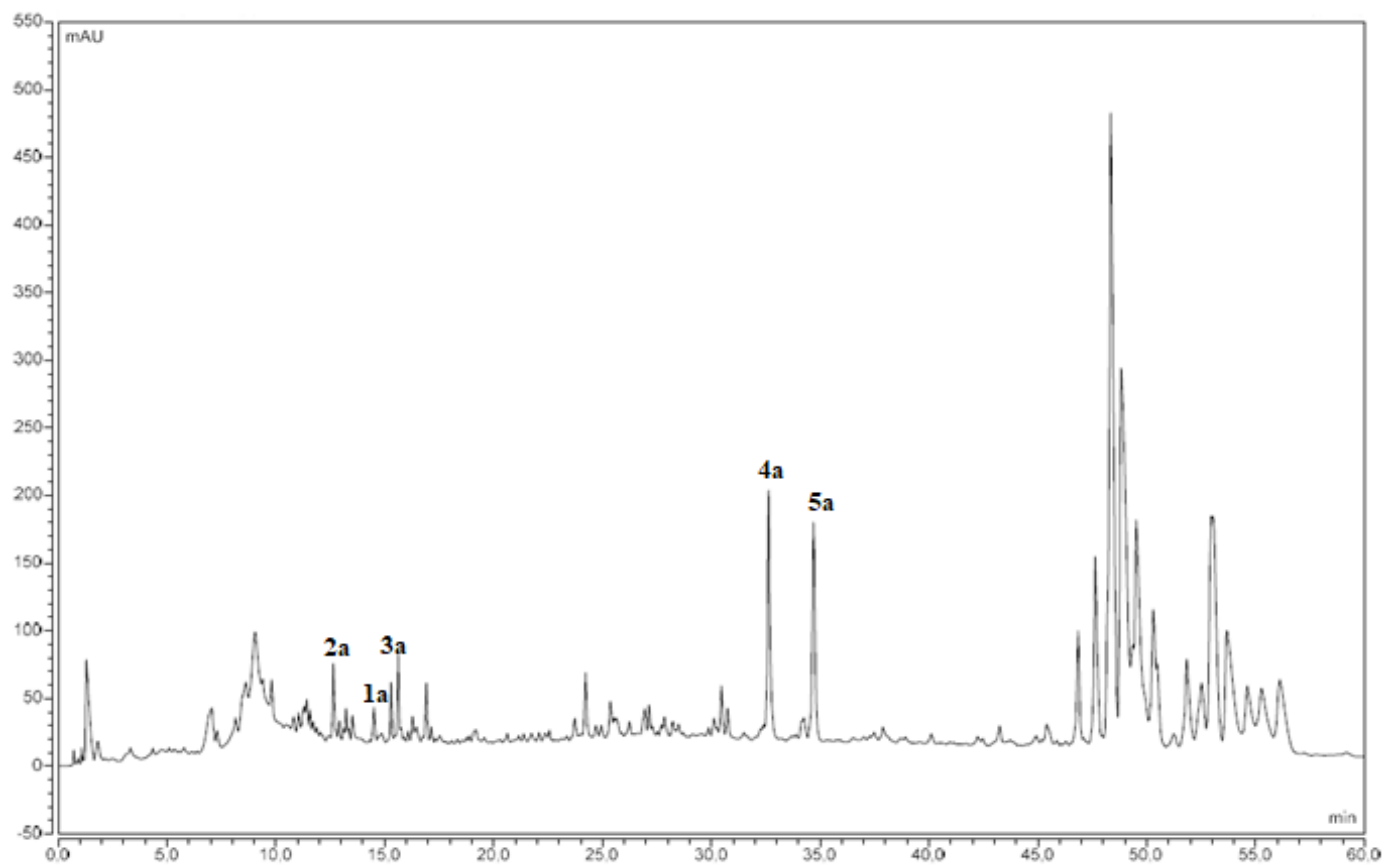
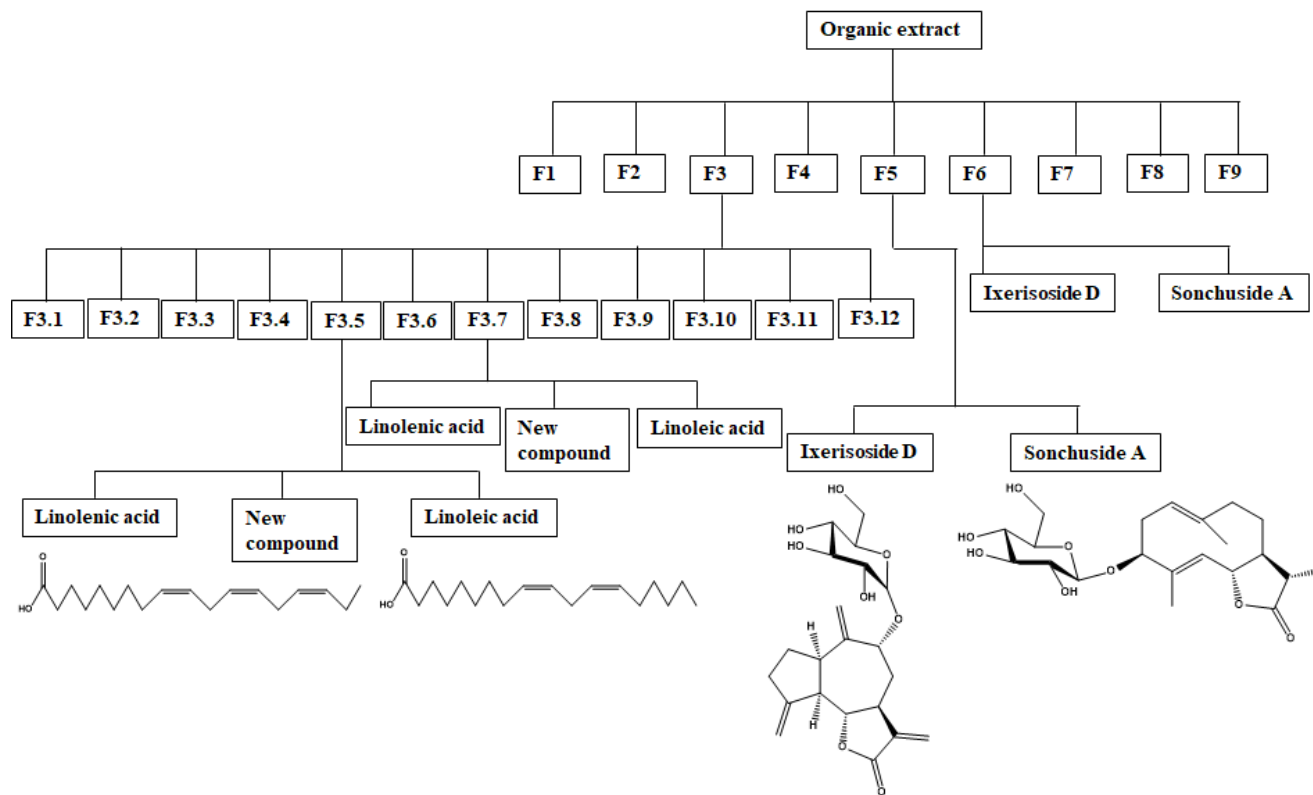


Figure 1a: UV HPLC trace recorded at 210 nm. 1a, ixeriside D; 2a, sonchuside A; 3a, unknown compound; 4a, linolenic acid; 5a, linoleic acid.



Scheme 1a: Purification scheme of *Leontodon tenuiflorus*

Ixeriside D (1a)

Ixeriside D (Fig. 2a, Page 205) was obtained as an amorphous solid and had: ^1H and ^{13}C data in agreement with those previously reported (Warashina *et al.*, 1990); ESIMS (+) spectrum m/z : 409 $[\text{M} + \text{H}]^+$.

Sonchuside A (4a)

Sonchuside A (Fig. 2a, Page 205) was afforded as an amorphous solid and had: ^1H and ^{13}C data in agreement with those previously reported (Zidorn *et al.*, 2005); ESIMS (+) spectrum m/z : 413 $[\text{M} + \text{H}]^+$.

Linolenic acid (4a)

Linolenic acid (Fig. 2a, Page 205), obtaining as an amorphous solid, had: ^1H and ^{13}C data in agreement with those previously reported (Lainer *et al.*, 2020); ESIMS (+) spectrum m/z : 279 $[\text{M} + \text{H}]^+$.

Linoleic acid (5a)

Linoleic acid (Fig. 2a, Page 205), yielded as an amorphous solid, had: ^1H and ^{13}C data in agreement with those previously reported (Lainer *et al.*, 2020); ESIMS (+) spectrum m/z : 281 $[\text{M} + \text{H}]^+$.

Results and discussion

The organic extract of dried roots of *L. tenuiflorus* was purified as detailed in the Experimental section (Scheme 1a), yielding five metabolites (**1a-5a**, Fig. 2a). An unknown compound (**3a**) was isolated together with already known metabolites identified as ixeriside D (**1a**), sonchuside A (**2a**), linolenic acid (**4a**) and linoleic acid (**5a**).

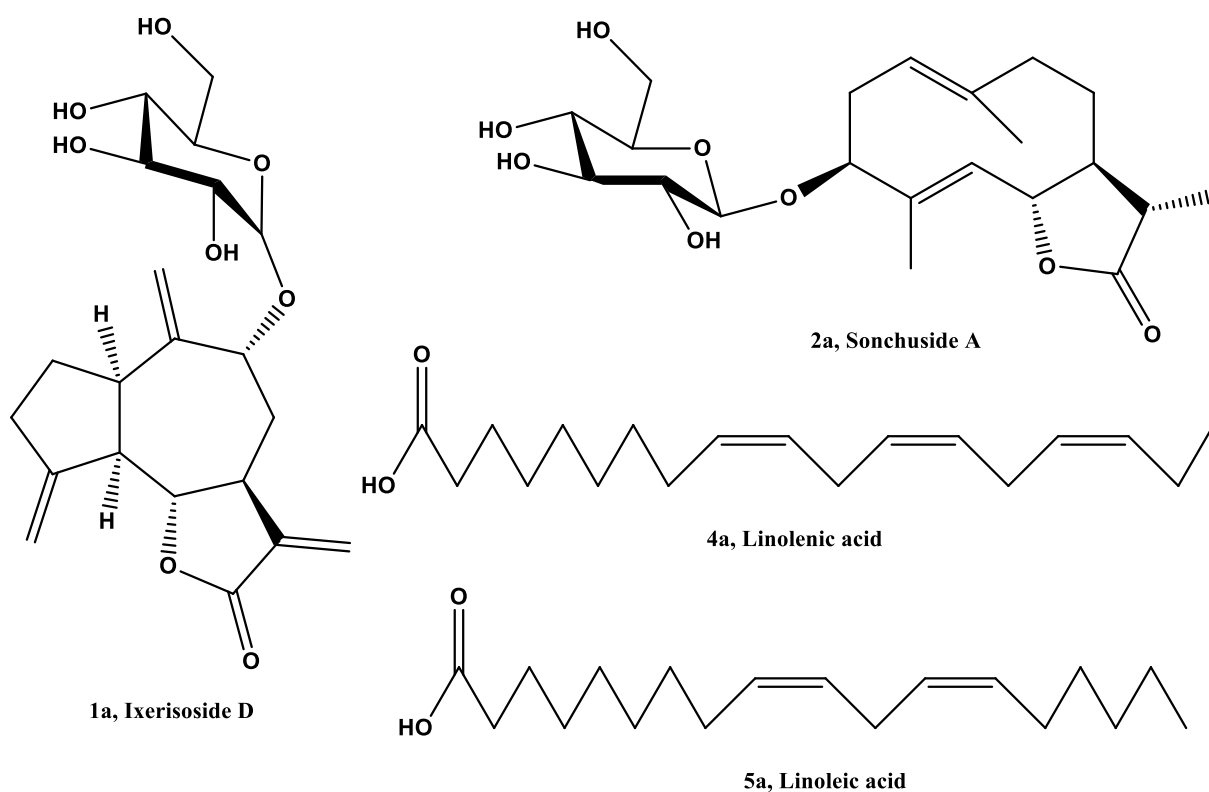


Figure 2a: Secondary metabolites isolated from *Leontodon tenuiflorus*.

They were identified comparing their spectroscopic data with those reported in literature: (Warashina *et al.*, 1990) for ixeriside D (**1a**), (Zidorn *et al.*, 2005) for sonchuside A (**2a**) and (Lainer *et al.*, 2020) for linolenic acid (**4a**) and for linoleic acid (**5a**).

Ixeriside D (**1a**) is a guaianolide glucoside that was isolated for the first time from *Ixeris repens* (Warashina *et al.*, 1990), then it was isolated from *Cichorium intybus* (Kisiel and Zielińska, 2001; Malarz *et al.*, 2002) and *C. endivia* var. *crispum* (Kisiel and Michalska, 2006). Recently, it has been identified as chemical constituent of roots of *Launaea sarmentosa* (Hanh *et al.*, 2020).

Sonchuside A (**2a**) is a germacranolide glucoside that was isolated for the first time from *Sonchus oleraceus* L. (Miyase and Fukushima, 1987). Successively, it was identified as chemical constituent of many plants: *Lactuca tatarica* (Kisiel *et al.*, 1997), *Cichorium intybus* (Malarz *et al.*, 2002), *Taraxacum obovatum* (Michalska and Kisiel, 2003), *Cicerbita alpina* (Zidorn *et al.*, 2005) and *Lactuca plumieri* (Michalska *et al.*, 2021).

Linolenic acid (**4a**) and linoleic acid (**5a**) are fatty acids commonly found as chemical constituents of many plants (Onivogui *et al.*, 2017; Lainer *et al.*, 2020; Saffaryazdi *et al.*, 2020; Ju *et al.*, 2021).

The chemical characterization of the unknown metabolite (**3a**) is still in progress.

References

- Enke, N., Gemeinholzer, B., Zidorn, C. (2012). Molecular and phytochemical systematics of the subtribe Hypochaeridinae (Asteraceae, Cichorieae). *Org. Divers. Evol.* *12*, 1–16.
- Hanh, L.H., Dung, P.D., Huy, L.D., Duong, N.T.T., Wacharasindhu, S., Phung, N.K.P., Chi, H.B.L. (2020). Chemical constituents of *Launaea sarmentosa* roots. *Vietnam J. Chem.* *58*, 637–642.
- Ju, Y.L., Yue, X.F., Cao, X.Y., Wei, X.F., Fang, Y.L. (2021). First study on the fatty acids and their derived volatile profiles from six Chinese wild spine grape clones (*Vitis davidii* Foex). *Sci. Hortic.* *275*, 109709.
- Kisiel, W., Barszcz, B., Szneler, E. (1997). Sesquiterpene lactones from *Lactuca tatarica*. *Phytochemistry*, *45*, 365–368.
- Kisiel, W., and Zielińska, K. (2001). Guaianolides from *Cichorium intybus* and structure revision of *Cichorium* sesquiterpene lactones. *Phytochemistry*, *57*, 523–527.
- Kisiel, W., and Michalska, K. (2006). Sesquiterpenoids and phenolics from roots of *Cichorium endivia* var. *crispum*. *Fitoterapia*, *77*, 354–357.
- Lainer, J., Dawid, C., Dunkel, A., Gläser, P., Wittl, S., Hofmann, T. (2020). Characterization of bitter-tasting oxylipins in poppy seeds (*Papaver somniferum* L.). *J. Agric. Food Chem.* *368*, 10361–10373.
- Malarz, J., Stojakowska, A., Kisiel, W. (2002). Sesquiterpene lactones in a hairy root culture of *Cichorium intybus*. *Z. Naturforsch. C* *57*, 994–997.
- Michalska, K., and Kisiel, W. (2003). Sesquiterpene lactones from *Taraxacum obovatum*. *Planta Med.* *69*, 181–183.

- Michalska, K., Malarz, J., Stojakowska, A. (2021). Chemical constituents from *Lactuca plumieri* (L.) Gren. & Godr. (Asteraceae). Nat. Prod. Res. 1–5.
- Miyase, T., and Fukushima, S. (1987). Studies on sesquiterpene glycosides from *Sonchus oleraceus* L. Chem. Pharm. Bull. 35, 2869–2874.
- Onivogui, G., Zhang, X., Diaby, M., Maomy, C.G., Song, Y. (2017). Potential nutritional and antioxidant activity of various solvent extracts from leaves and stem bark of *Anisophyllea laurina* R. Br ex Sabine used in folk medicine. Braz. J. Pharm. Sci. 53.
- Saffaryazdi, A., Ganjeali, A., Farhoosh, R., Cheniany, M. (2020). Variation in phenolic compounds, α -linolenic acid and linoleic acid contents and antioxidant activity of purslane (*Portulaca oleracea* L.) during phenological growth stages. Physiol. Mol. Biol. Plants 26, 1519–1529.
- Sareedenchai, V., and Zidorn, C. (2010). Flavonoids as chemosystematic markers in the tribe Cichorieae of the Asteraceae. Biochem. Syst. Ecol. 38, 935–957.
- Warashina, T., Ishino, M., Miyase, T., Ueno, A. (1990). Sesquiterpene glycosides from *Ixeris debilis* and *Ixeris repens*. Phytochemistry 29, 3217–3224.
- Zidorn, C., Schwaha, R.E., Ellmerer, E.P., Stuppner, H. (2005). On the occurrence of sonchuside A in *Cicerbita alpina* and its chemosystematic significance. J. Serb. Chem. Soc. 70, 171–175.
- Zidorn, C. (2012). *Leontodon* and *Scorzoneroides* (Asteraceae, Cichorieae) in Italy. Plant Biosyst. 146, 41–51.

9 PUBLICATIONS LIST

The results herein reported have been published:

- Masi, M., Di Lecce, R., Tuzi, A., Linaldeddu, B. T., Montecchio, L., Maddau, L., Evidente, A. (2019) “Hyfraxinic acid, a phytotoxic tetrasubstituted octanoic acid, produced by the ash (*Fraxinus excelsior* L.) pathogen *Hymenoscyphus fraxineus* together with viridiol and some of its analogues”. *Journal of Agricultural and Food Chemistry*, 67.49, 13617-13623. DOI: 10.1021/acs.jafc.9b06055.
- Bashiri, S., Abdollahzadeh, J., Di Lecce, R., Alioto, D., Górecki, M., Pescitelli, G., Masi, M., Evidente, A. (2020) “Rabenchromenone and rabenzophenone, phytotoxic tetrasubstituted chromenone and hexasubstituted benzophenone constituents produced by the oak-decline-associated fungus *Fimetariella rabenhorstii*”. *Journal of Natural Products*, 83.2, 447-452. DOI: 10.1021/acs.jnatprod.9b01017.
- Di Lecce, R., Bashiri, S., Masi, M., Alioto, D., Tuzi, A., Abdollahzadeh, J., Evidente, A. (2020) “Phytotoxic metabolites from *Stilbocrea macrostoma*, a fungal pathogen of *Quercus brantii* in Iran”. *Natural Product Research*, 1-5. DOI: 10.1080/14786419.2020.1797731.
- Di Lecce, R., Masi, M., Linaldeddu, B.T., Pescitelli, G., Maddau, L., Evidente, A. (2021) “Bioactive secondary metabolites produced by the emerging pathogen *Diplodia olivarum*”. *Phytopathologia Mediterranea*, 60.1, 129-138. DOI: 10.36253/phyto-12170.
- Masi, M., Di Lecce, R., Marsico, G., Linaldeddu, B. T., Maddau, L., Superchi, S., Evidente, A. (2021) “Pinofuranoxins A and B, bioactive trisubstituted furanones produced by the invasive pathogen *Diplodia sapinea*”. *Journal of natural products*, 84.9, 2600-2605. DOI: 10.1021/acs.jnatprod.1c00365.
- Masi, M., Di Lecce, R., Maddau, L., Marsico, G., Superchi, S., Evidente, A. (2021) “Argyrotoxins A-C, a trisubstituted dihydroisobenzofuranone, a tetrasubstituted 2-hydroxyethylbenzamide and a tetrasubstitutedphenyl trisubstitutedbutyl ether produced by *Alternaria argyroxiphii*, the causal agent of leaf spot on African mahogany trees (*Khaya senegalensis*)”. *Phytochemistry*, 191, 112921. DOI: 10.1016/j.phytochem.2021.112921.

Acknowledgment

Immeasurable appreciation and gratitude for the help and support are extended to the following scientists that contributed in these studies.

Firstly, I would like to express my gratitude to my supervisor Prof. Antonio Evidente for his support during my PhD with his enthusiasm and immense knowledge. His guidance helped me in all the time of the research and writing this thesis.

I would like to thank my co-supervisor Dr. Marco Masi for his help and support in these studies, for the stimulating discussions and for motivating me during the hardest times.

Besides my supervisors, I thank the other members of the research group: in particular, Prof. Alessio Cimmino for the time spent together to discuss about many fields and to help me, Dr. Paola Nocera for her support, unreserved presence and friendship.

My sincere thanks also go to Prof. Christian Zidorn for the opportunity to spend a stage in his group learning new techniques and using different machines and to believe immediately in my potentials. In that time, I had the precious help of Dr. Mayra Perez also, who was present in all the moments.

Finally, I would like to thank all the other people that contribute to these researches: Prof. Lucia Maddau of the University of Sassari that grown fungi and performed the biological assays; Prof. Jafar Abdollahzadeh and Dr. Samaneh Bashiri of the University of Kurdistan that grown the fungi pathogens of Iranian oak trees and performed the biological assays; Prof. Stefano Superchi at the University of Basilicata and Prof. Gennaro Pescitelli at the University of Pisa that performed ECD experiments and the computational calculations; Prof. Angela Tuzi of the University of Naples Federico II that performed the crystallographic analyses.